What can we learn about donor metrology from transport measurements?

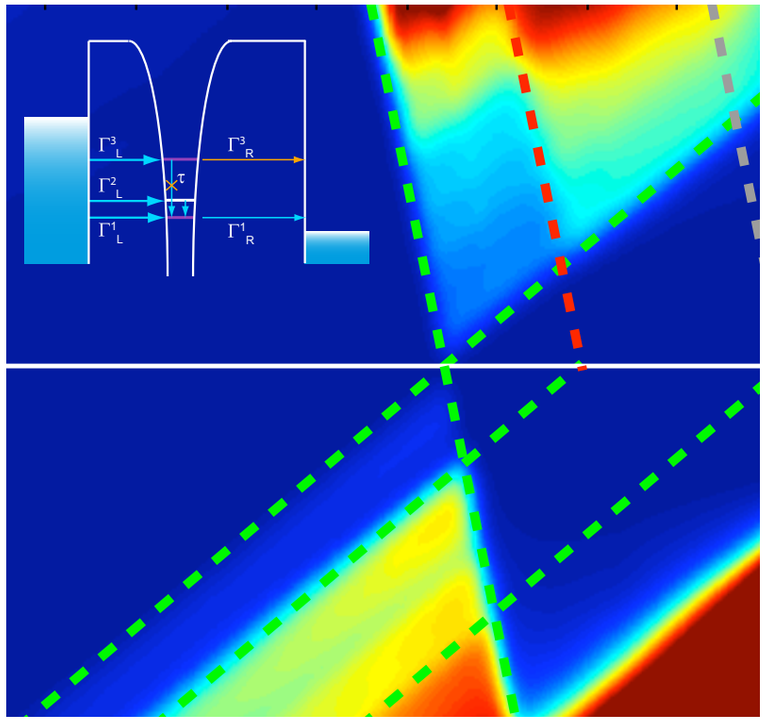

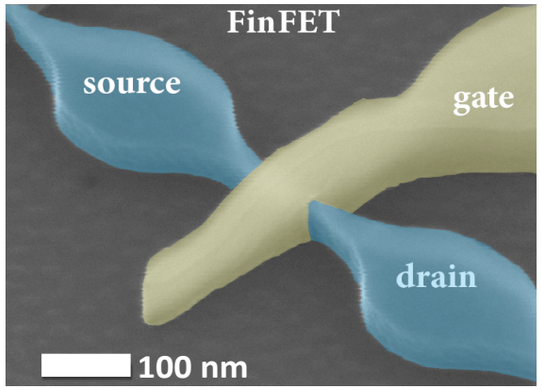

Sven Rogge
Kavli Institute for NanoScience

Knowledge of dopant location and their electronic properties is essential

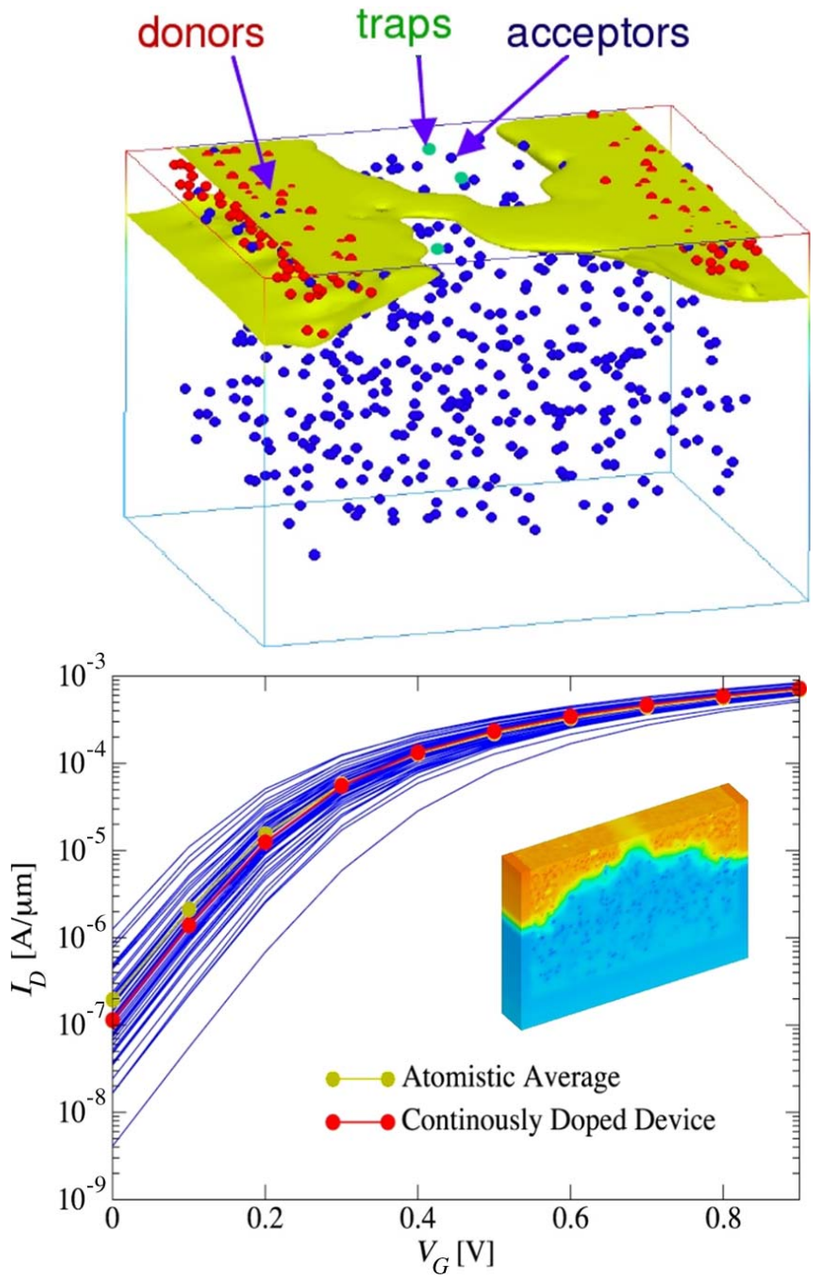

Bukhori et al. IEEE Trans. Electron Devices 57, 795 (2010)

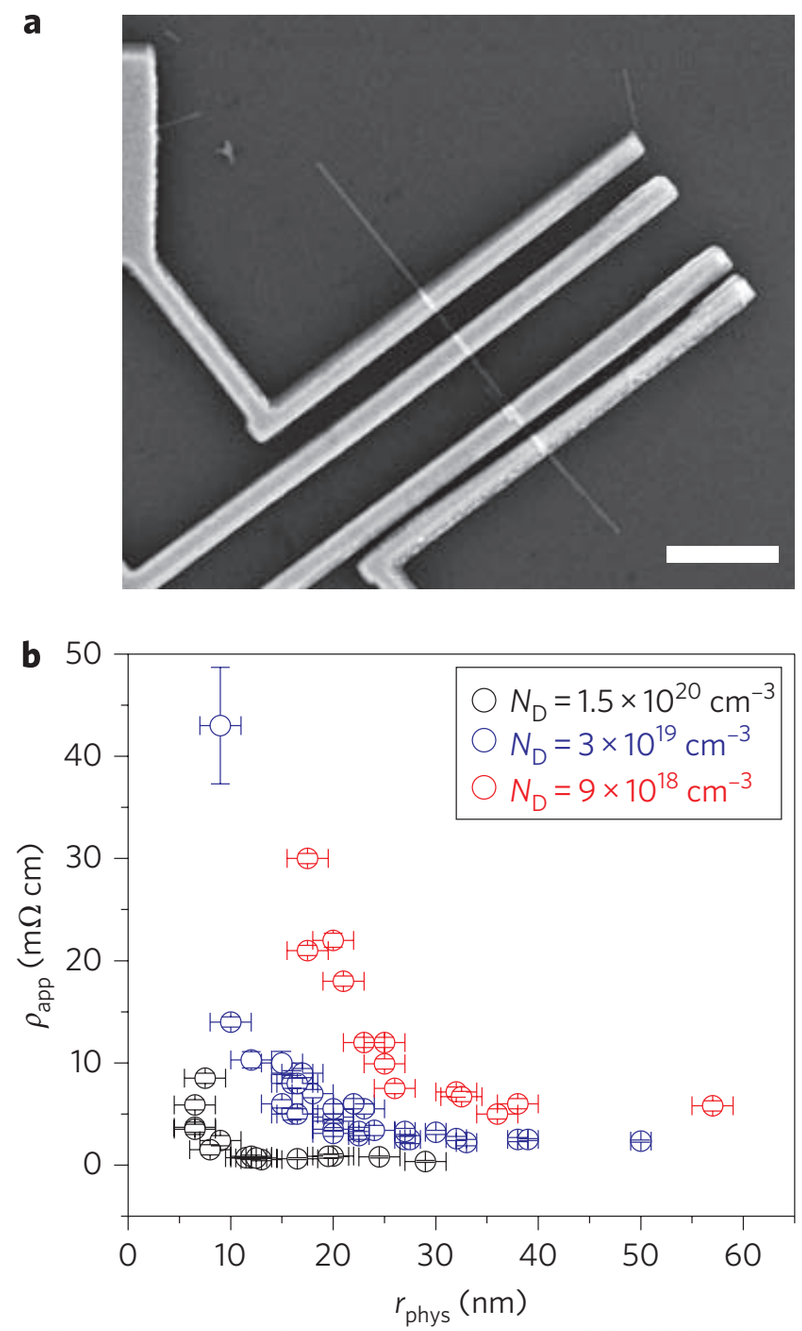

Bjork et al. Nature NT 4, 103 (2009)

Transport through localized states

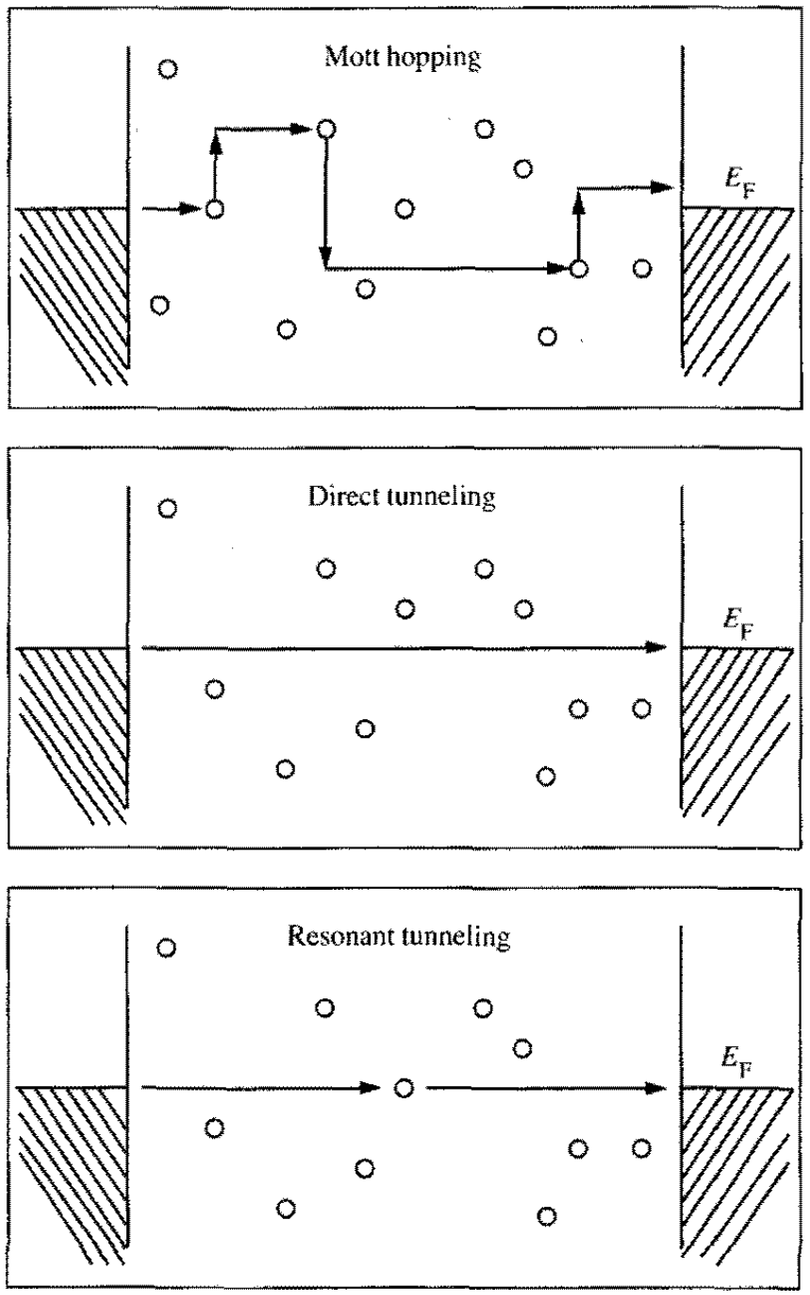

Sellier PRL 97, 206805 (2006)

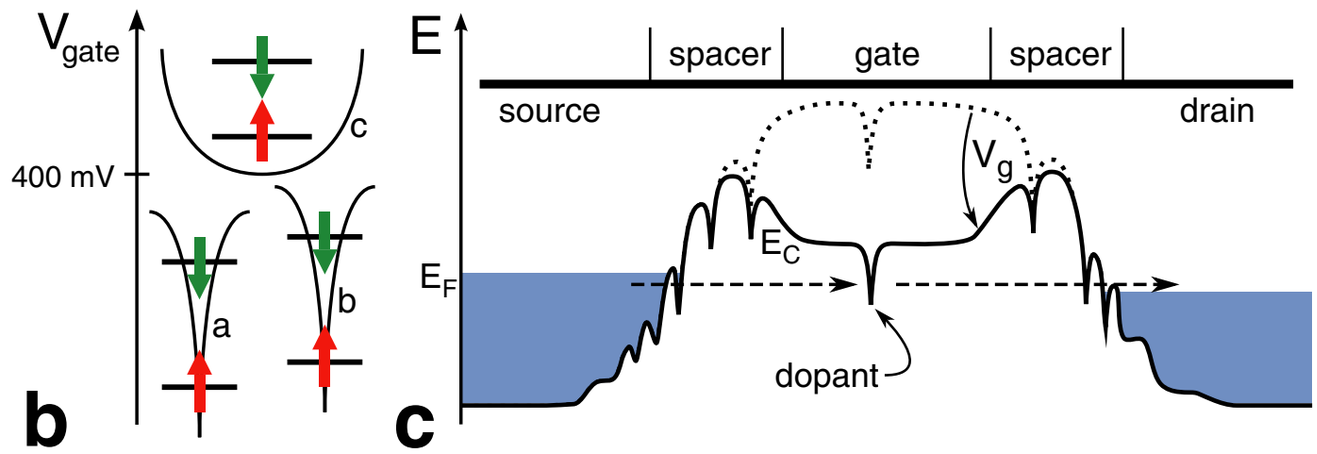

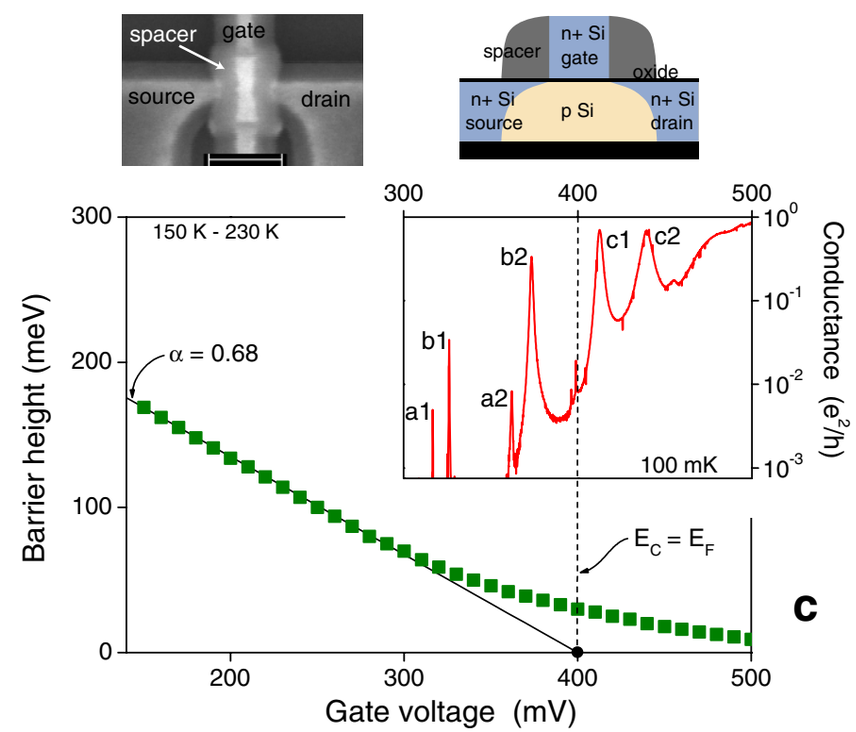

Link LT spectroscopy to RT performance

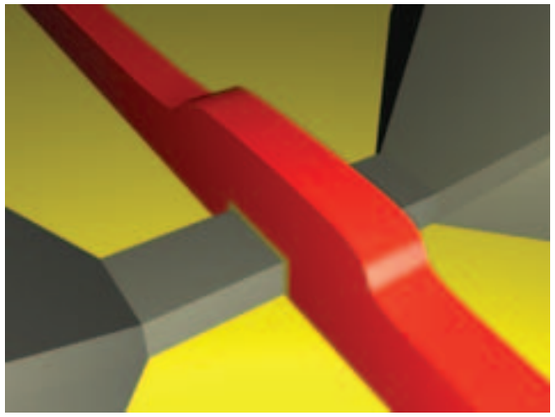

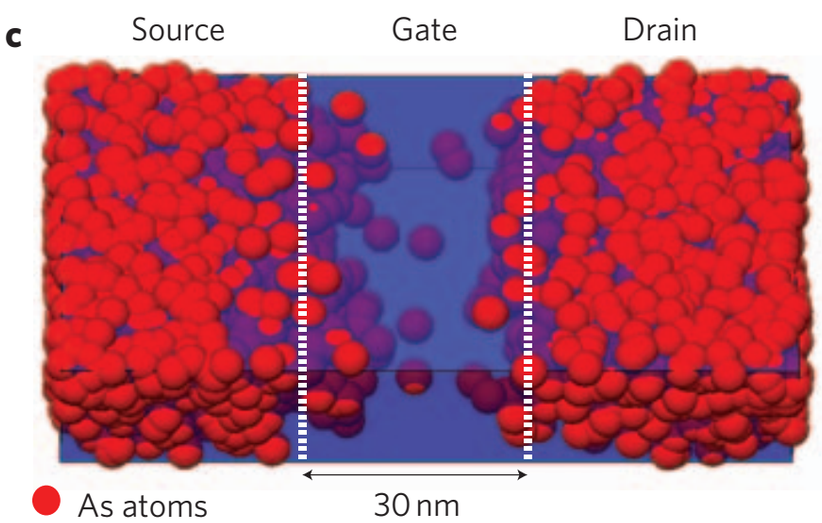

room temperature

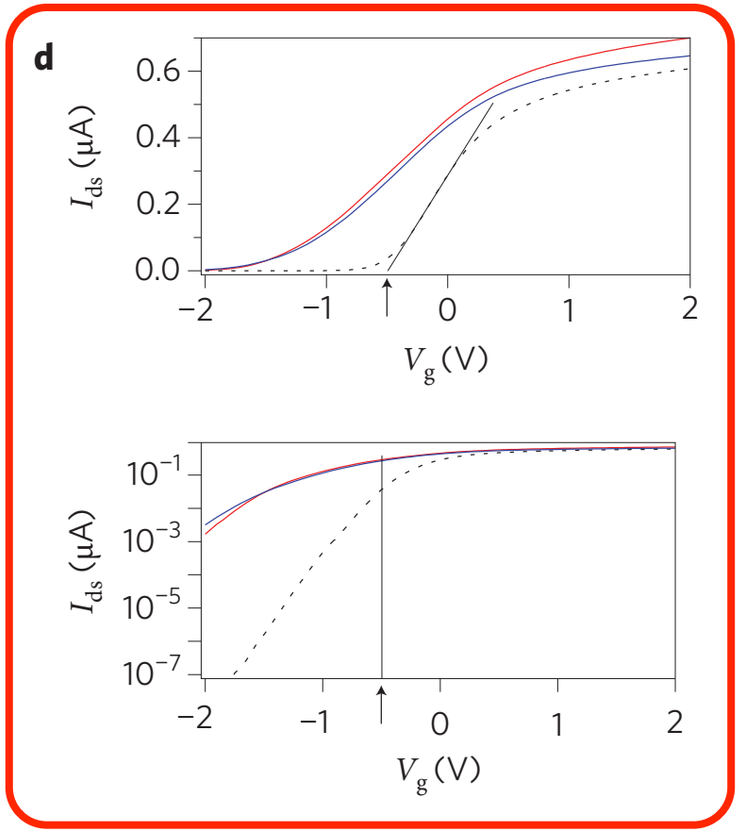

cryogenic

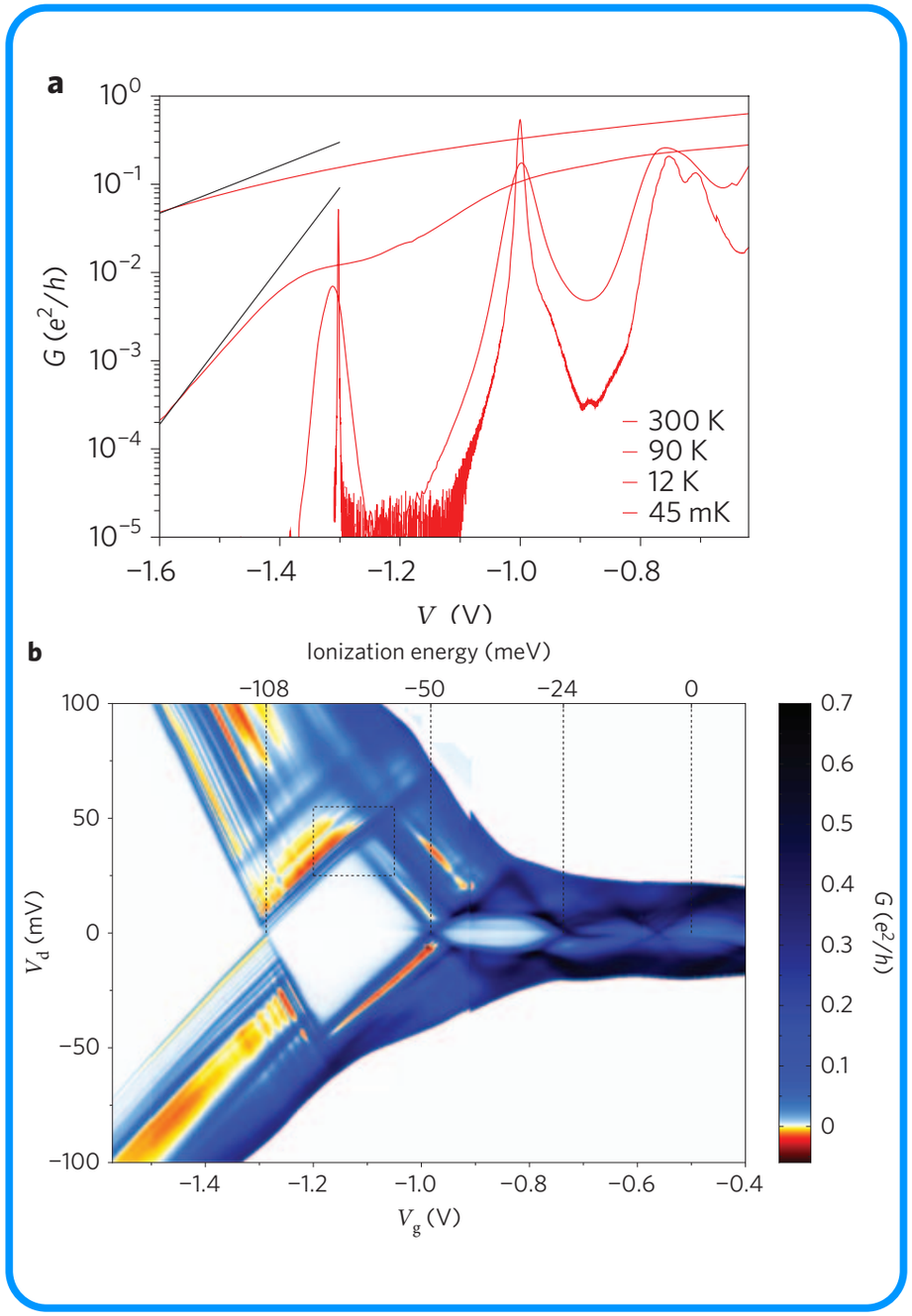

Pierre et al. Nature Nanotechology 5, 133 (2010) & VLSI (2010)

Single-ion implantation in a nano FET

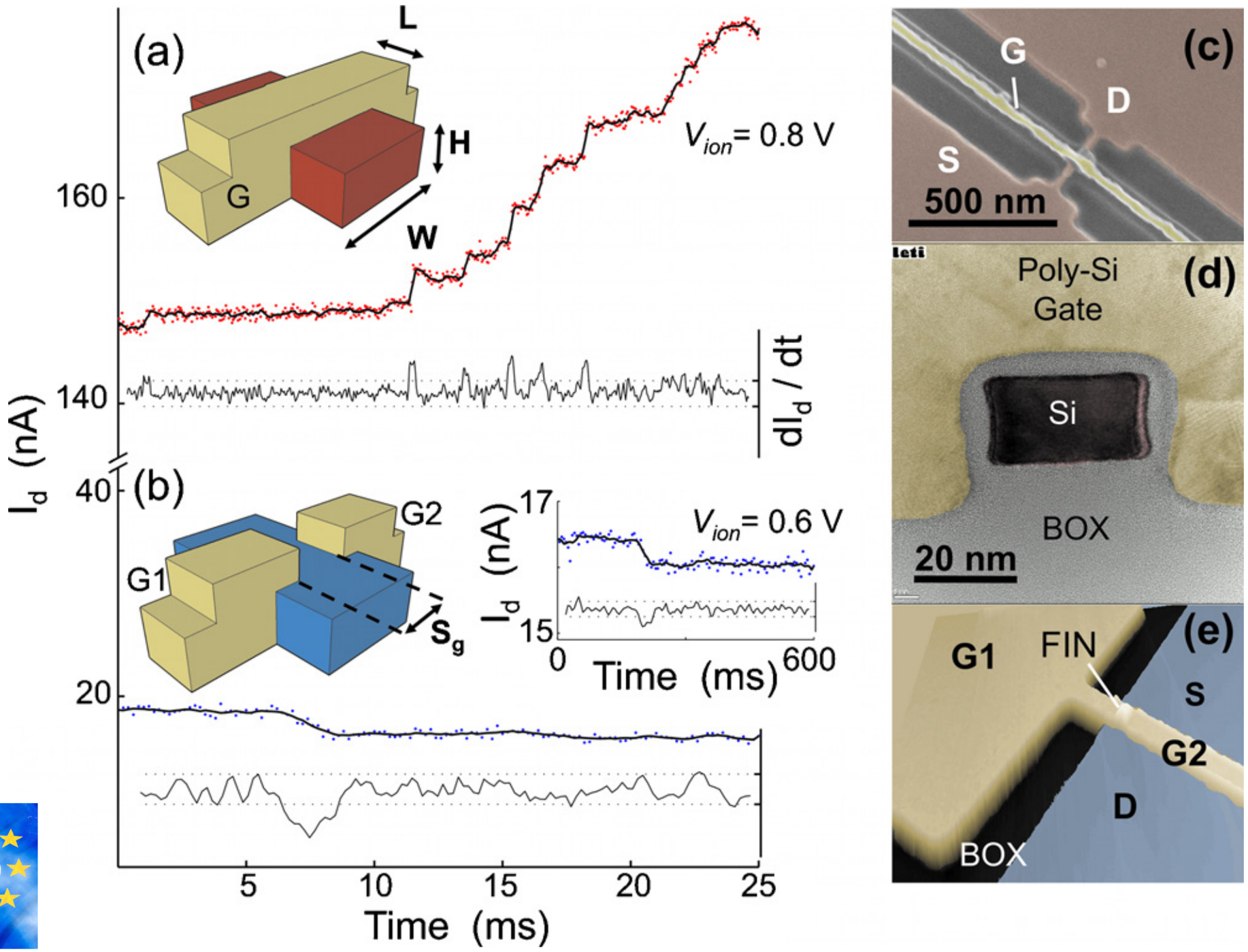

Johnson et al. APL 96, 264102 (2010)

Determination of the position of a single acceptor in a nanoFET

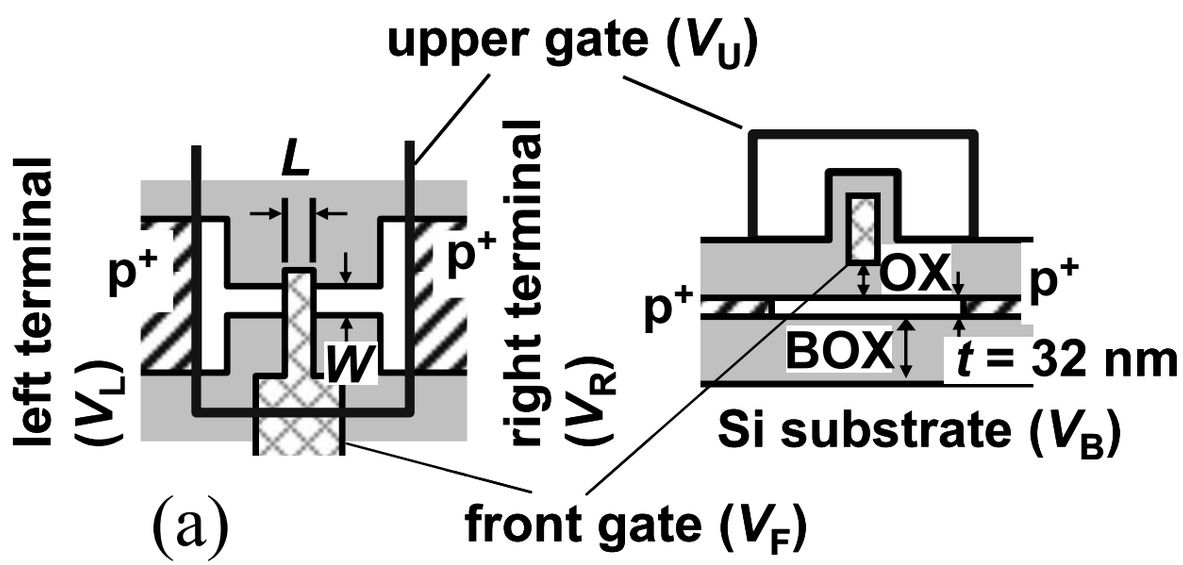

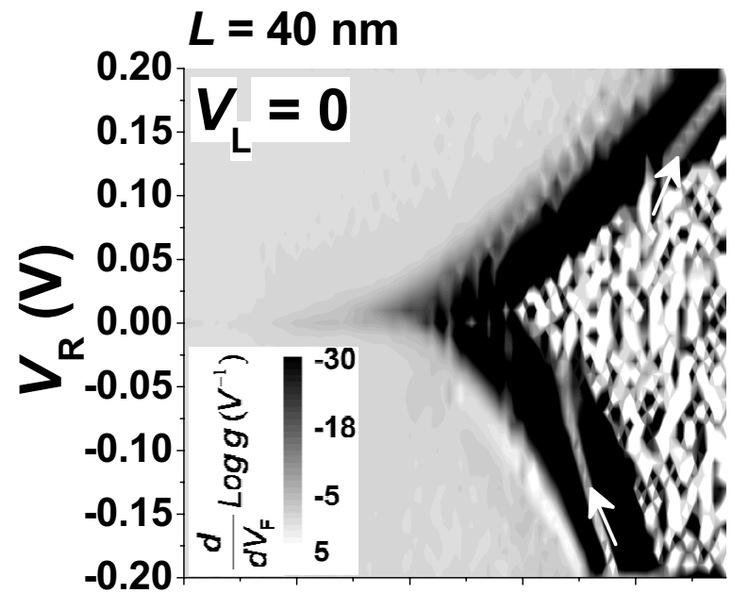

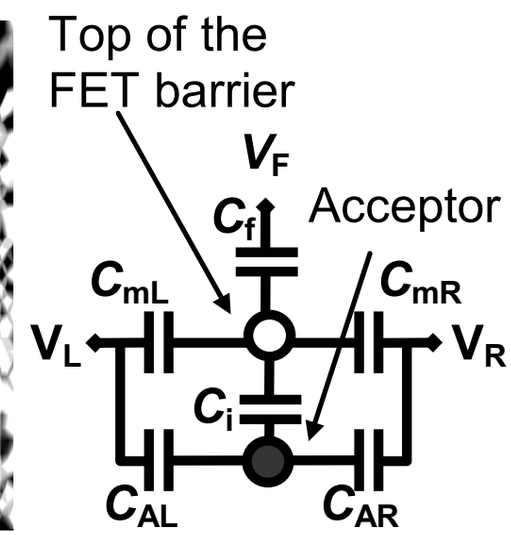

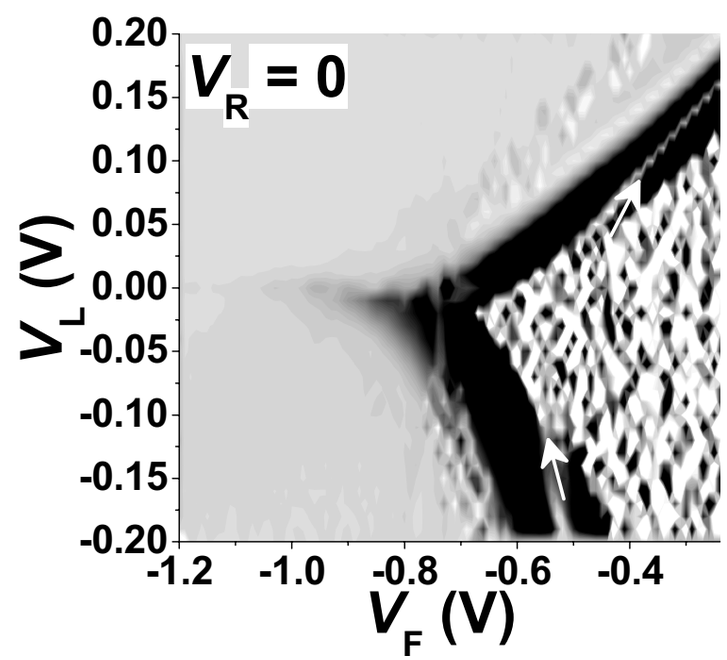

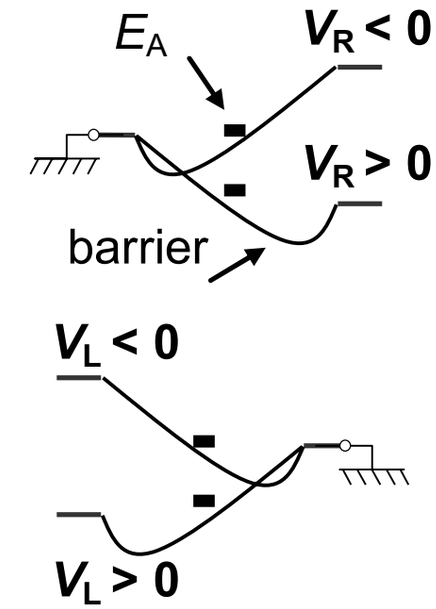

p++,p,p++ undoped pFET location of the channel can be scanned and a single acceptor is located by trapping/detrapping

Khalafalla APL 94, 223501 (2009)

Outline

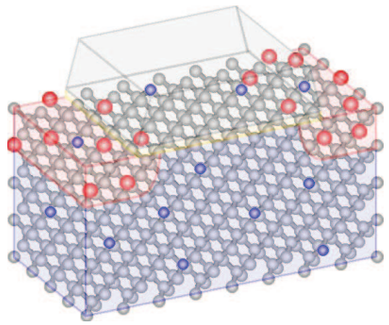

- Background

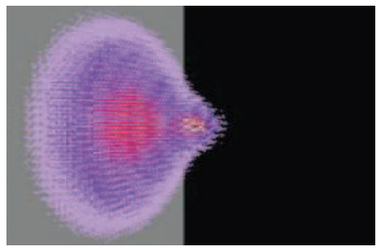

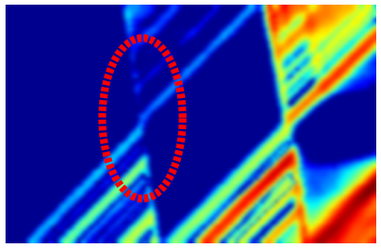

- From I(Vg) peaks → spectra & environmental information

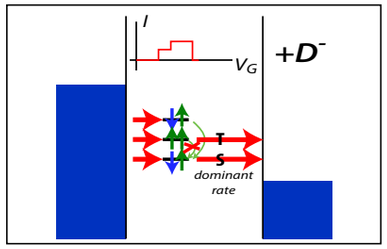

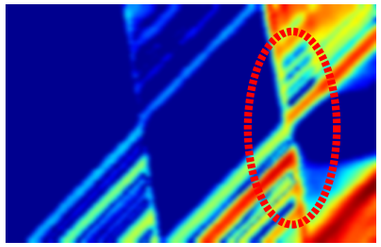

- Beyond level spectroscopy

Σ

- Summary

Shallow dopants in Si: restricted momentum space atoms

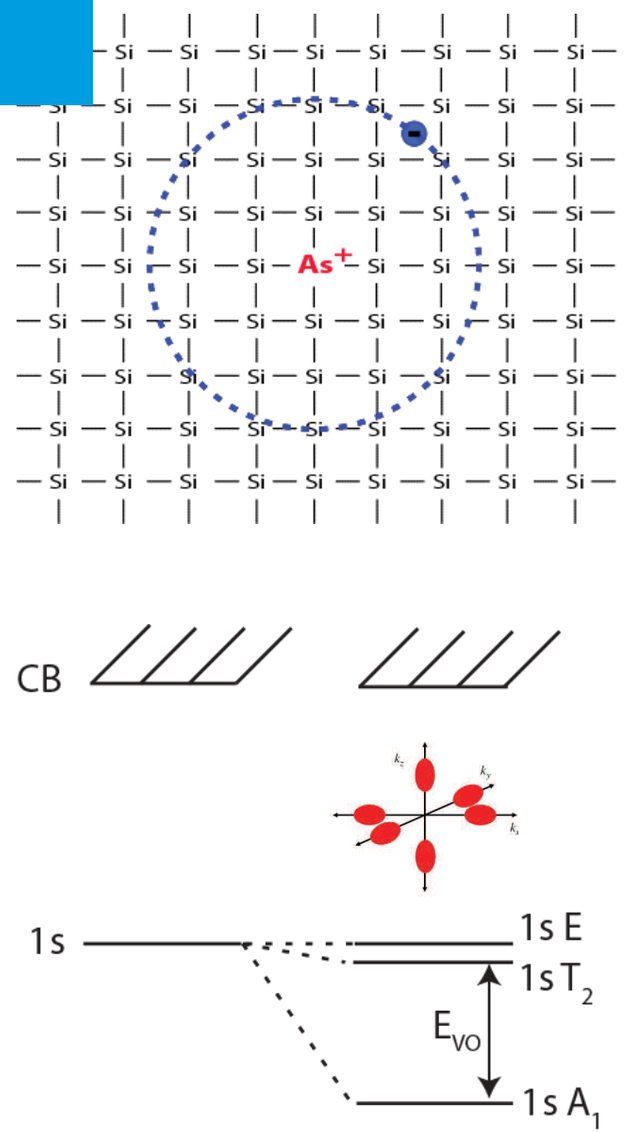

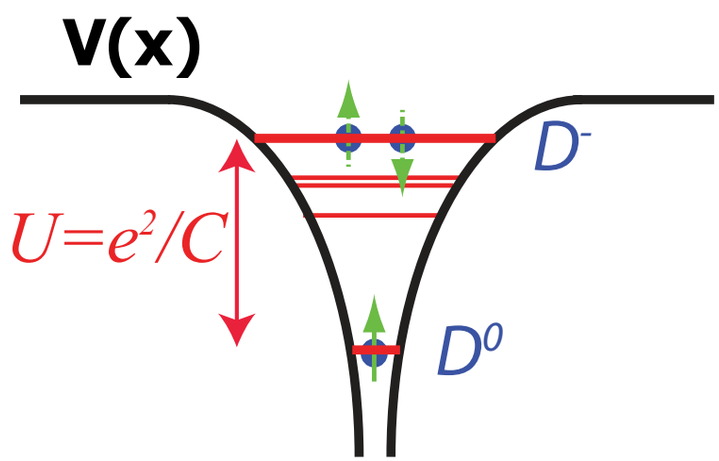

- 3D Coulomb potential
  - Can bind up to two electrons
  - Hydrogen-like level spectrum (D^0)
  - Valley-orbit

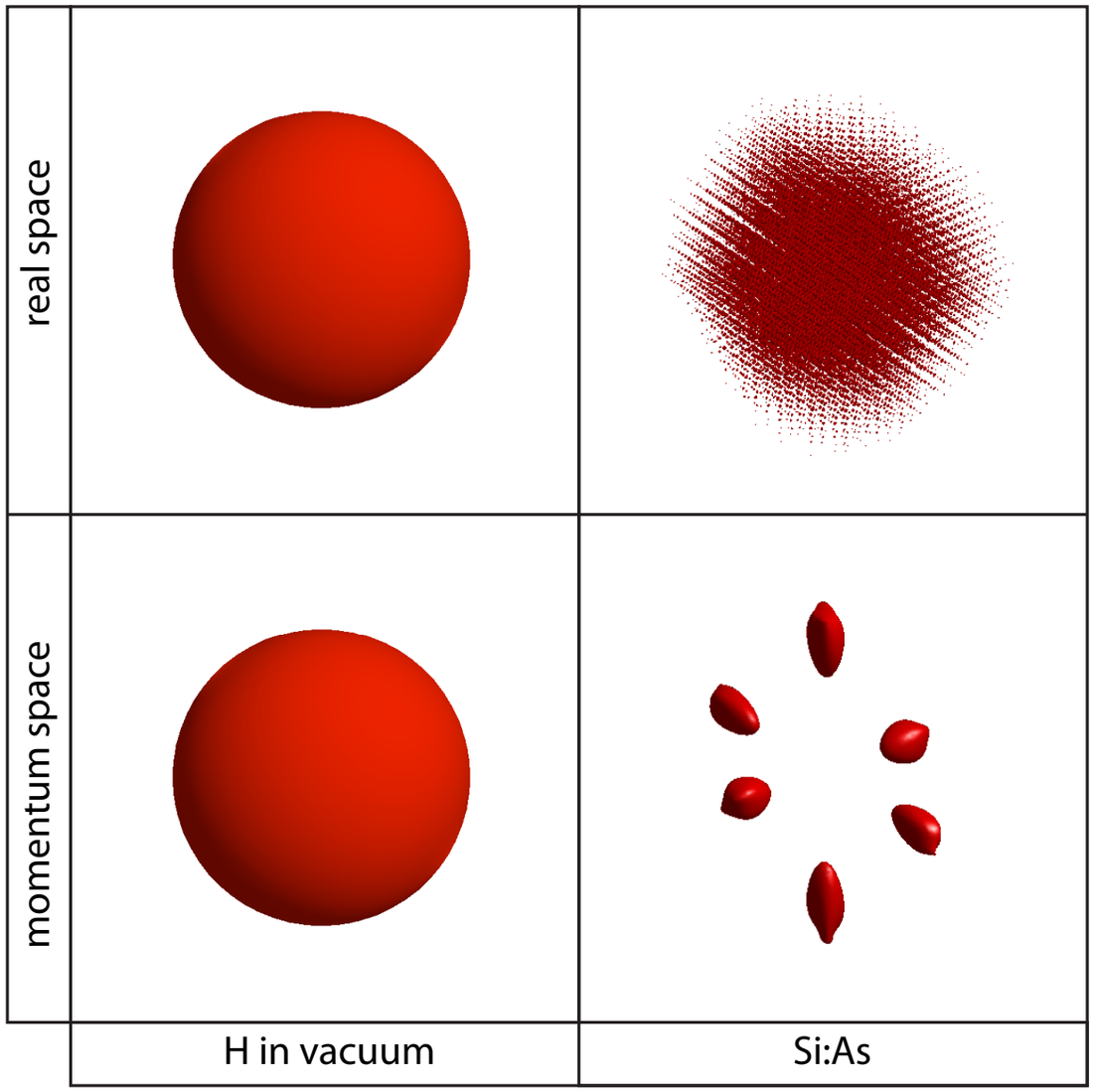

Multi-gate devices: FinFETs from the Biesemans group at IMEC

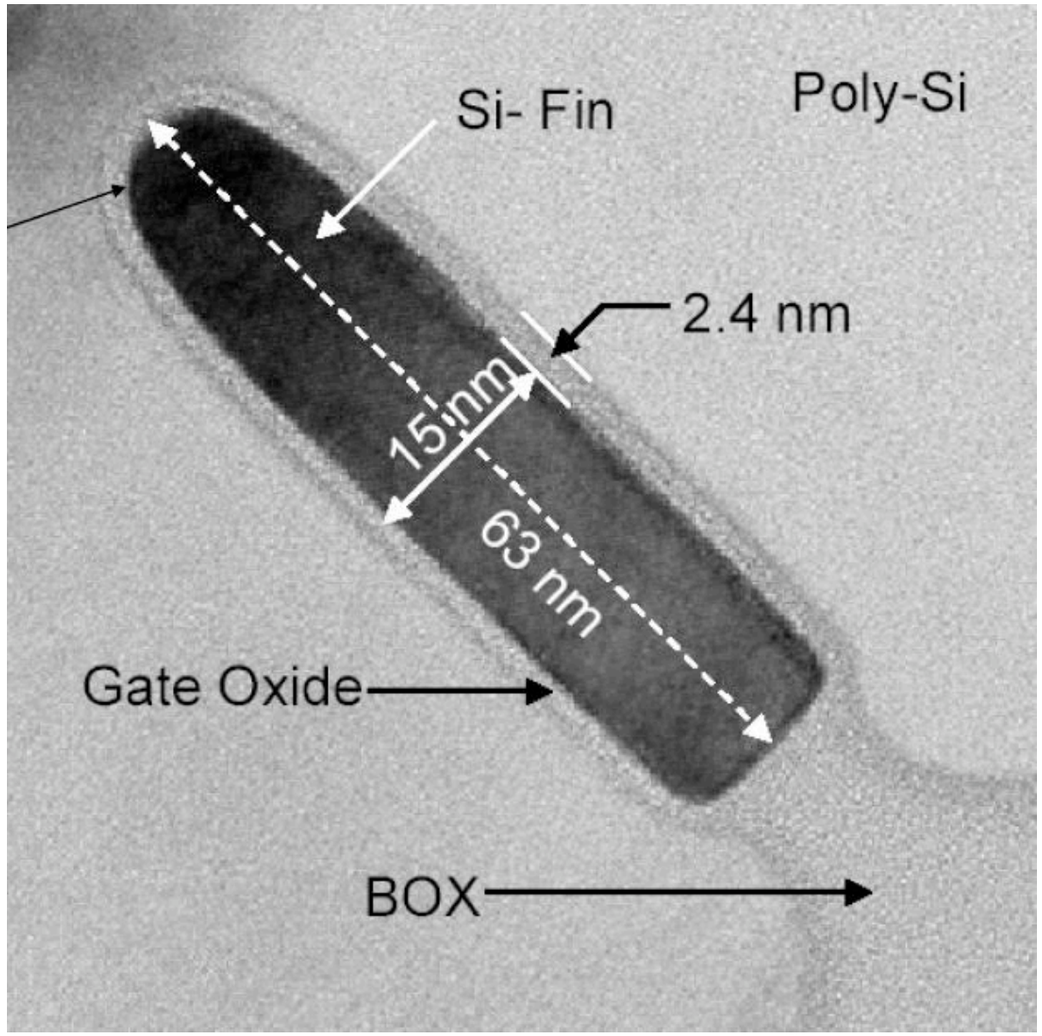

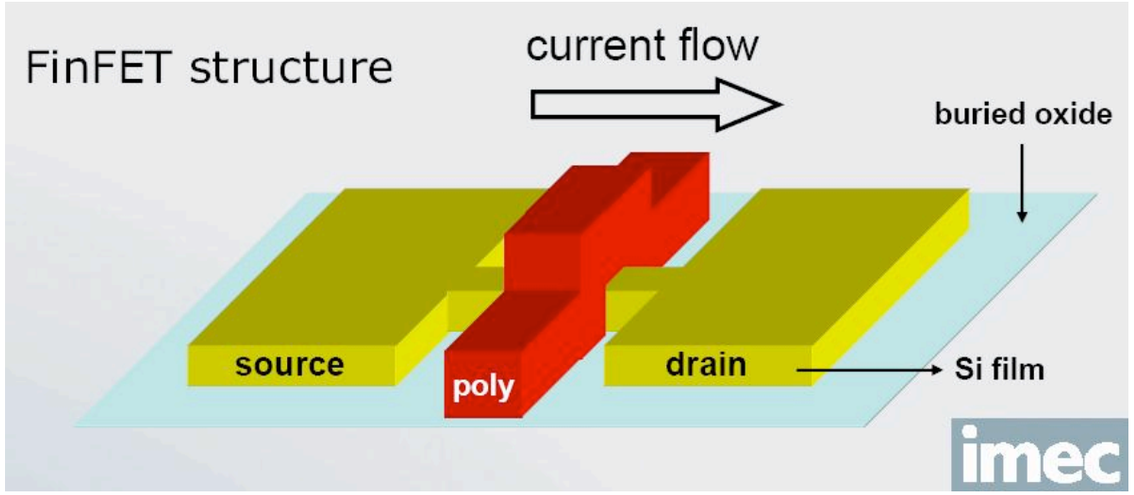

[Nadine Collaert, IMEC]

- application: lithographically defined Si nanowires (fins) covered by a single gate
- our experiments: single fin devices, here fin width 15 nm & gate length 20 nm

Detect states below the bandedge by resonant tunneling

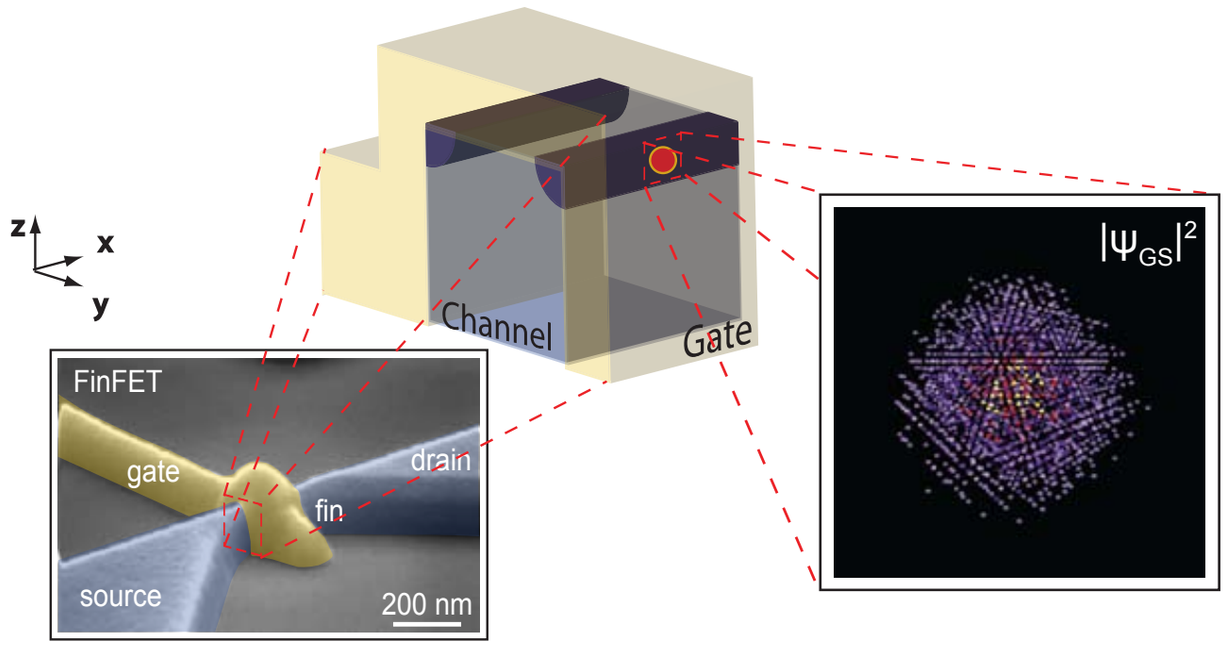

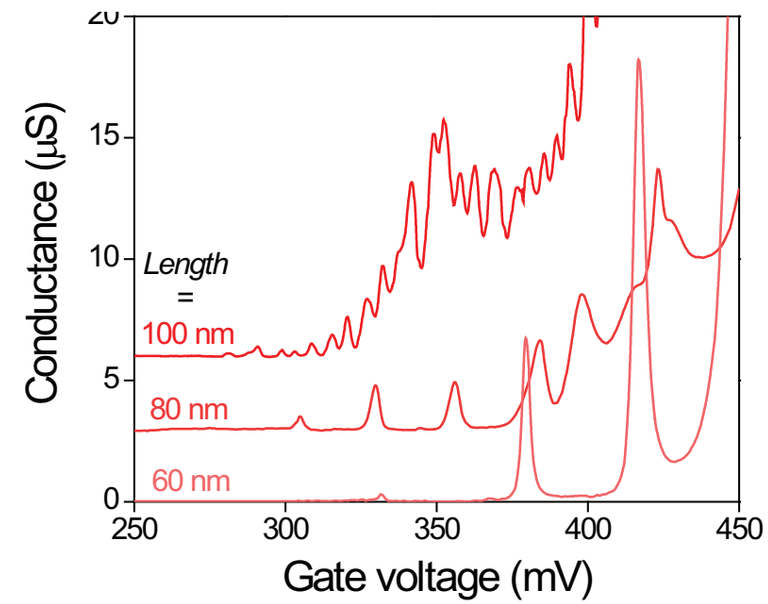

$$G_{res} = \frac{4e^2}{h}\frac{\Gamma_1\Gamma_2}{(\Gamma_1+\Gamma_2)^2}$$

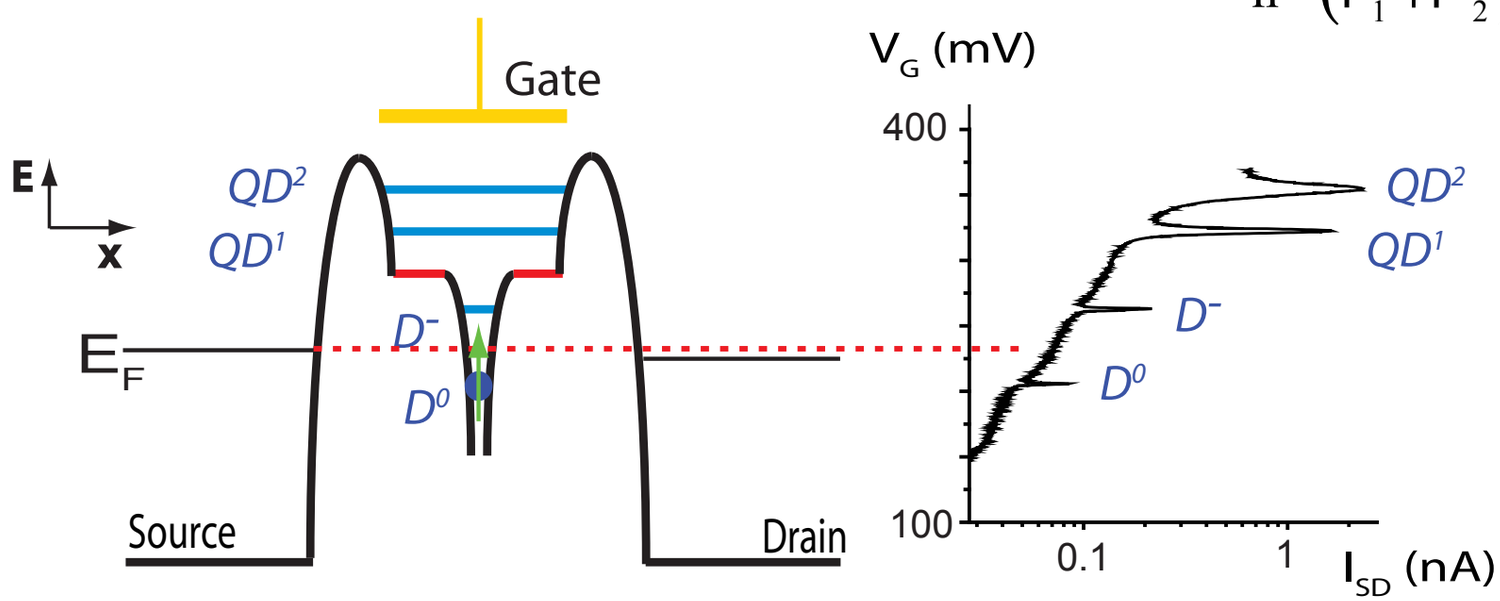

1 in 7 samples has peaks below bandedge (two, lower conductance, larger peak separation)

Sellier PRL 97, 206805 (2006)

Stability diagram: determine addition- & level-spectrum

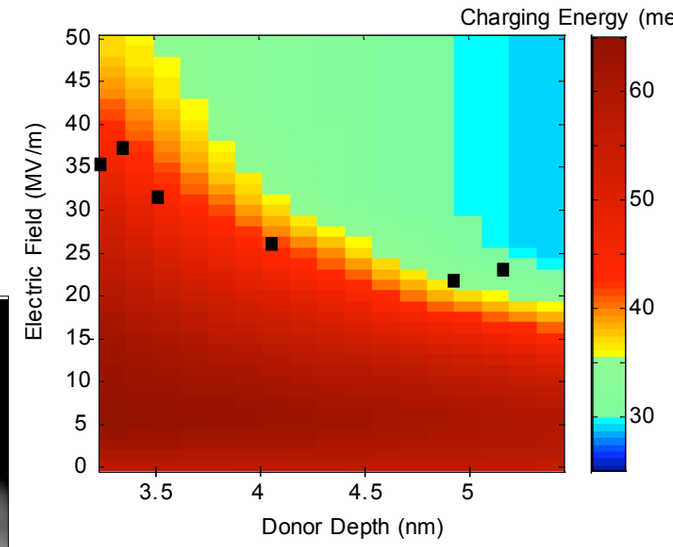

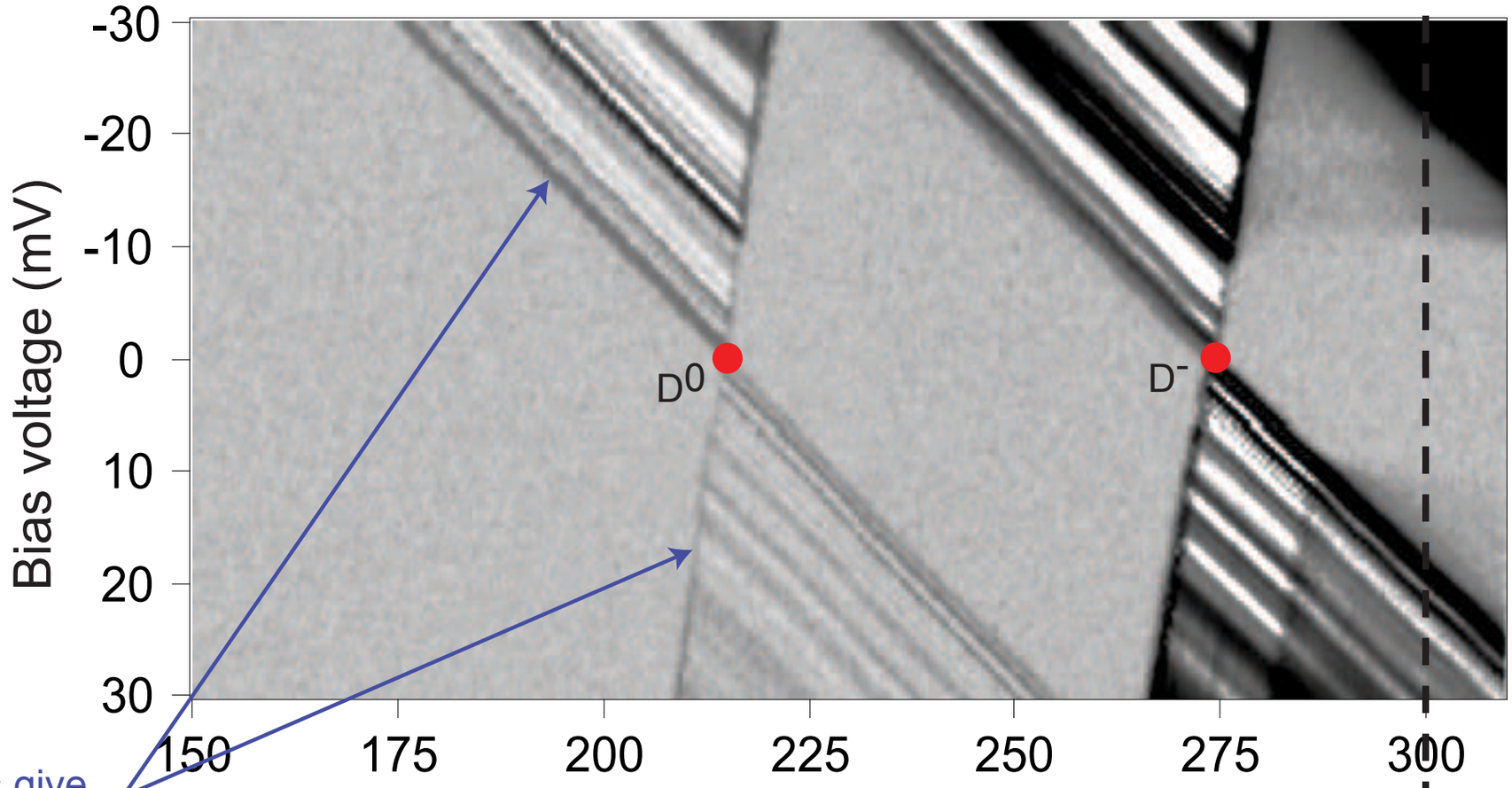

Slopes give voltage to energy conversion α = 0.7

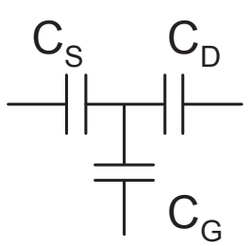

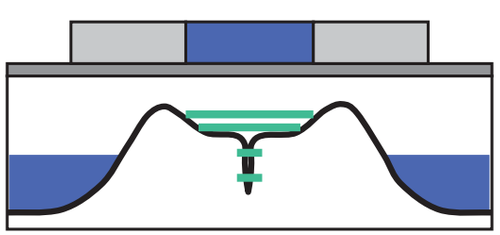

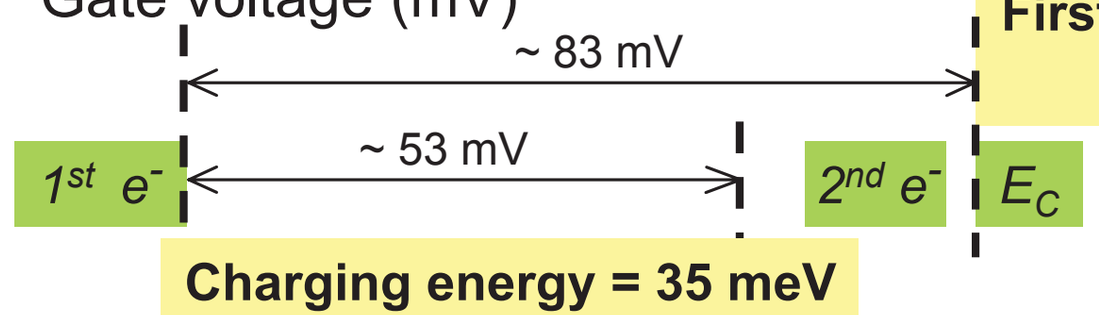

First binding energy = 55 meV

As: 54 meV
(P: 46 meV)

Charging energy = 35 meV

- lower than 52 meV (As: 2 meV second binding energy)
- **increased capacitance** due to nearby electrodes

[Sellier PRL 97, 206805, 2006]

Assignment of the level spectrum

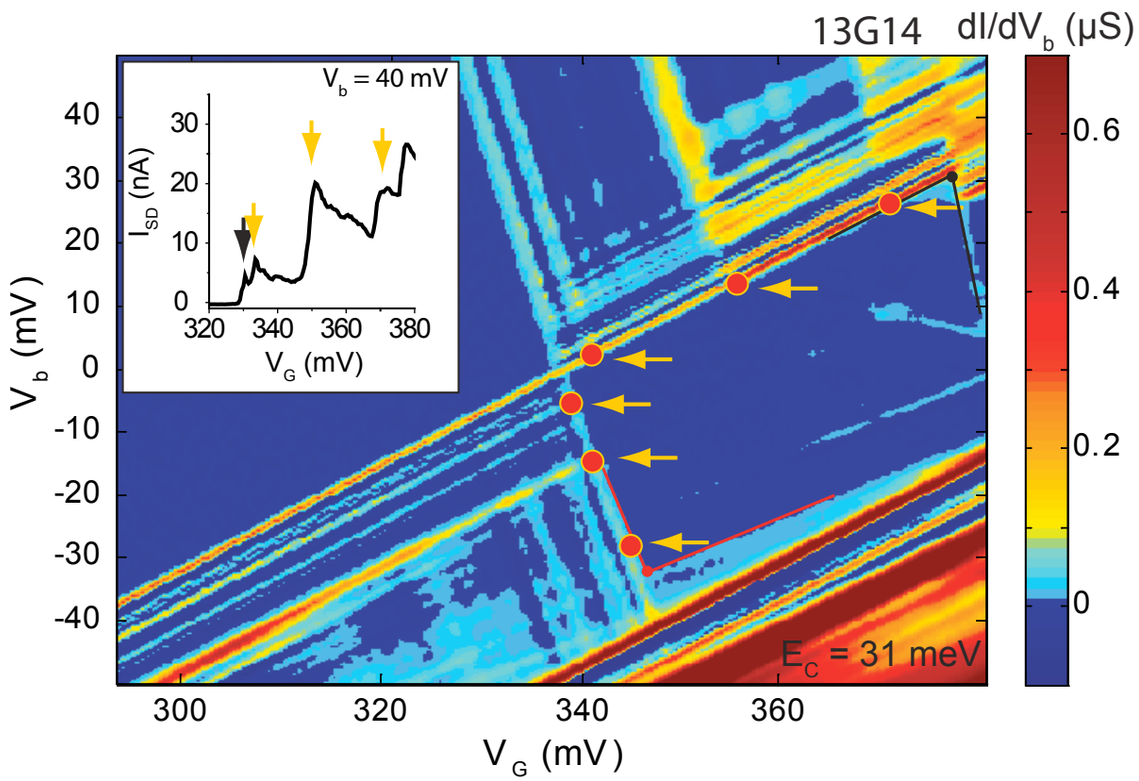

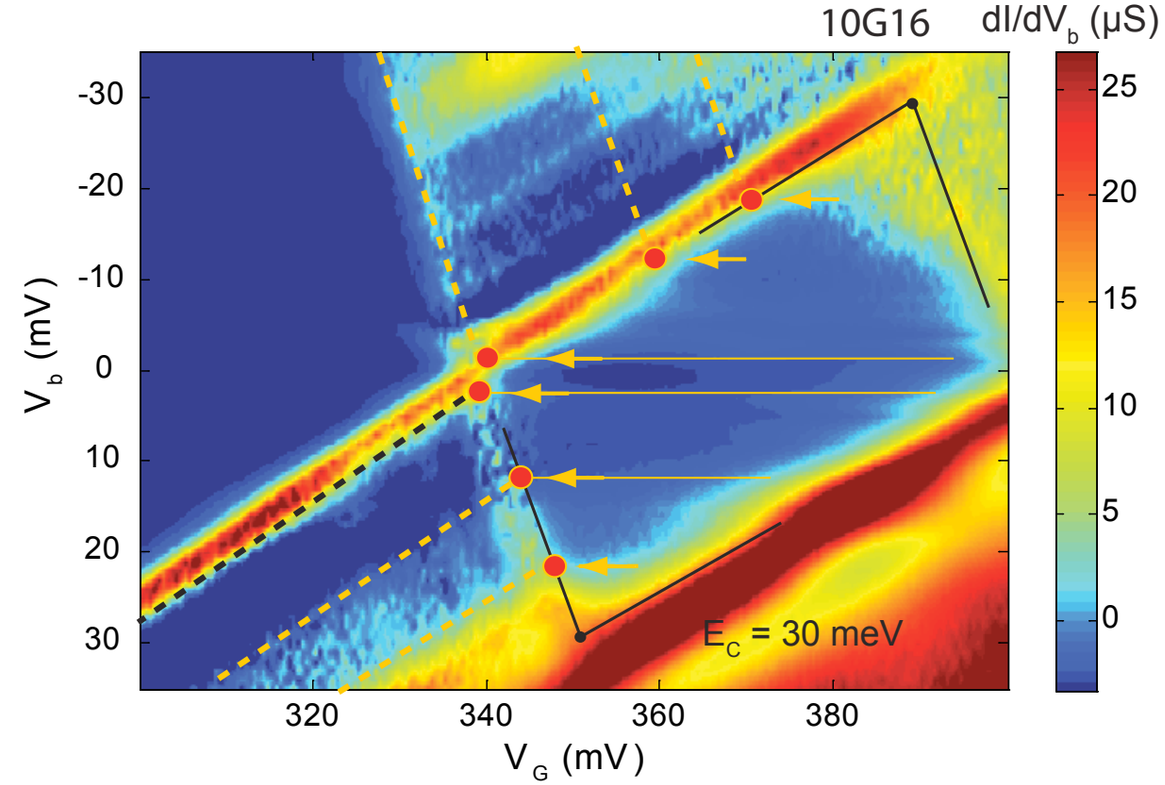

The "stability diagram" reveals the higher orbitals / excited states of a charge state.

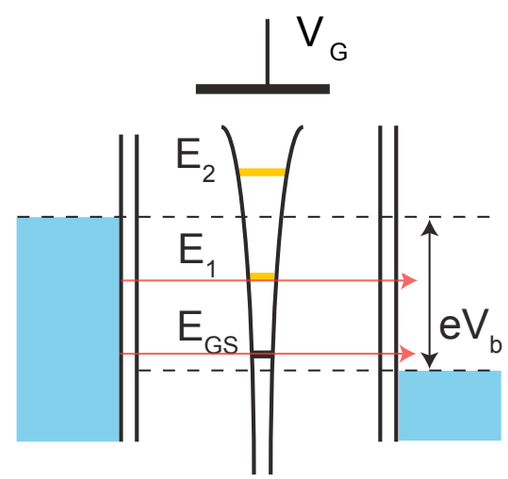

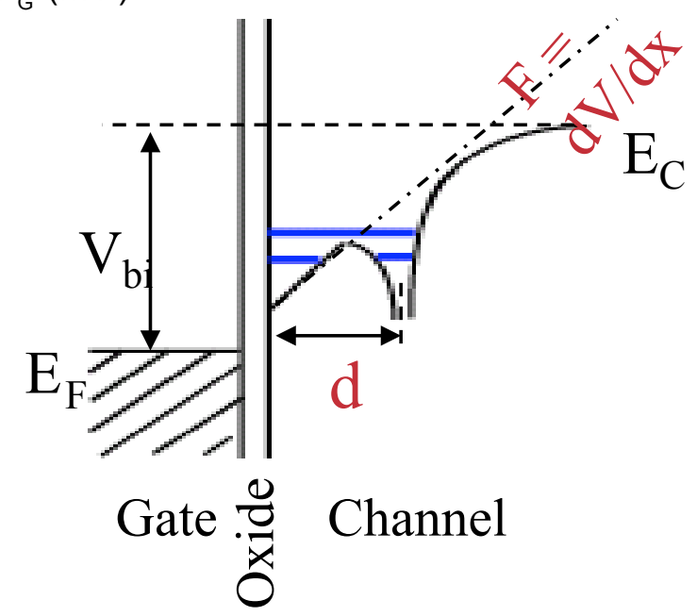

Hybridization with well state leads to a molecular system

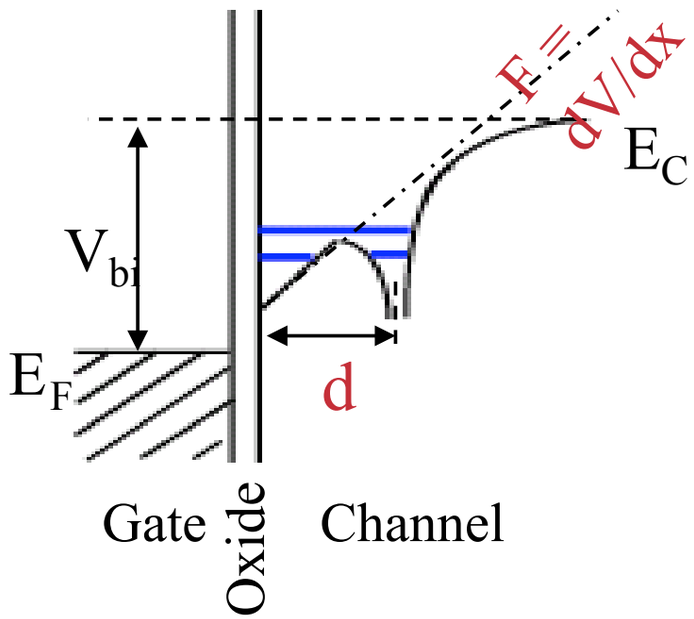

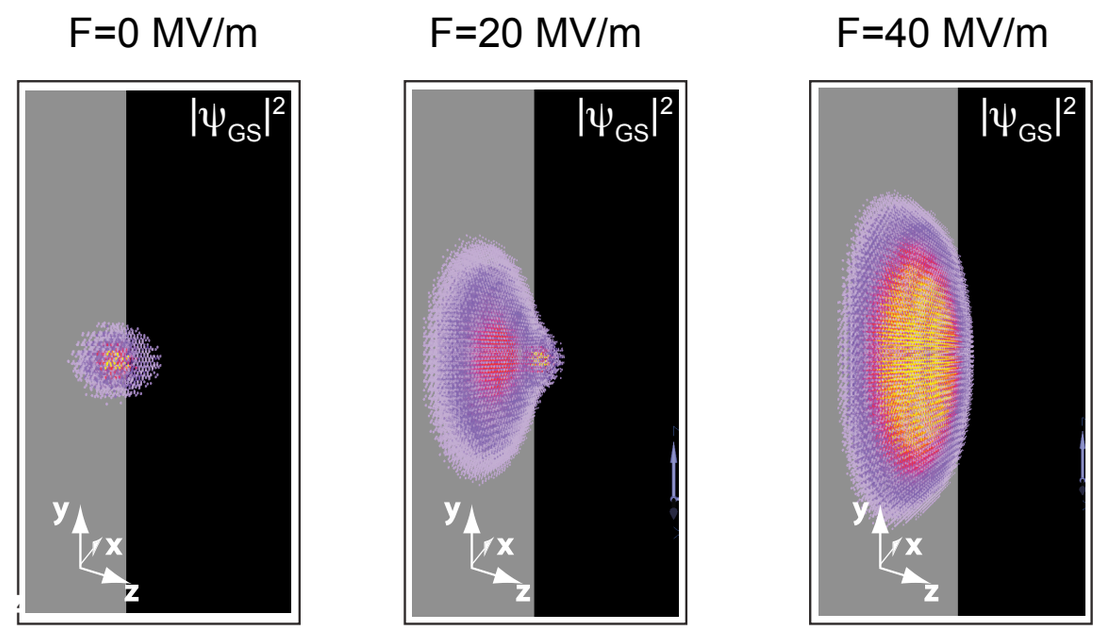

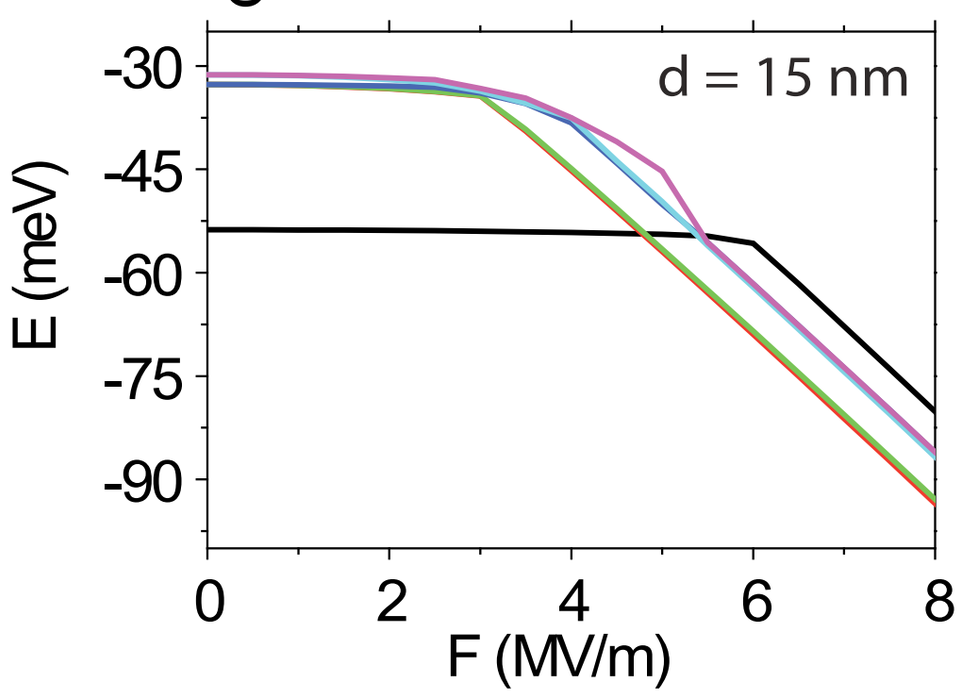

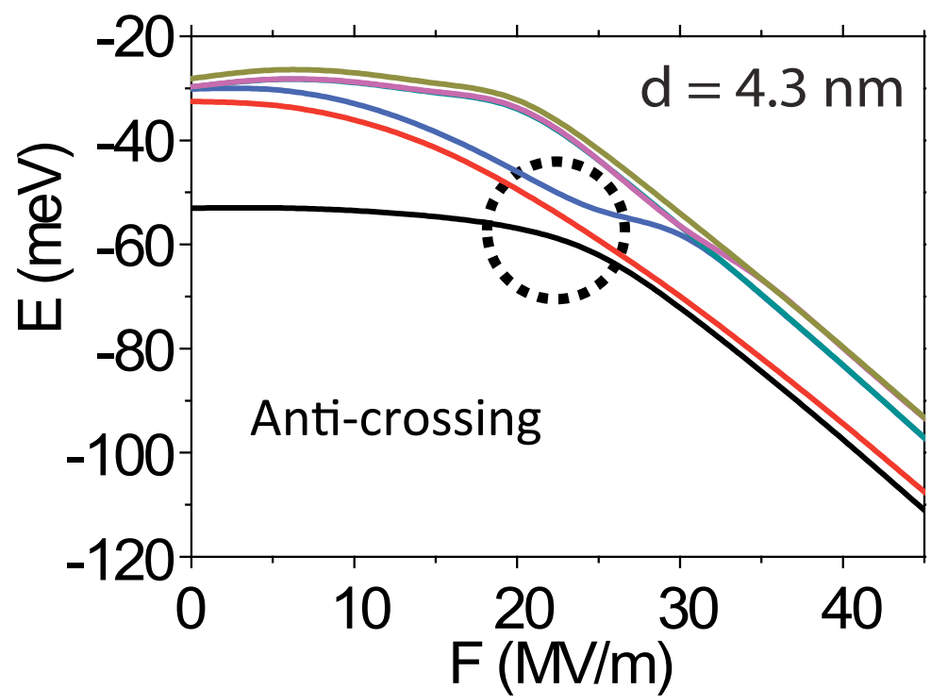

hybridization first theoretically predicted by Martins, PRB 69, 085320 (2004)
→ adiabatic regime for charge manipulation

Fit excited states of the dopants to model

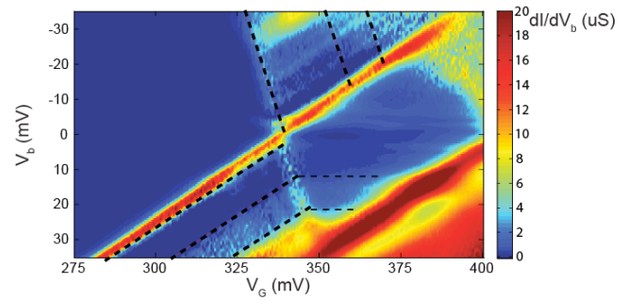

Measured

$E_{x,i}$

F ? , d ?

Predicted

$E_{x,i}$ (F,d)

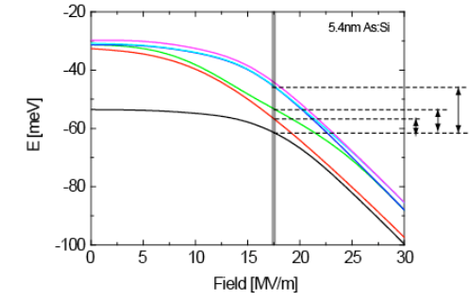

Device		E_1 (meV)	E_2 (meV)	E_3 (meV)	E_C (meV)	d (nm)	F (MV m^{-1})	s (meV)
10G16	Exp.	2	15	23	30	3.3		
	TB	2.2	15.6	23.0		3.3	37.3	0.59
11G14	Exp.	4.5	13.5	25	29	3.2		
	TB	4.5	13.5	25.0		3.5	31.6	0.04
13G14	Exp.	3.5	15.5	26.4	31	3.5		
	TB	3.6	15.7	26.3		3.2	35.4	0.17
HSJ18	Exp.	5	10	21.5	33	4.0		
	TB	4.5	9.9	21.8		4.1	26.1	0.63
GLG14	Exp.	1.3	10	13.2	35	4.7		
	TB	1.3	10	12.4		5.2	23.1	0.28
GLJ17	Exp.	2	7.7	15.5	33	4.0		
	TB	1.3	7.7	15.8		4.9	21.9	0.77

$E_C \rightarrow d$

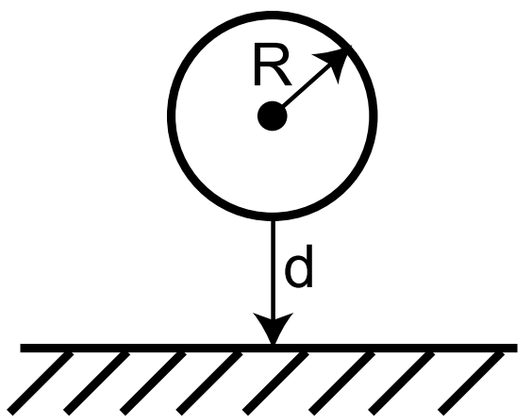

- a 2D (F, d) fit of the first 3 excited states of the model works well for the 6 samples
- overdetermined, since we fit 3 parameters of 6 samples to a 2D space

Chemically selective donor-tomography

Single donor fingerprint in transport characteristics combined with large scale device-simulations yields:

- chemical species (VO in Si)
- local field
- depth below the interface
- concentration

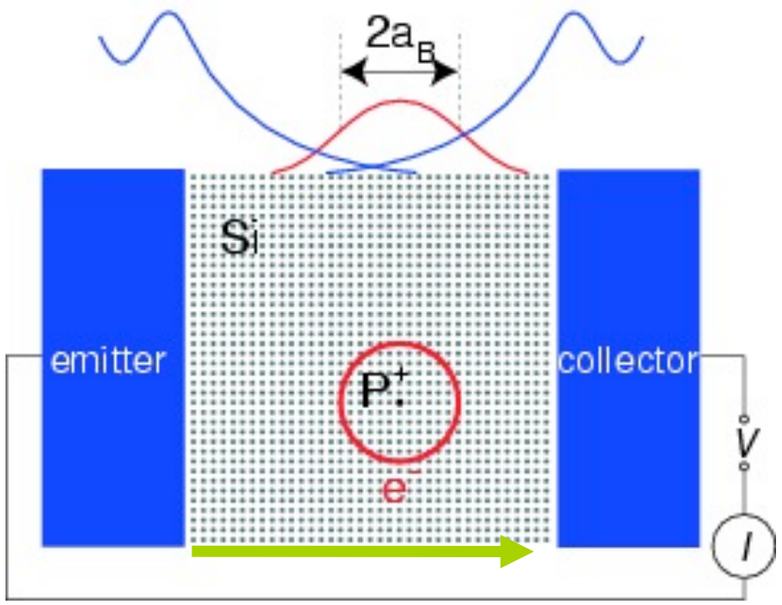

Jagannath et al. PRB 23, 2082 (1981)

Level	P[a]	As[a]	Sb[b]	Bi[c]	Li[a]	Li-O[a]	Mg+[d]	Mg[d]	S[e]	Theory[f]
$1s(A_1)$	45.59	53.76	42.74	70.98	31.24 ± 0.02	39.67	256.47	107.50	186.42	31.27
$1s(E)$	32.58[b,g,h]	31.26[b,h]	30.47[b,h]							31.27
$1s(E+T_2)$					33.02	32.00				31.27
			32.89	32.89[i]					30.92	
$1s(T_2)$	33.89	32.67[b]							26.22	31.27
			32.91	31.89[i]					24.02	
$2p_0$	11.48	11.50	11.51	11.44	11.51	11.57	47.84	11.70	11.4	11.51
$2s$		9.11[j]		8.78[j]						8.83
$2p\pm$	6.40	6.40	6.38	6.37	6.40	6.40	26.25 26.05	6.38	6.2	6.40

Outline

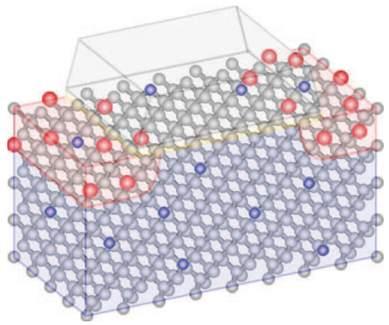

- Background

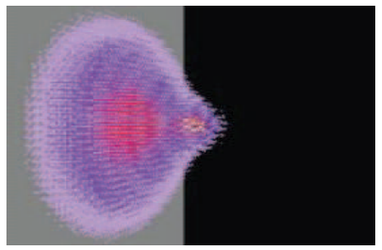

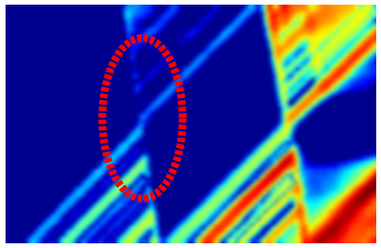

- From I(Vg) peaks → spectra & environmental information

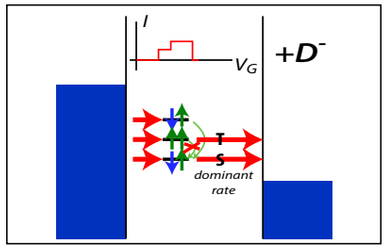

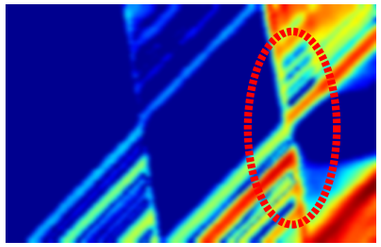

- Beyond level spectroscopy

Σ

- Summary

Information about relaxation processes

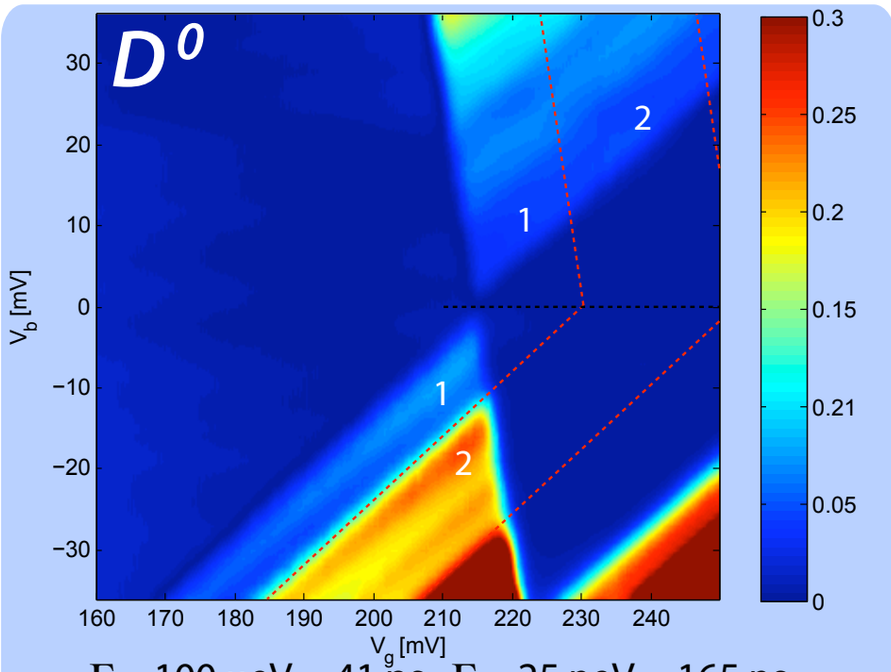

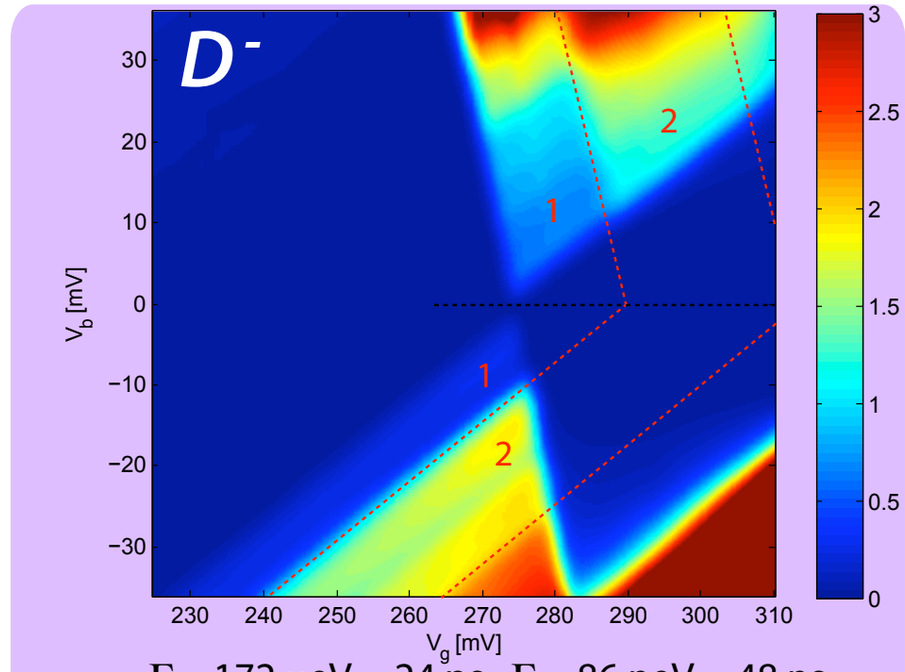

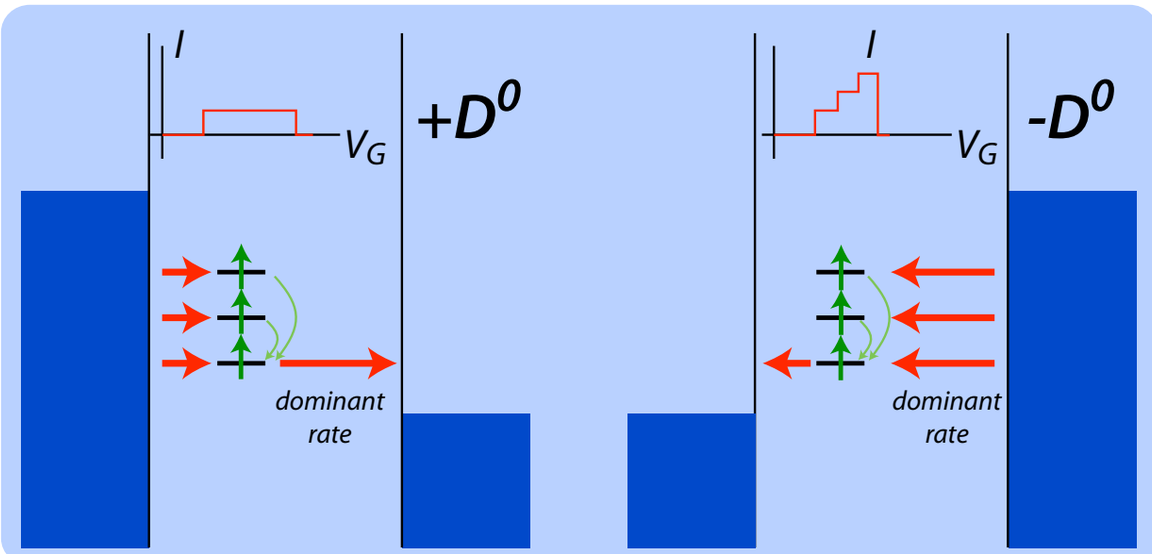

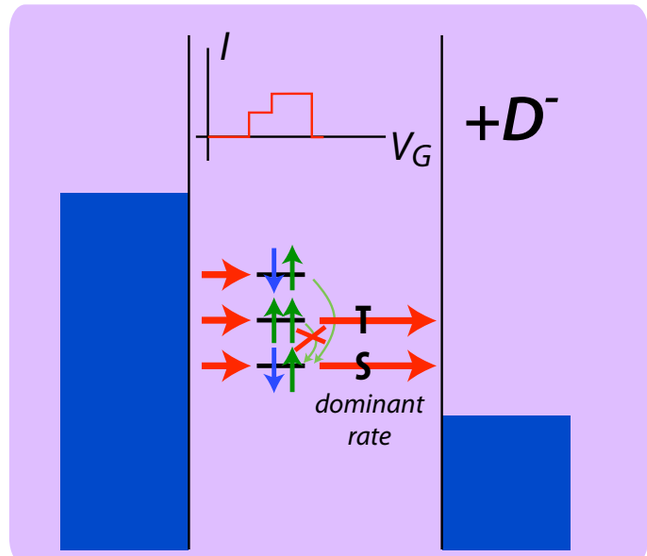

- electron leaves from ground state unless this transition is blocked ⇒ LET [NP 4, 540, 2008]
- orbital exited lifetimes are short (~30ps [JAP 102, 093104, 2007]), gated D^- relaxation observed as slow as 50ns!?

Summary

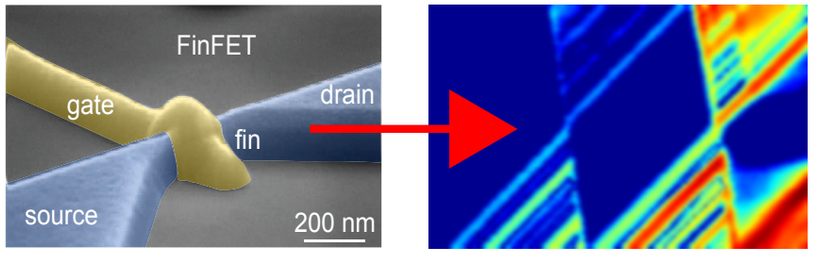

- **What can we learn from transport in nanoFETs?**
  - electrical channel length / extend of the SD region
  - variability - dopant density in the channel
  - spectrum: chemical species & environment

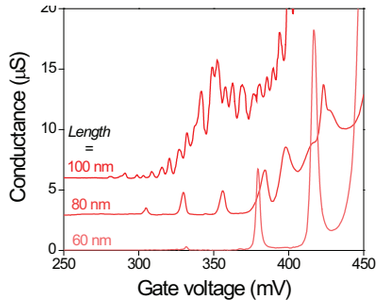

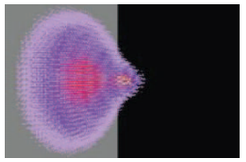

- **Beyond level spectroscopy**
  - spin and orbital relaxations
  - probe coherence
  - determine scattering in channel
  - future: manipulate spin and orbital state

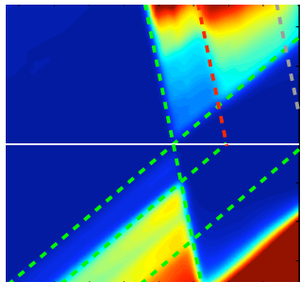

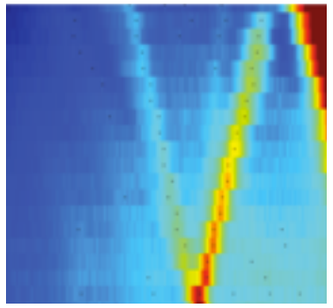

Acknowledgments

- **IMEC**
  N. Collaert, S. Biesemans (FinFETs)
- **Purdue**
  R. Rahman (→SNL), G. Klimeck (tight-binding)
- **Melbourne**
  L.C.L. Hollenberg (theory)
  B.C. Johnson, C. Yang, D.N. Jamieson (single-ion implantation)
- **Grenoble**
  R. Wacquez, M. Vinet, M. Sanquer (multi-gate FinFETs)
- **Delft**
  J.Heijden, J.Verduijn, J.Mol, G.C.Tettamanzi, G.P.Lansbergen (→NTT)

What can we learn about donor metrology from transport measurements?

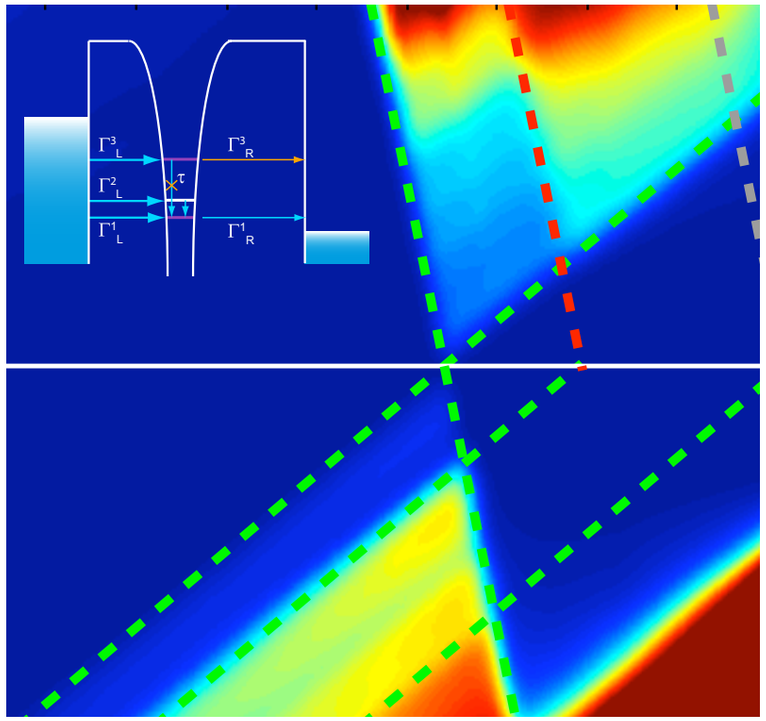

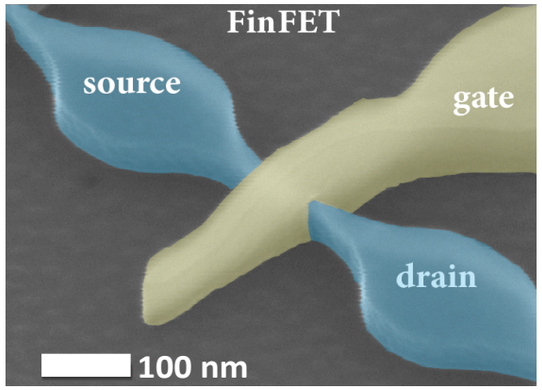

Sven Rogge
Kavli Institute for NanoScience

Knowledge of dopant location and their electronic properties is essential

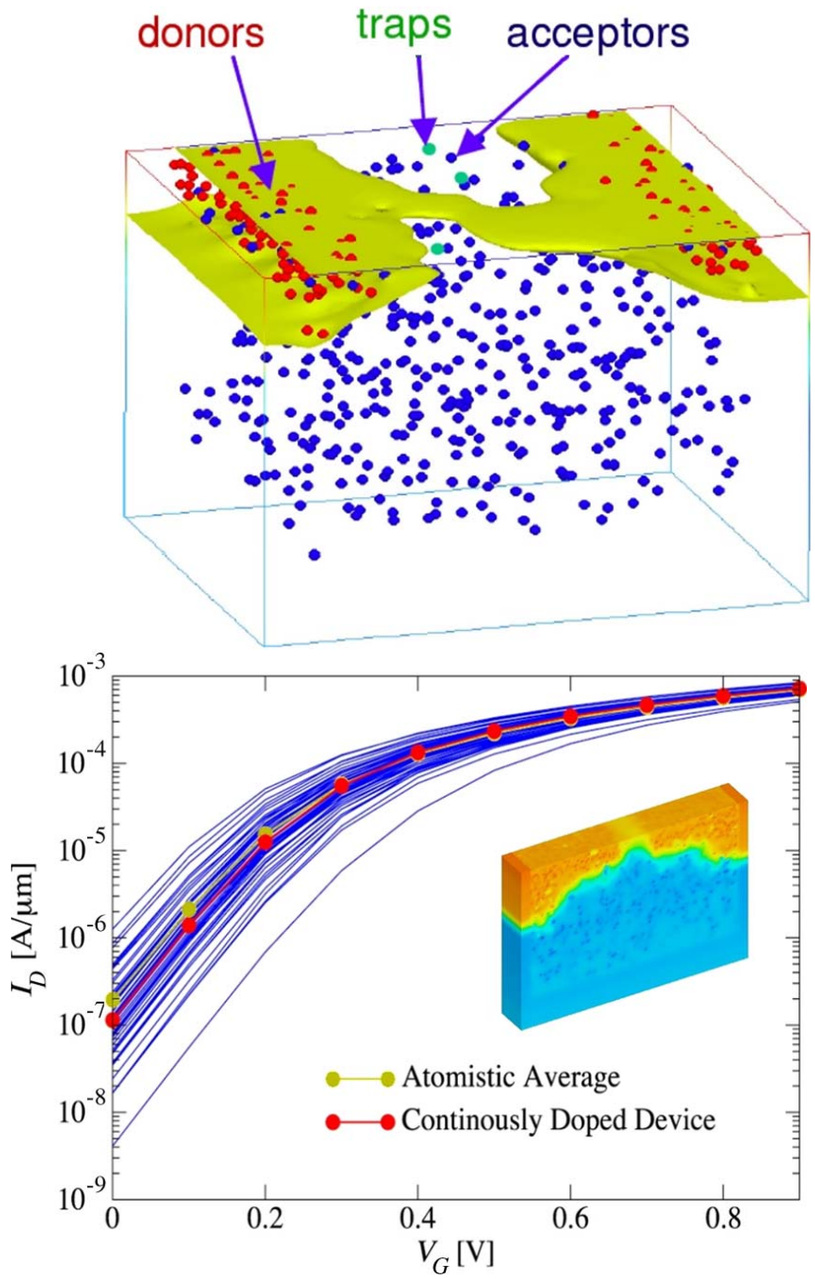

Bukhori et al. IEEE Trans. Electron Devices 57, 795 (2010)

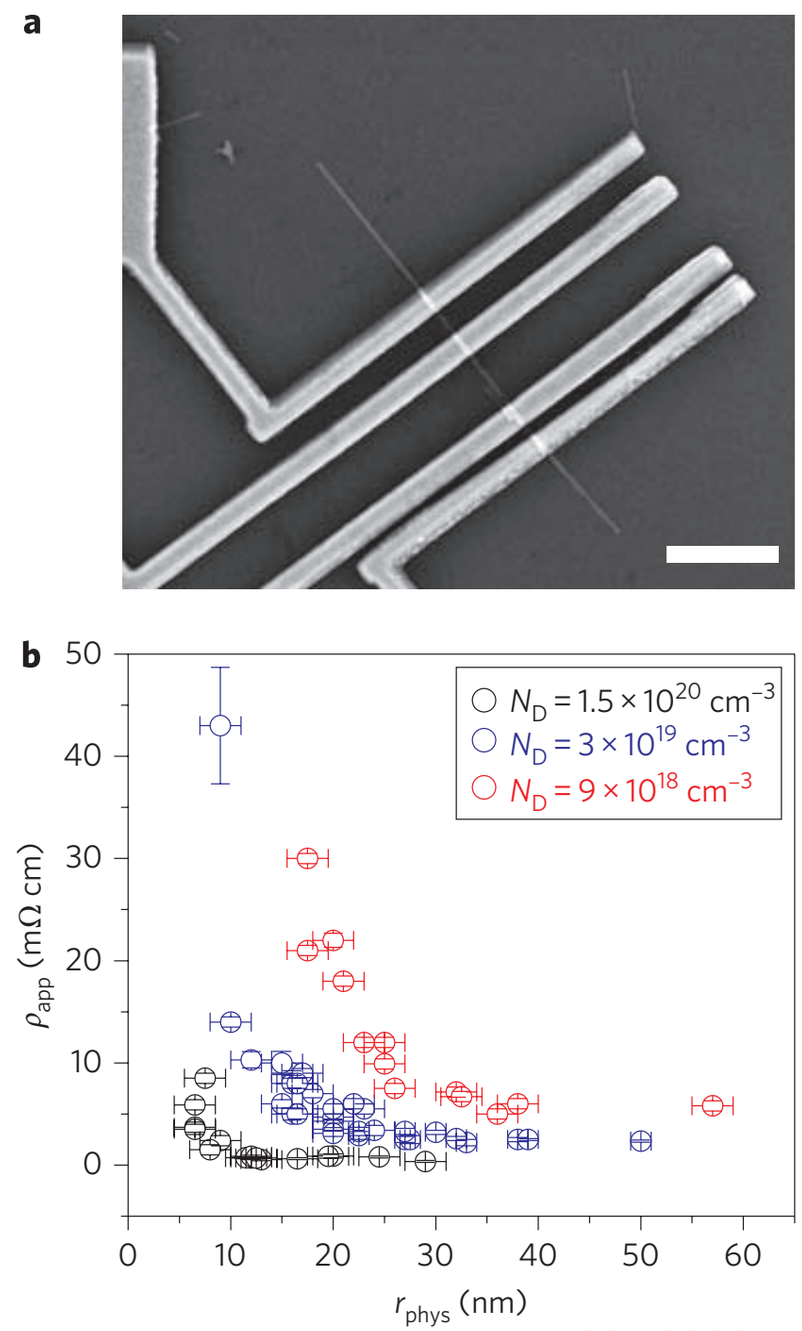

Bjork et al. Nature NT 4, 103 (2009)

Transport through localized states

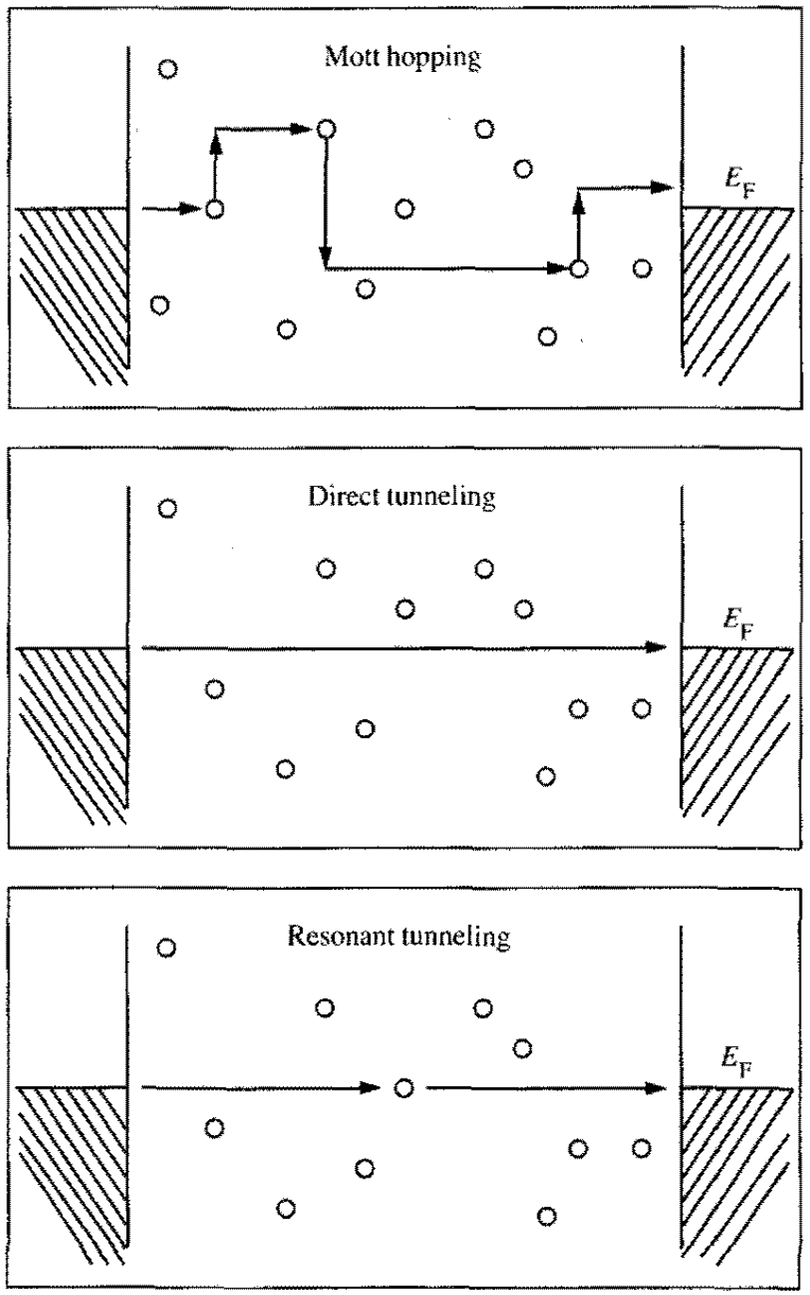

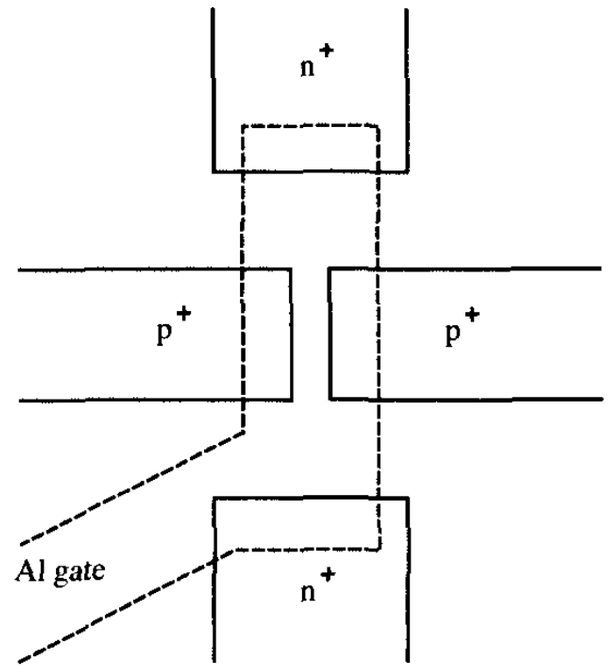

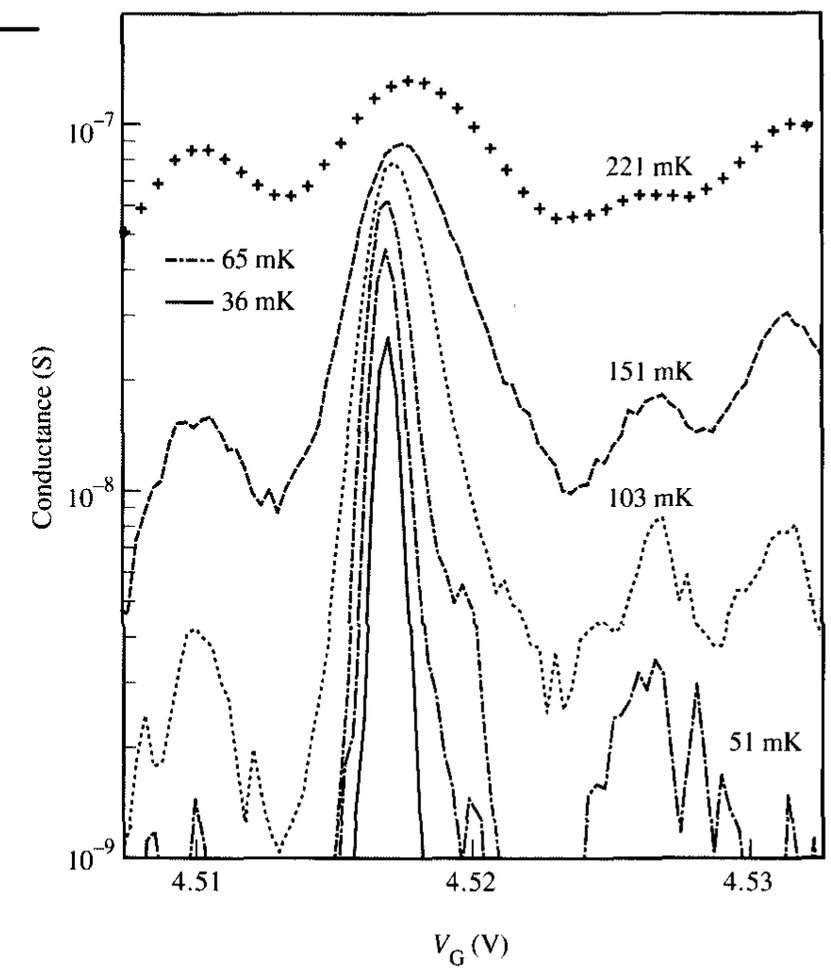

Transport through localized states

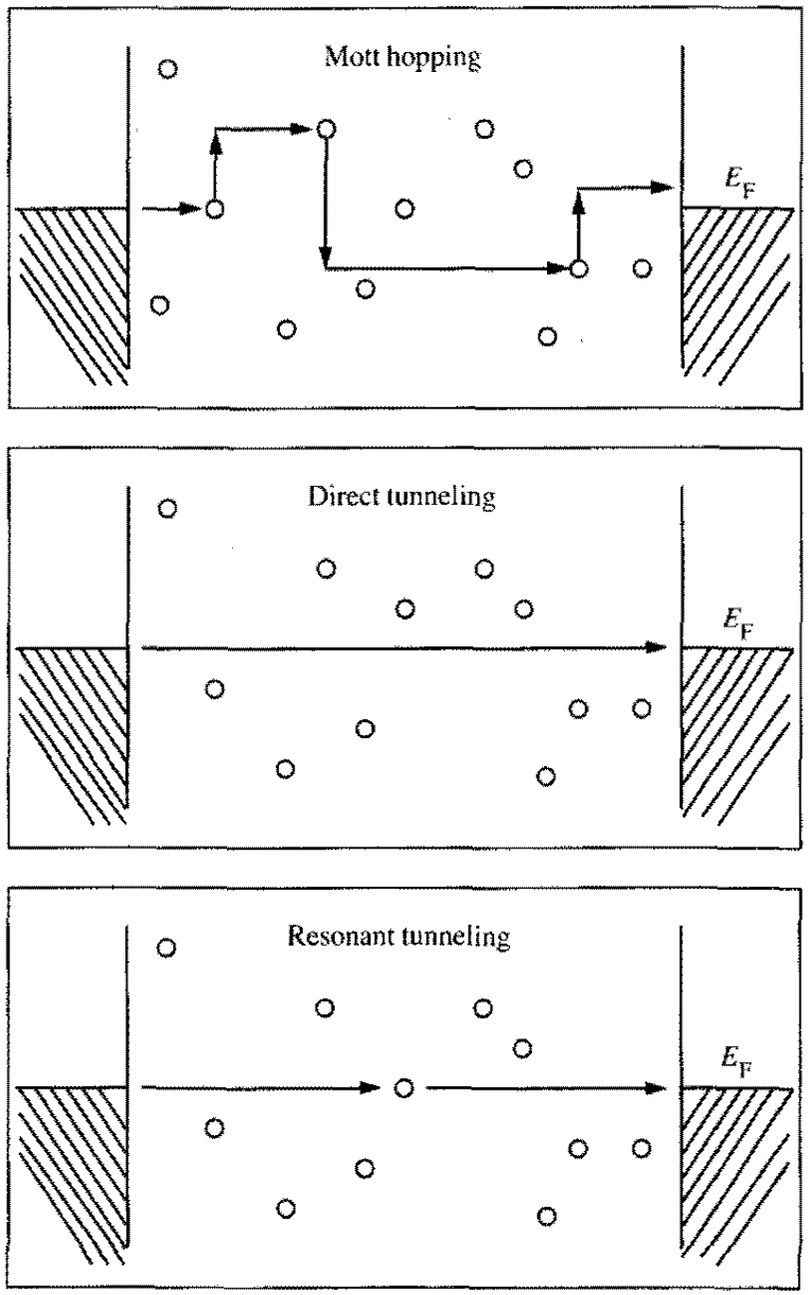

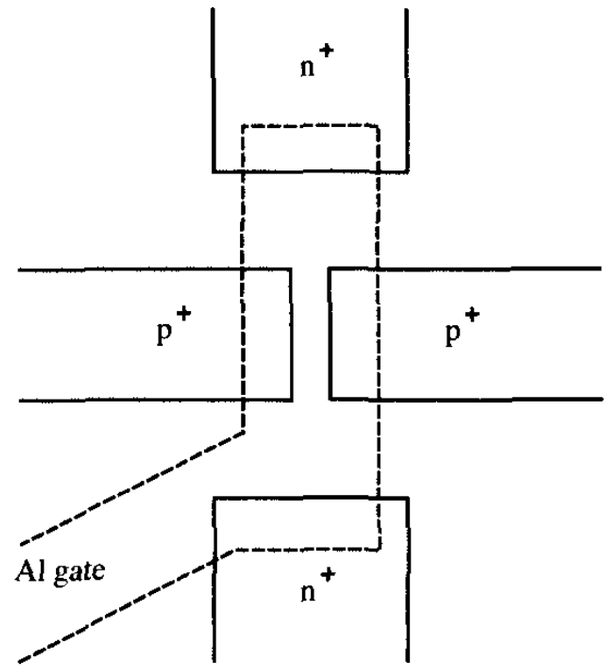

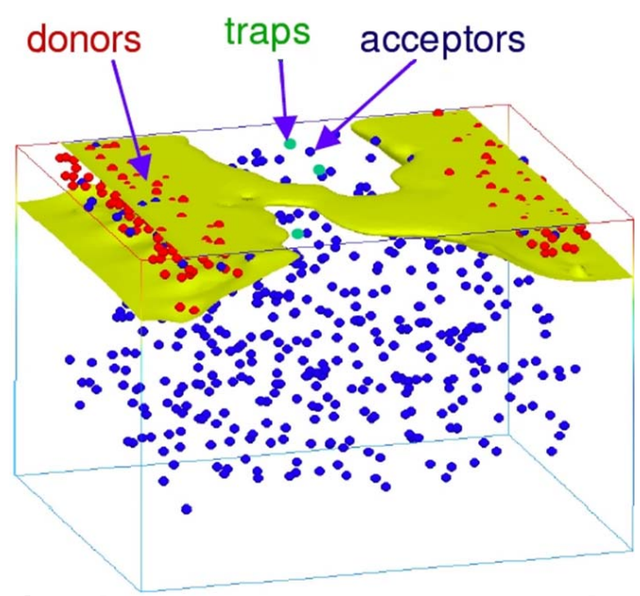

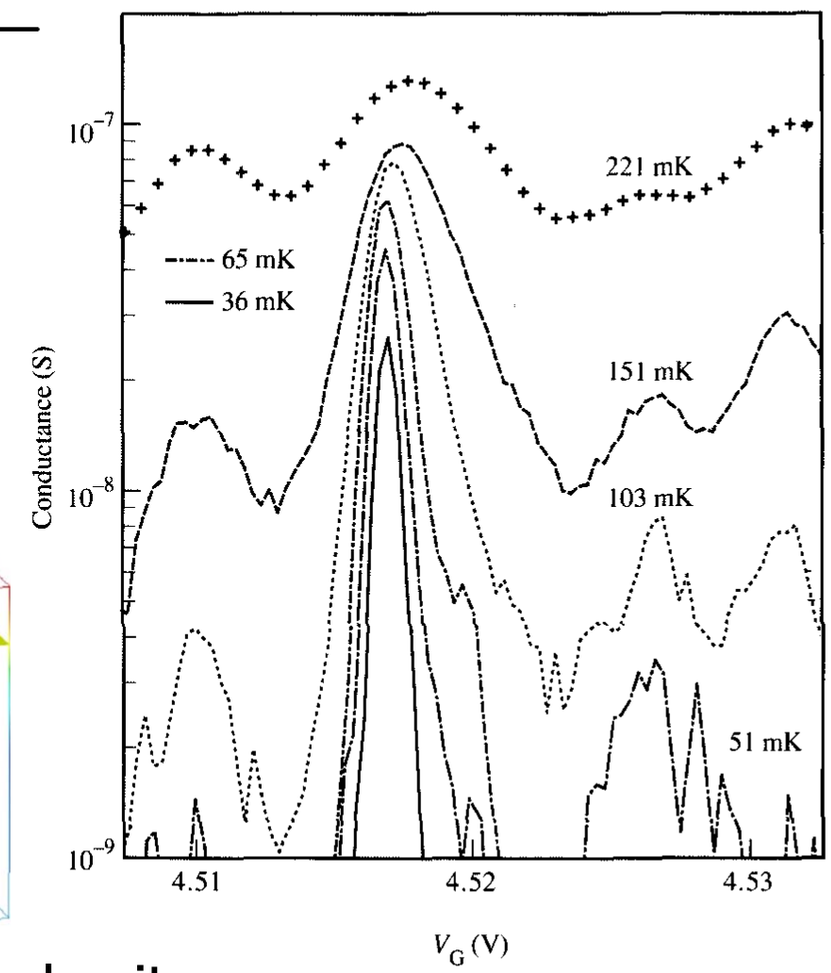

smaller devices → access to single sites

review: Fowler, Wainer, Webb, IBM J Res Dev 32, 273 (1988)

Transport through localized states

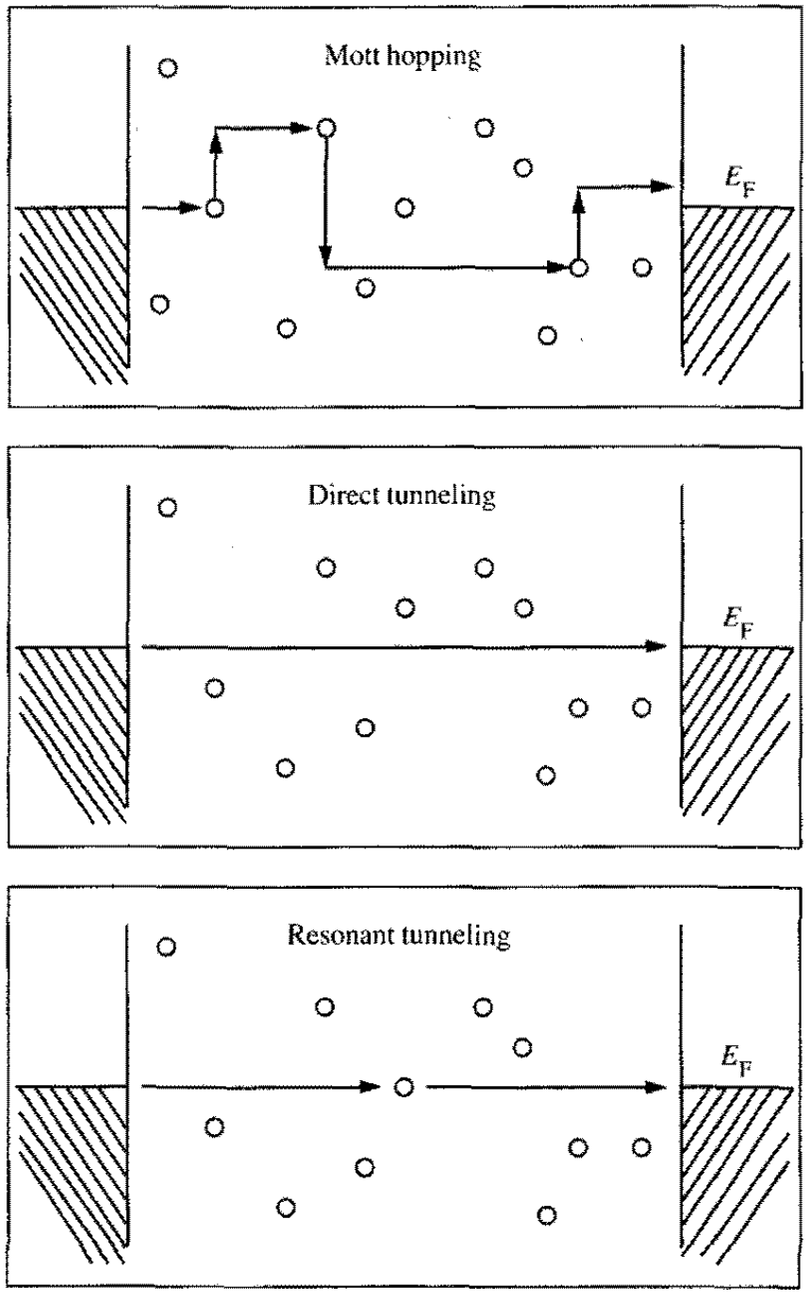

Sellier PRL 97, 206805 (2006)

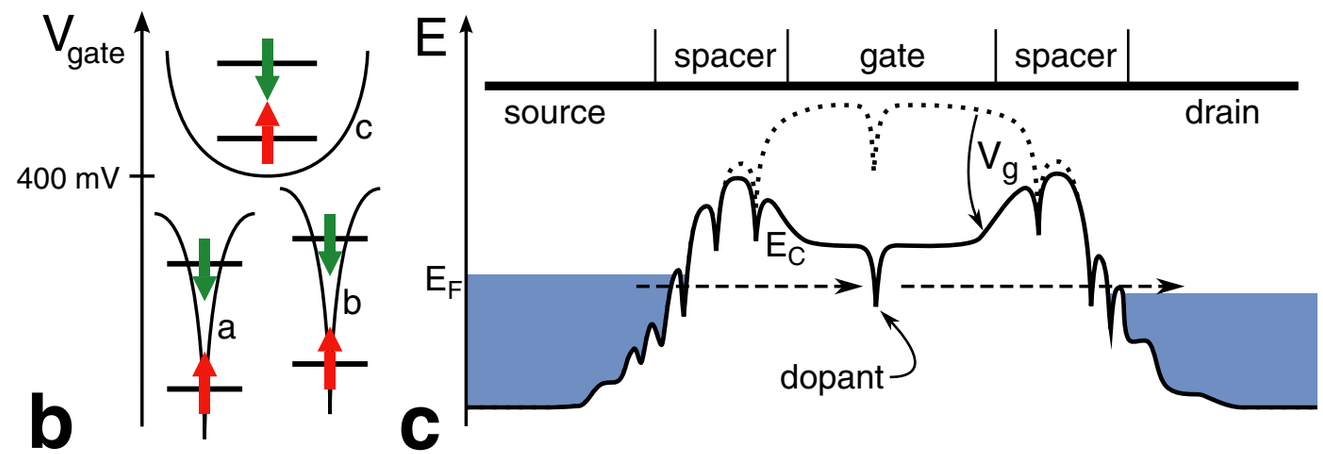

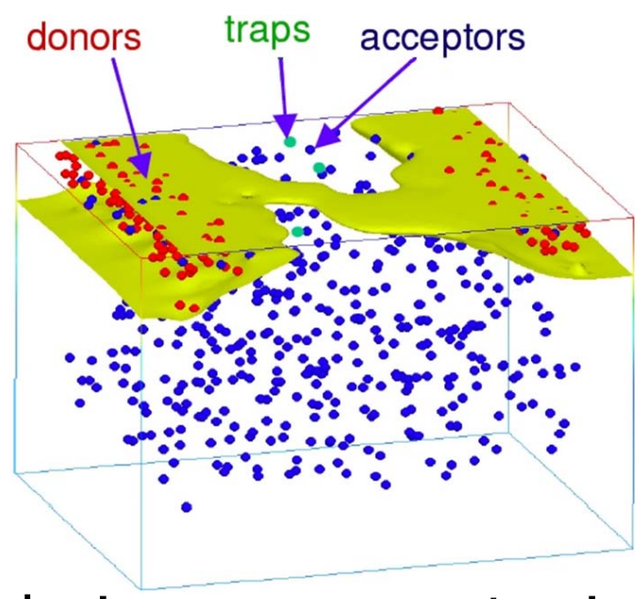

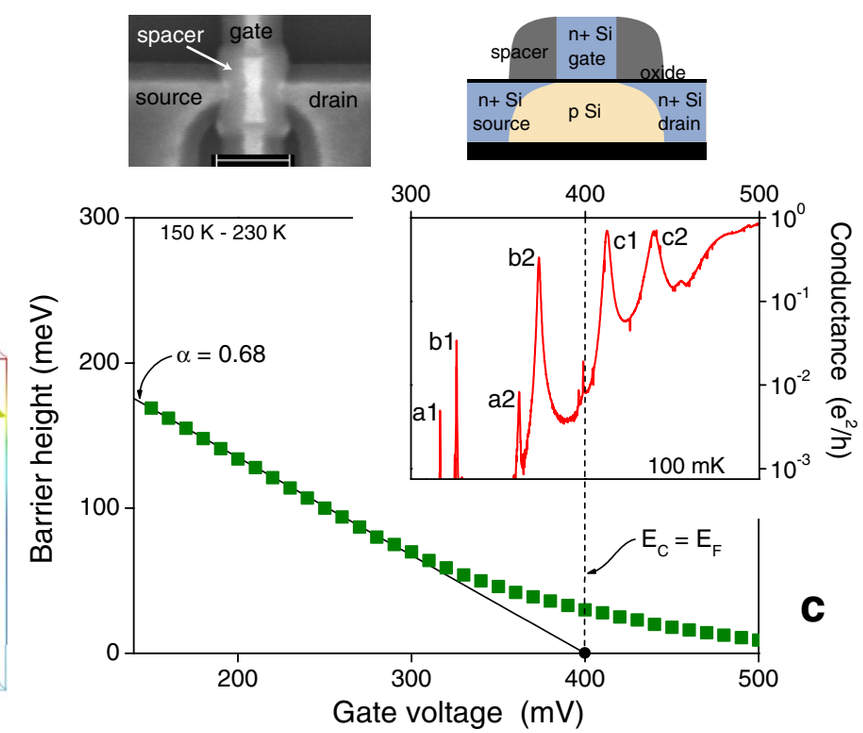

smaller devices → access to single sites

review: Fowler, Wainer, Webb, IBM J Res Dev 32, 273 (1988)

Link LT spectroscopy to RT performance

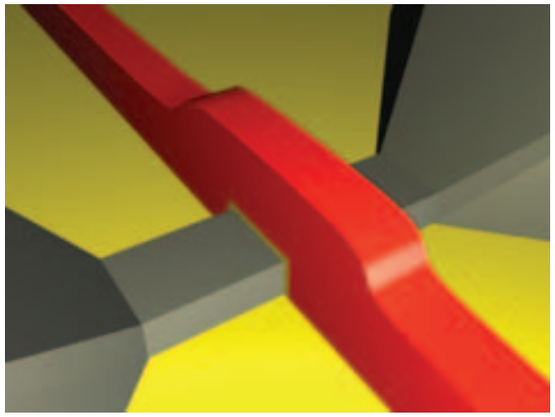

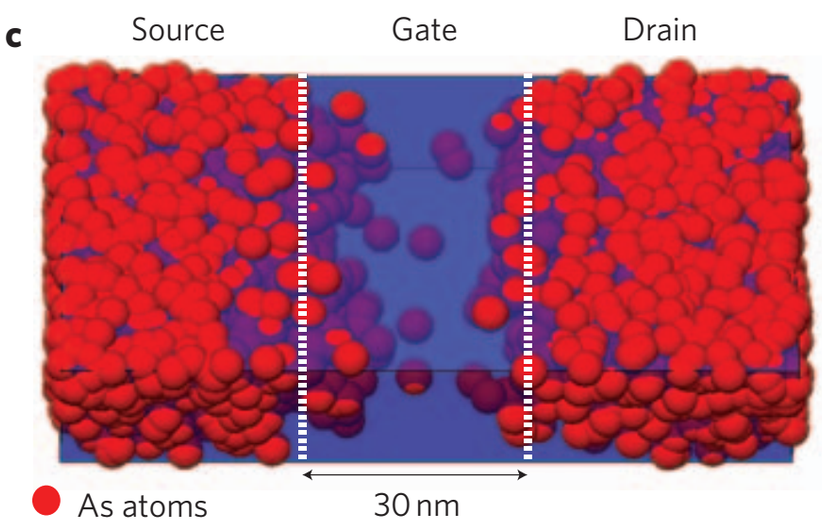

room temperature

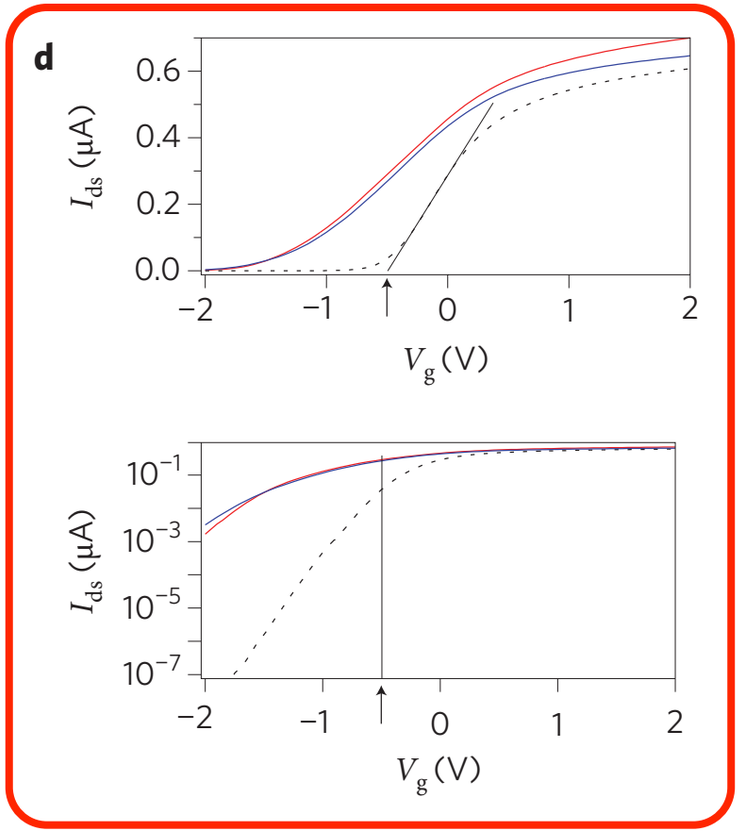

cryogenic

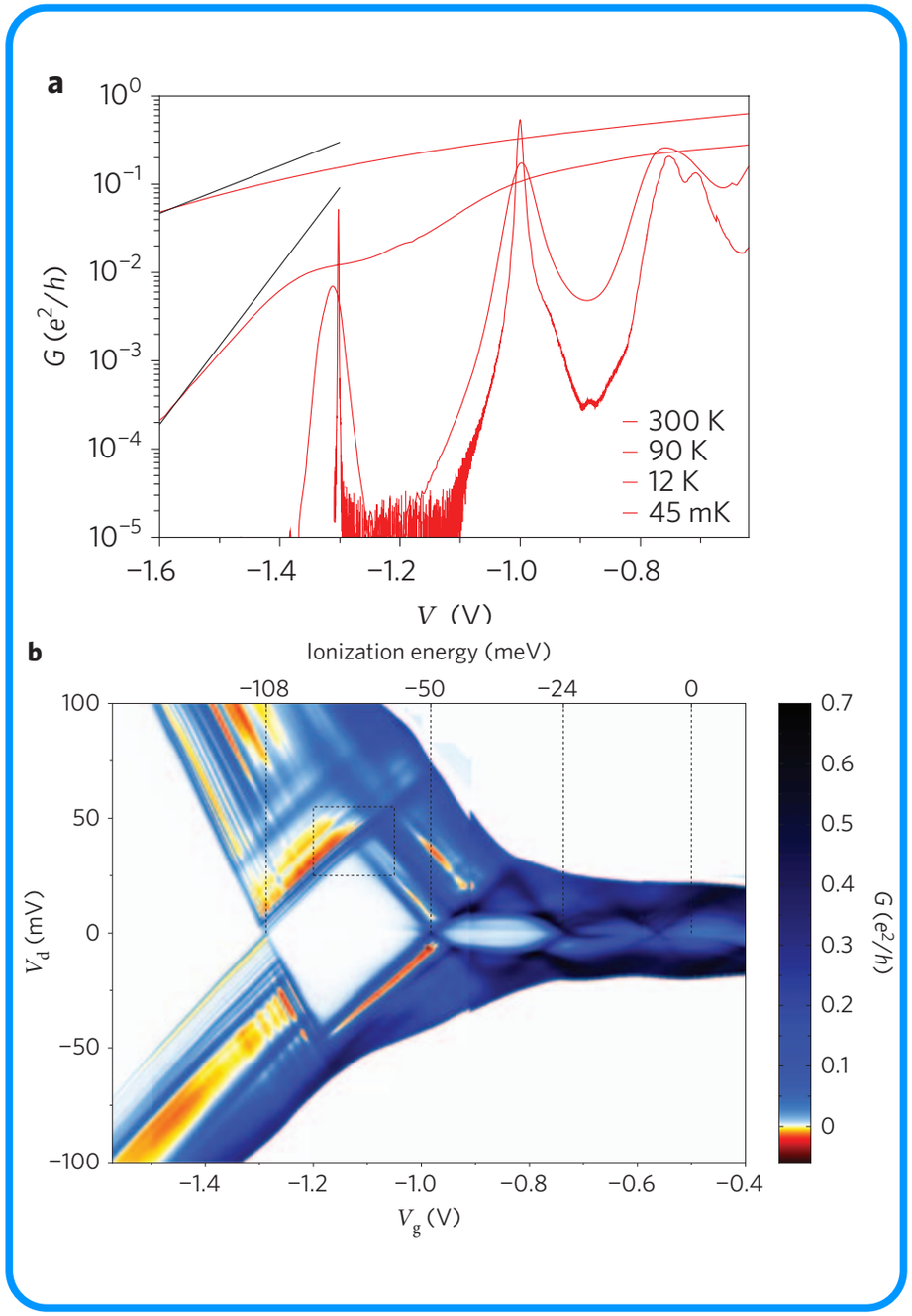

Pierre et al. Nature Nanotechology 5, 133 (2010) & VLSI (2010)

Single-ion implantation in a nano FET

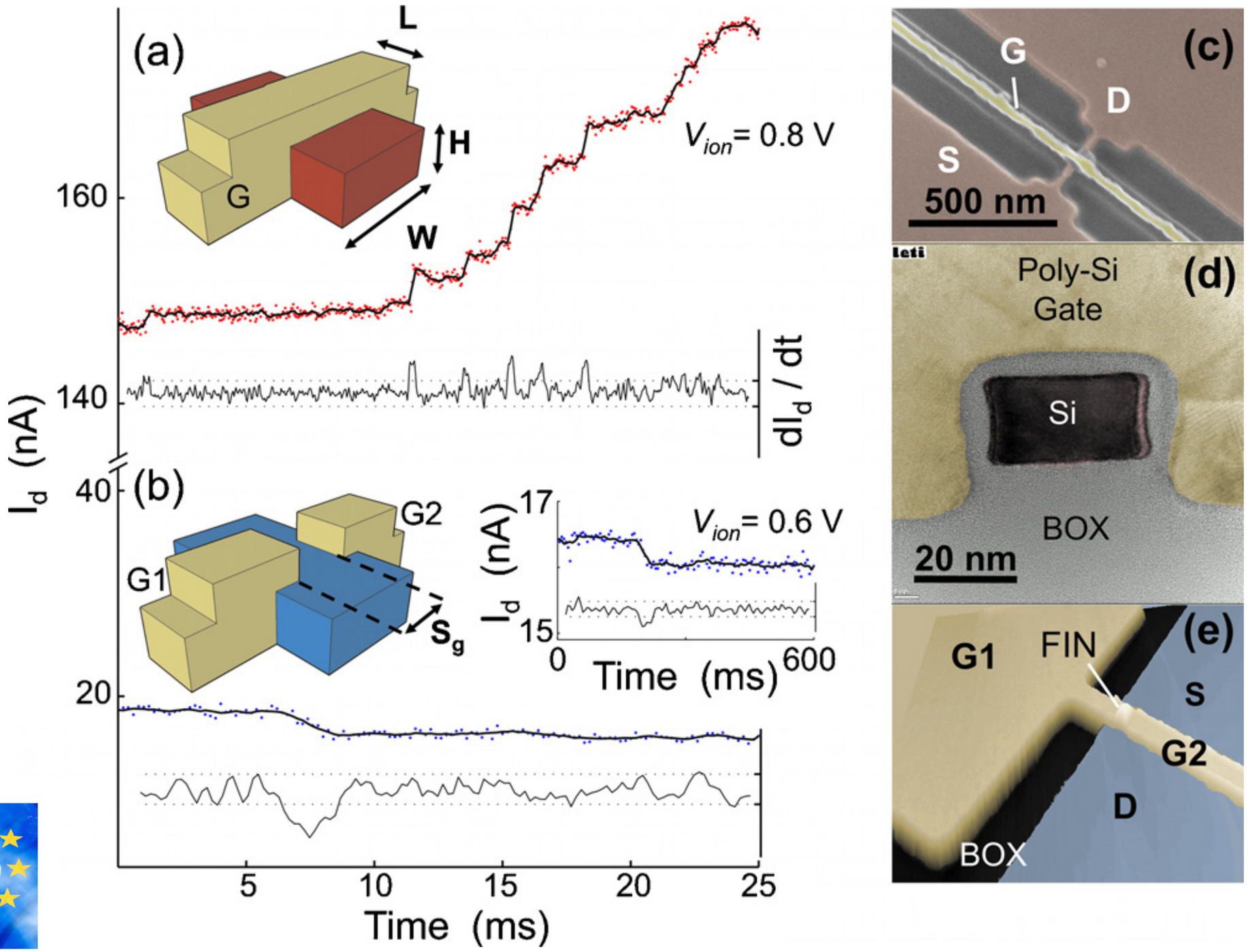

Johnson et al. APL 96, 264102 (2010)

Determination of the position of a single acceptor in a nanoFET

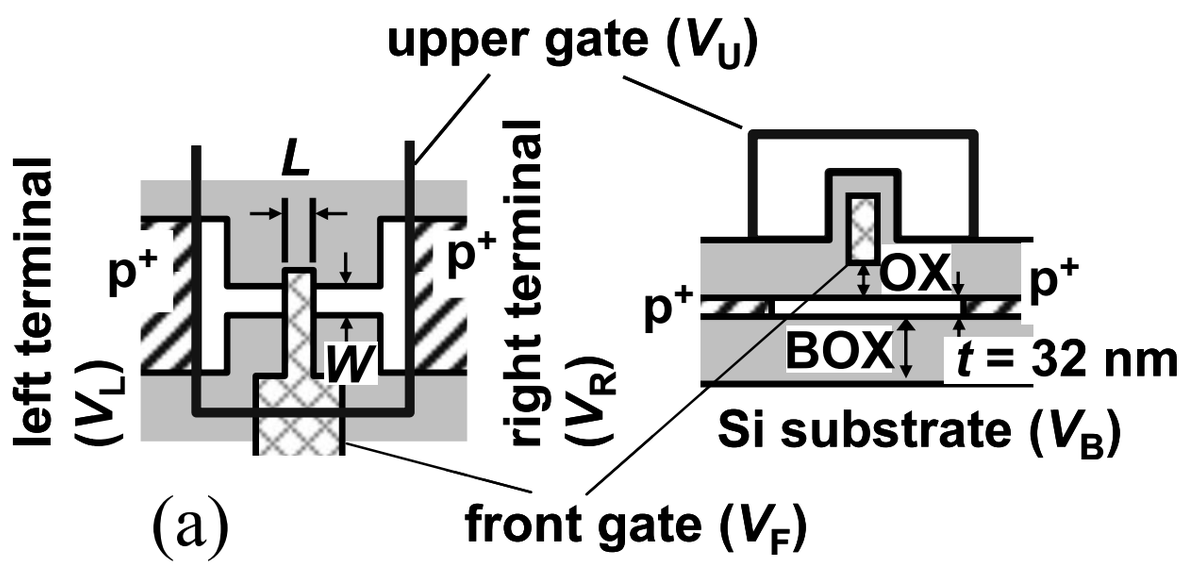

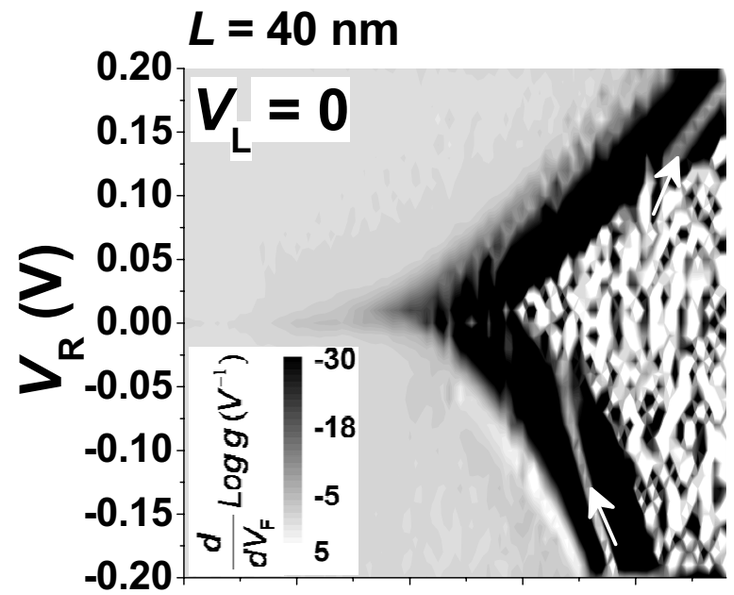

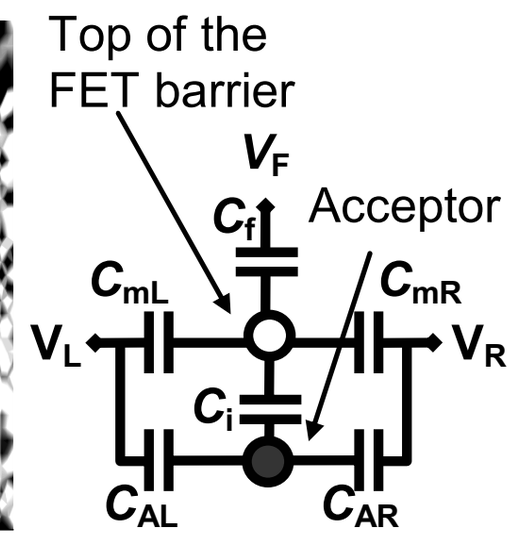

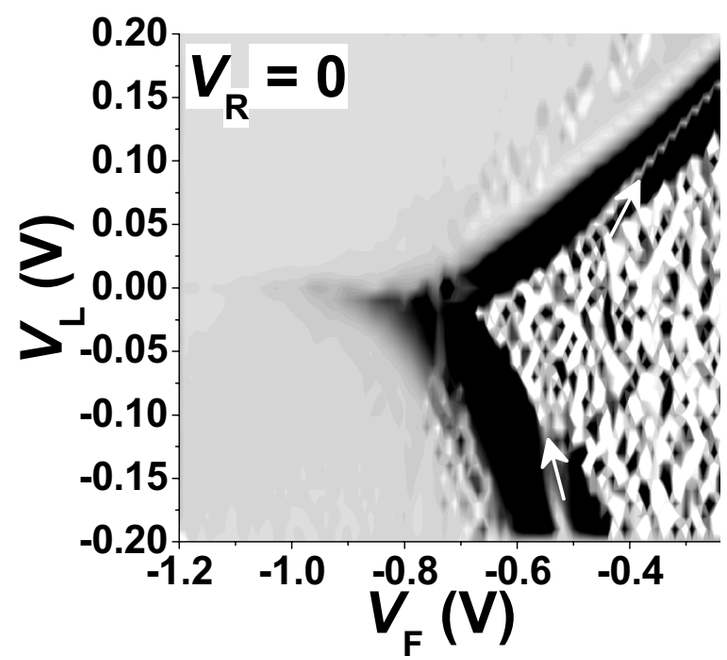

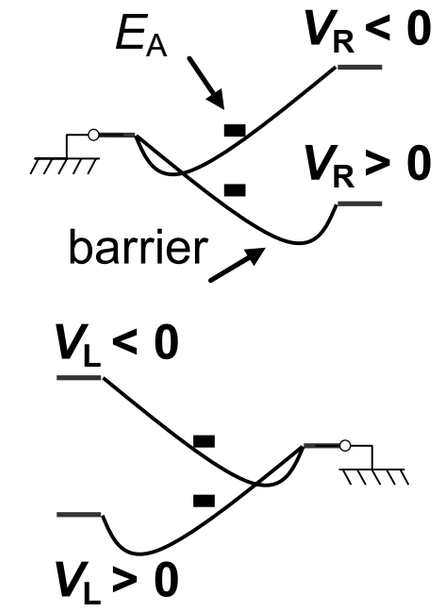

p++,p,p++ undoped pFET location of the channel can be scanned and a single acceptor is located by trapping/detrapping

Khalafalla APL 94, 223501 (2009)

Outline

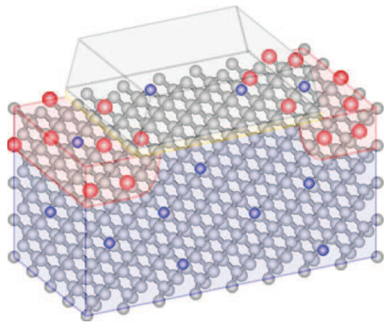

- Background

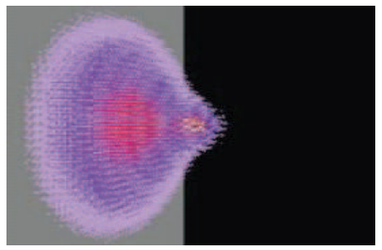

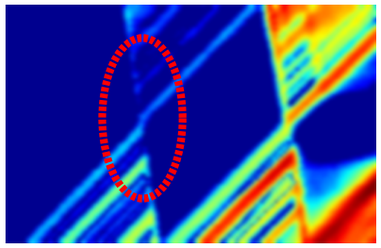

- From I(Vg) peaks → spectra & environmental information

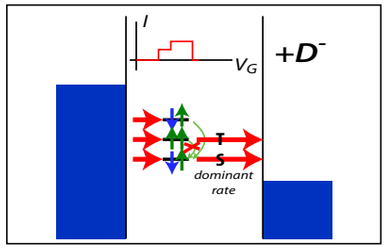

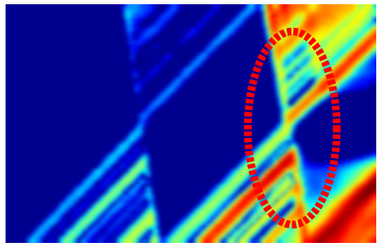

- Beyond level spectroscopy

Σ

- Summary

Shallow dopants in Si: restricted momentum space atoms

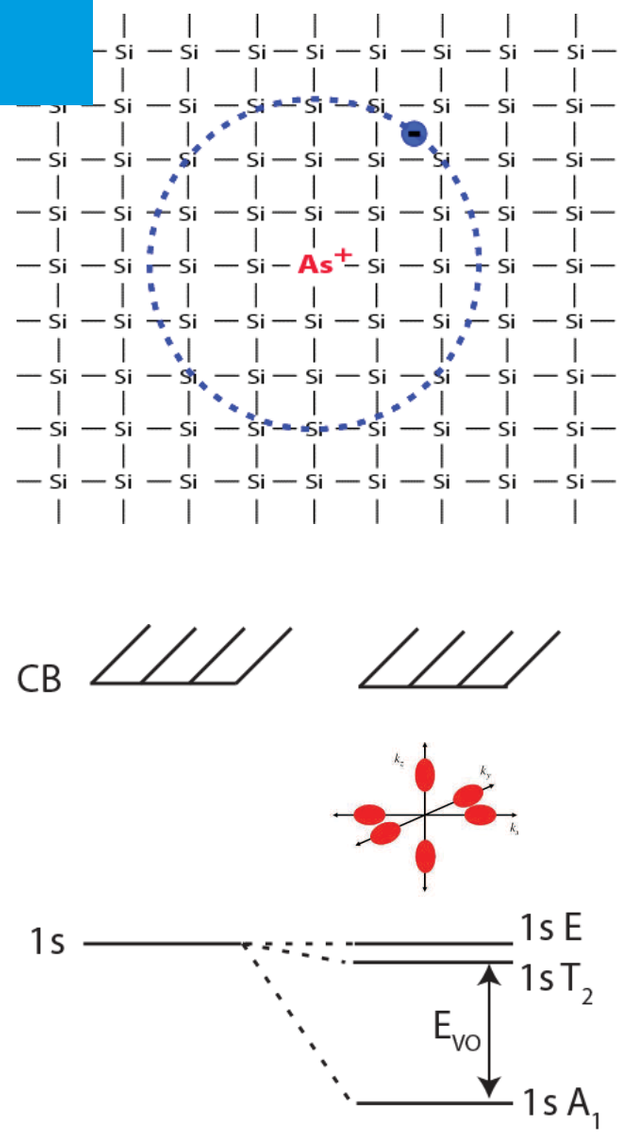

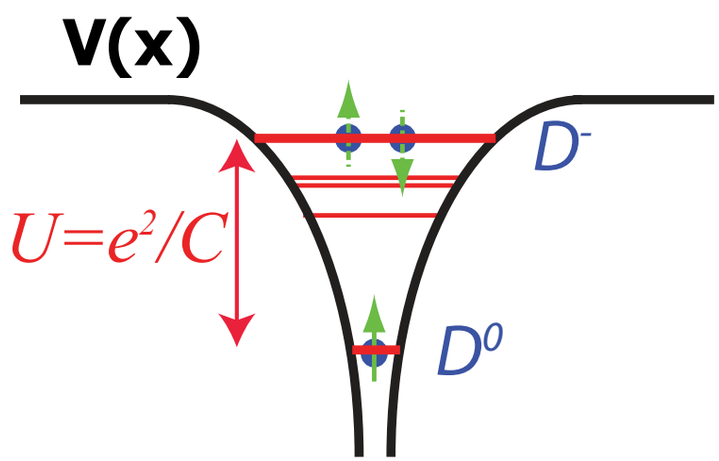

- 3D Coulomb potential
  - Can bind up to two electrons
  - Hydrogen-like level spectrum (D^0)
  - Valley-orbit

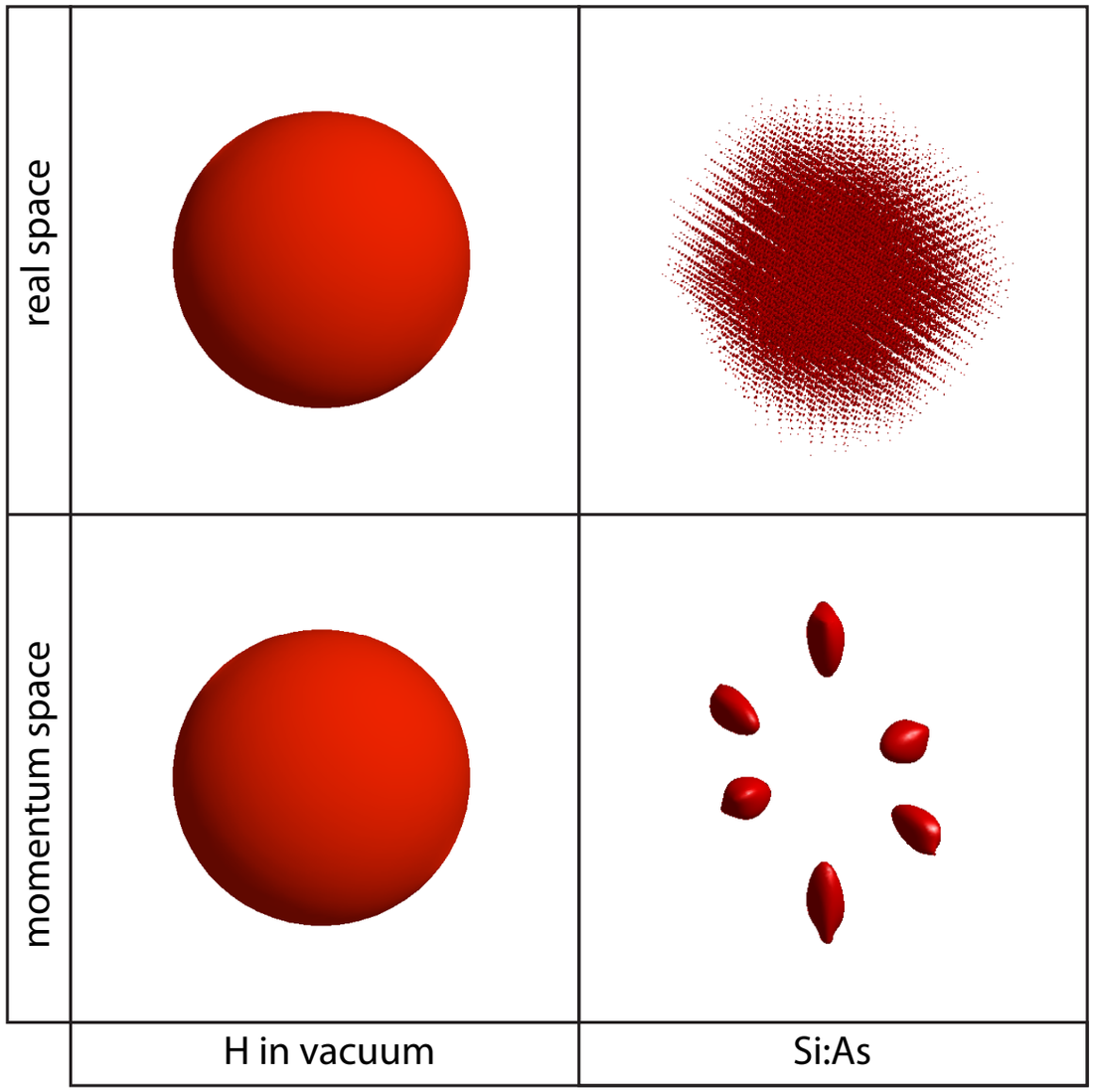

Multi-gate devices: FinFETs from the Biesemans group at IMEC

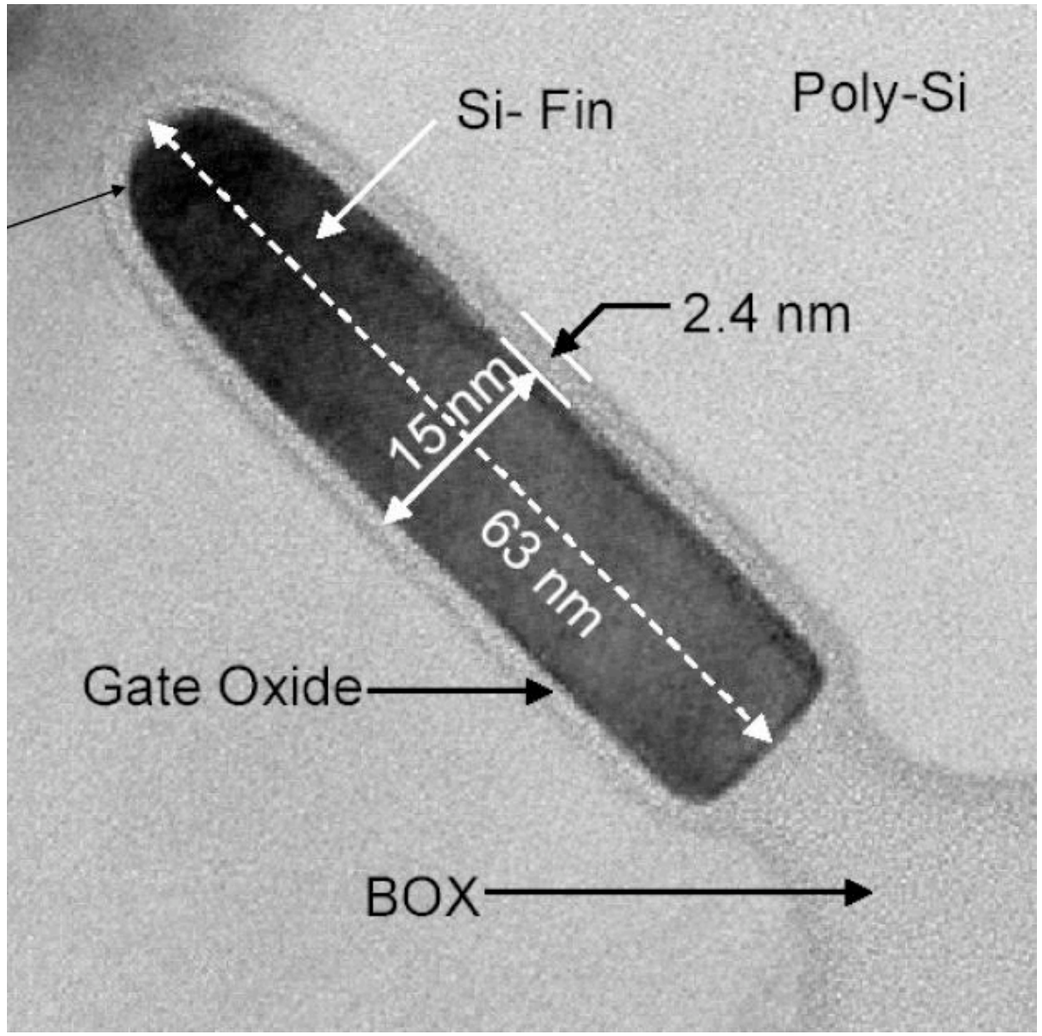

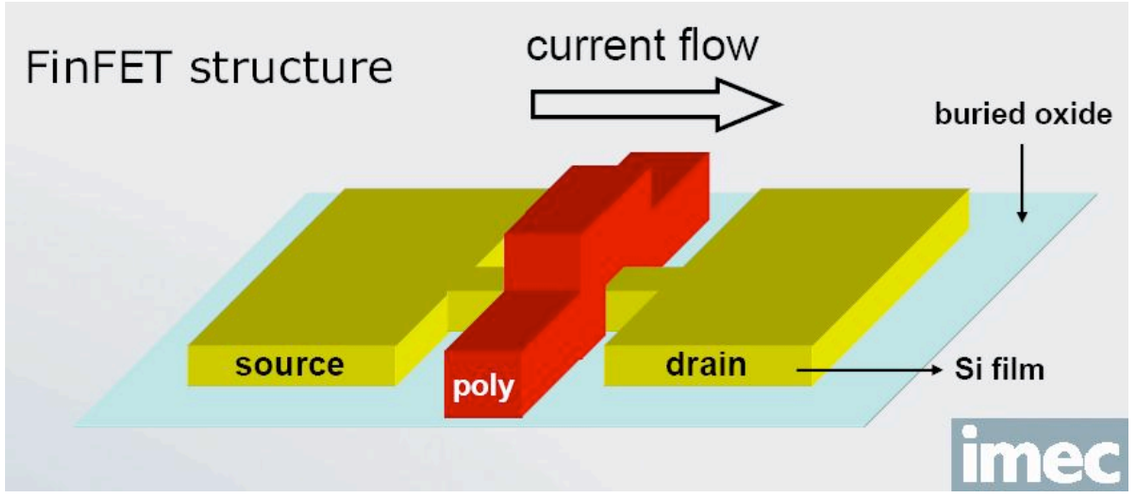

[Nadine Collaert, IMEC]

- application: lithographically defined Si nanowires (fins) covered by a single gate
- our experiments: single fin devices, here fin width 15 nm & gate length 20 nm

Detect states below the bandedge by resonant tunneling

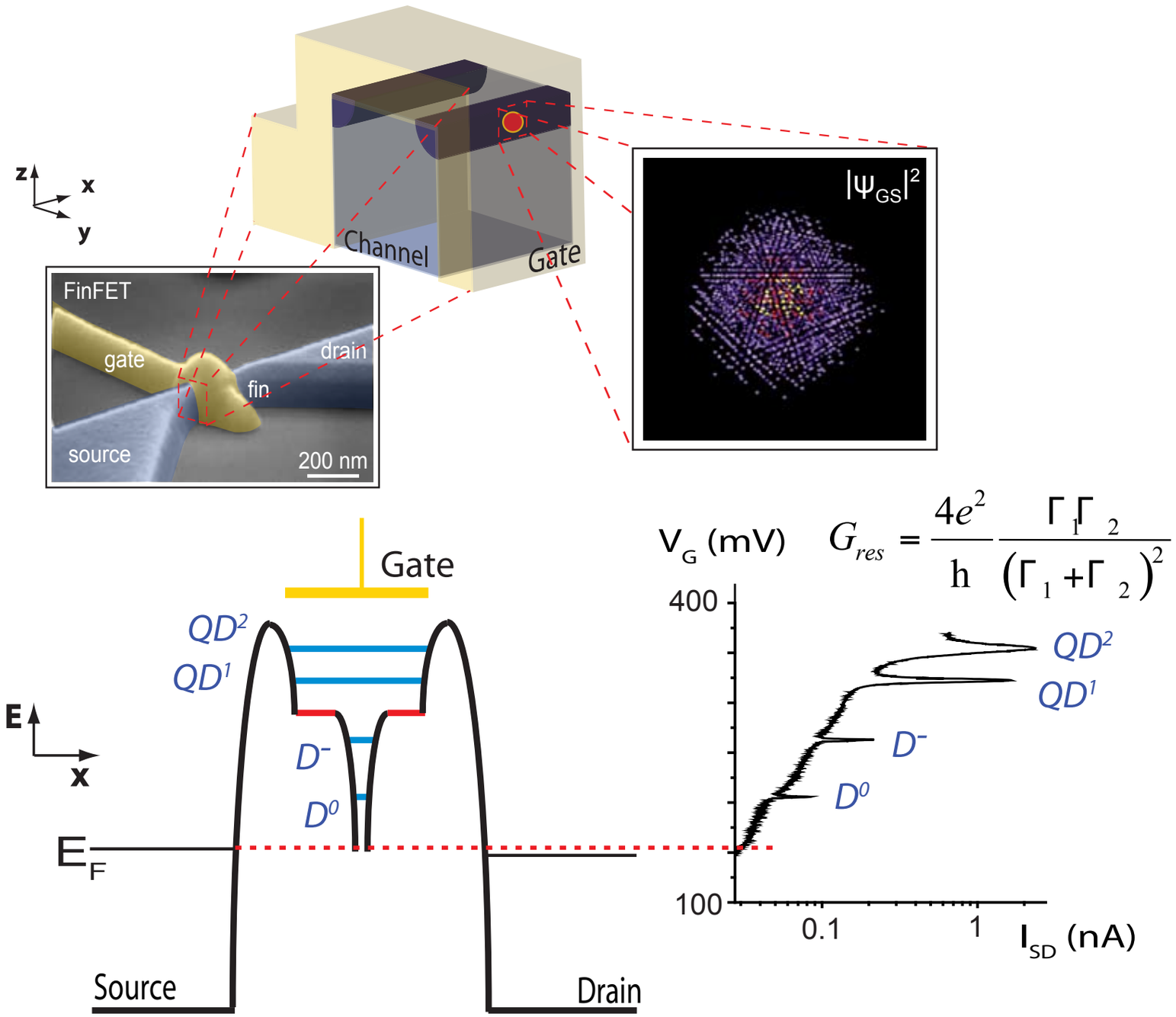

1 in 7 samples has peaks below bandedge (two, lower conductance, larger peak separation)

Sellier PRL 97, 206805 (2006)

Detect states below the bandedge by resonant tunneling

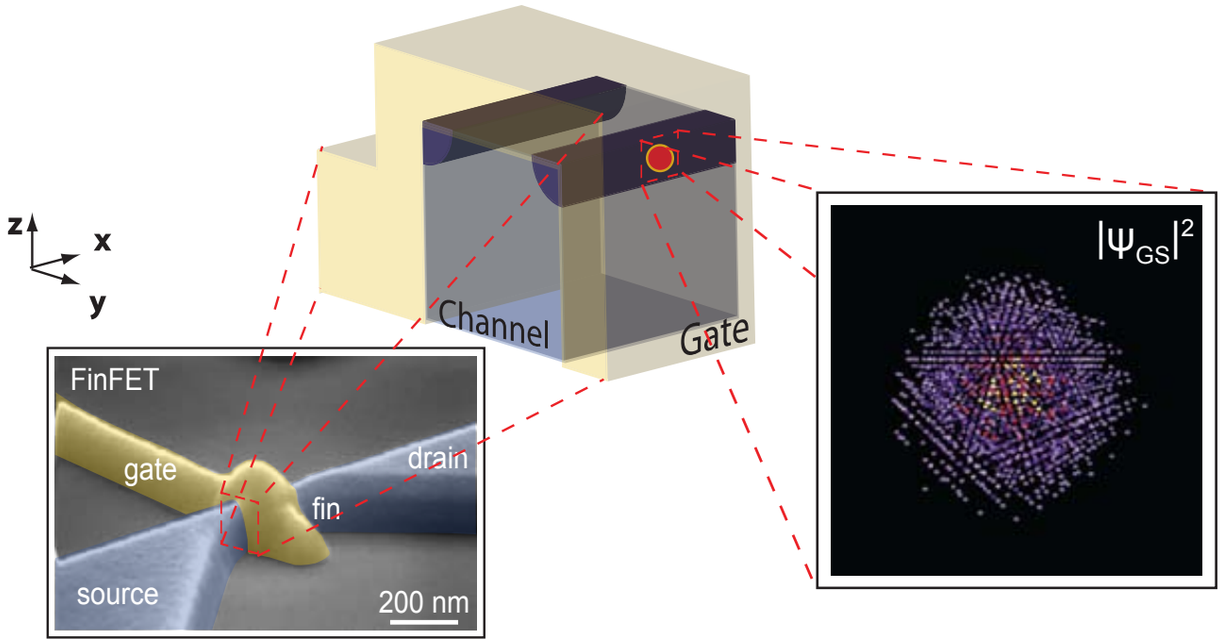

$$G_{res} = \frac{4e^2}{h}\frac{\Gamma_1\Gamma_2}{(\Gamma_1+\Gamma_2)^2}$$

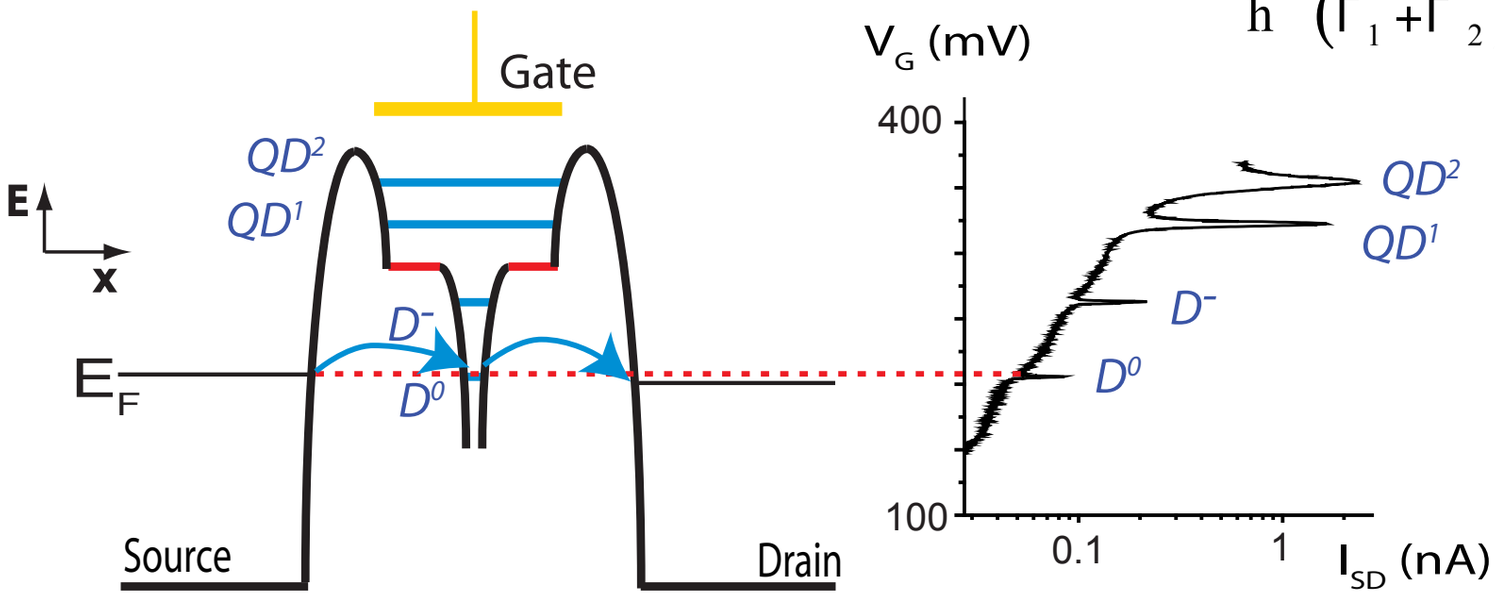

1 in 7 samples has peaks below bandedge (two, lower conductance, larger peak separation)

Sellier PRL 97, 206805 (2006)

Detect states below the bandedge by resonant tunneling

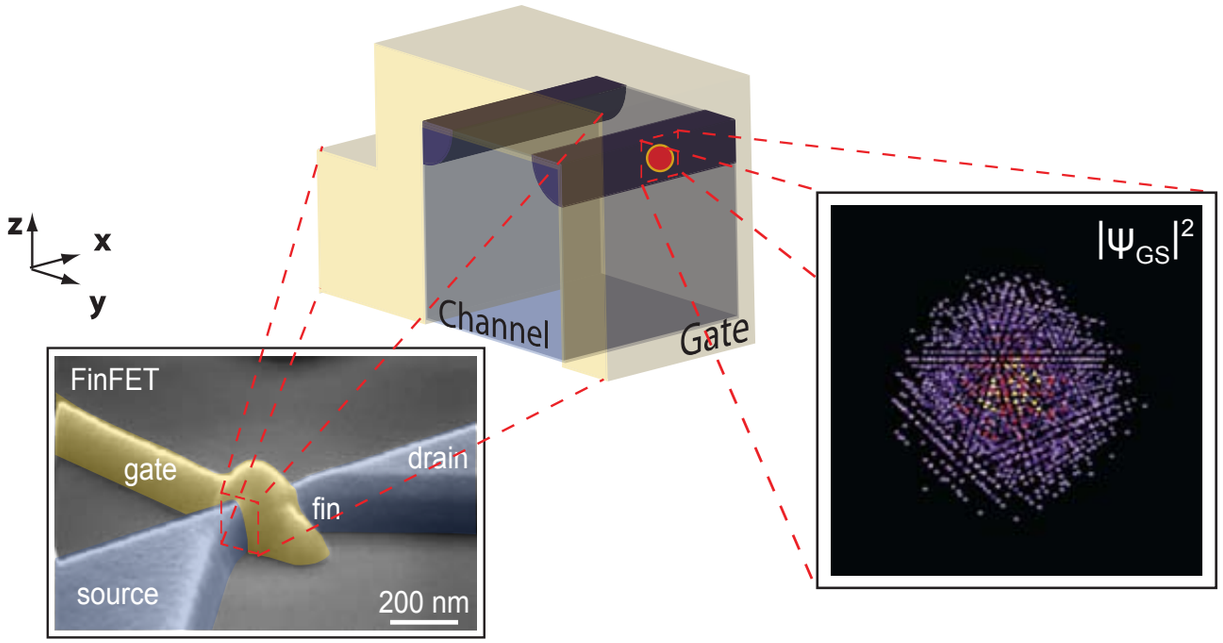

$$G_{res} = \frac{4e^2}{h}\frac{\Gamma_1\Gamma_2}{(\Gamma_1+\Gamma_2)^2}$$

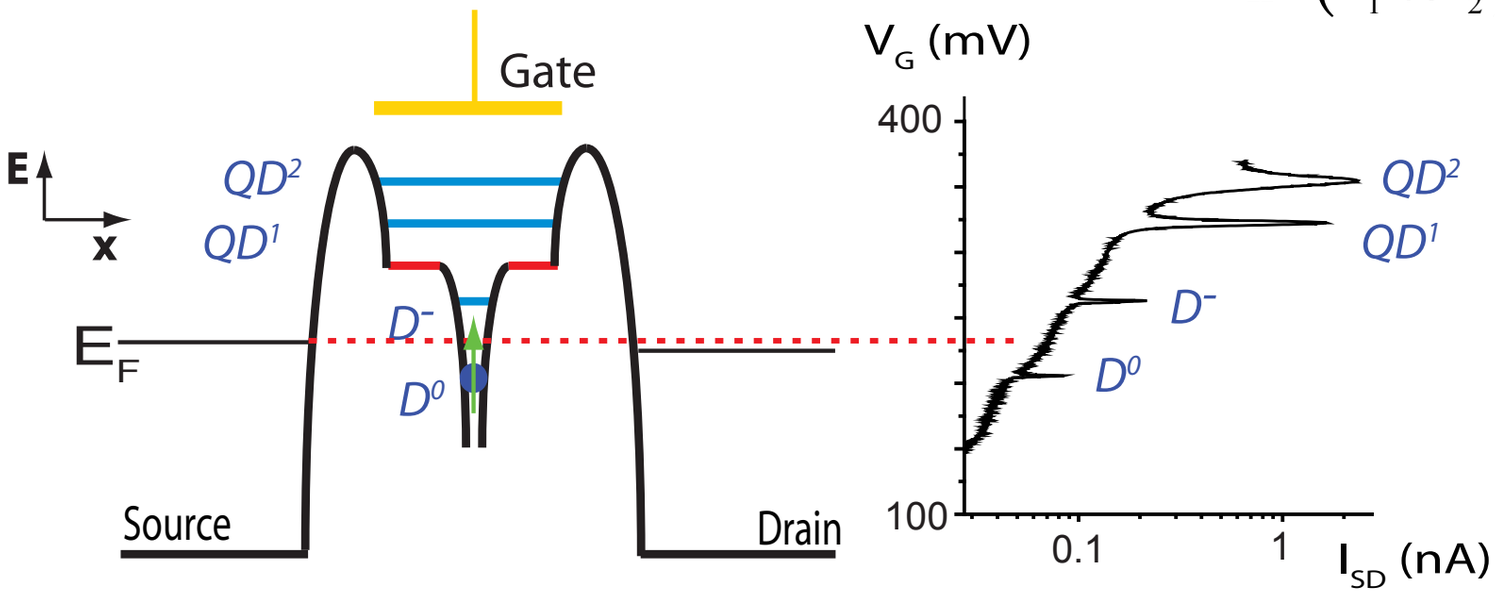

1 in 7 samples has peaks below bandedge (two, lower conductance, larger peak separation)

Sellier PRL 97, 206805 (2006)

Detect states below the bandedge by resonant tunneling

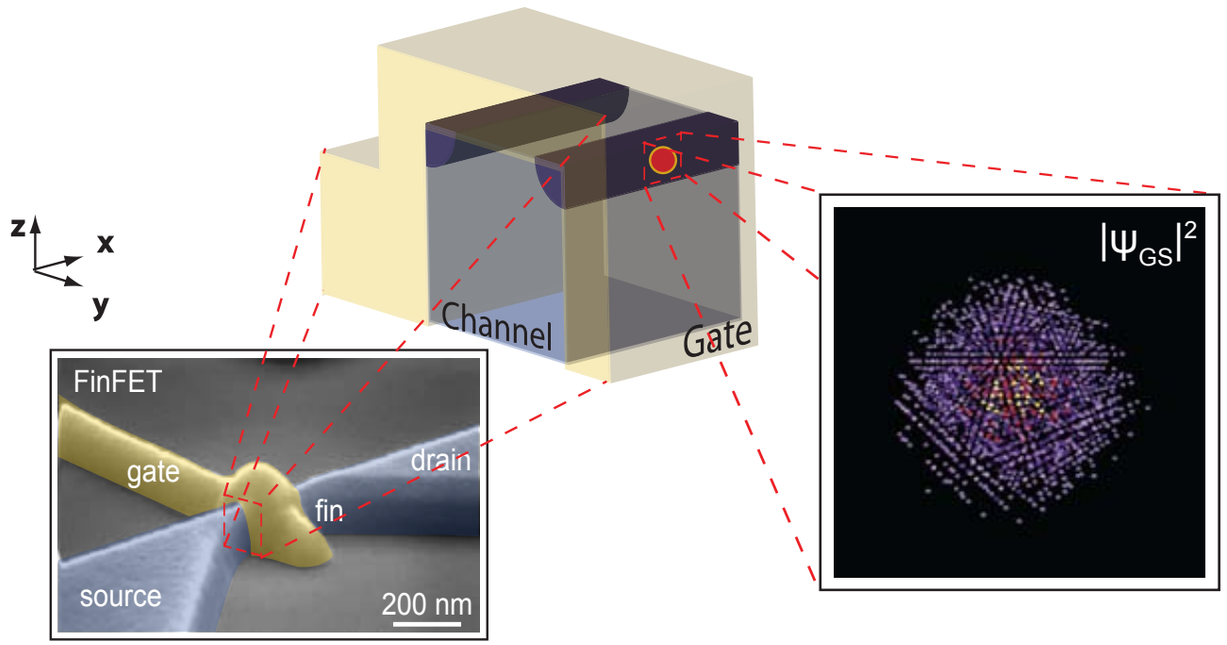

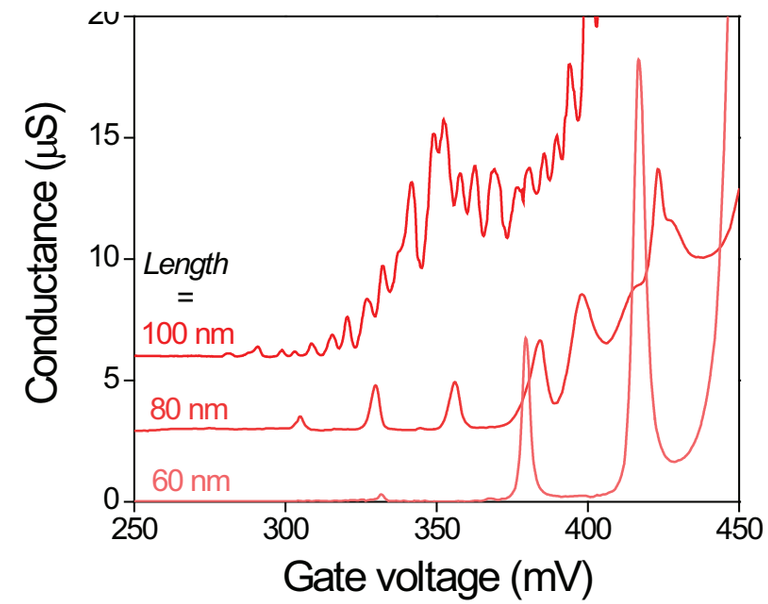

$$G_{res} = \frac{4e^2}{h}\frac{\Gamma_1\Gamma_2}{(\Gamma_1+\Gamma_2)^2}$$

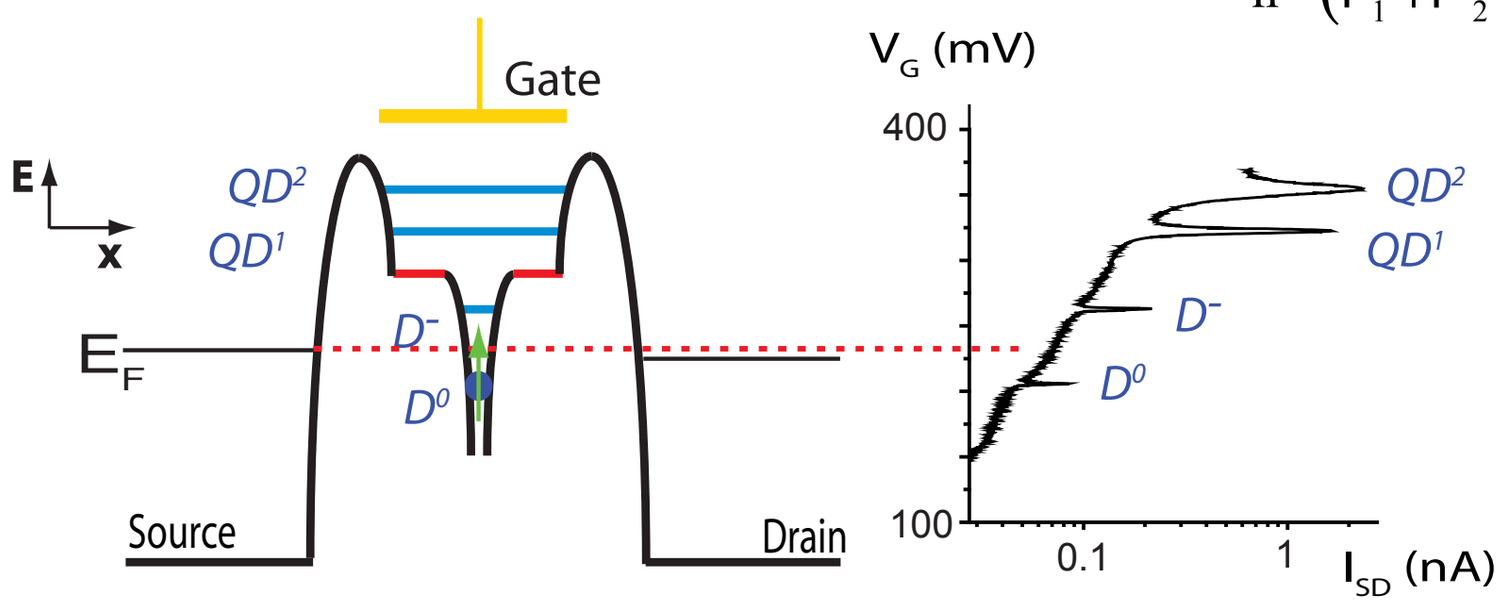

1 in 7 samples has peaks below bandedge (two, lower conductance, larger peak separation)

Sellier PRL 97, 206805 (2006)

Stability diagram: determine addition- & level-spectrum

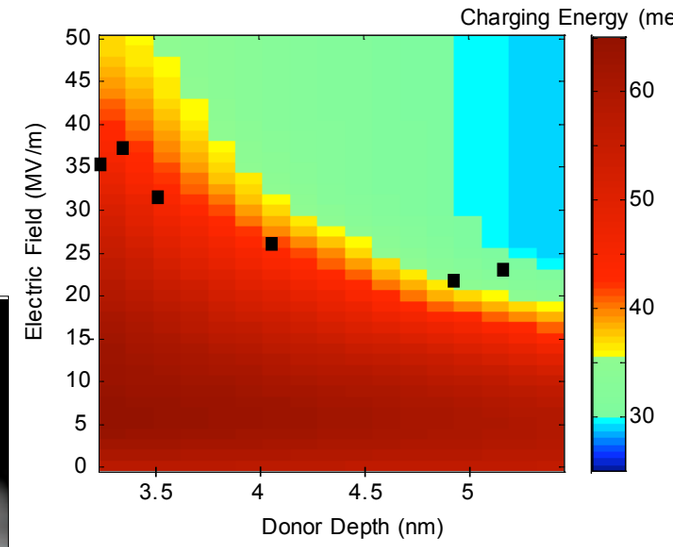

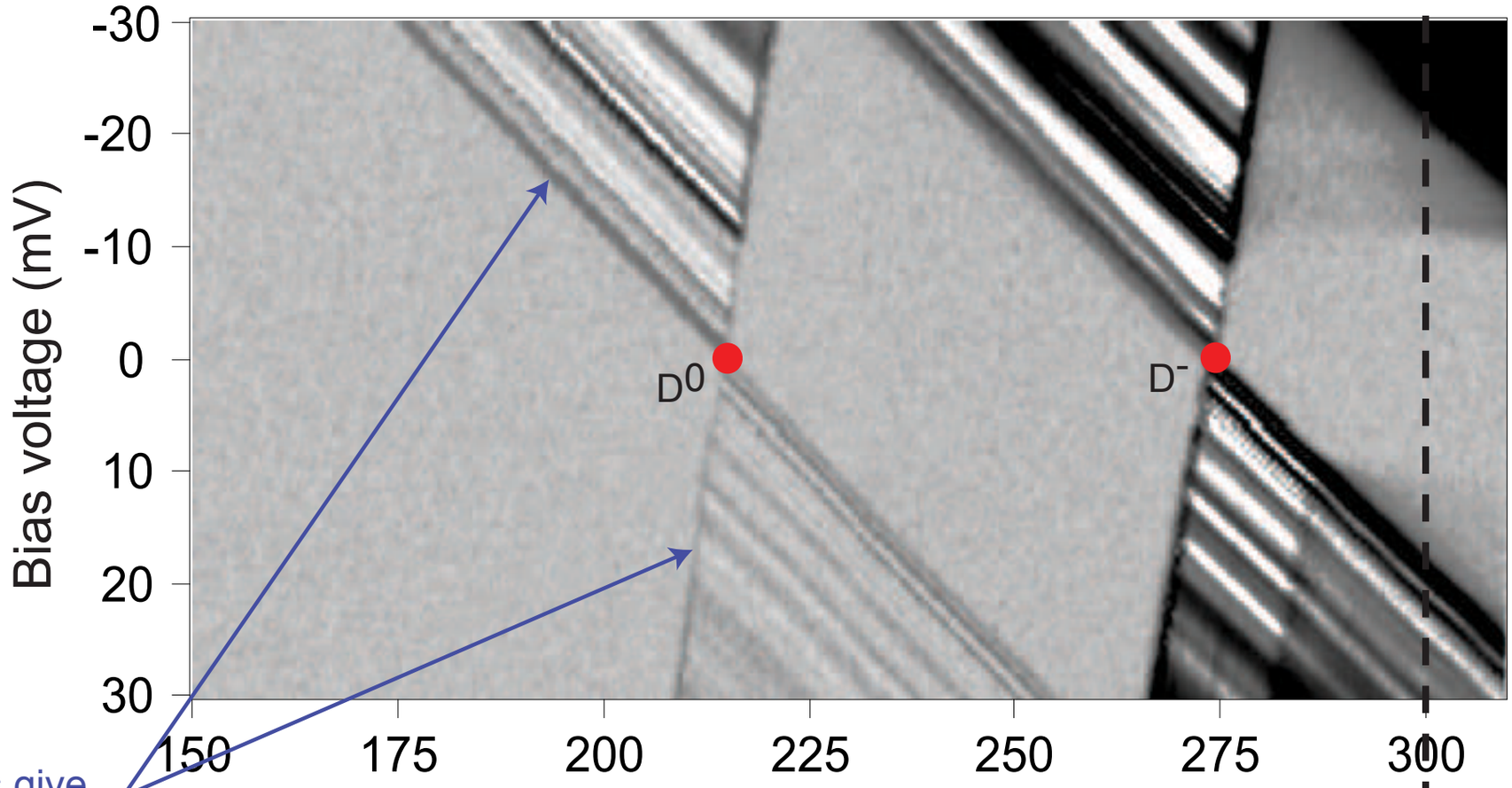

Slopes give voltage to energy conversion α = 0.7

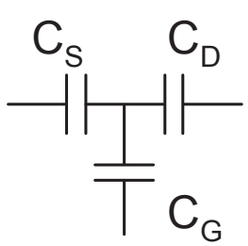

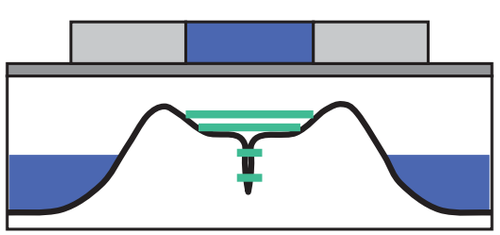

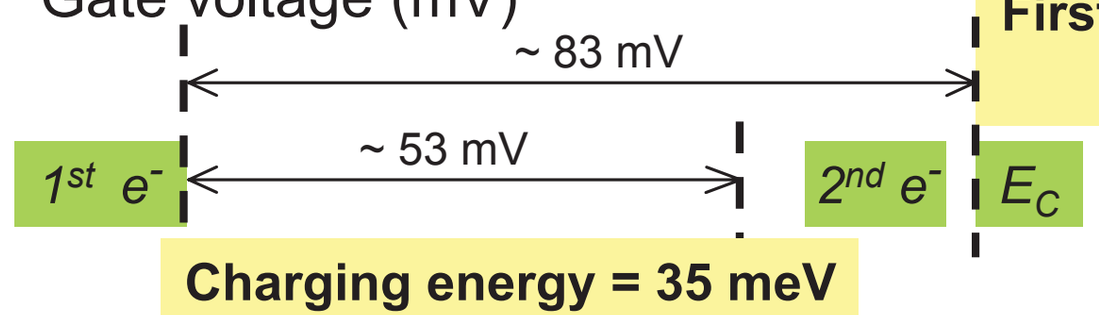

First binding energy = 55 meV

As: 54 meV
(P: 46 meV)

Charging energy = 35 meV

- lower than 52 meV (As: 2 meV second binding energy)
- **increased capacitance** due to nearby electrodes

[Sellier PRL 97, 206805, 2006]

Assignment of the level spectrum

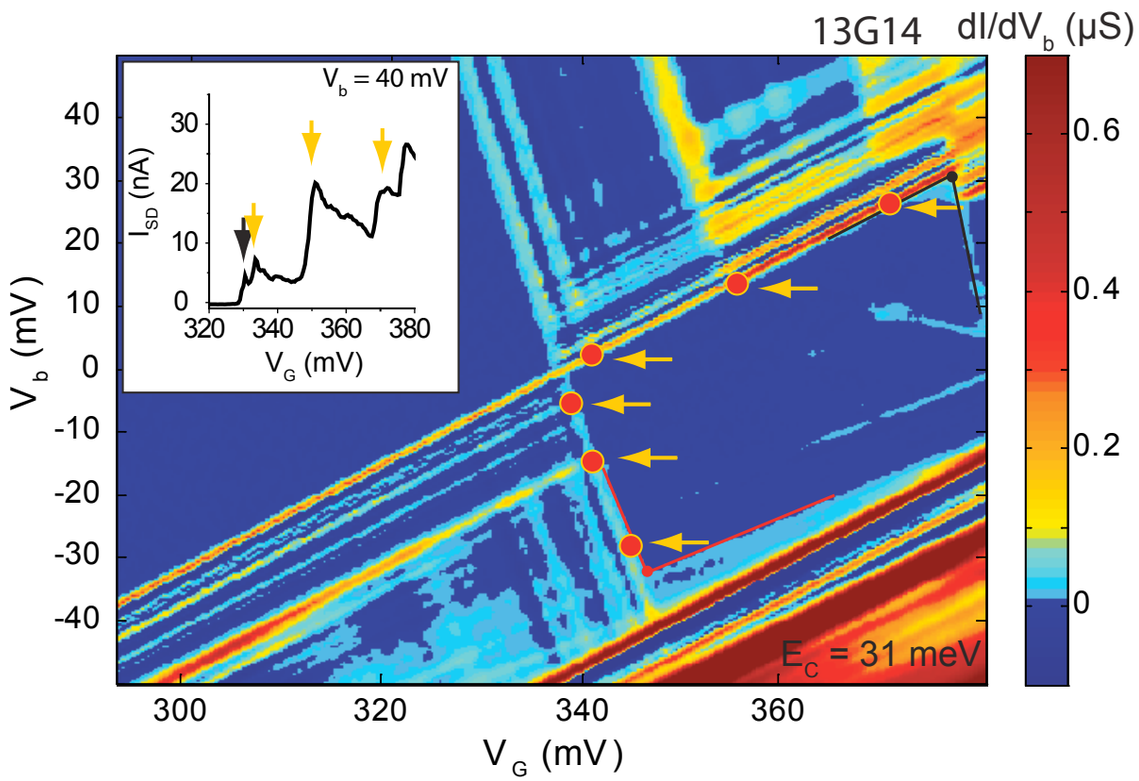

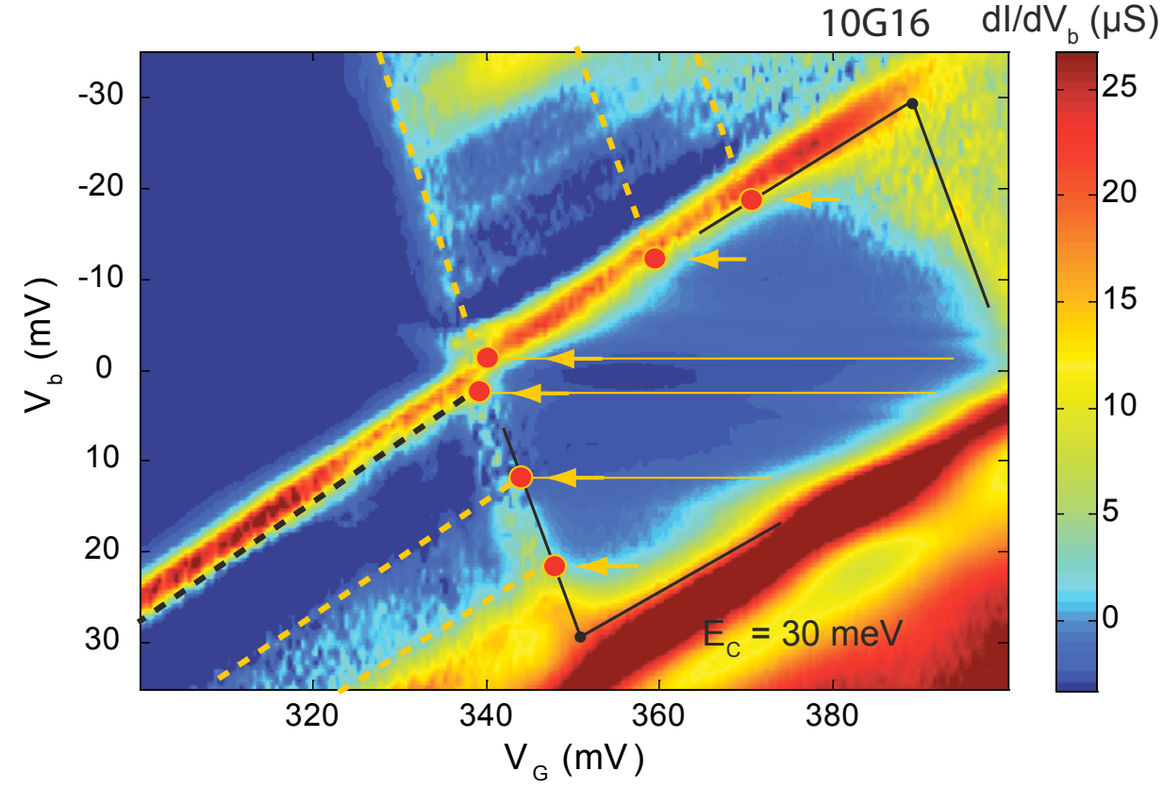

The "stability diagram" reveals the higher orbitals / excited states of a charge state.

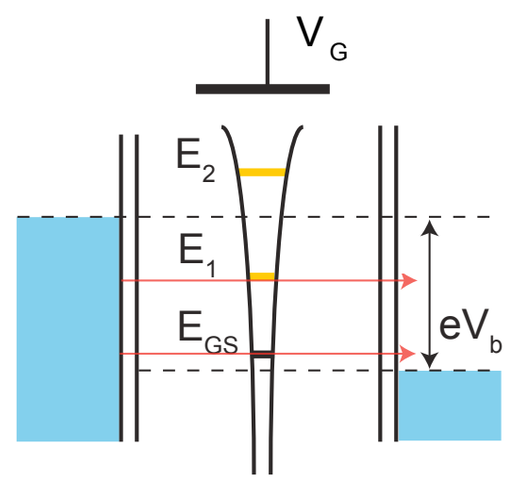

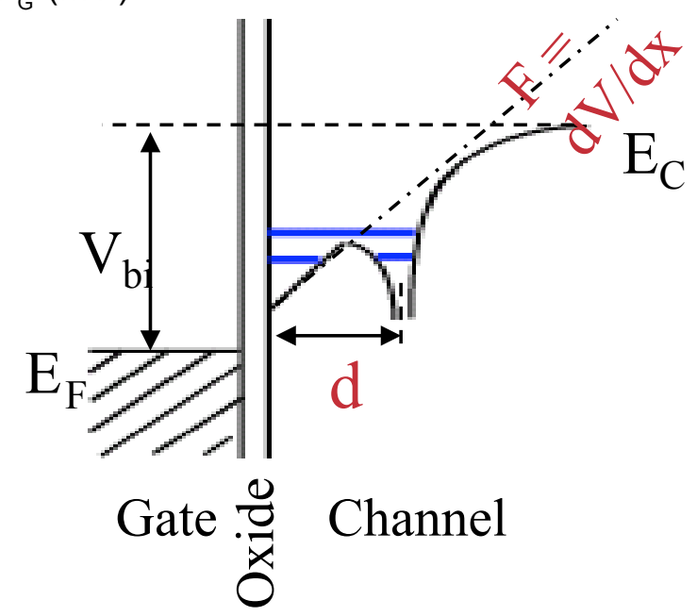

Hybridization with well state leads to a molecular system

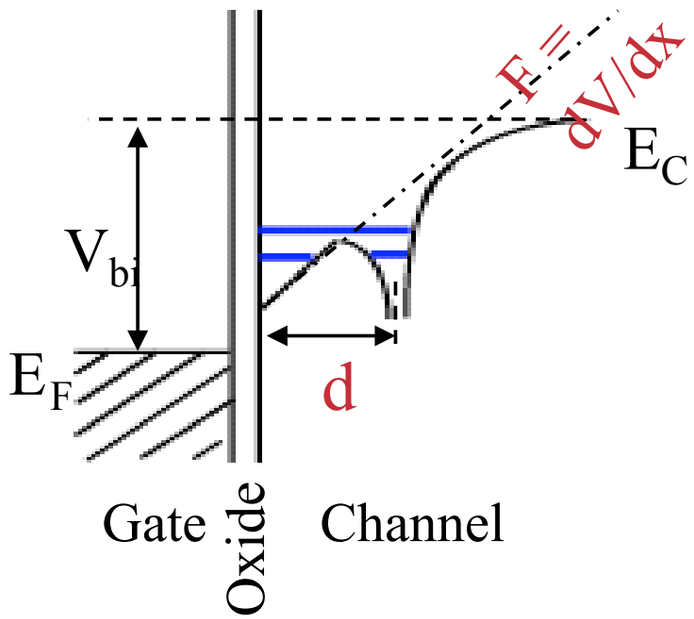

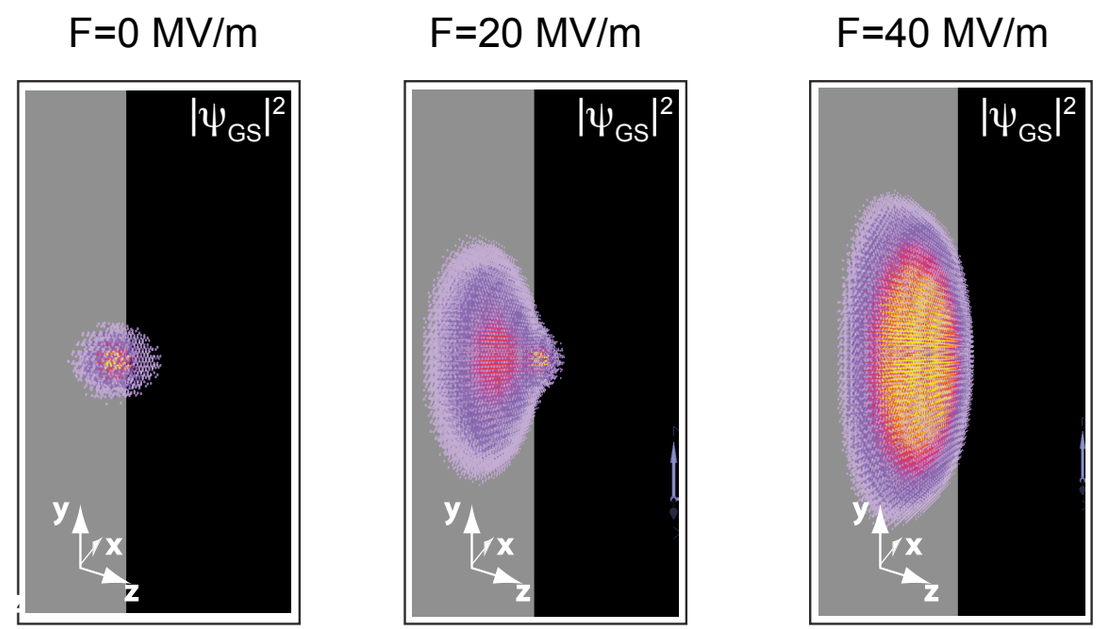

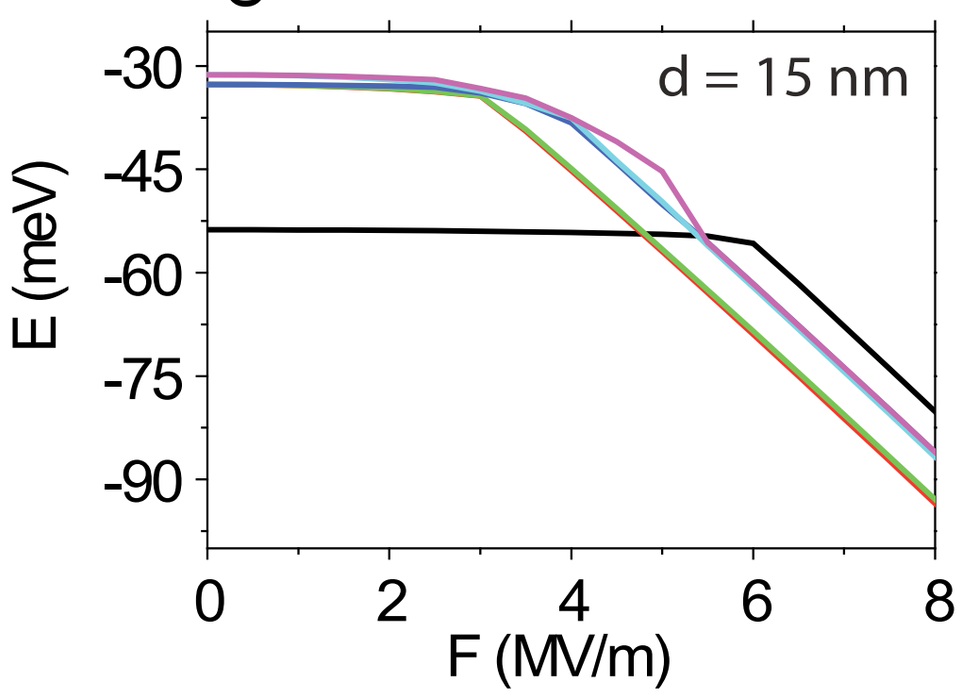

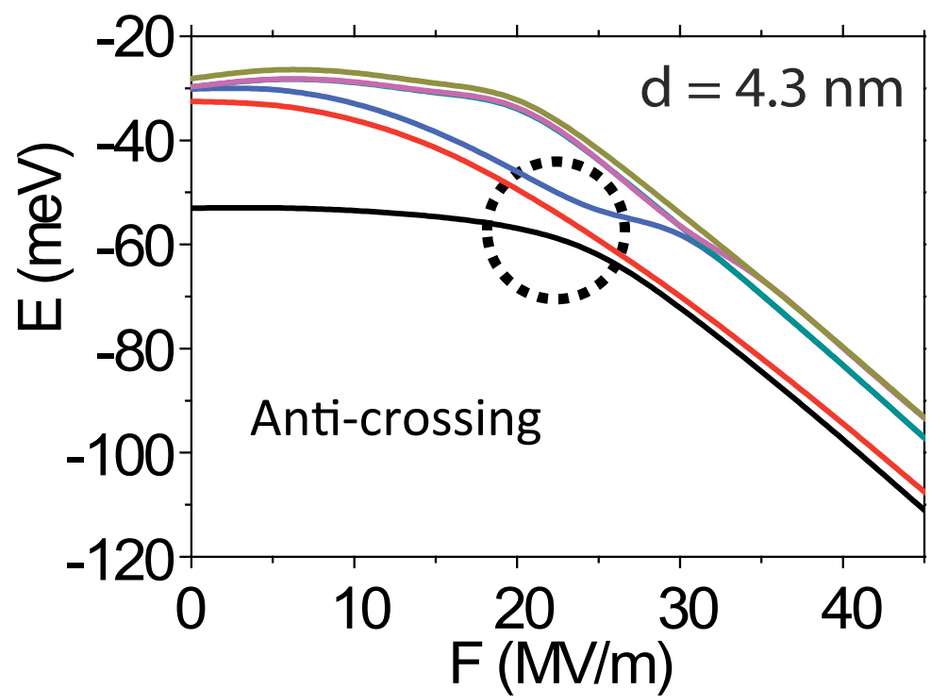

hybridization first theoretically predicted by Martins, PRB 69, 085320 (2004)
→ adiabatic regime for charge manipulation

Fit excited states of the dopants to model

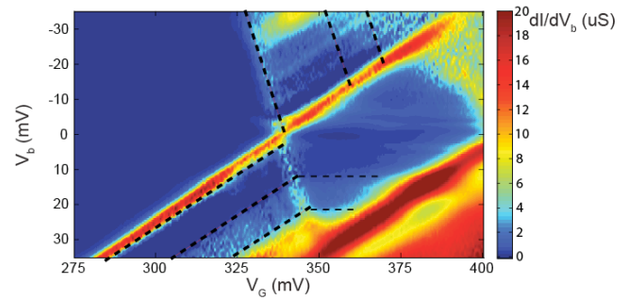

Measured

$E_{x,i}$

F ? , d ?

Predicted

$E_{x,i}$ (F,d)

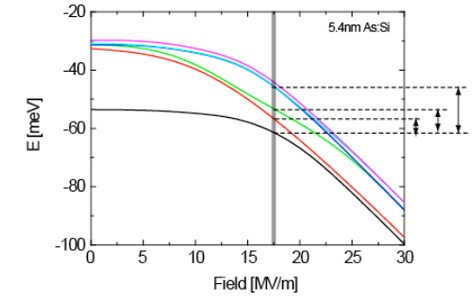

Device		E_1 (meV)	E_2 (meV)	E_3 (meV)	E_C (meV)	d (nm)	F (MV m^{-1})	s (meV)
10G16	Exp.	2	15	23	30	3.3		
	TB	2.2	15.6	23.0		3.3	37.3	0.59
11G14	Exp.	4.5	13.5	25	29	3.2		
	TB	4.5	13.5	25.0		3.5	31.6	0.04
13G14	Exp.	3.5	15.5	26.4	31	3.5		
	TB	3.6	15.7	26.3		3.2	35.4	0.17
HSJ18	Exp.	5	10	21.5	33	4.0		
	TB	4.5	9.9	21.8		4.1	26.1	0.63
GLG14	Exp.	1.3	10	13.2	35	4.7		
	TB	1.3	10	12.4		5.2	23.1	0.28
GLJ17	Exp.	2	7.7	15.5	33	4.0		
	TB	1.3	7.7	15.8		4.9	21.9	0.77

$E_C \rightarrow d$

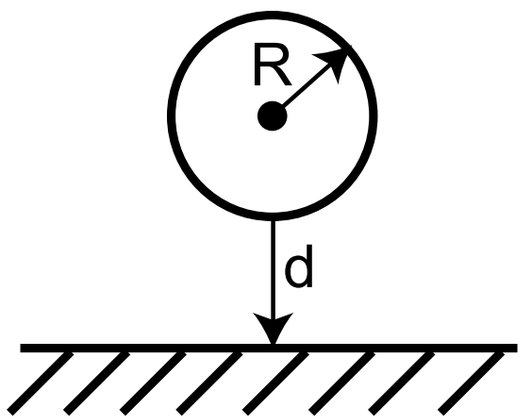

- a 2D (F, d) fit of the first 3 excited states of the model works well for the 6 samples
- overdetermined, since we fit 3 parameters of 6 samples to a 2D space

Fit excited states of the dopants to model

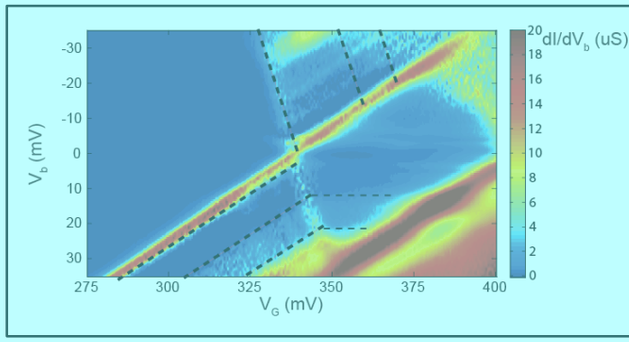

Measured

$E_{x,i}$

F ? , d ?

Predicted

$E_{x,i}$ (F,d)

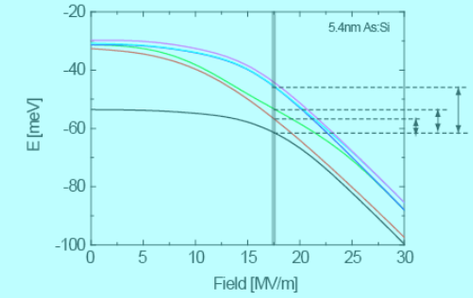

Device		E_1 (meV)	E_2 (meV)	E_3 (meV)	E_C (meV)	d (nm)	F (MV m^{-1})	s (meV)
10G16	Exp.	2	15	23	30	3.3		
	TB	2.2	15.6	23.0		3.3	37.3	0.59
11G14	Exp.	4.5	13.5	25	29	3.2		
	TB	4.5	13.5	25.0		3.5	31.6	0.04
13G14	Exp.	3.5	15.5	26.4	31	3.5		
	TB	3.6	15.7	26.3		3.2	35.4	0.17
HSJ18	Exp.	5	10	21.5	33	4.0		
	TB	4.5	9.9	21.8		4.1	26.1	0.63
GLG14	Exp.	1.3	10	13.2	35	4.7		
	TB	1.3	10	12.4		5.2	23.1	0.28
GLJ17	Exp.	2	7.7	15.5	33	4.0		
	TB	1.3	7.7	15.8		4.9	21.9	0.77

$E_C \rightarrow d$

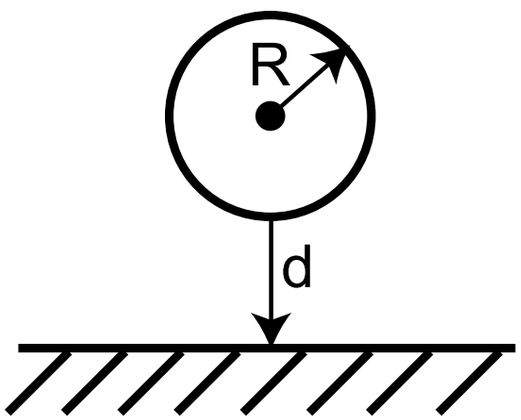

- a 2D (F, d) fit of the first 3 excited states of the model works well for the 6 samples
- overdetermined, since we fit 3 parameters of 6 samples to a 2D space

Fit excited states of the dopants to model

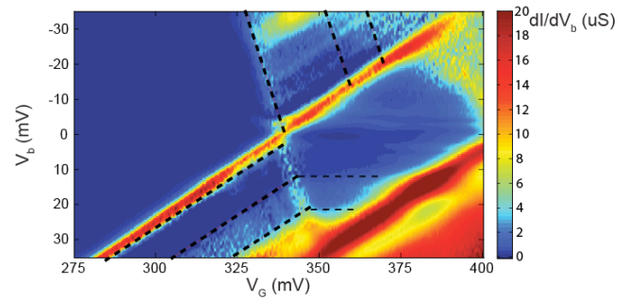

Measured

$E_{x,i}$

F ? , d ?

Predicted

$E_{x,i}$ (F,d)

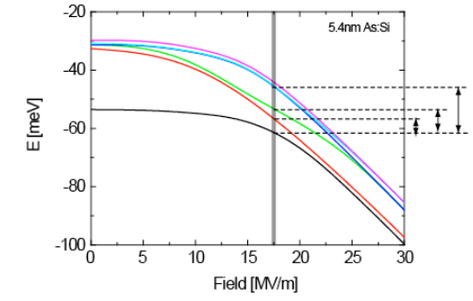

Device		E_1 (meV)	E_2 (meV)	E_3 (meV)	E_C (meV)	d (nm)	F (MV m^{-1})	s (meV)
10G16	Exp.	2	15	23	30	3.3		
	TB	2.2	15.6	23.0		3.3	37.3	0.59
11G14	Exp.	4.5	13.5	25	29	3.2		
	TB	4.5	13.5	25.0		3.5	31.6	0.04
13G14	Exp.	3.5	15.5	26.4	31	3.5		
	TB	3.6	15.7	26.3		3.2	35.4	0.17
HSJ18	Exp.	5	10	21.5	33	4.0		
	TB	4.5	9.9	21.8		4.1	26.1	0.63
GLG14	Exp.	1.3	10	13.2	35	4.7		
	TB	1.3	10	12.4		5.2	23.1	0.28
GLJ17	Exp.	2	7.7	15.5	33	4.0		
	TB	1.3	7.7	15.8		4.9	21.9	0.77

$E_C \rightarrow d$

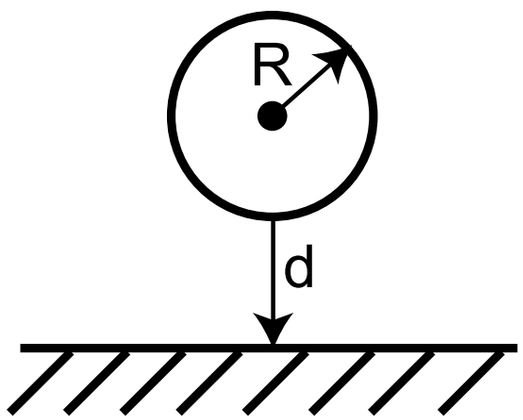

- a 2D (F, d) fit of the first 3 excited states of the model works well for the 6 samples
- overdetermined, since we fit 3 parameters of 6 samples to a 2D space

Fit excited states of the dopants to model

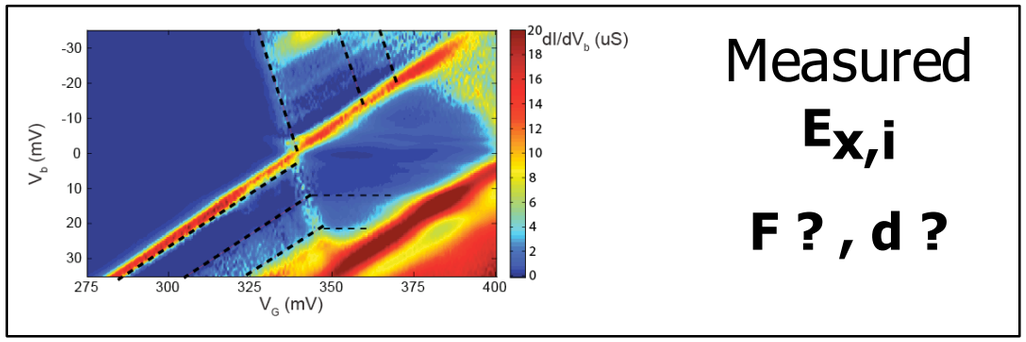

Measured

$E_{x,i}$

F ? , d ?

Predicted

$E_{x,i}$ (F,d)

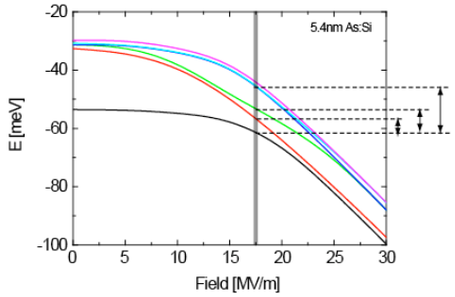

Device		E_1 (meV)	E_2 (meV)	E_3 (meV)	E_C (meV)	d (nm)	F (MV m^{-1})	s (meV)
10G16	Exp.	2	15	23	30	3.3		
	TB	2.2	15.6	23.0		3.3	37.3	0.59
11G14	Exp.	4.5	13.5	25	29	3.2		
	TB	4.5	13.5	25.0		3.5	31.6	0.04
13G14	Exp.	3.5	15.5	26.4	31	3.5		
	TB	3.6	15.7	26.3		3.2	35.4	0.17
HSJ18	Exp.	5	10	21.5	33	4.0		
	TB	4.5	9.9	21.8		4.1	26.1	0.63
GLG14	Exp.	1.3	10	13.2	35	4.7		
	TB	1.3	10	12.4		5.2	23.1	0.28
GLJ17	Exp.	2	7.7	15.5	33	4.0		
	TB	1.3	7.7	15.8		4.9	21.9	0.77

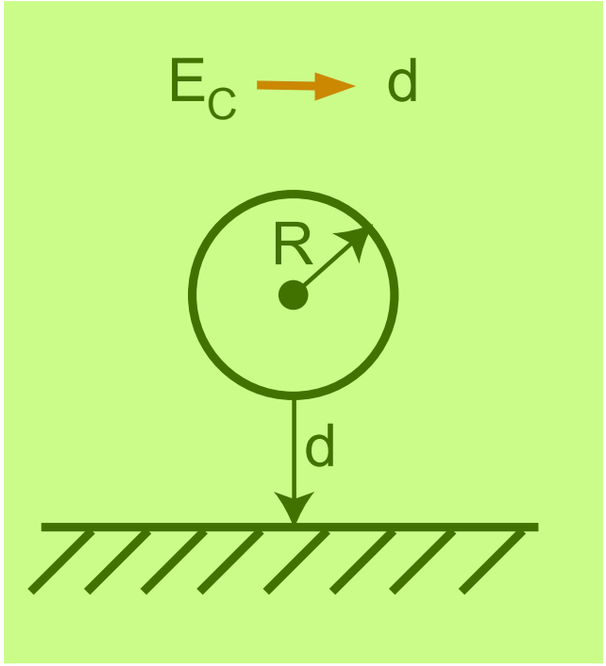

- a 2D (F, d) fit of the first 3 excited states of the model works well for the 6 samples
- overdetermined, since we fit 3 parameters of 6 samples to a 2D space

Lansbergen Nature Physics 4, 656 (2008)

Fit excited states of the dopants to model

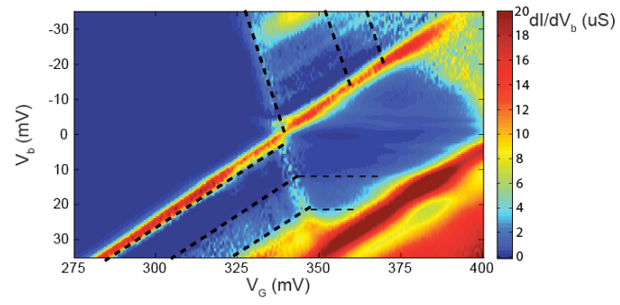

Measured

$E_{x,i}$

F ? , d ?

Predicted

$E_{x,i}$ (F,d)

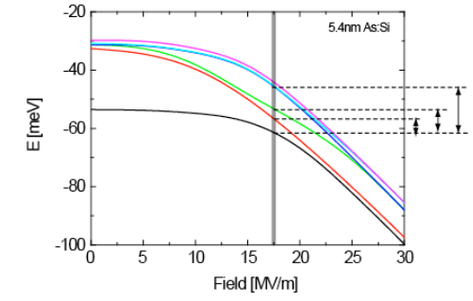

Device		E_1 (meV)	E_2 (meV)	E_3 (meV)	E_C (meV)	d (nm)	F (MV m^{-1})	s (meV)
10G16	Exp.	2	15	23	30	3.3		
	TB	2.2	15.6	23.0		3.3	37.3	0.59
11G14	Exp.	4.5	13.5	25	29	3.2		
	TB	4.5	13.5	25.0		3.5	31.6	0.04
13G14	Exp.	3.5	15.5	26.4	31	3.5		
	TB	3.6	15.7	26.3		3.2	35.4	0.17
HSJ18	Exp.	5	10	21.5	33	4.0		
	TB	4.5	9.9	21.8		4.1	26.1	0.63
GLG14	Exp.	1.3	10	13.2	35	4.7		
	TB	1.3	10	12.4		5.2	23.1	0.28
GLJ17	Exp.	2	7.7	15.5	33	4.0		
	TB	1.3	7.7	15.8		4.9	21.9	0.77

$E_C \rightarrow d$

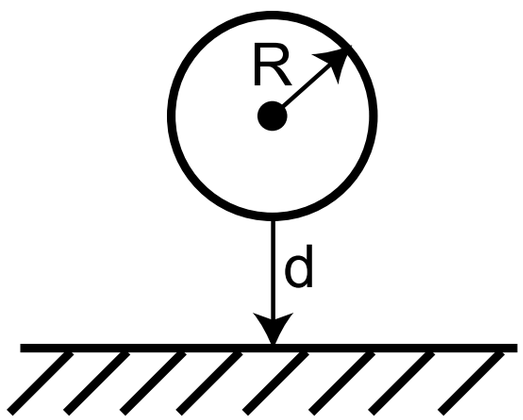

- a 2D (F, d) fit of the first 3 excited states of the model works well for the 6 samples
- overdetermined, since we fit 3 parameters of 6 samples to a 2D space

Chemically selective donor-tomography

Single donor fingerprint in transport characteristics combined with large scale device-simulations yields:

- chemical species (VO in Si)
- local field
- depth below the interface
- concentration

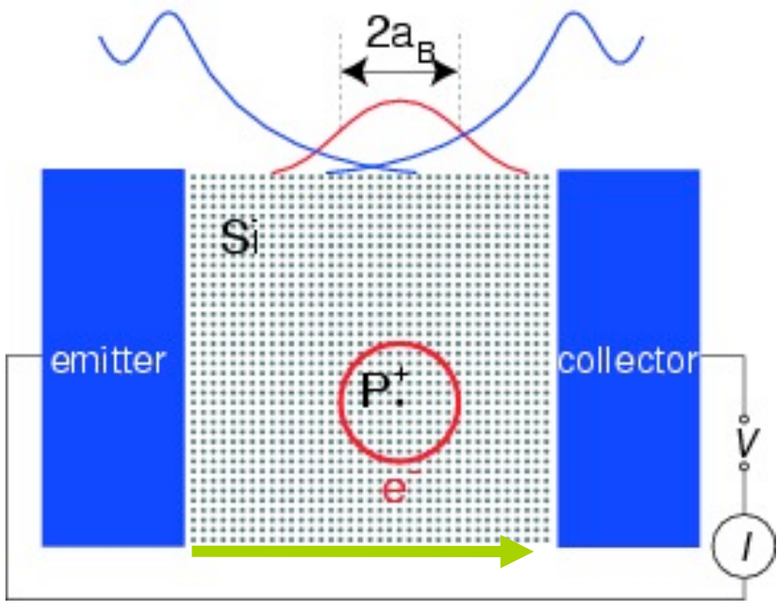

Jagannath et al. PRB 23, 2082 (1981)

Level	P[a]	As[a]	Sb[b]	Bi[c]	Li[a]	Li-O[a]	Mg+[d]	Mg[d]	S[e]	Theory[f]
$1s(A_1)$	45.59	53.76	42.74	70.98	31.24 ± 0.02	39.67	256.47	107.50	186.42	31.27
$1s(E)$	32.58[b,g,h]	31.26[b,h]	30.47[b,h]							31.27
$1s(E+T_2)$					33.02	32.00				31.27
			32.89	32.89[i]					30.92	
$1s(T_2)$	33.89	32.67[b]							26.22	31.27
			32.91	31.89[i]					24.02	
$2p_0$	11.48	11.50	11.51	11.44	11.51	11.57	47.84	11.70	11.4	11.51
$2s$		9.11[j]		8.78[j]						8.83
$2p\pm$	6.40	6.40	6.38	6.37	6.40	6.40	26.25 26.05	6.38	6.2	6.40

Outline

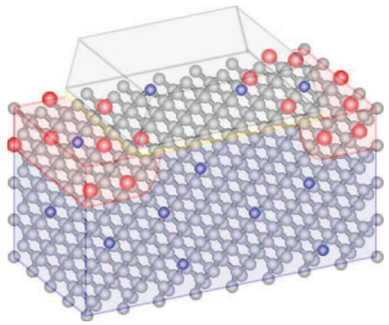

- Background

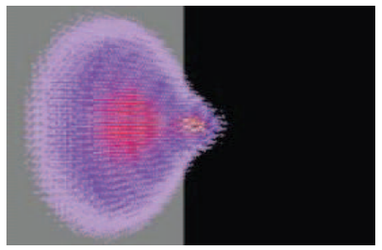

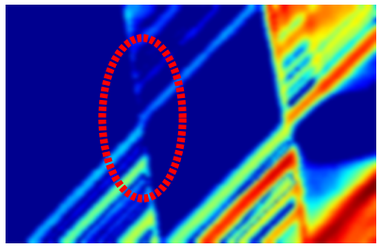

- From I(Vg) peaks → spectra & environmental information

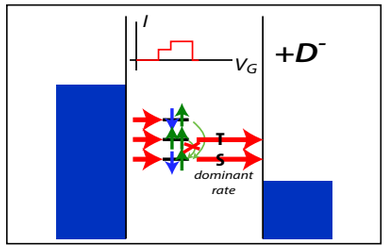

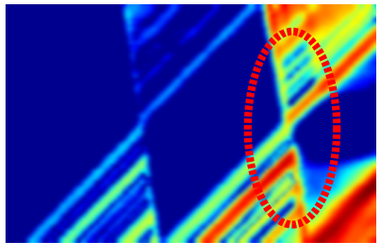

- Beyond level spectroscopy

Σ

- Summary

Information about relaxation processes

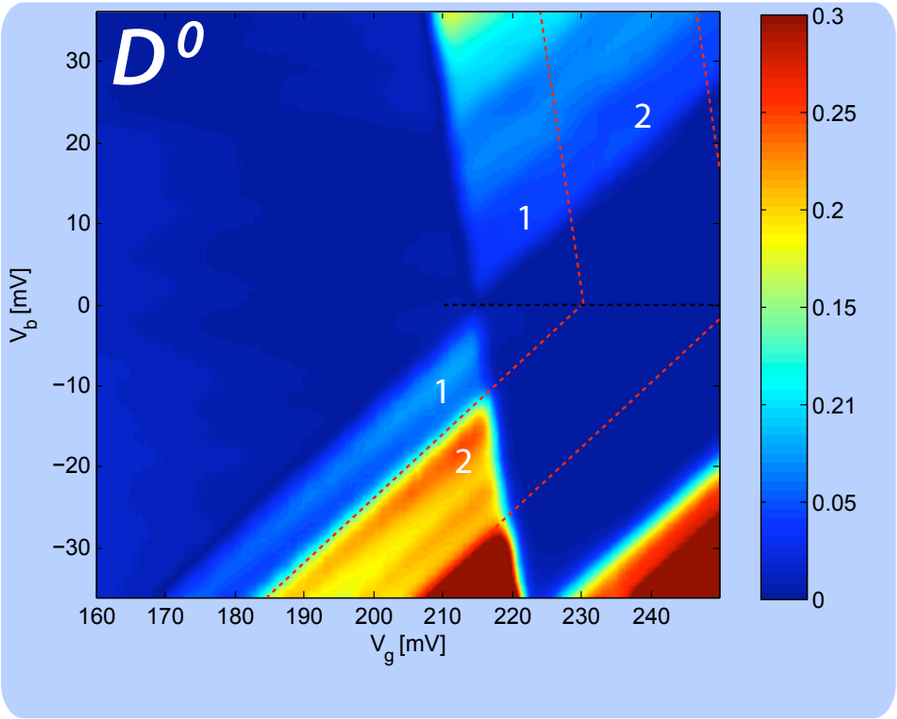

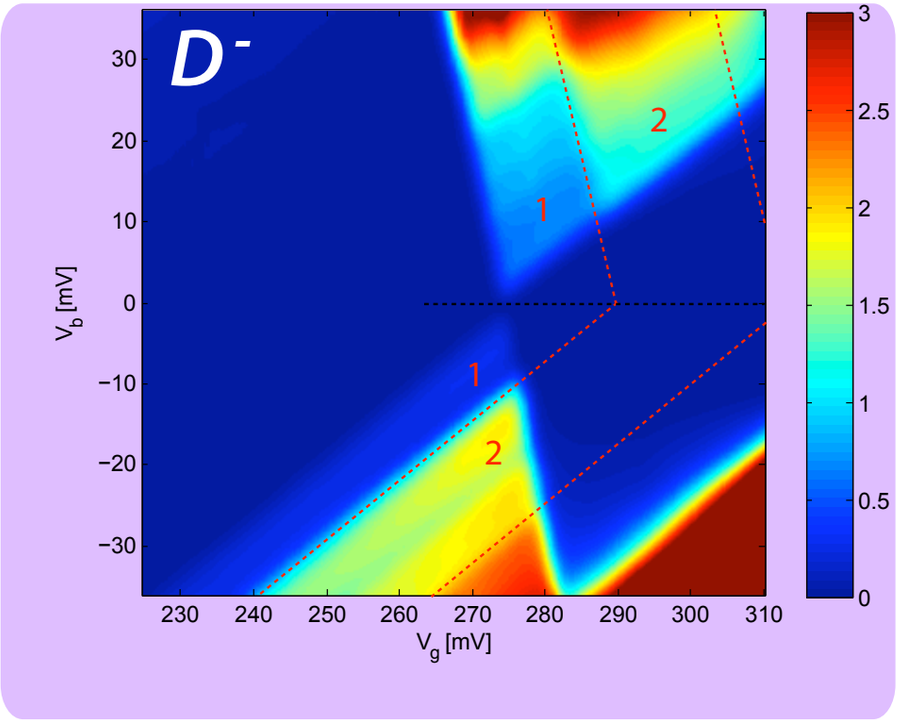

Information about relaxation processes

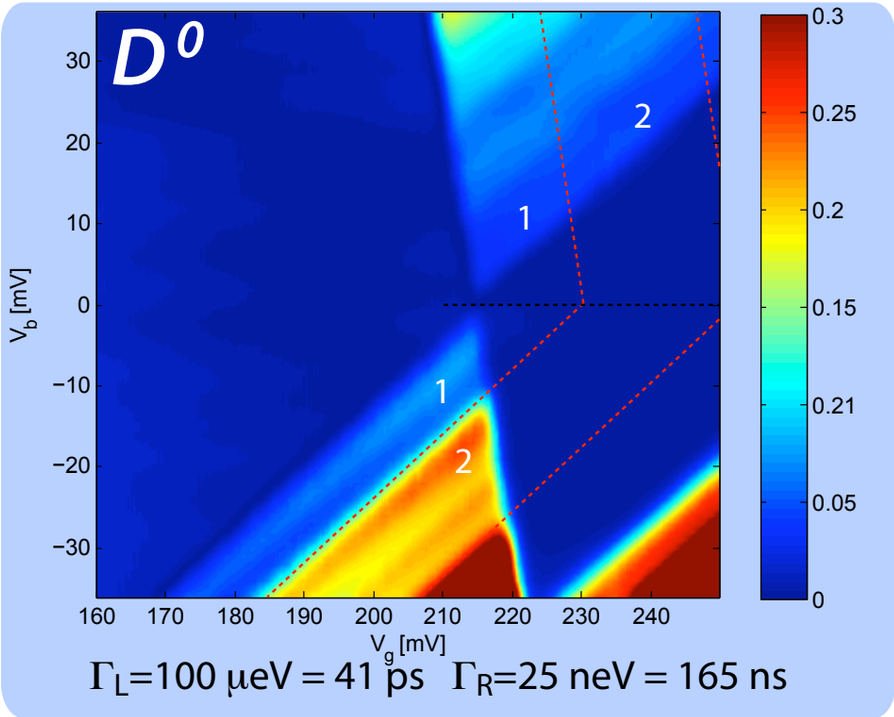

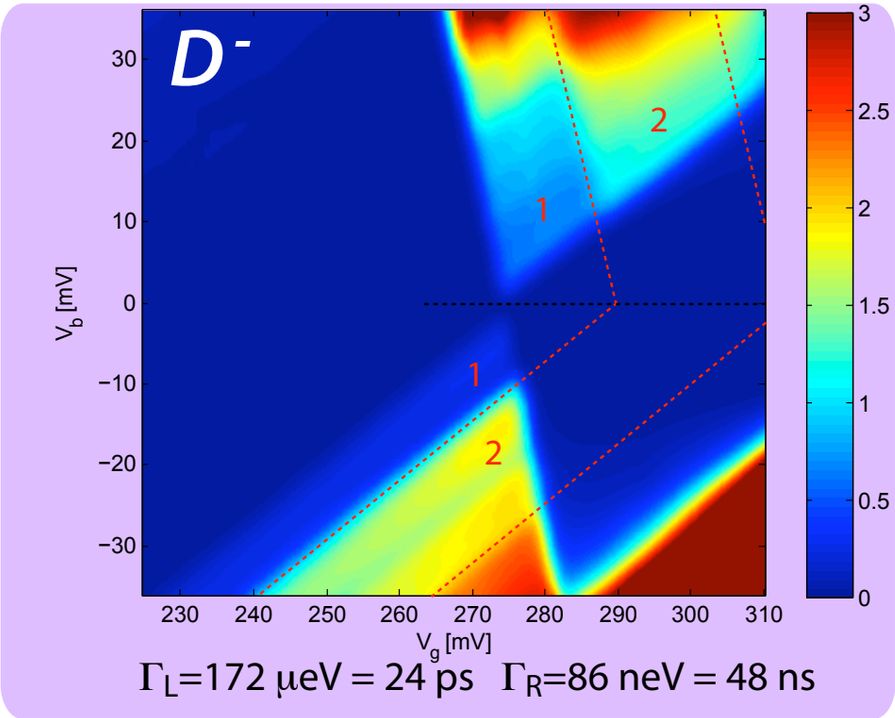

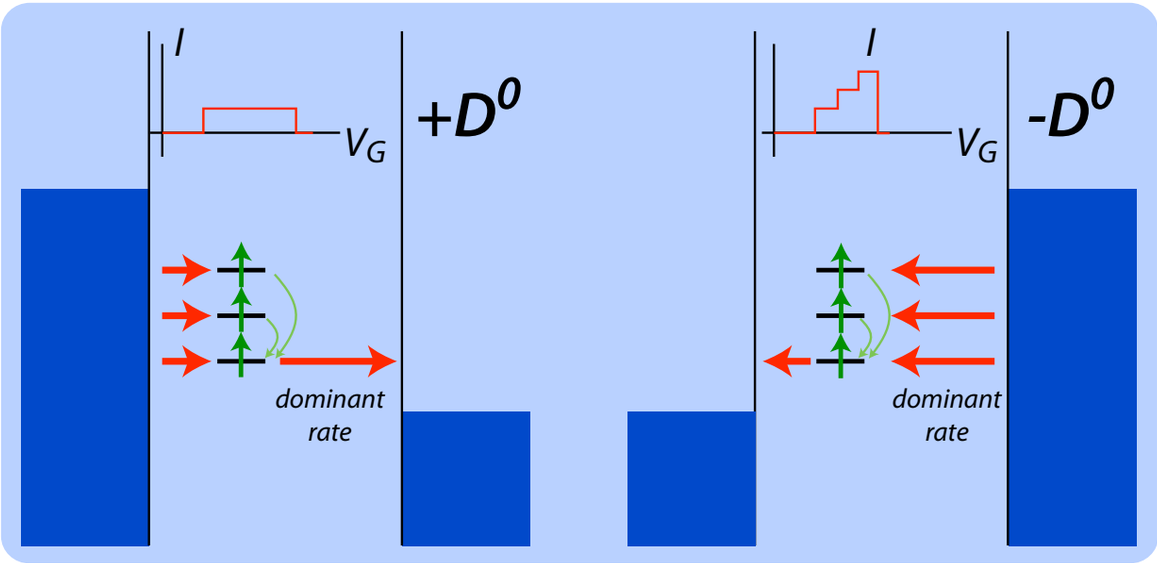

Information about relaxation processes

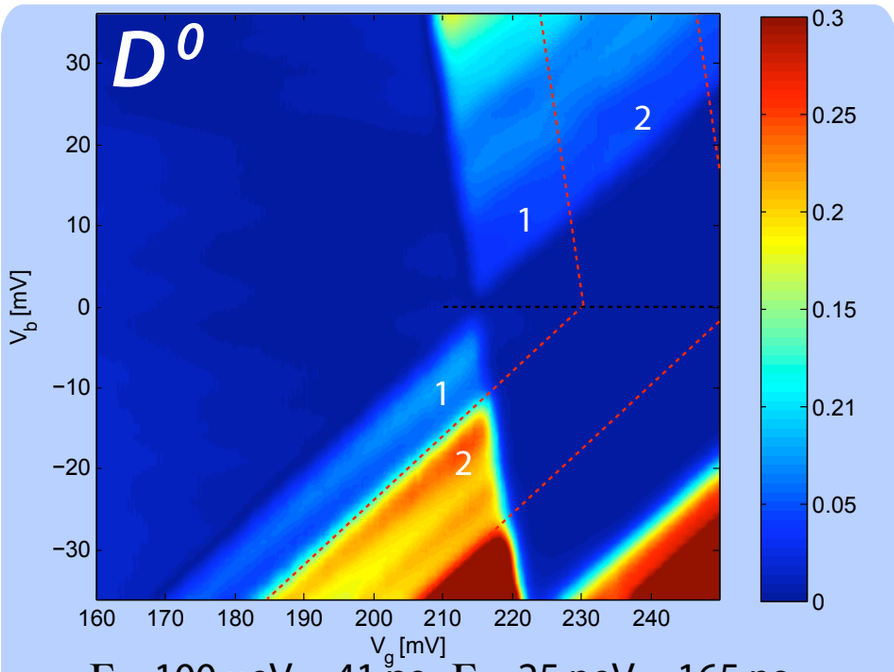

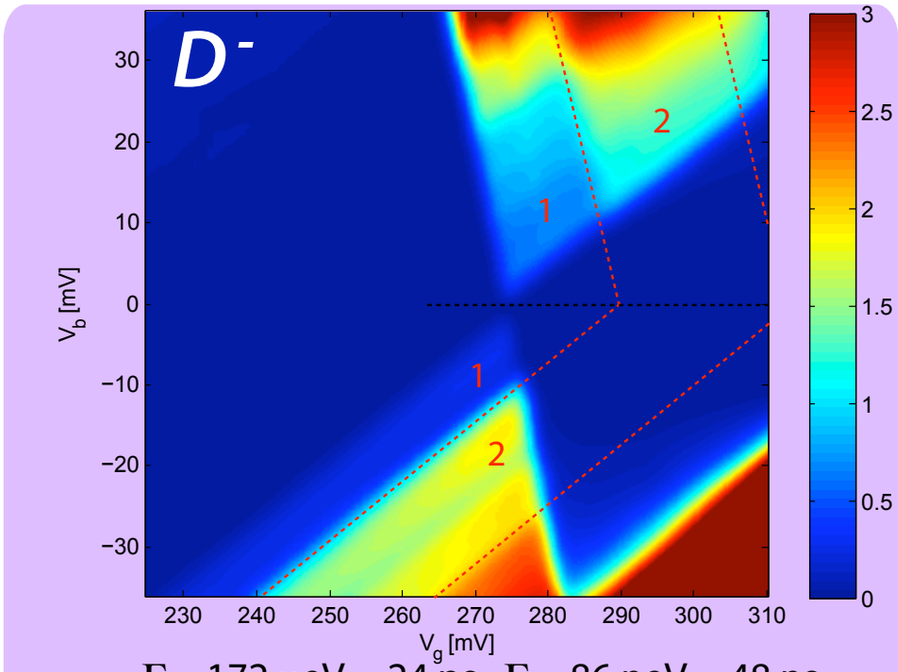

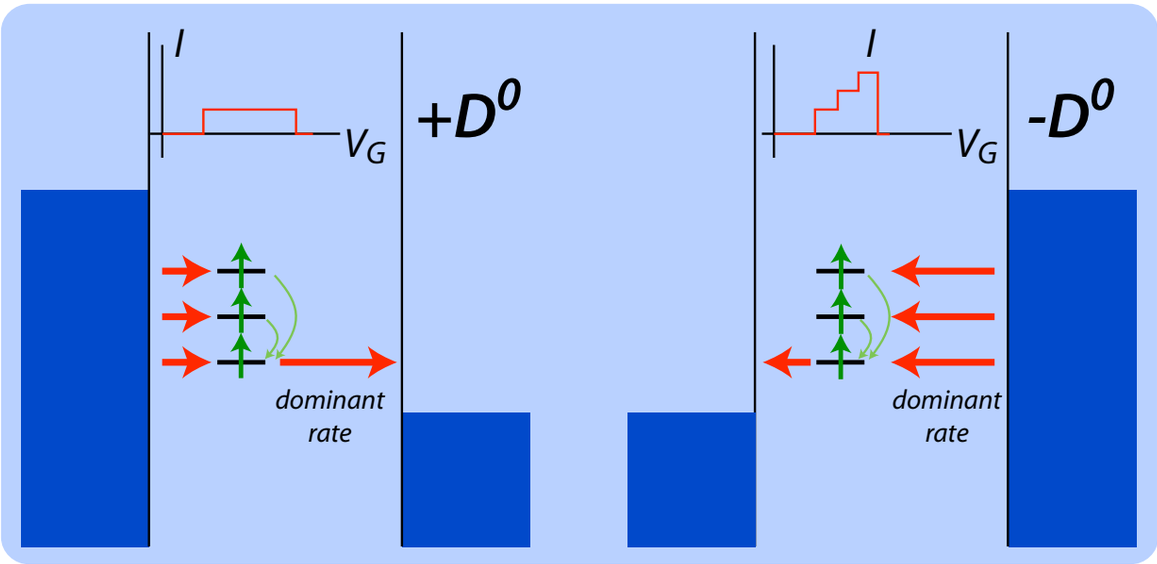

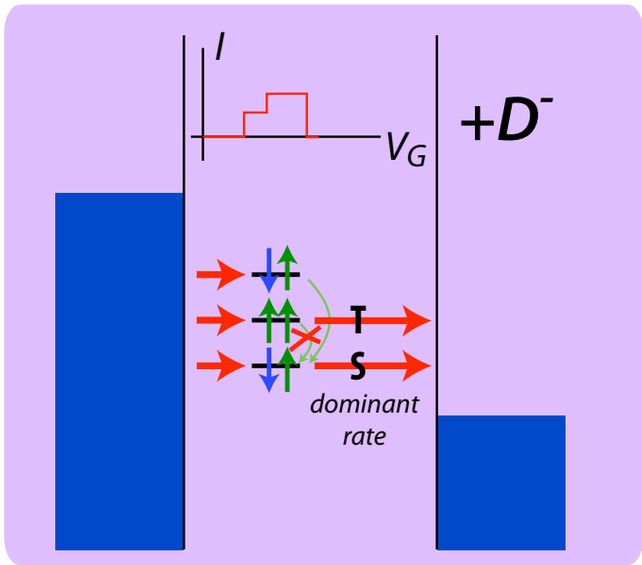

Information about relaxation processes

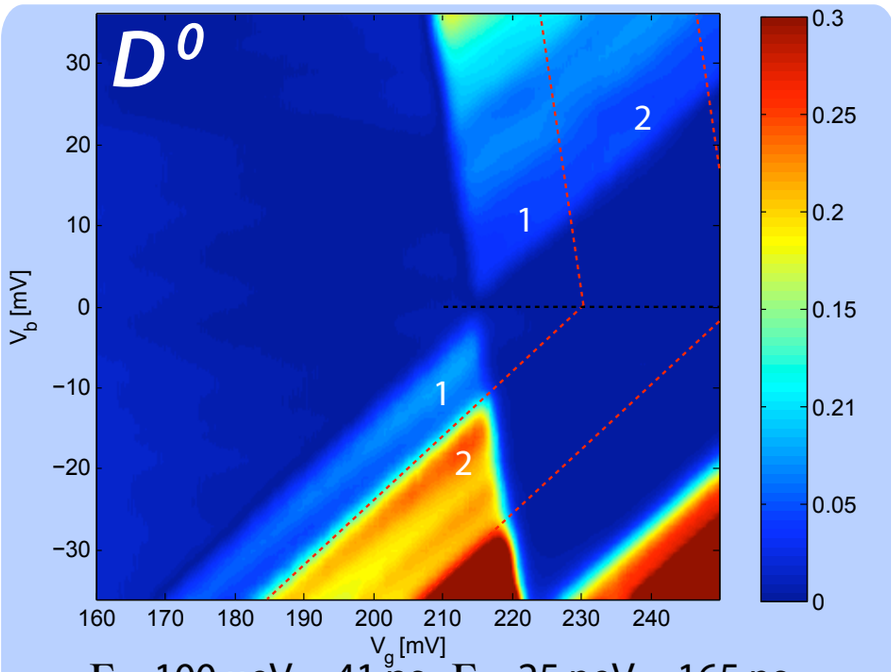

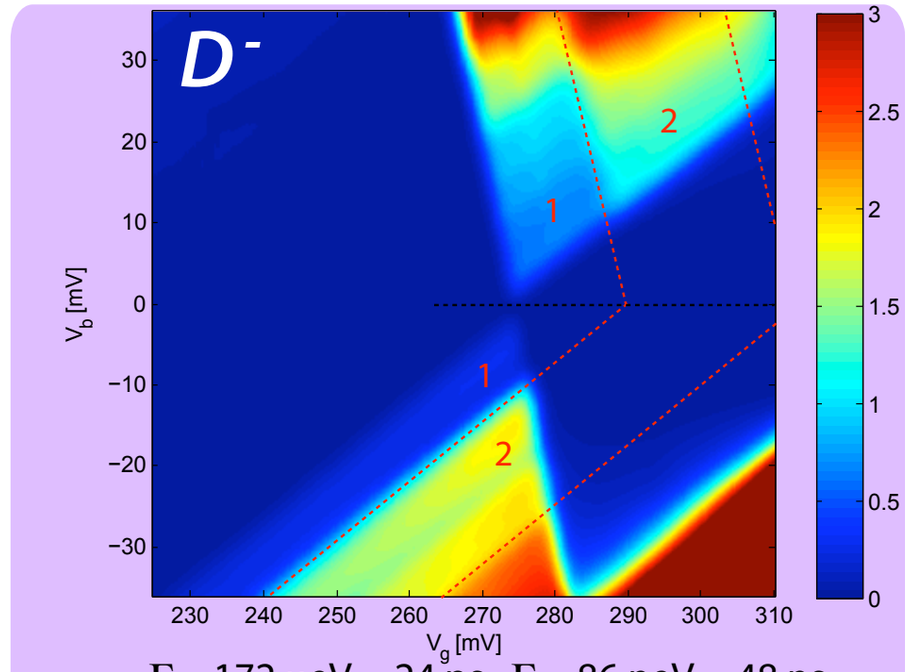

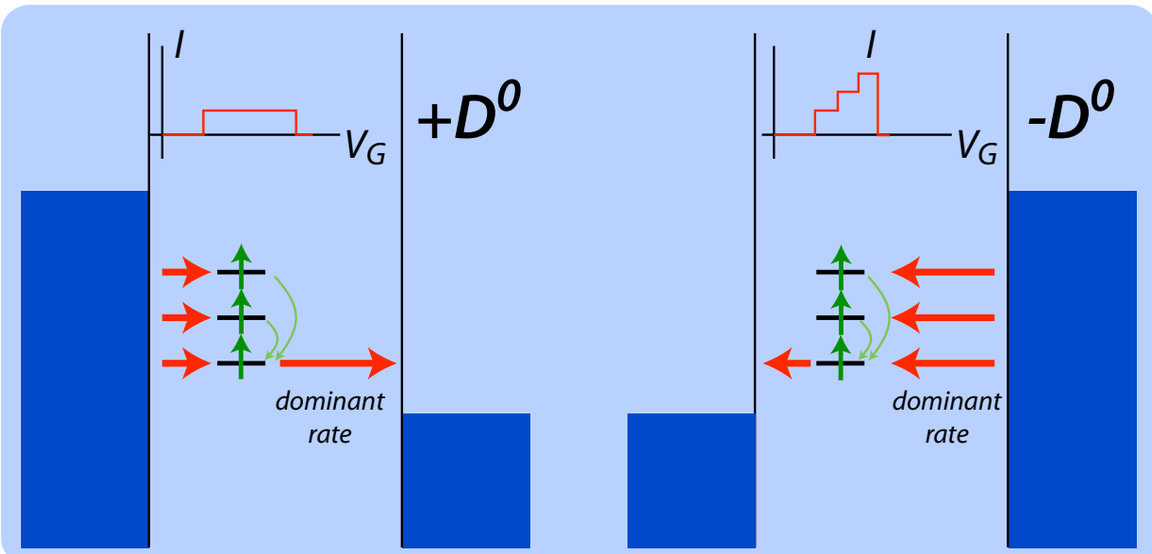

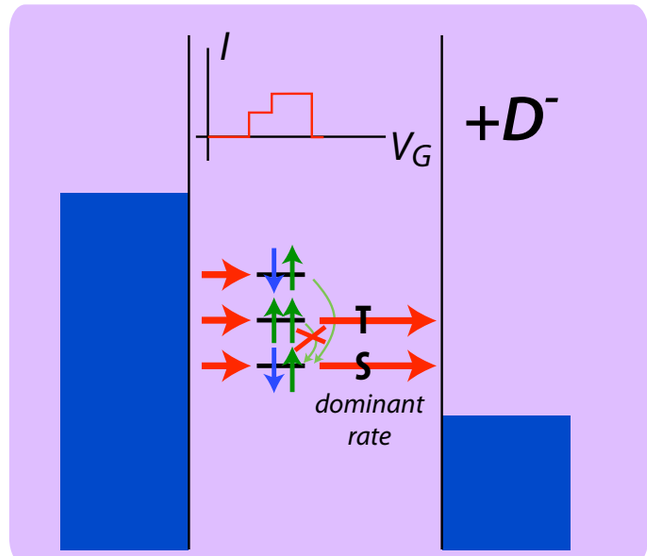

- electron leaves from ground state unless this transition is blocked ⇒ LET [NP 4, 540, 2008]
- orbital exited lifetimes are short (~30ps [JAP 102, 093104, 2007]), gated D^- relaxation observed as slow as 50ns!?

Slow relaxation due to spin & valley selection rules

theory symmetry	theory [meV]	exp. [meV]
singlet ee	0.0	0
triplet eo	1.5	1
singlet eo	1.6	
singlet oo	1.7	
2nd manifold	7.9	9
triplet ee	11.2	

F, d value from D0 data

$\varphi_e = |k_+\rangle + |k_-\rangle$ or $\varphi_o = |k_+\rangle - |k_-\rangle$

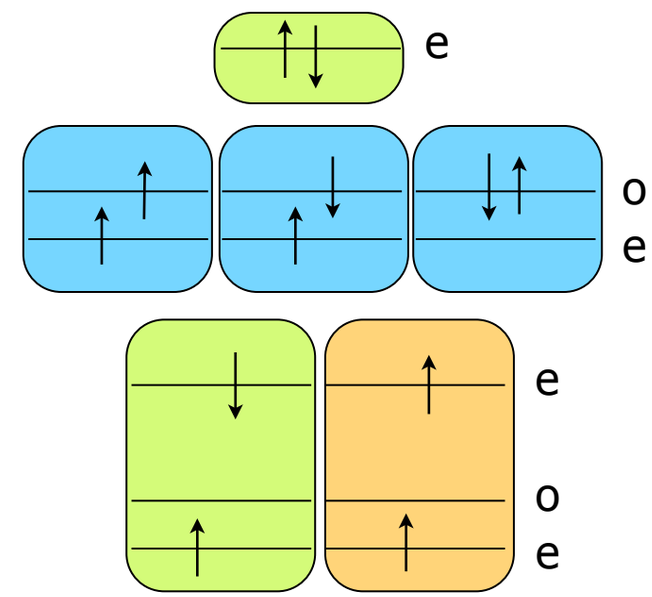

spin & valley configuration

- model fits: charging energy & excited manifolds qualitatively agree
- first excited manifold presides in orthogonal valleys and shows **vanishing exchange***
- slow decay ⇒ LET due to combined spin **& valley selection rules**

* Y. Hada and M. Eto, Phys. Rev. B **68**, 155322 (2003)

Single-dopants transient-current spectroscopy

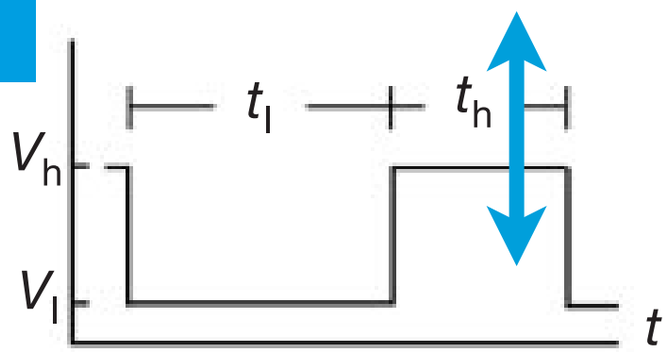

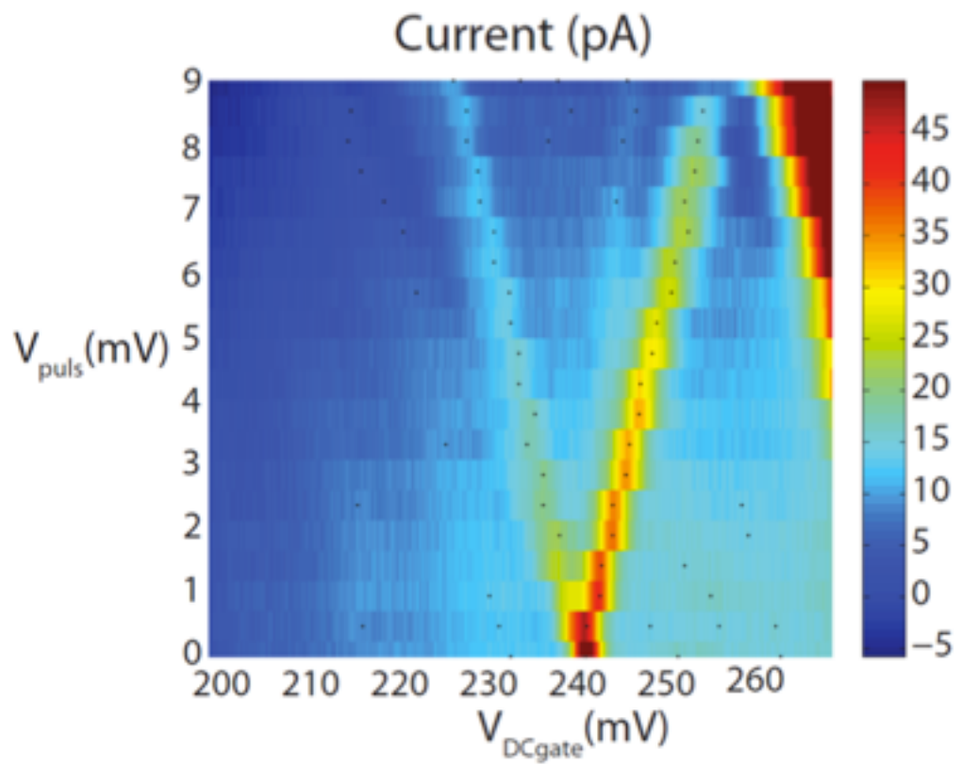

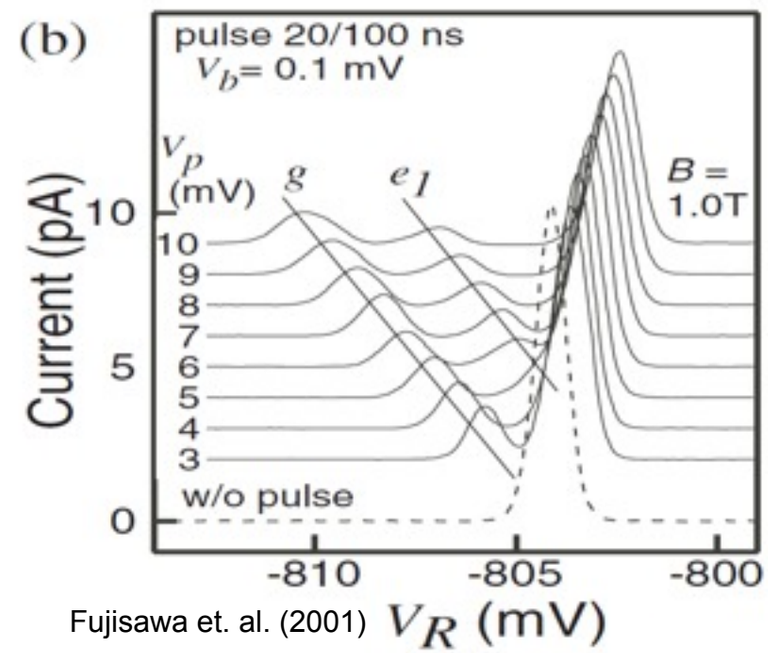

Fujisawa et. al. (2001)

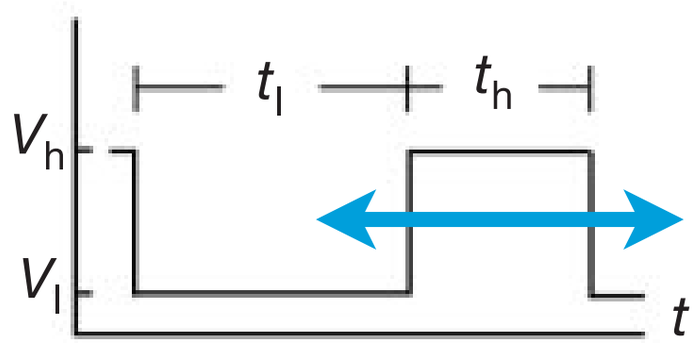

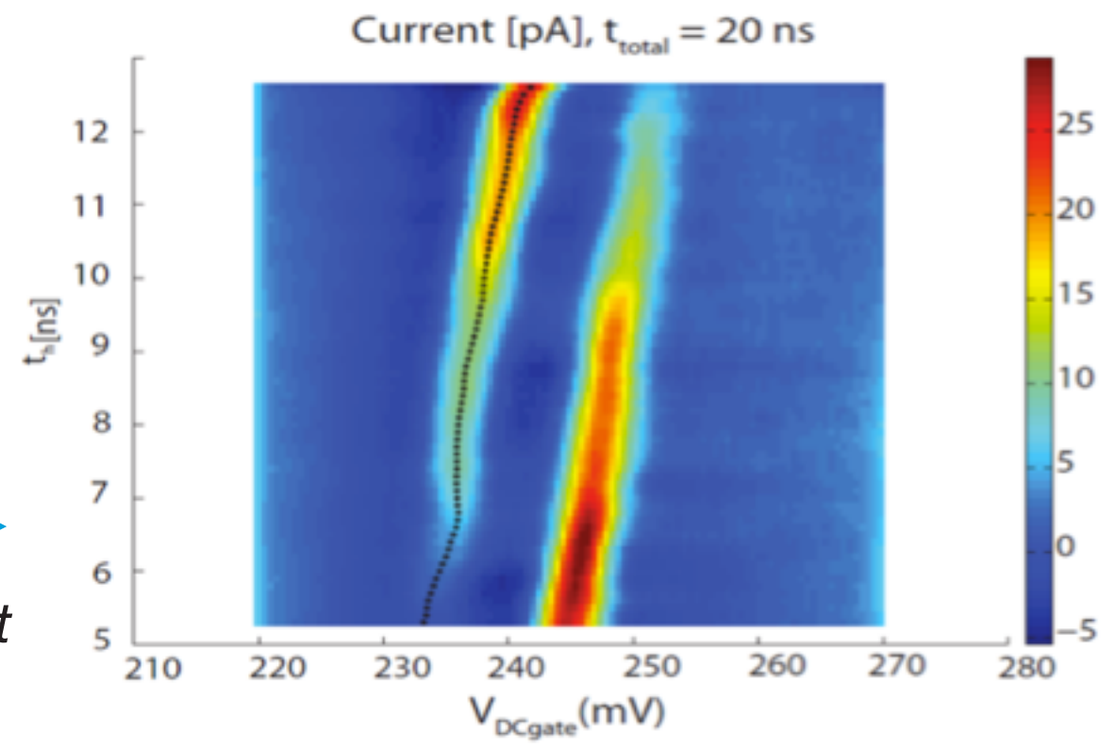

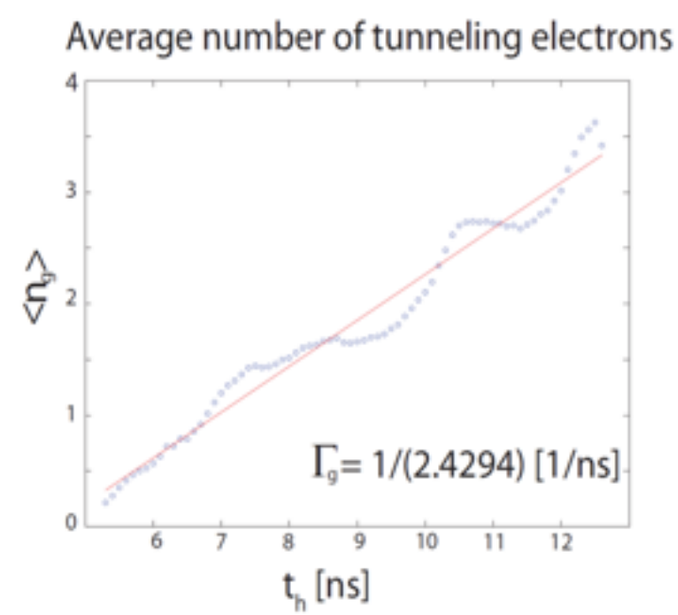

Determination of scattering in the channel: shot noise

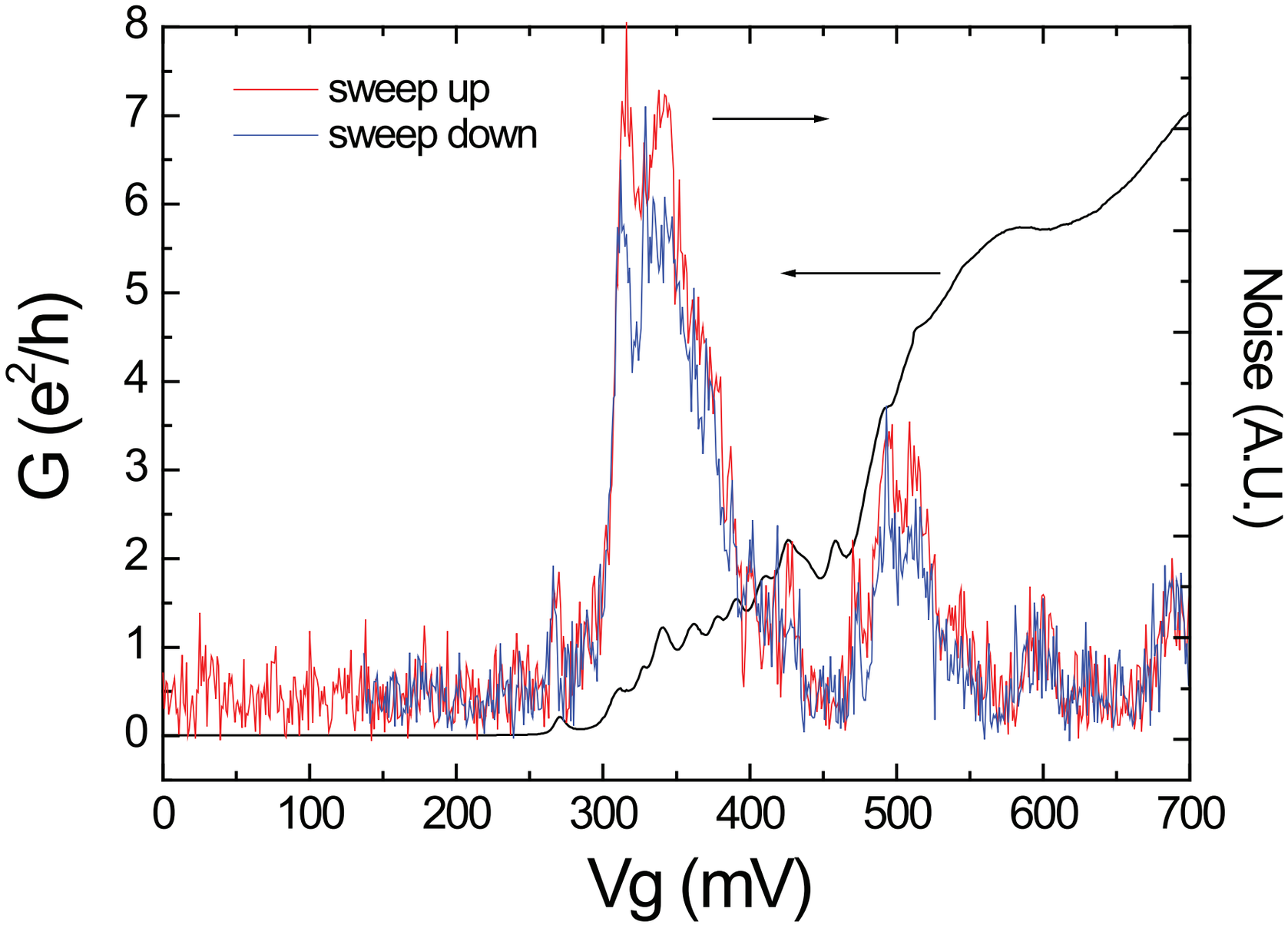

Shot-noise suppression [Reznikov PRL 75, 3340, 1995] when channel is fully open consistent with blastic transport in these narrow channels.

Summary

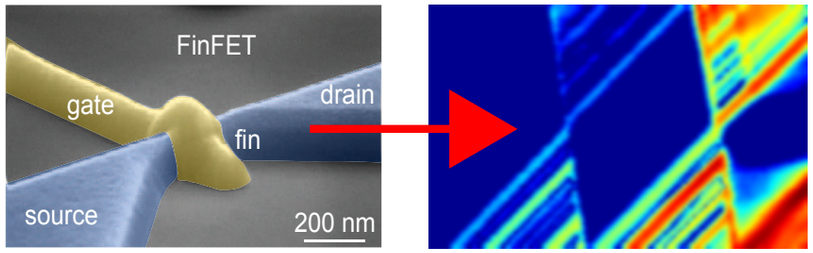

- **What can we learn from transport in nanoFETs?**
  - electrical channel length / extend of the SD region
  - variability - dopant density in the channel
  - spectrum: chemical species & environment

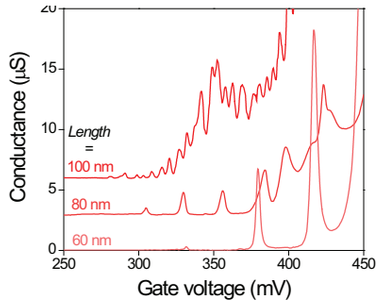

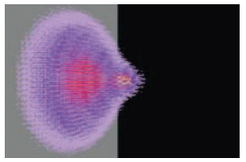

- **Beyond level spectroscopy**
  - spin and orbital relaxations
  - probe coherence
  - determine scattering in channel
  - future: manipulate spin and orbital state

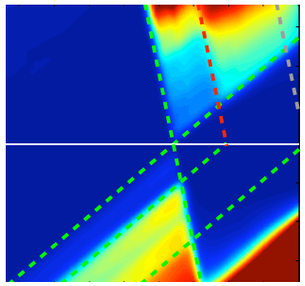

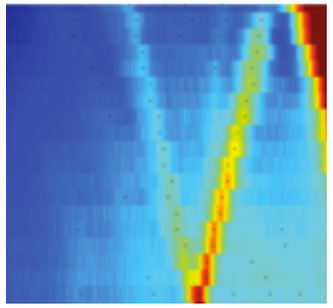

Acknowledgments

- **IMEC**
  N. Collaert, S. Biesemans (FinFETs)
- **Purdue**
  R. Rahman (→SNL), G. Klimeck (tight-binding)
- **Melbourne**
  L.C.L. Hollenberg (theory)
  B.C. Johnson, C. Yang, D.N. Jamieson (single-ion implantation)
- **Grenoble**
  R. Wacquez, M. Vinet, M. Sanquer (multi-gate FinFETs)
- **Delft**
  J.Heijden, J.Verduijn, J.Mol, G.C.Tettamanzi, G.P.Lansbergen (→NTT)

Single-dopant devices: Single-electron transport through single-dopants

Michiharu Tabe and Daniel Moraru

Research Institute of Electronics
SHIZUOKA UNIVERSITY

OUTLINE

1. Introduction

2. Progress over the past five years
   - 1-donor FET: single-electron transistor
   - 2-donor FET: single-electron memory
   - 3-donor FET: single-electron turnstile
   - Single photon detection
   - Observation of dopants by LT-KFM

3. Challenges for the next ten years

4. Summary

self-capacitance of single donor

P in Si

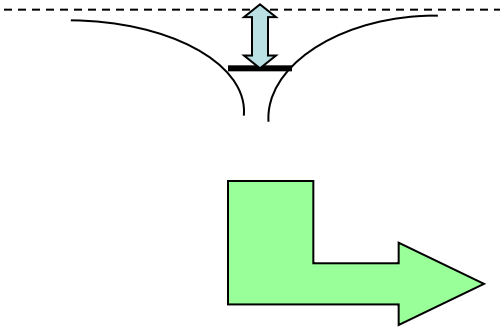

metal dot & outer shell approximation

r = a

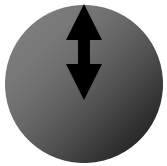

self-capacitance of single donor

P in Si

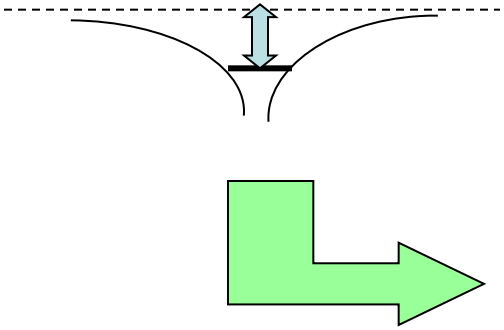

metal dot & outer shell approximation

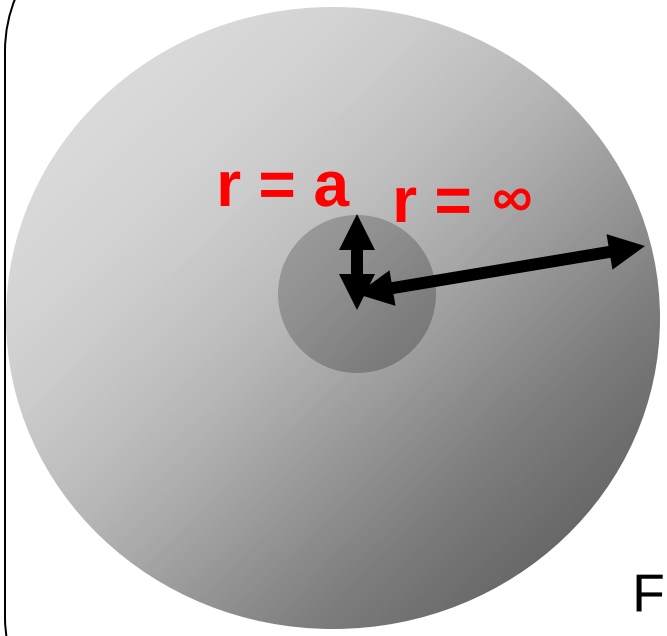

$C = 4\pi\varepsilon_0\varepsilon\, a = 3aF$

(a=3nm)

$E_{charge} = e^2 / 2C$

$= 30$ meV

For 2nd electron, potential well almost disappears due to e-e interaction.

self-capacitance of single donor

P in Si

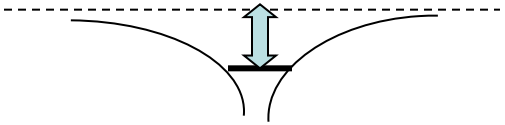

metal dot & outer shell approximation

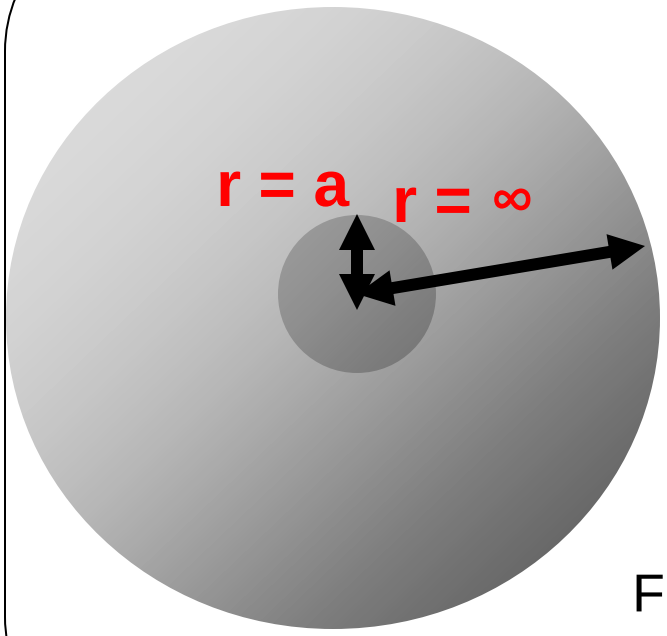

$C = 4\pi\varepsilon_0\varepsilon\, a = 3aF$
(a=3nm)

$E_{charge} = e^2 / 2C$
$= 30$ meV

For 2nd electron, potential well almost disappears due to e-e interaction.

The donor quantum dot effectively works as one-electron trap.

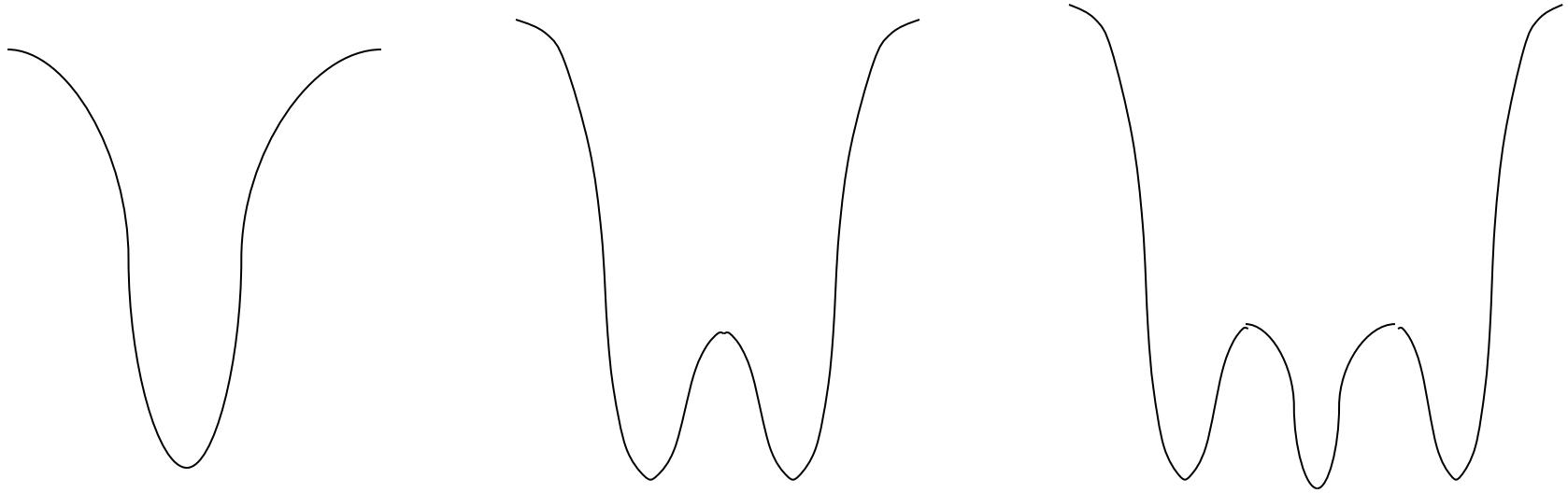

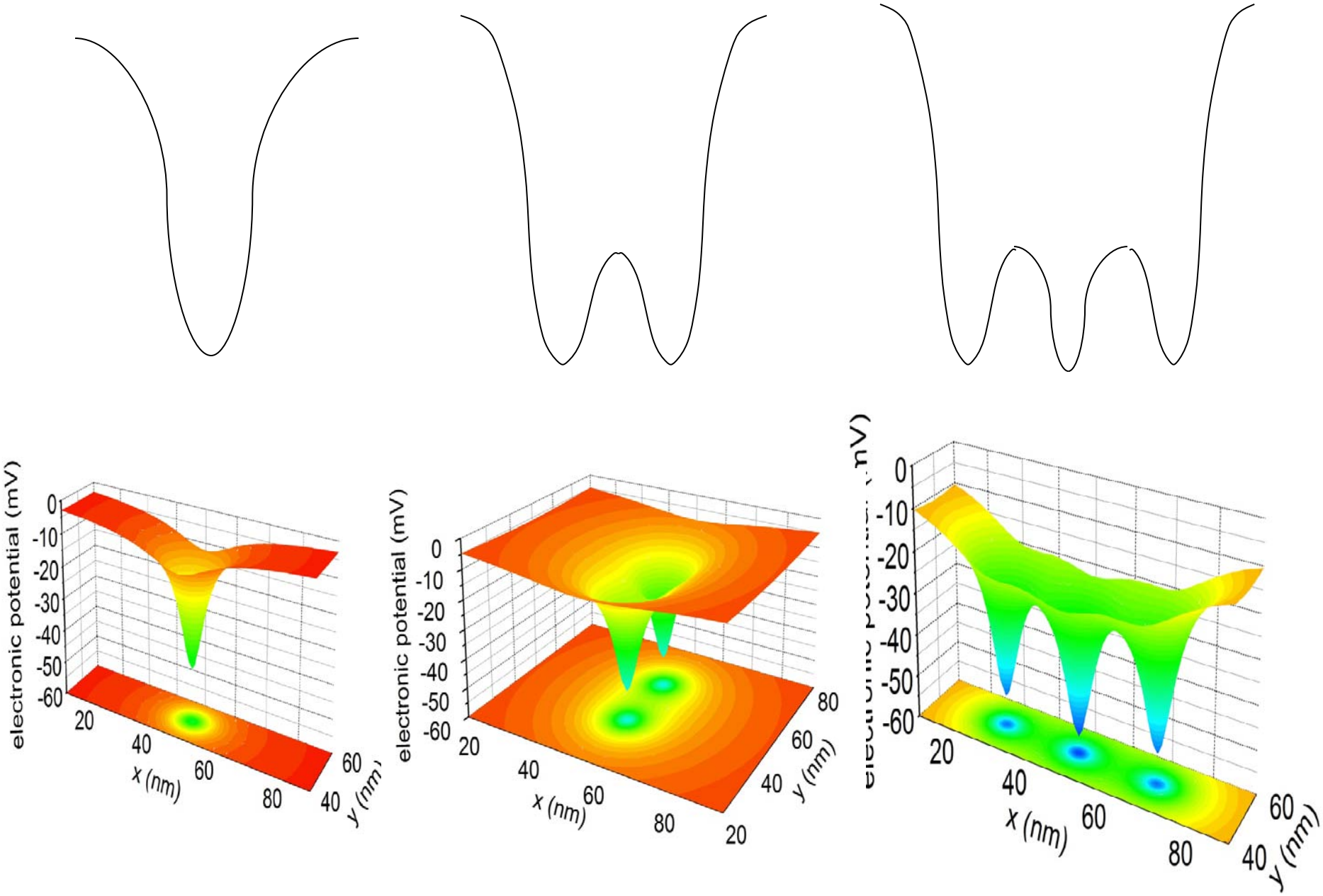
electronic potential (mV)
0
-10
-20
-30
-40
-50
-60
20
40
60
80
x (nm)
y (nm)

OUTLINE

1. Introduction

2. Progress over the past five years
   - 1-donor FET: single-electron transistor
   - 2-donor FET: single-electron memory
   - 3-donor FET: single-electron turnstile
   - Single photon detection
   - Observation of dopants by LT-KFM

3. Challenges for the next ten years

4. Summary

1-donor FET: single-electron transistor

single-dopant FET

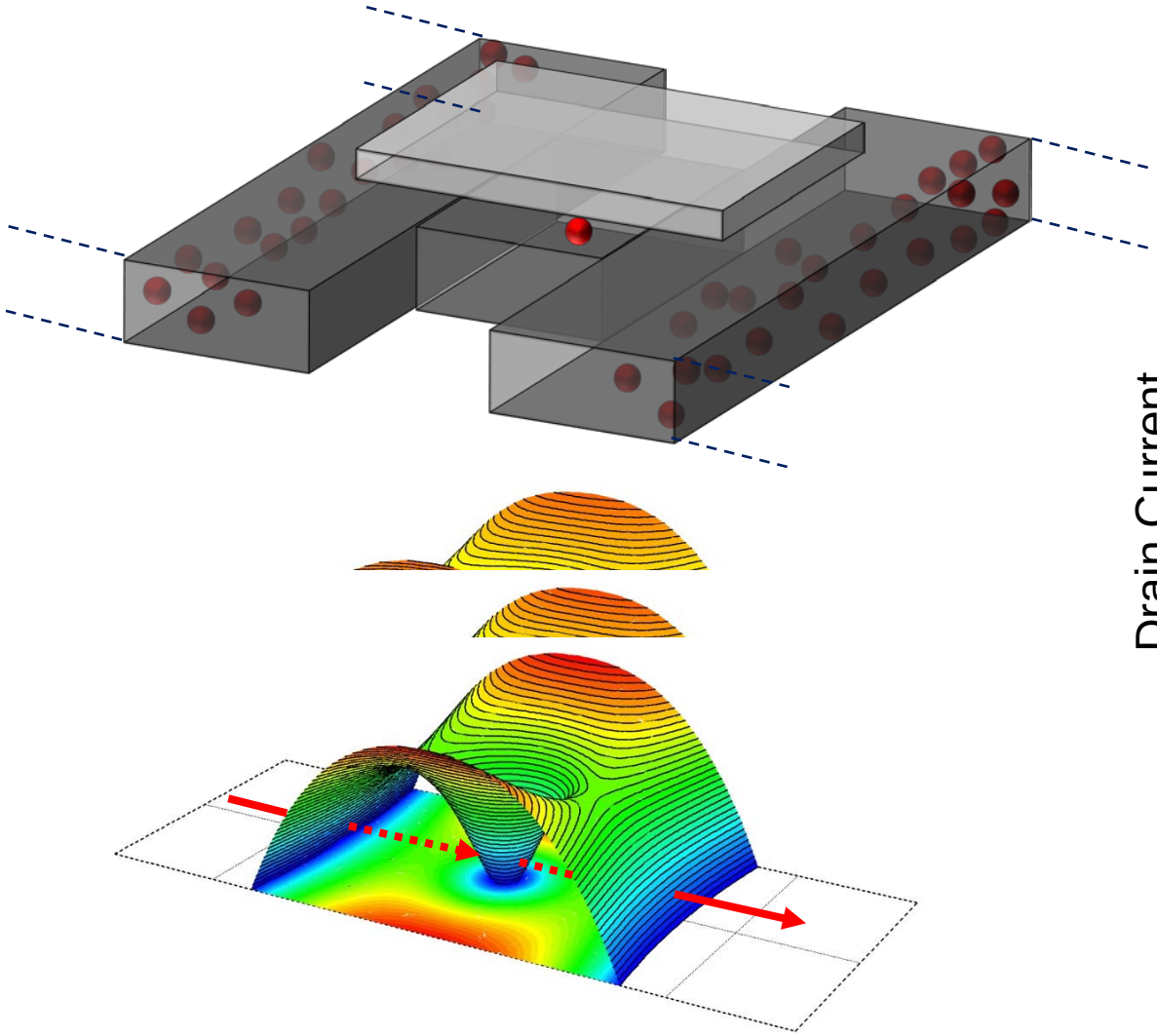

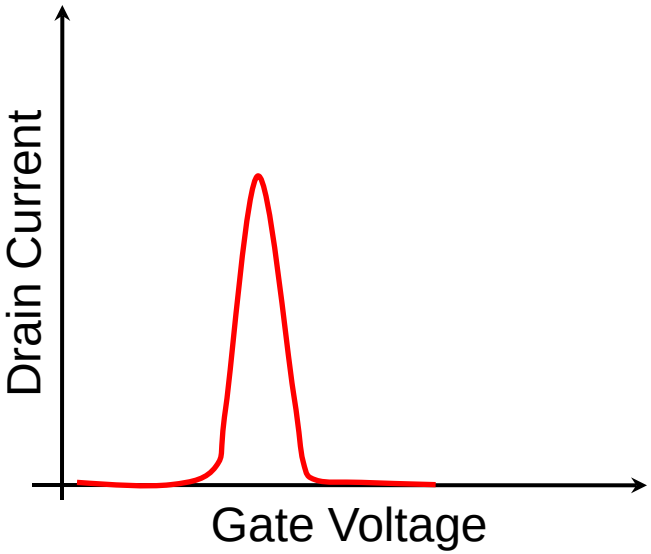

Single donor effect in Si FinFET

PRL vol. 97, 206805 (2006)

Transport Spectroscopy of a Single Dopant in a Gated Silicon Nanowire

H. Sellier,* G. P. Lansbergen, J. Caro, and S. Rogge
Kavli Institute of Nanoscience, Delft University of Technology, Lorentzweg 1, 2628 CJ Delft, The Netherlands

N. Collaert, I. Ferain, M. Jurczak, and S. Biesemans
InterUniversity Microelectronics Center (IMEC), Kapeldreef 75, 3001 Leuven, Belgium
(Received 17 July 2006; published 16 November 2006)

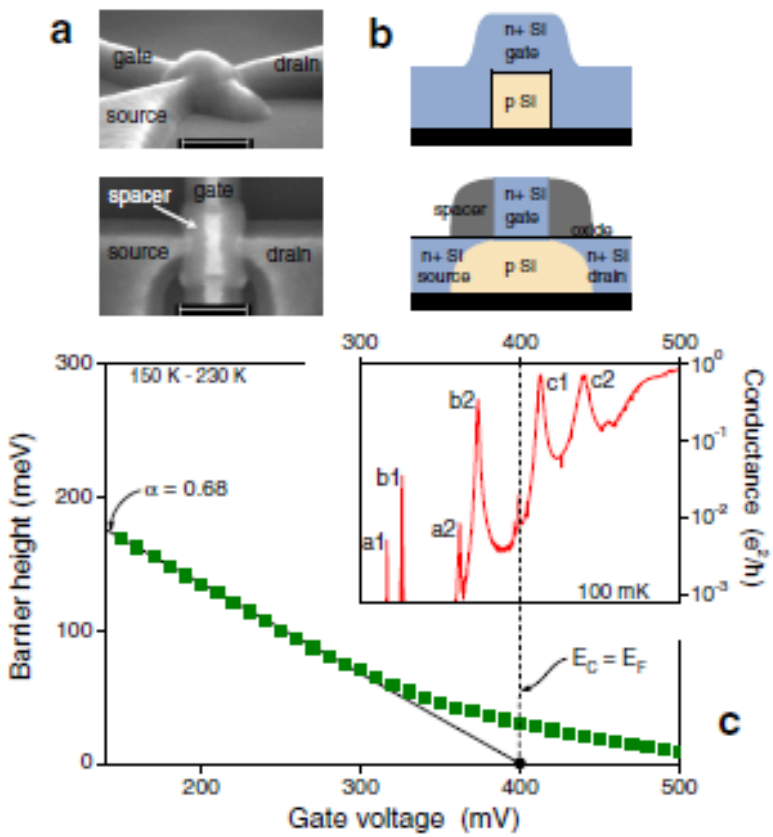

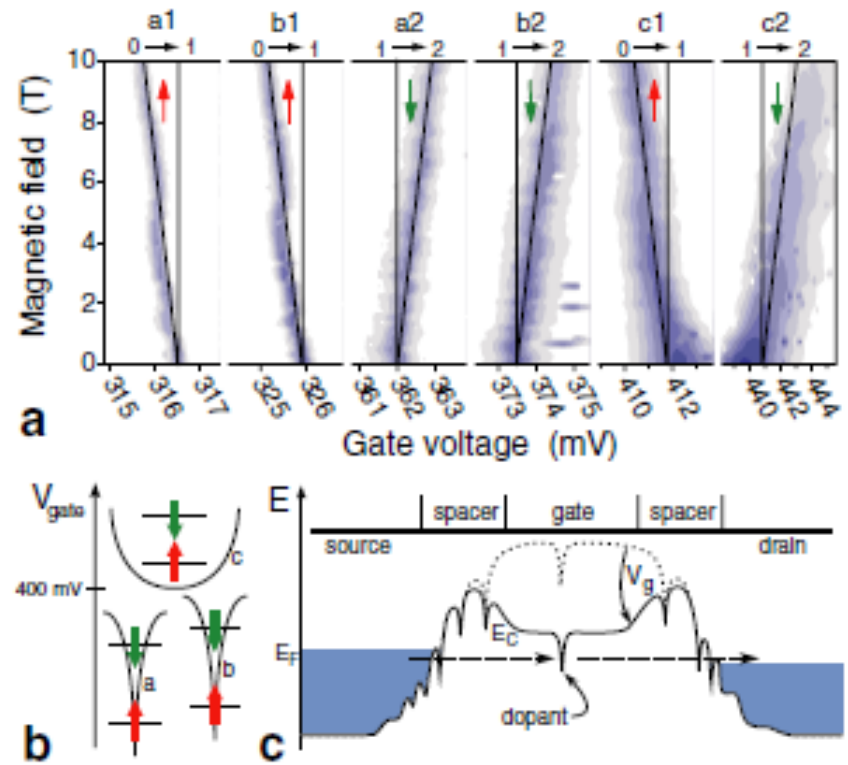

Single acceptor effect in Si FET

Appl. Phys. Lett. **90**, 102106 (2007)

Conductance modulation by individual acceptors in Si nanoscale field-effect transistors

Y. Ono,[a] K. Nishiguchi, A. Fujiwara, and H. Yamaguchi
NTT Basic Research Laboratories, NTT Corporation, 3-1 Morinosato- Wakamiya, Atsugi, Kanagawa 243-0198, Japan

H. Inokawa
Research Institute of Electronics, Shizuoka University, 3-5-1 Johoku, Hamamatsu 432-8011, Japan

Y. Takahashi
Graduate School of Information Science and Technology, Hokkaido University, Sapporo, Hokkaido 060-0814, Japan

(Received 18 November 2006; accepted 22 January 2007; published online 6 March 2007)

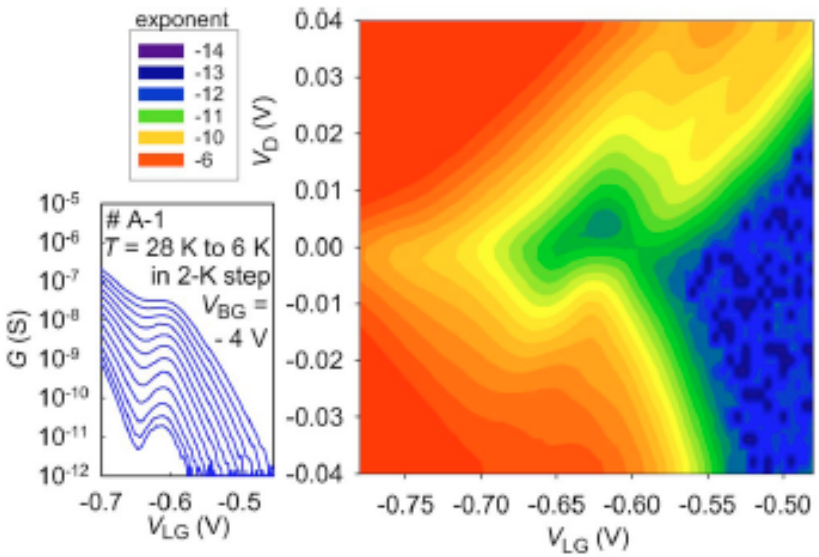

FIG. 3. (Color online) Left: Temperature dependence of the hump of sample A-1 (Fig. 2). V_{UG}=−5 V and V_D=−3 mV. Right: Contour diagram of the differential conductance in the V_D-V_{LG} plane measured at 6 K at V_{UG}= −5 V.

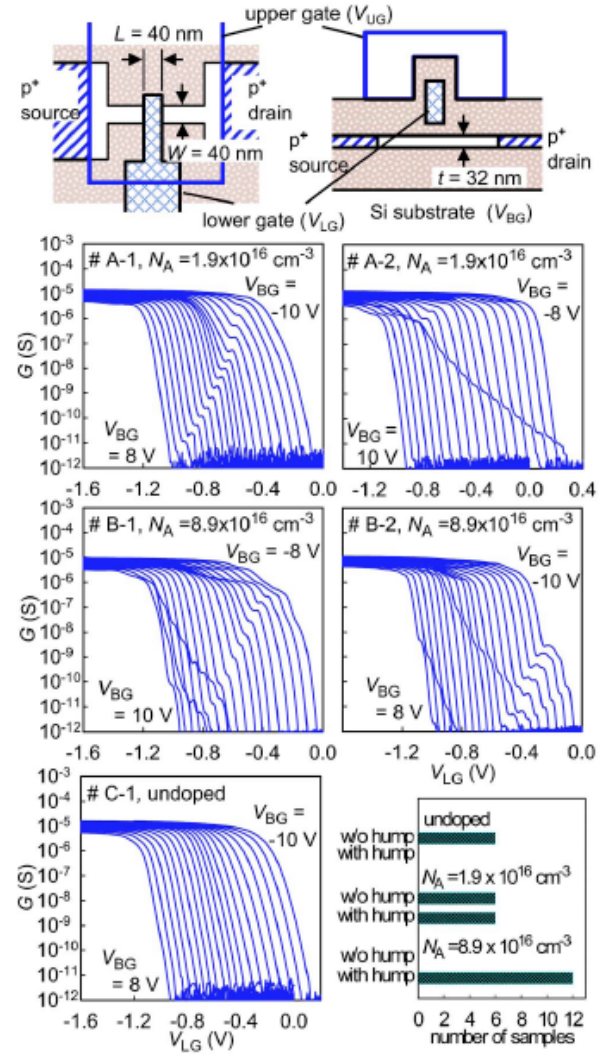

FIG. 2. (Color online) Top: Top and cross-sectional views of the nano-MOSFETs. Middle and bottom left: Conductance curve for doped and undoped MOSFETs measured at 26 K with V_{UG}=−5 V and V_D=−10 mV. The V_{BG} is changed in 1 V step. Bottom right: Histogram of the number of samples with and without the hump structures, based on the measurements at 26 K.

Single-dopant features in many dopants environment

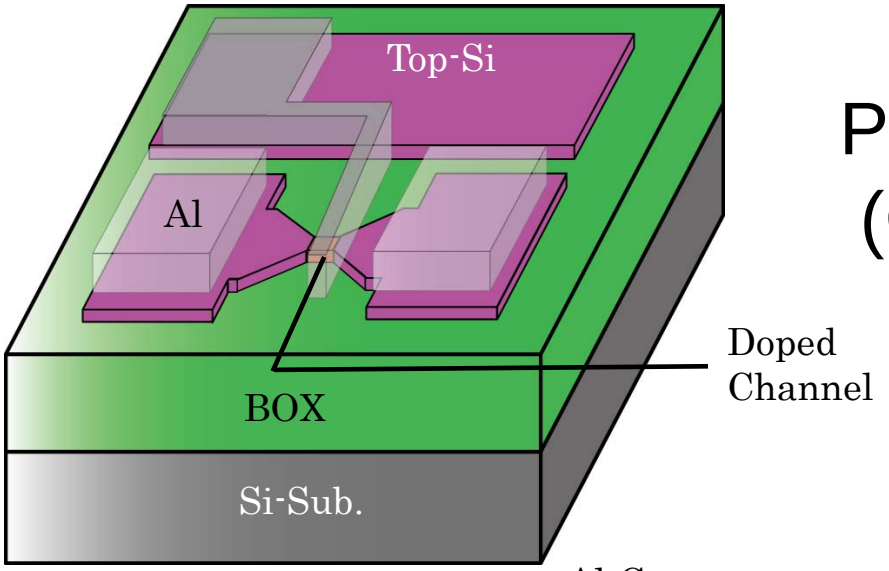

P-doped SOI MOSFET
(Cp=1E18 cm-3)

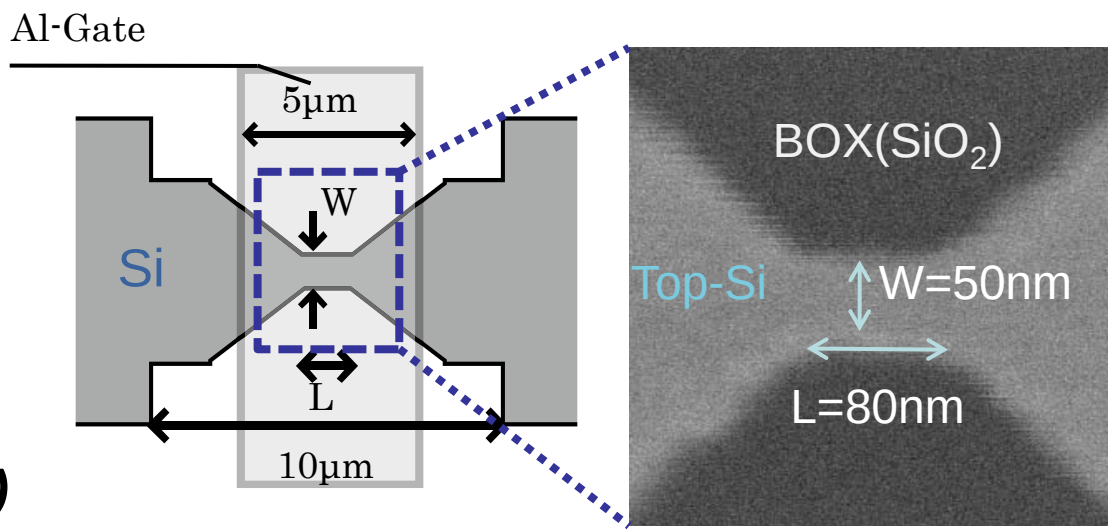

M.Tabe et al., PRL (2010)

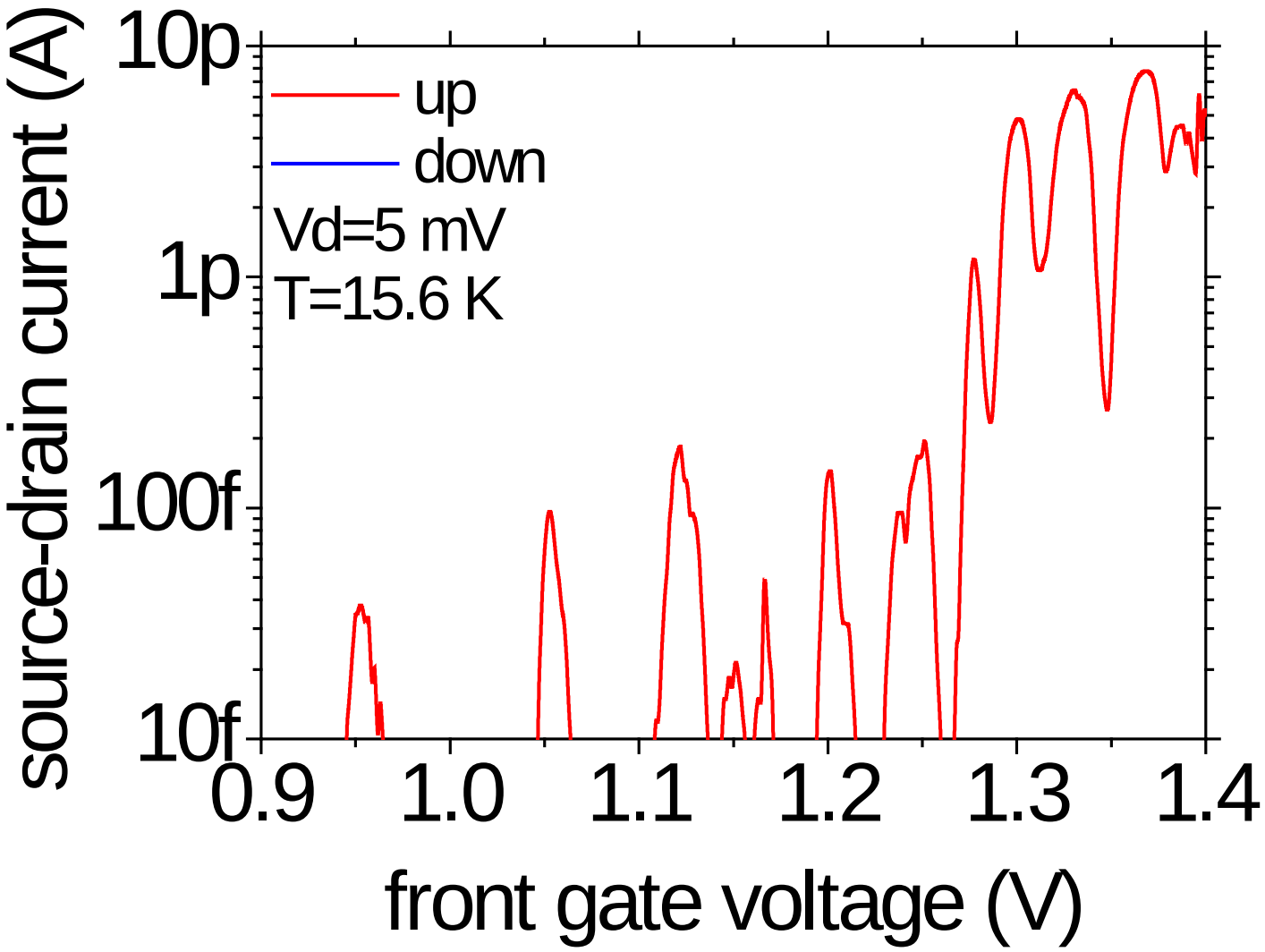
source-drain current (A)
10p
1p
100f
10f
up
down
Vd=5 mV
T=15.6 K
0.9
1.0
1.1
1.2
1.3
1.4
front gate voltage (V)

50nm×50nm FET

50nm×100nm-nanowire FET

50nm×150nm-nanowire FET

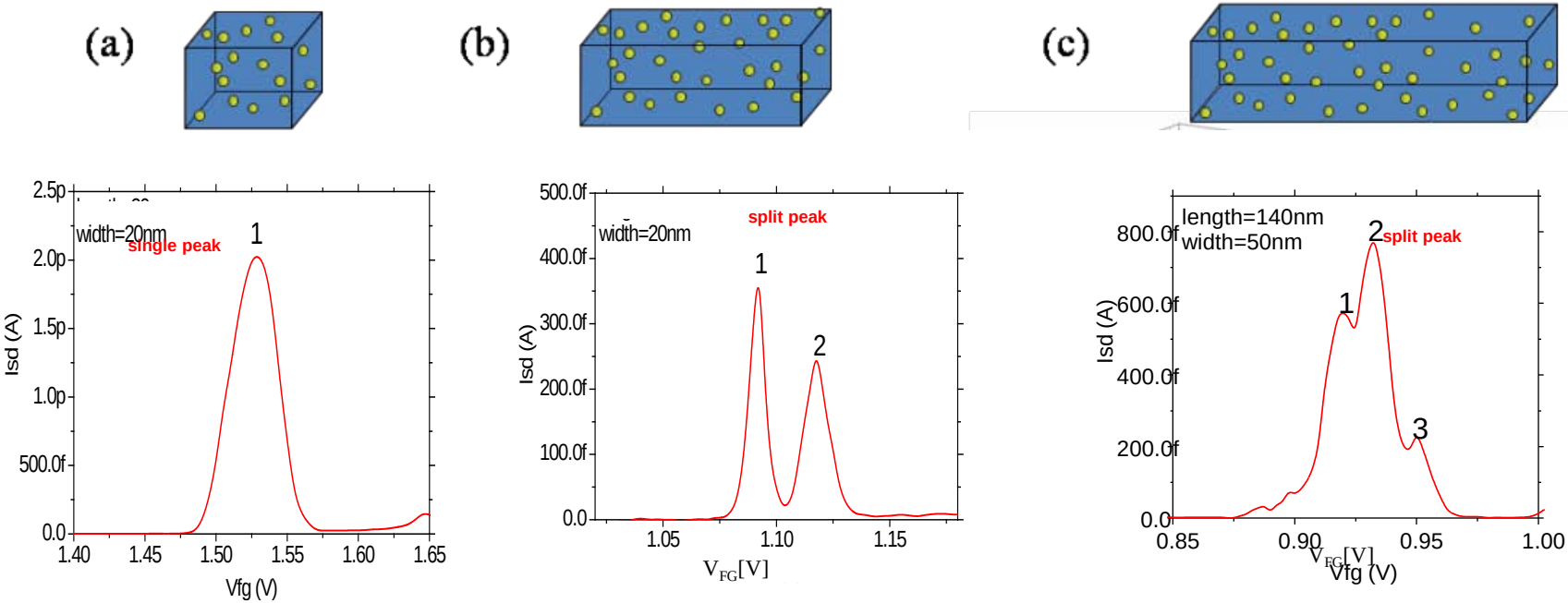

50nm×50nm FET

50nm×100nm-nanowire FET

50nm×150nm-nanowire FET

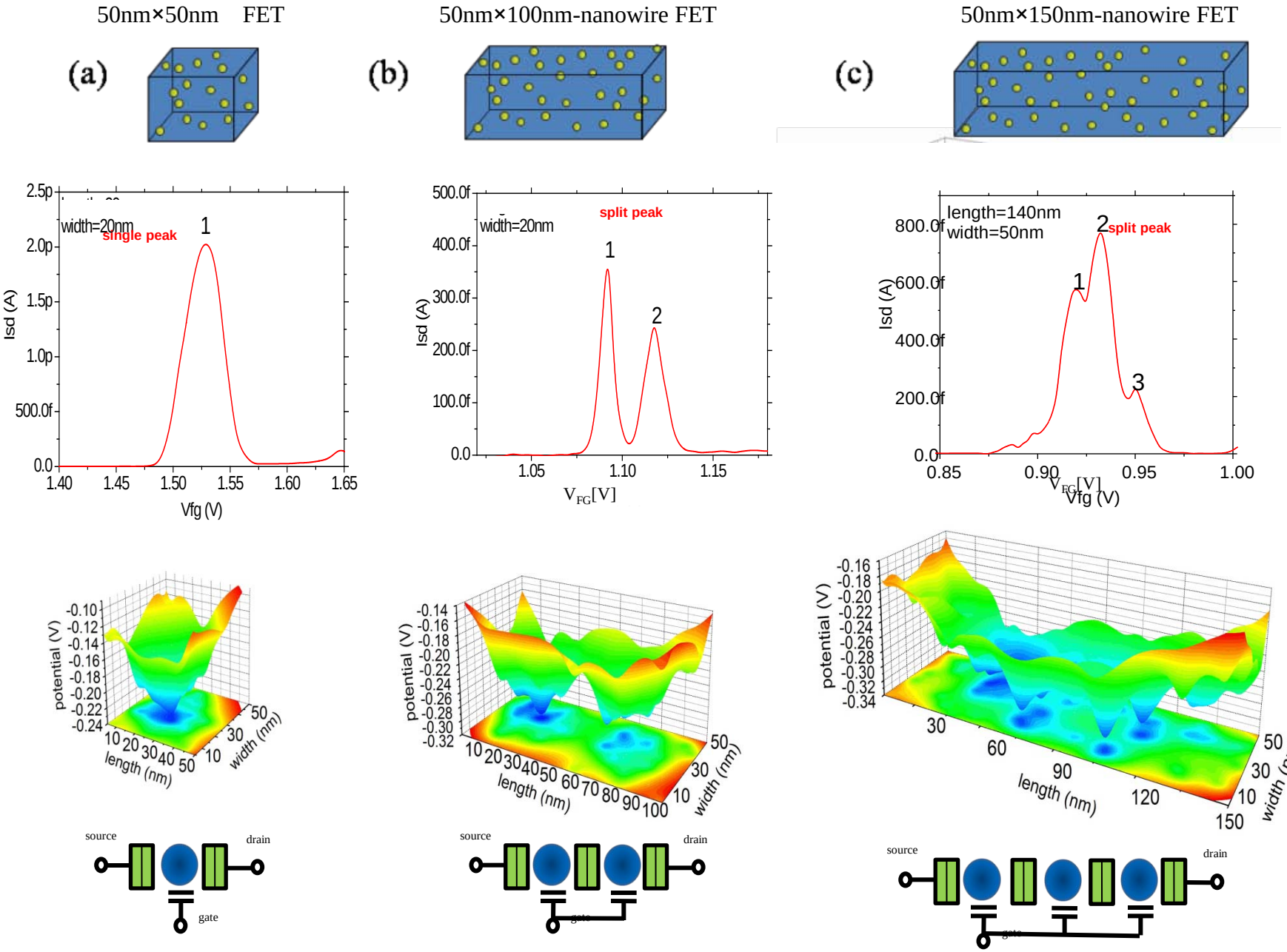

Channel length dependence - statistics

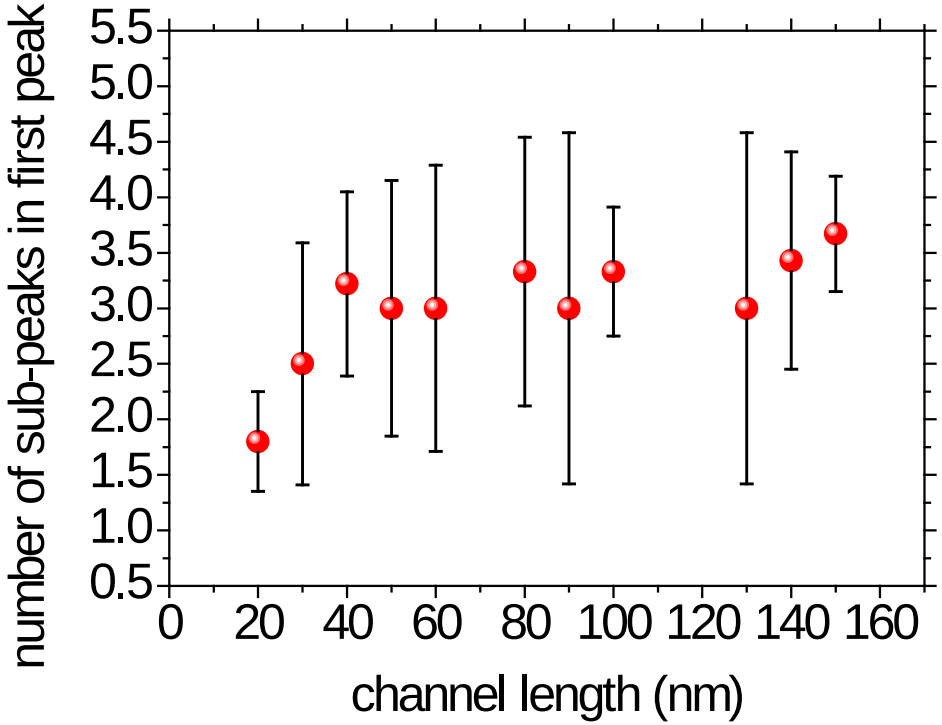

Number of sub-peaks increases with channel length !!!

In P-doped FETs, a single donor dominates I_d *vs*. V_g, statistically.

Can we make better control for this single dopant nature ?

Disk-shaped channel FETs

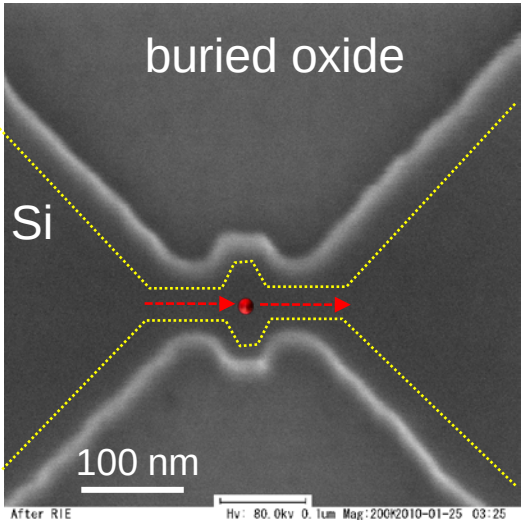

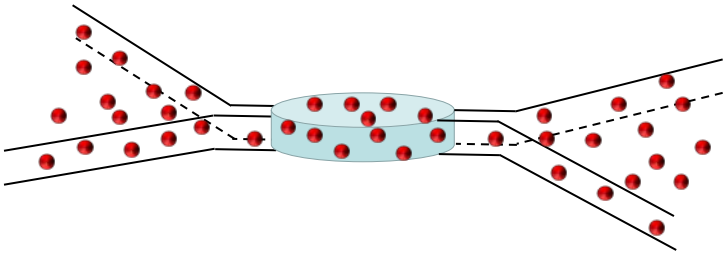

Disk-shaped channel FETs

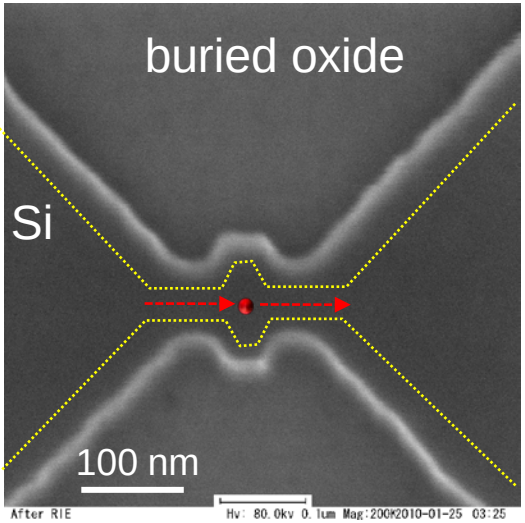

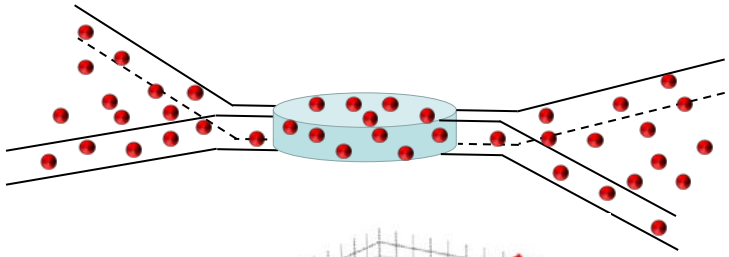

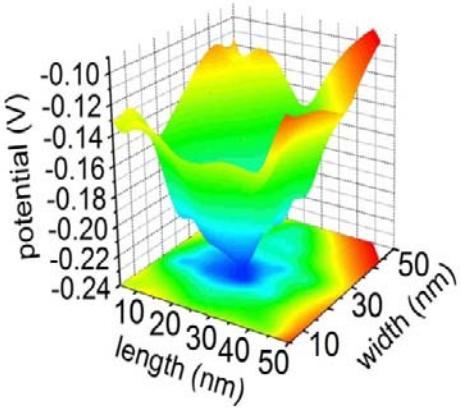

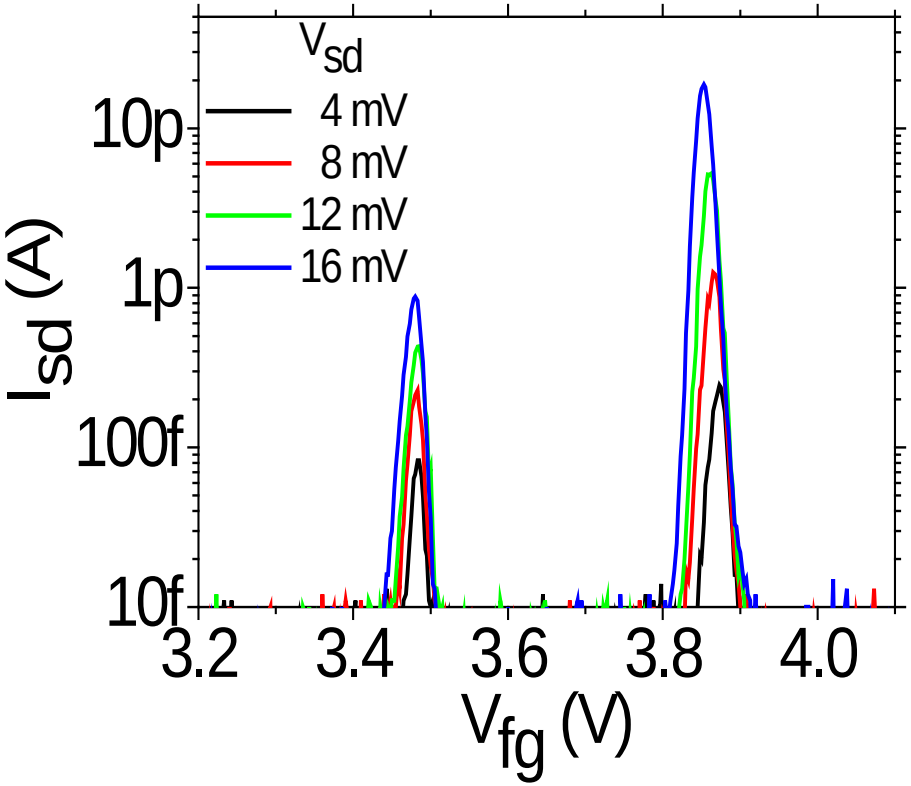

Isolated single-peaks

Single donor SET

M.Tabe et al., PRL (2010)

Disk-shaped channel FETs

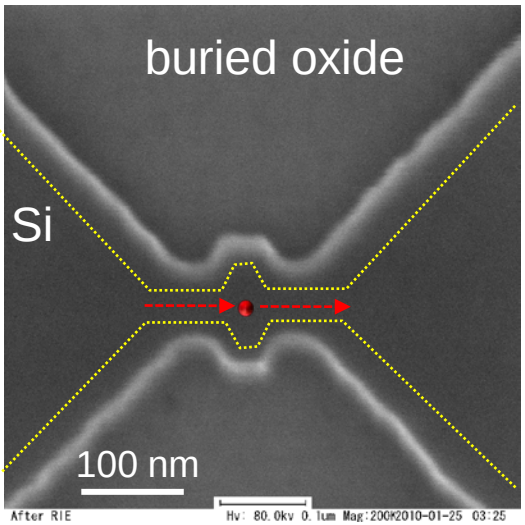

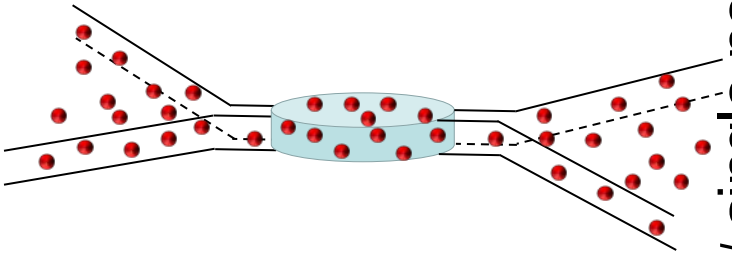

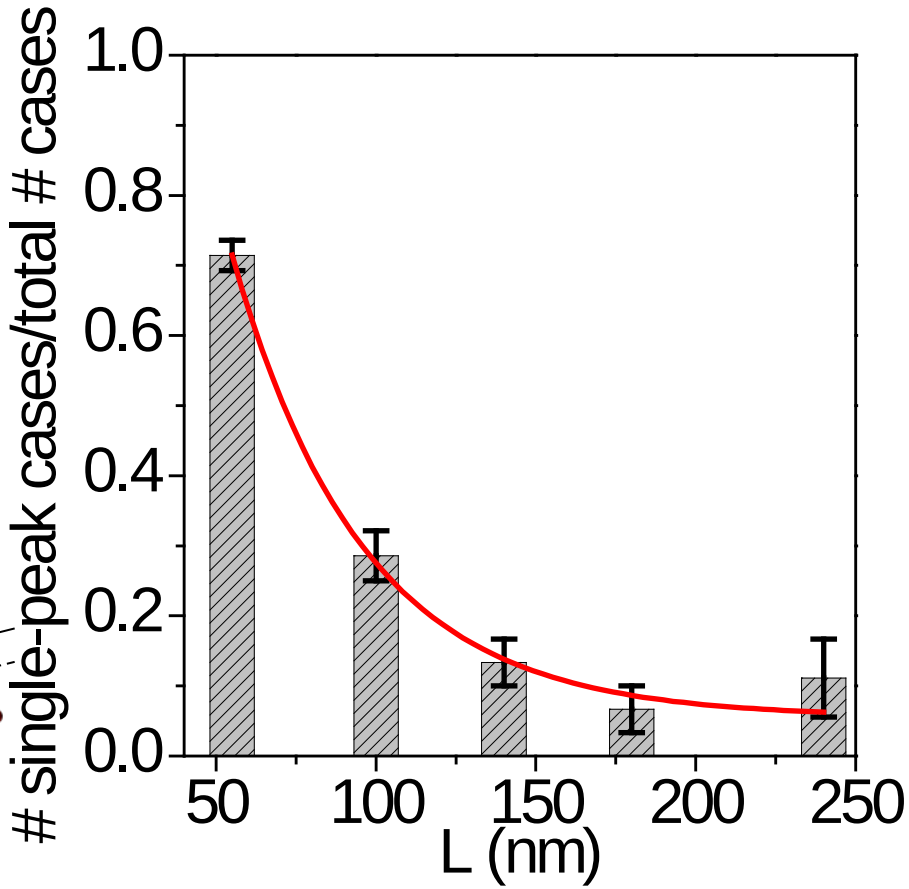

Disk pattern is effective for single-dopant-QD

2-donor FET: memory effect

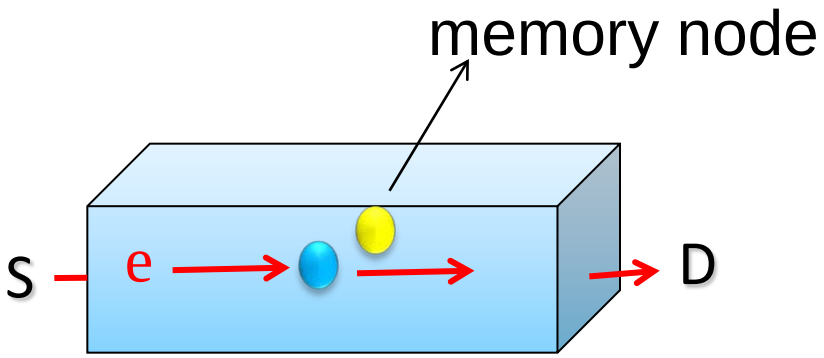

E. Hamid *et al*., Si Nanoelectronics Workshop (2010)

Device structure

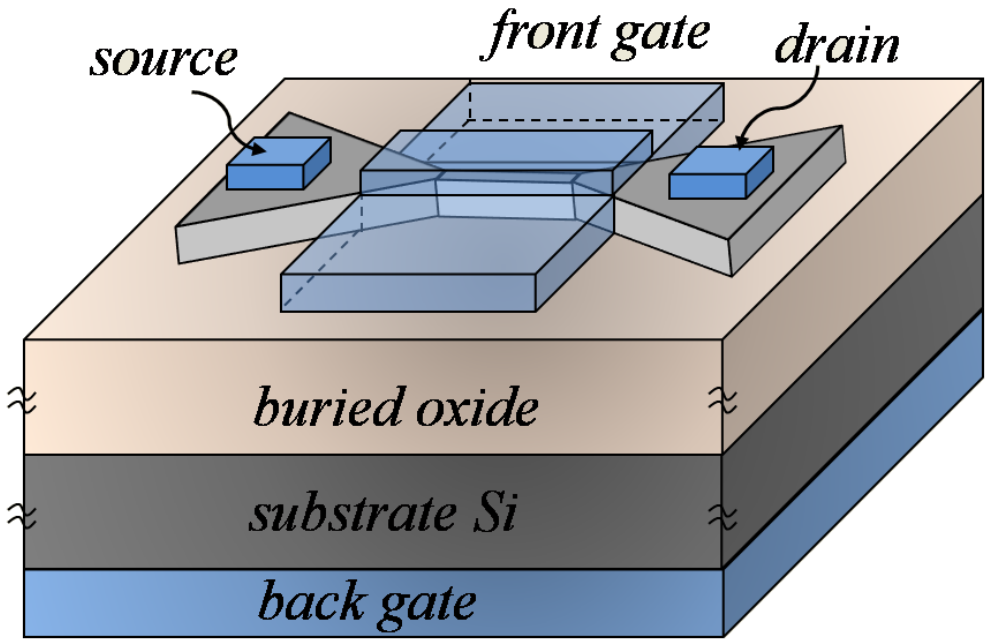

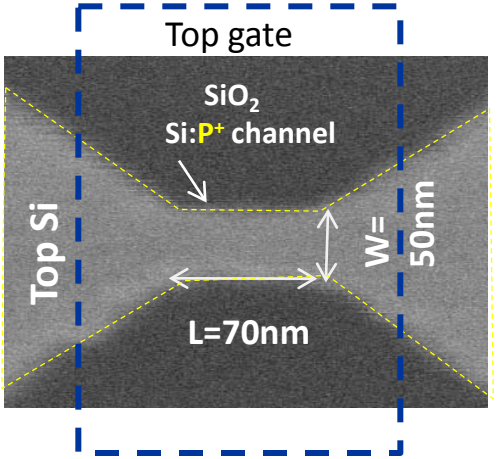

- Nd=1-3×10^{18} cm^{-3}
- Gate Oxide=10nm
- Top Si=10nm
- Buried oxide=400nm

I-V characteristics of the first peak

Charging effect

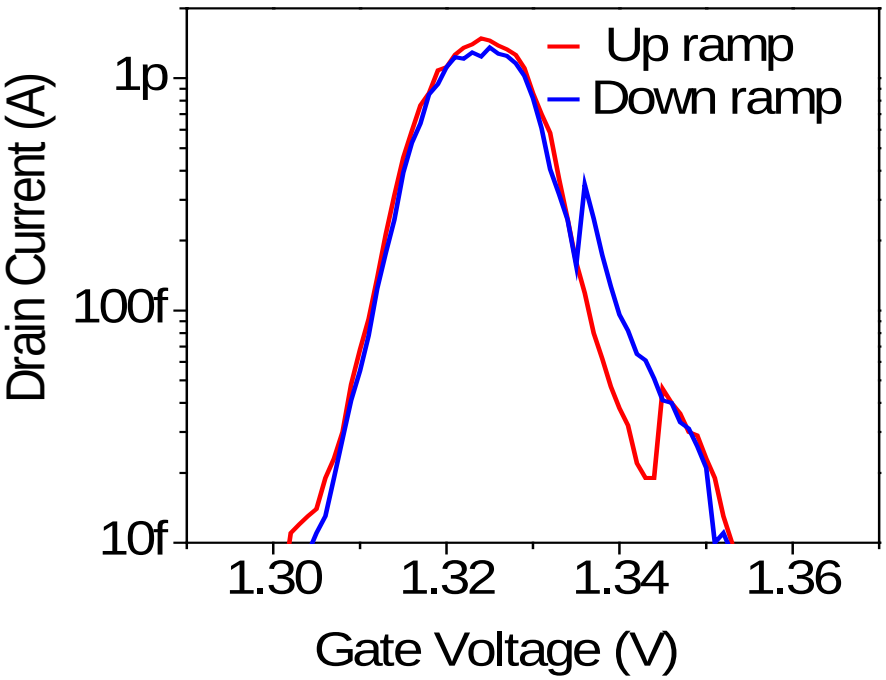

No charging effect

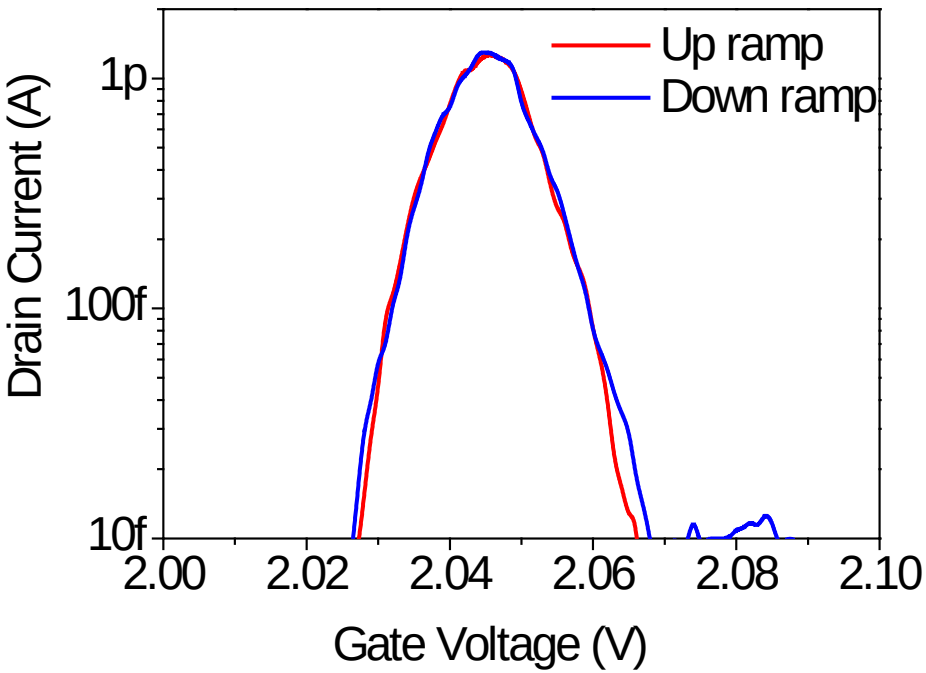

Model of charging effect

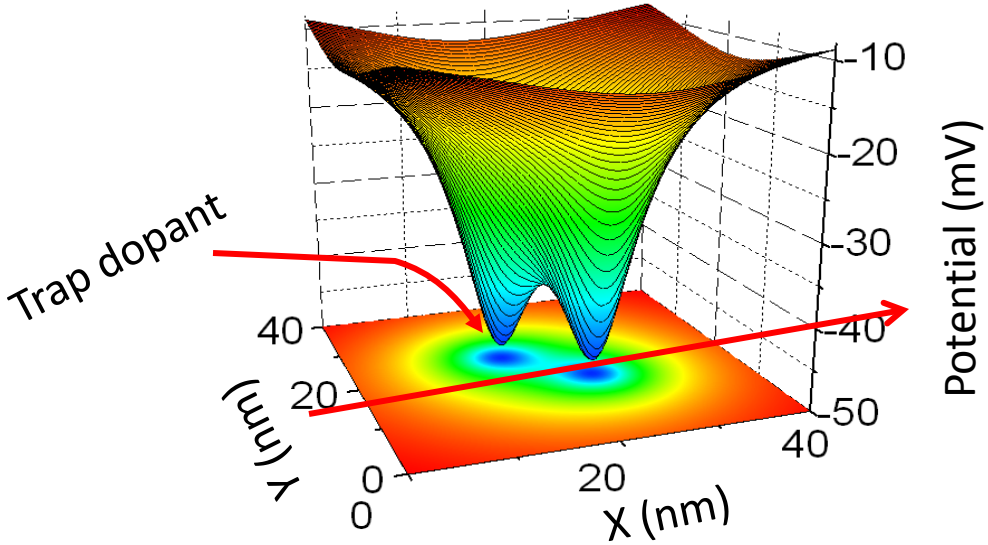

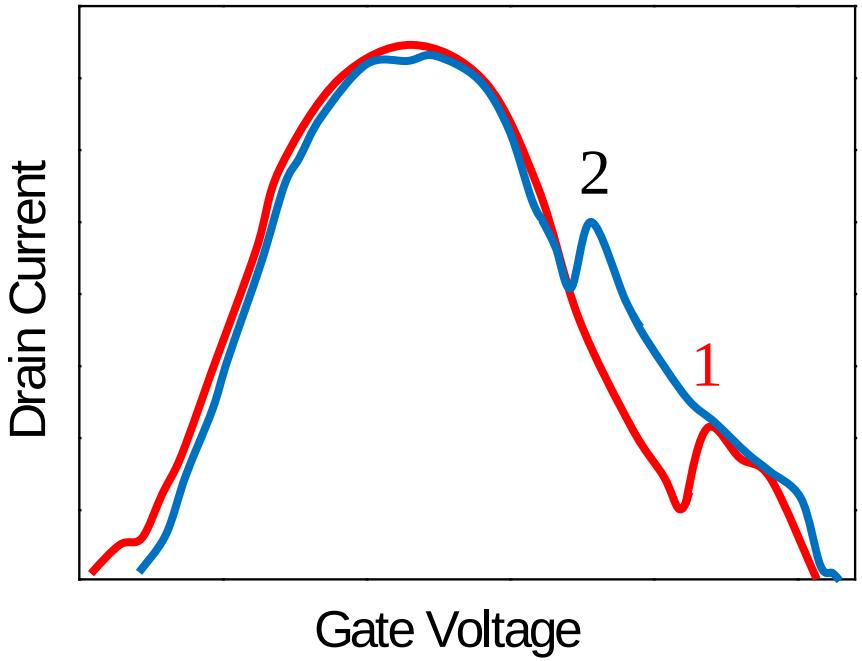

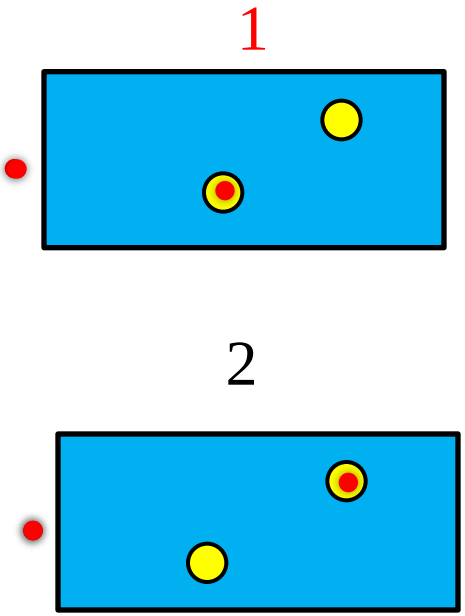

Id-time measurement

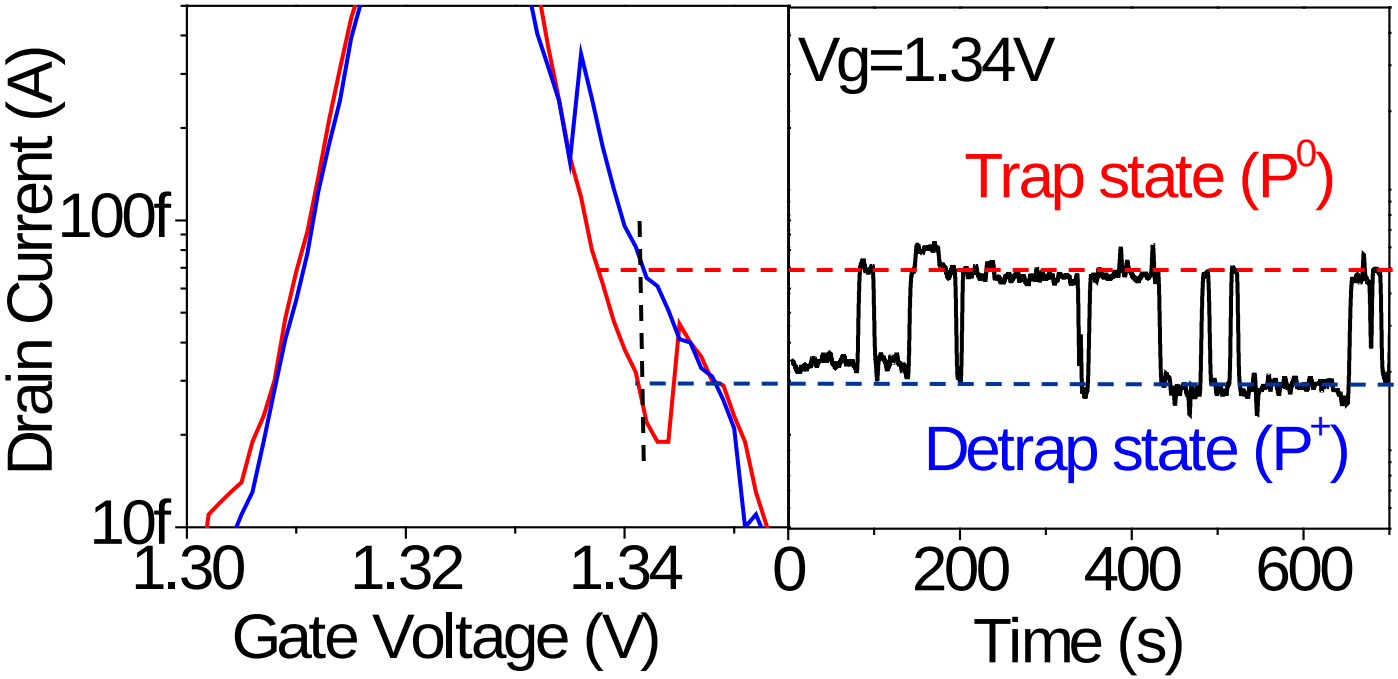

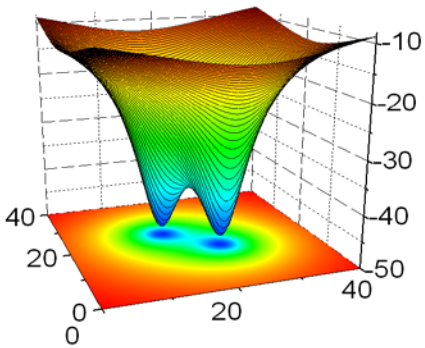

Two level-jump indicates single dopant trap in ionized (P^+) and neutral (P^0) states.

Model of charging effect

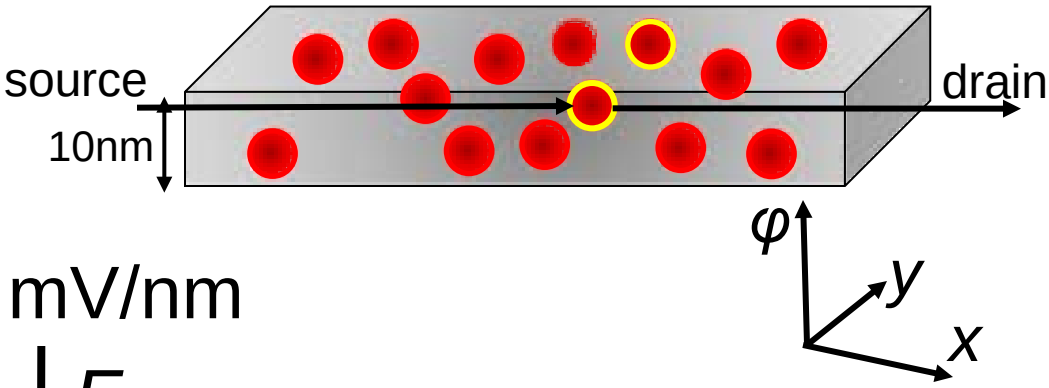

Field = 0 mV/nm

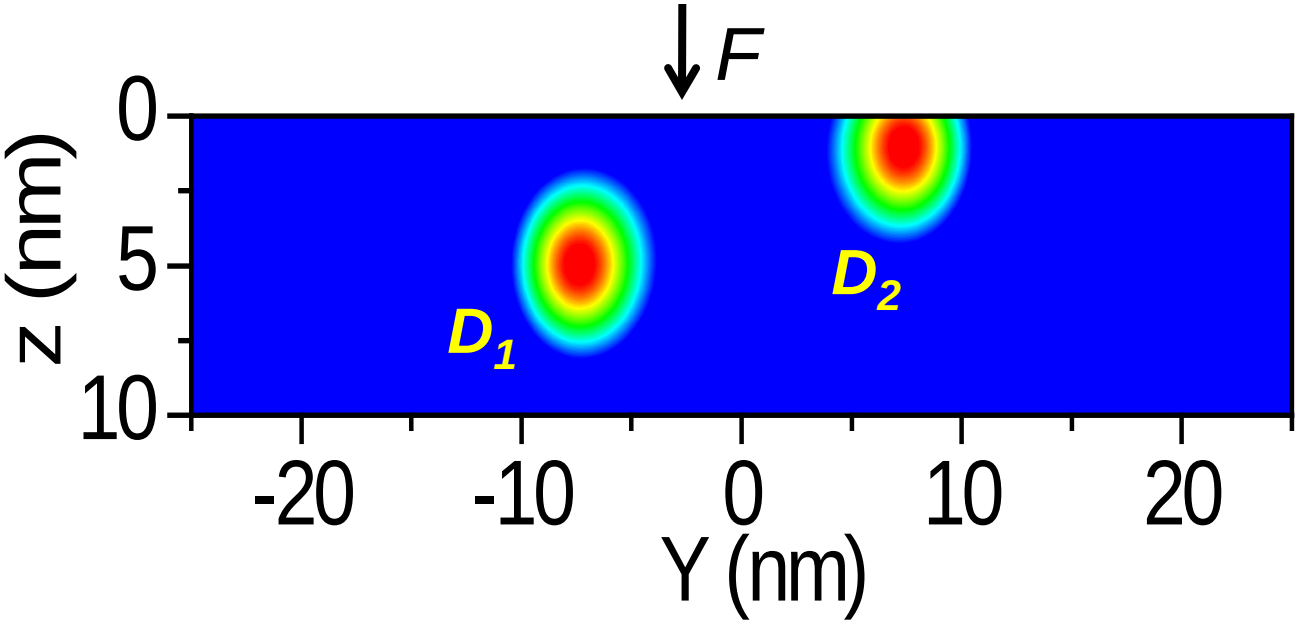

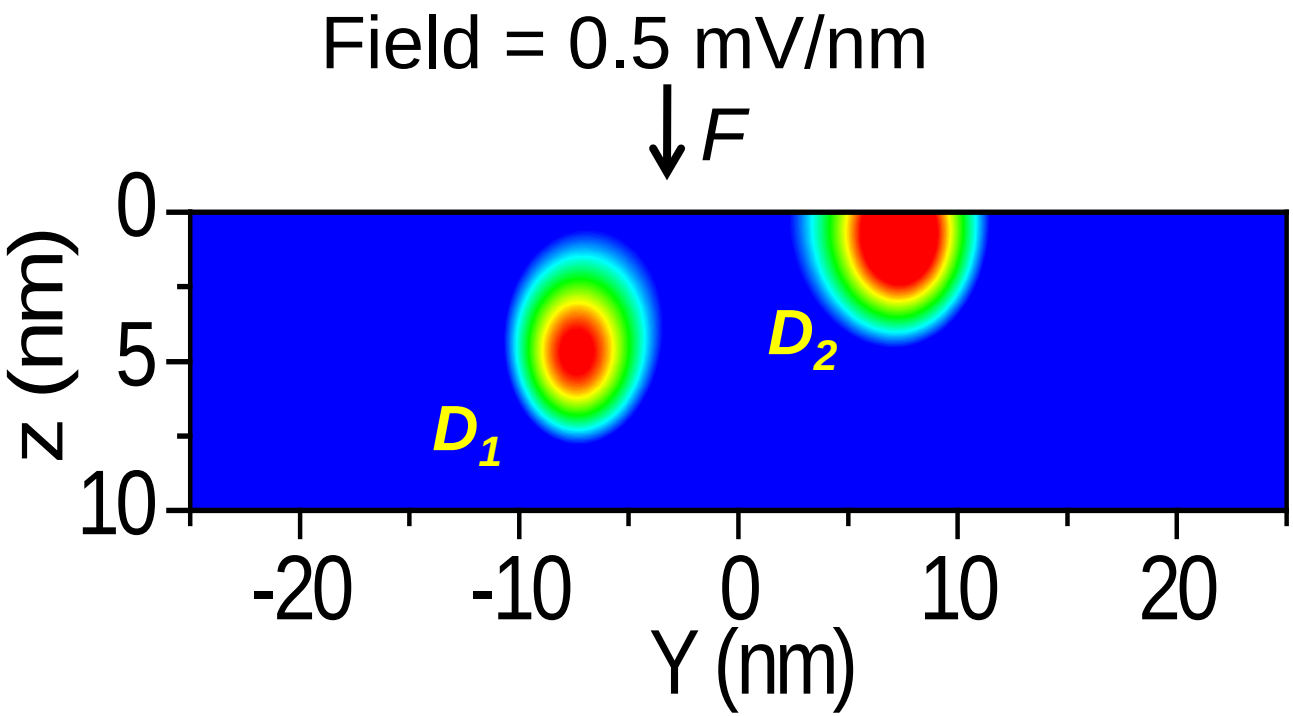
Field = 0.5 mV/nm
F
0
5
10
z (nm)
D1
D2
-20
-10
0
10
20
Y (nm)

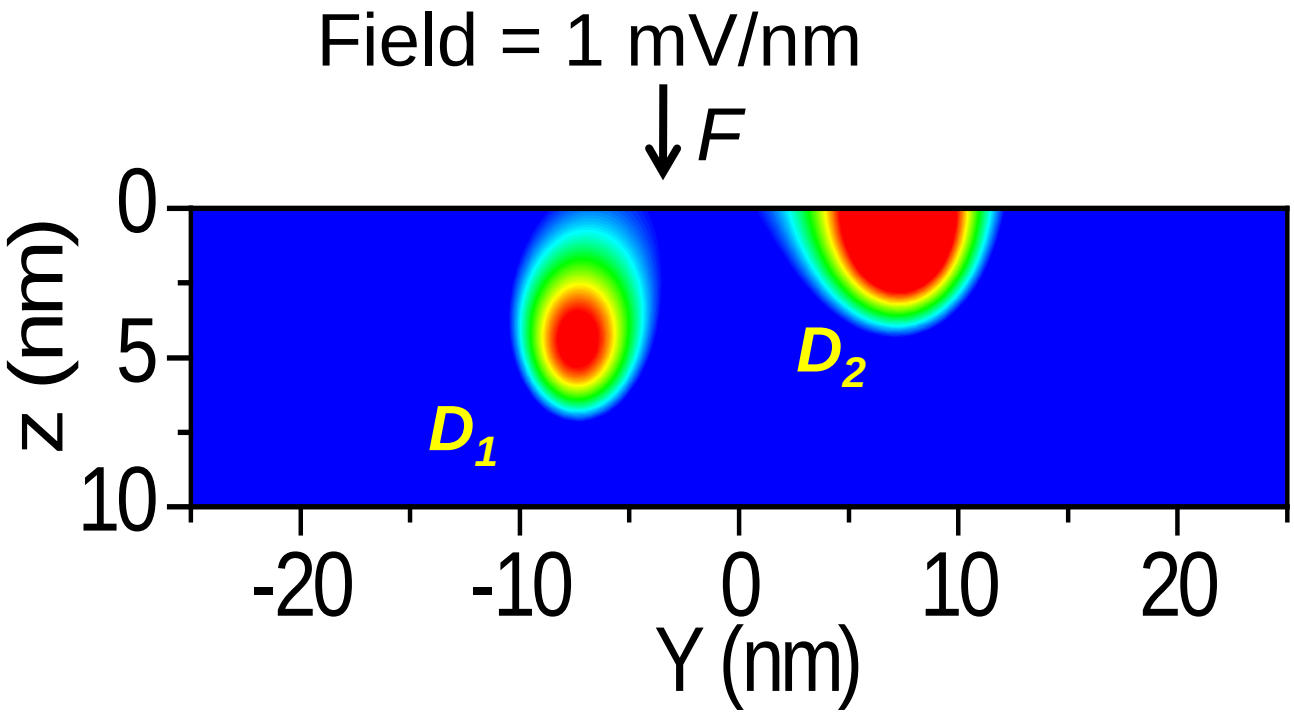
Field = 1 mV/nm
F
0
5
10
z (nm)
D1
D2
-20
-10
0
10
20
Y (nm)

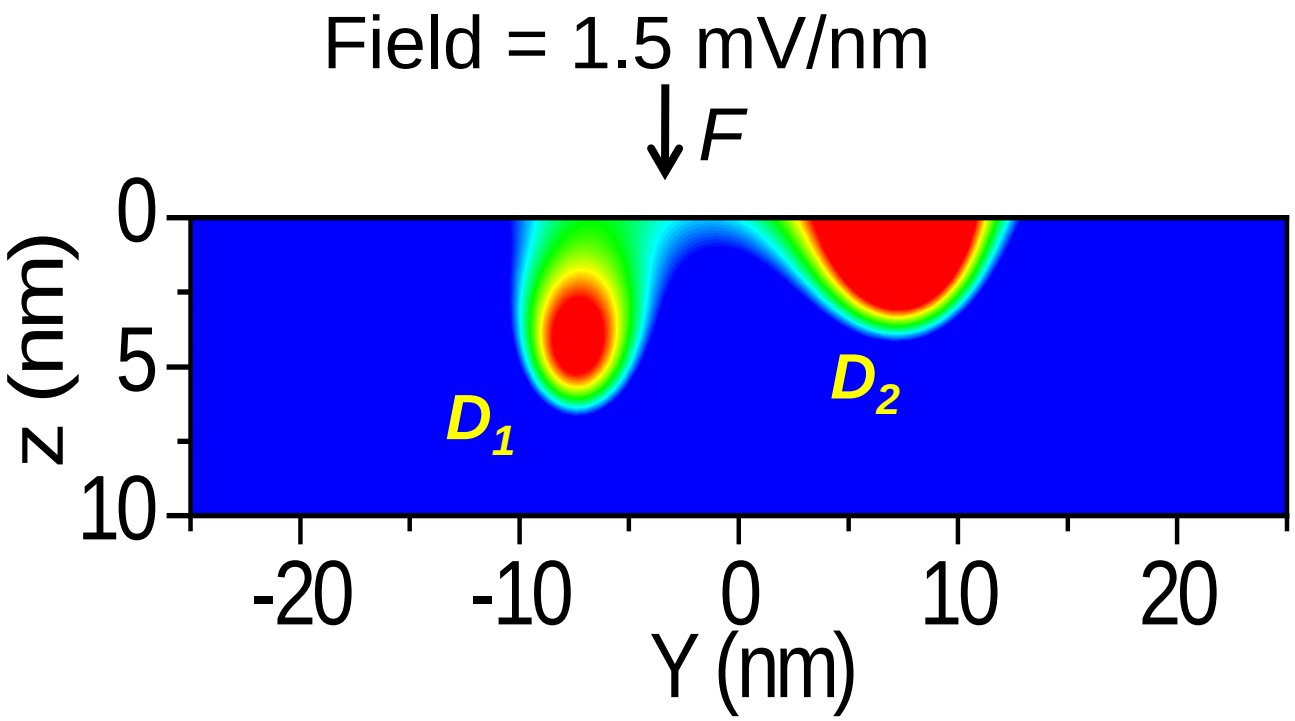
Field = 1.5 mV/nm
F
0
5
10
z (nm)
D1
D2
-20
-10
0
10
20
Y (nm)

Simulation approach

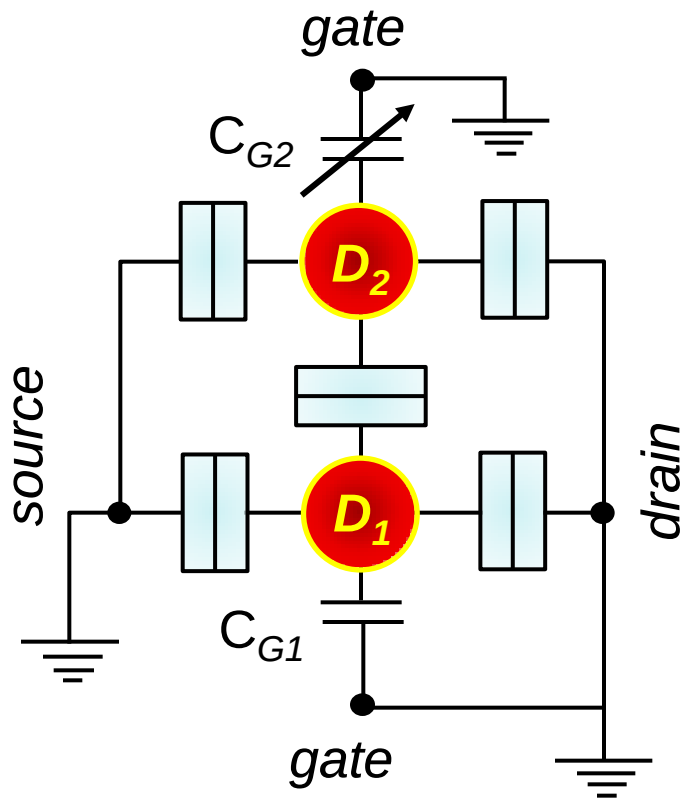

We introduce variable donor-gate capacitance in this simulation.

E. Hamid *et al*., Si Nanoelectronics Workshop (2010)

Comparison between simulation and experimental results

Experimental

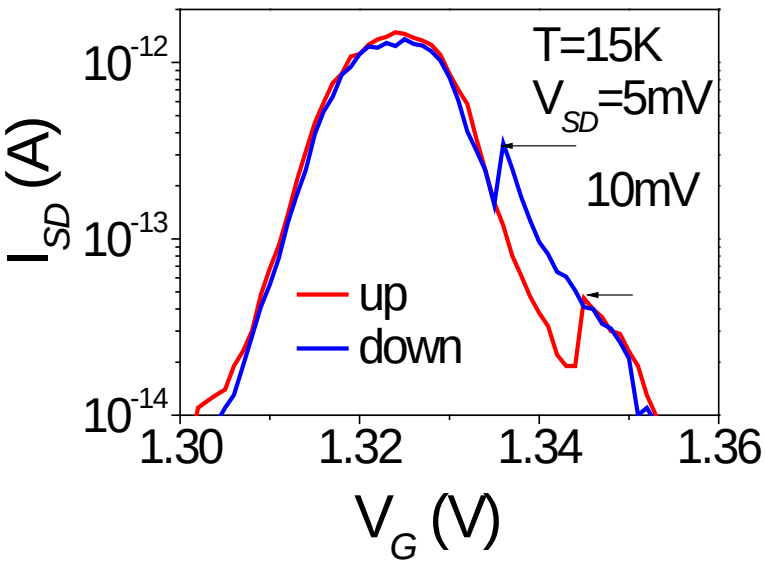

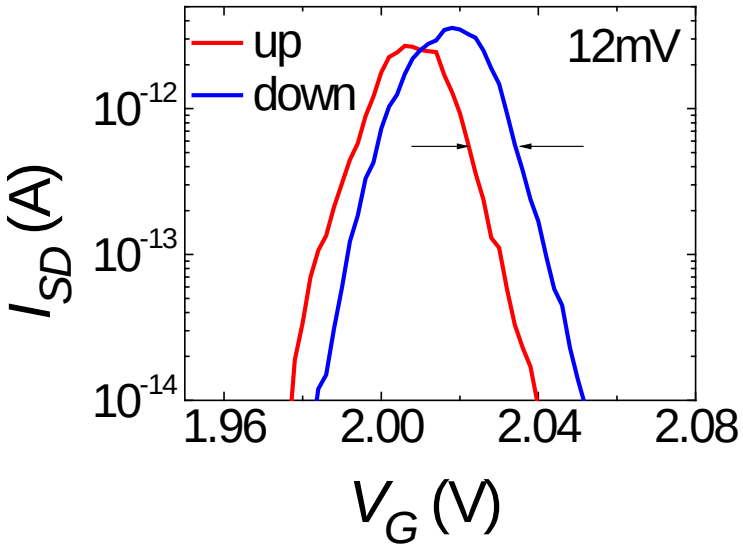

Simulation

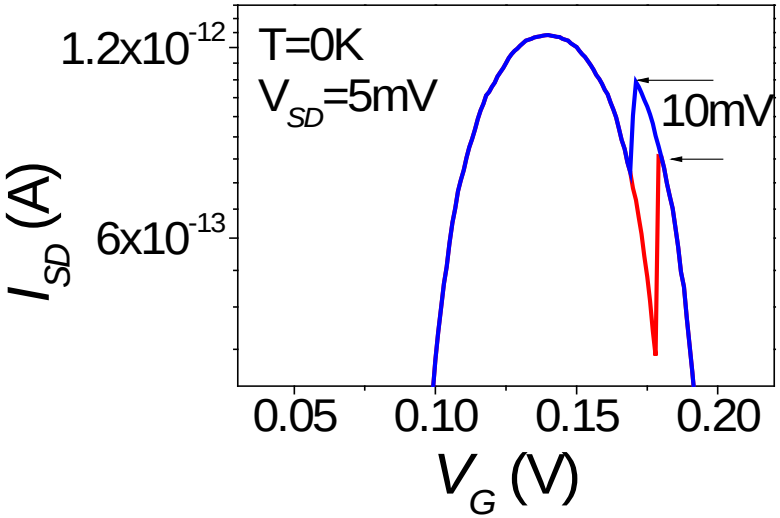

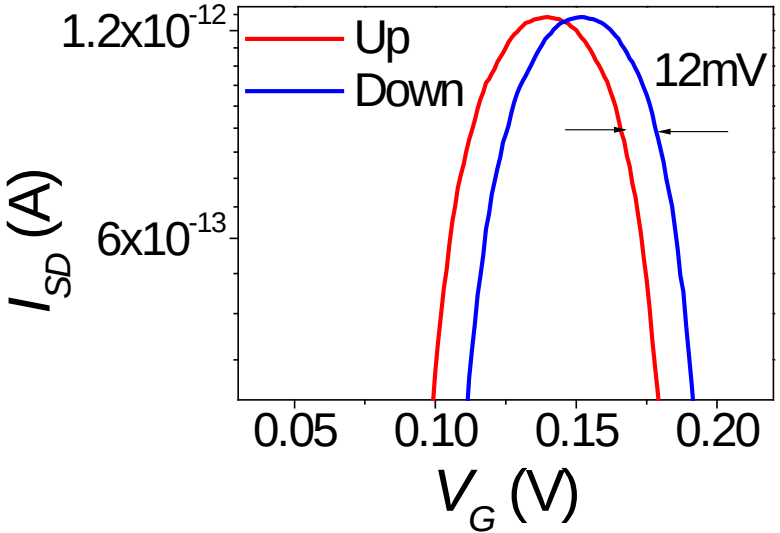

Discrete dopants may work as:

- ✓ conduction path, as well as traps for single electrons
- ✓ basic concept of dopant-based memory

3-donor FET: single-electron turnstile

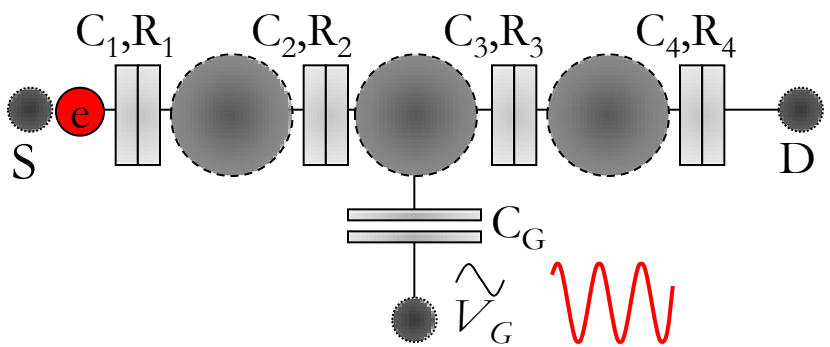

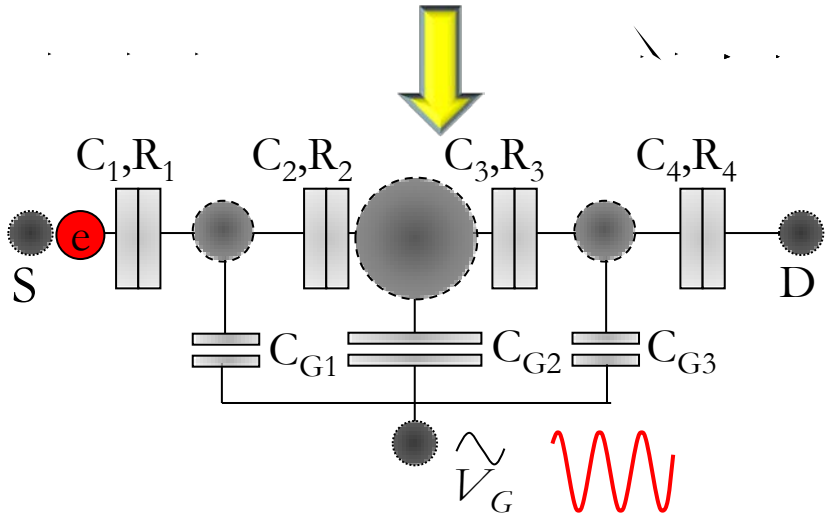

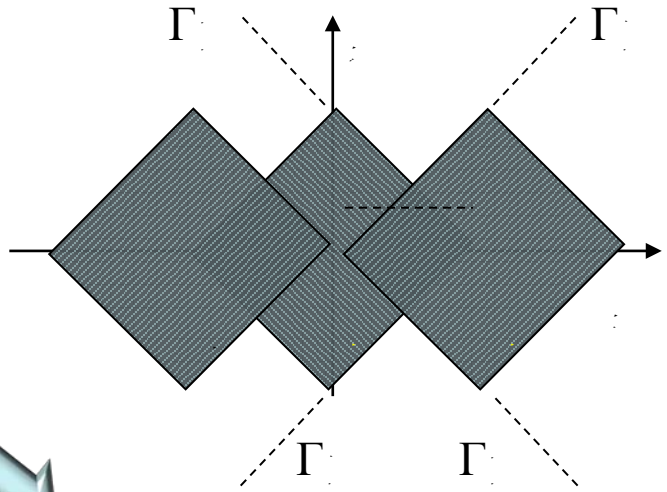

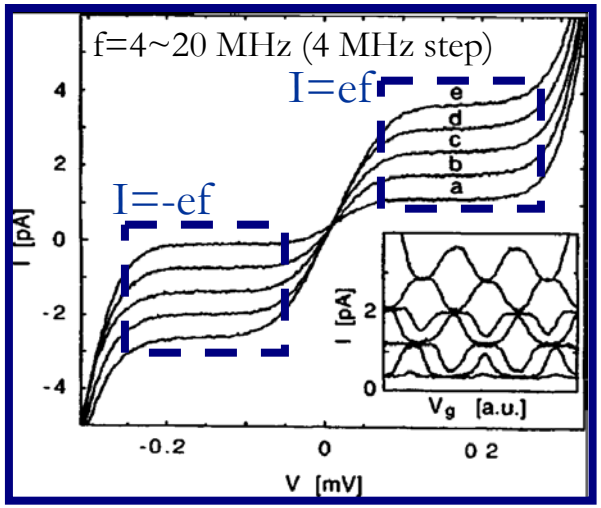

K. Yokoi *et al*., Jpn. J. Appl. Phys. (2009), JAP (2010).

D. Moraru *et al.*, Phys. Rev. B (2007).

In some devices, we may find
3-QD array created by discrete dopants

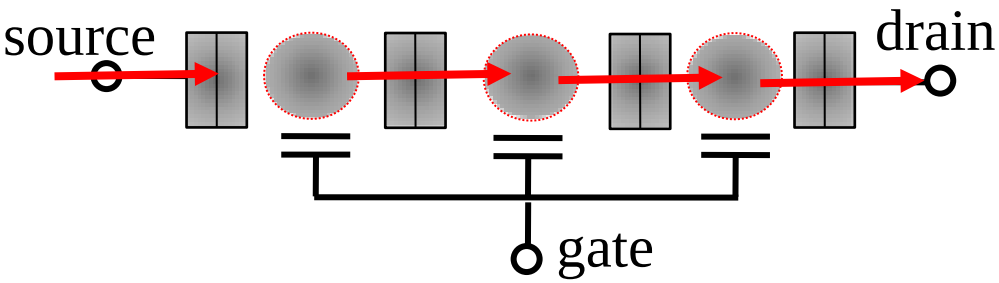

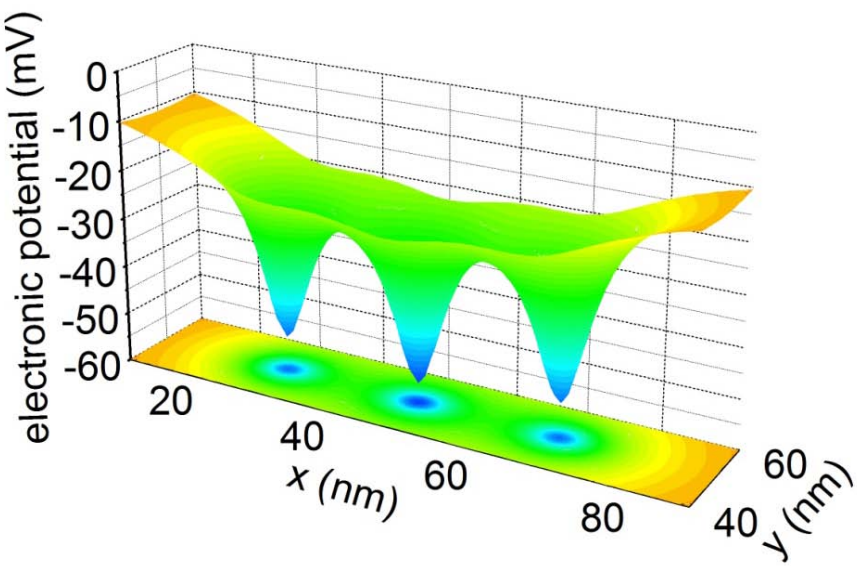

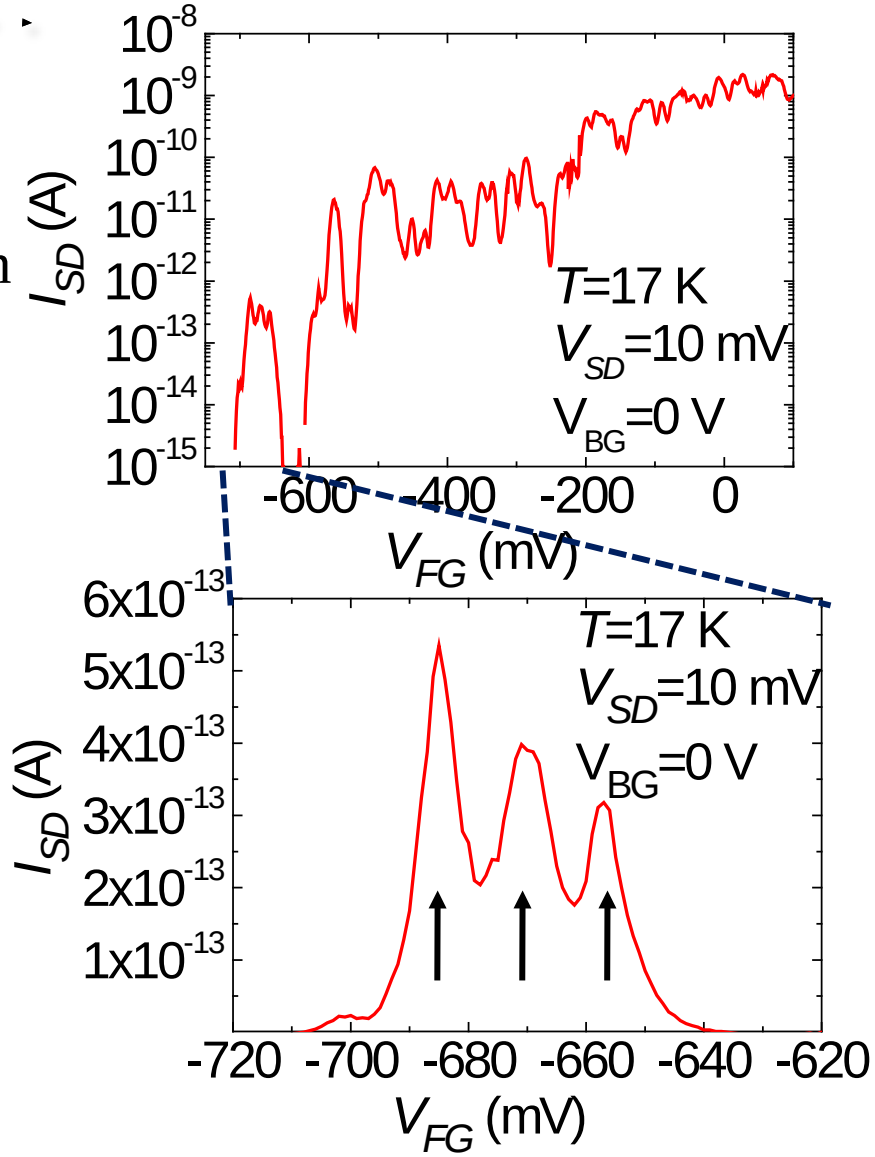

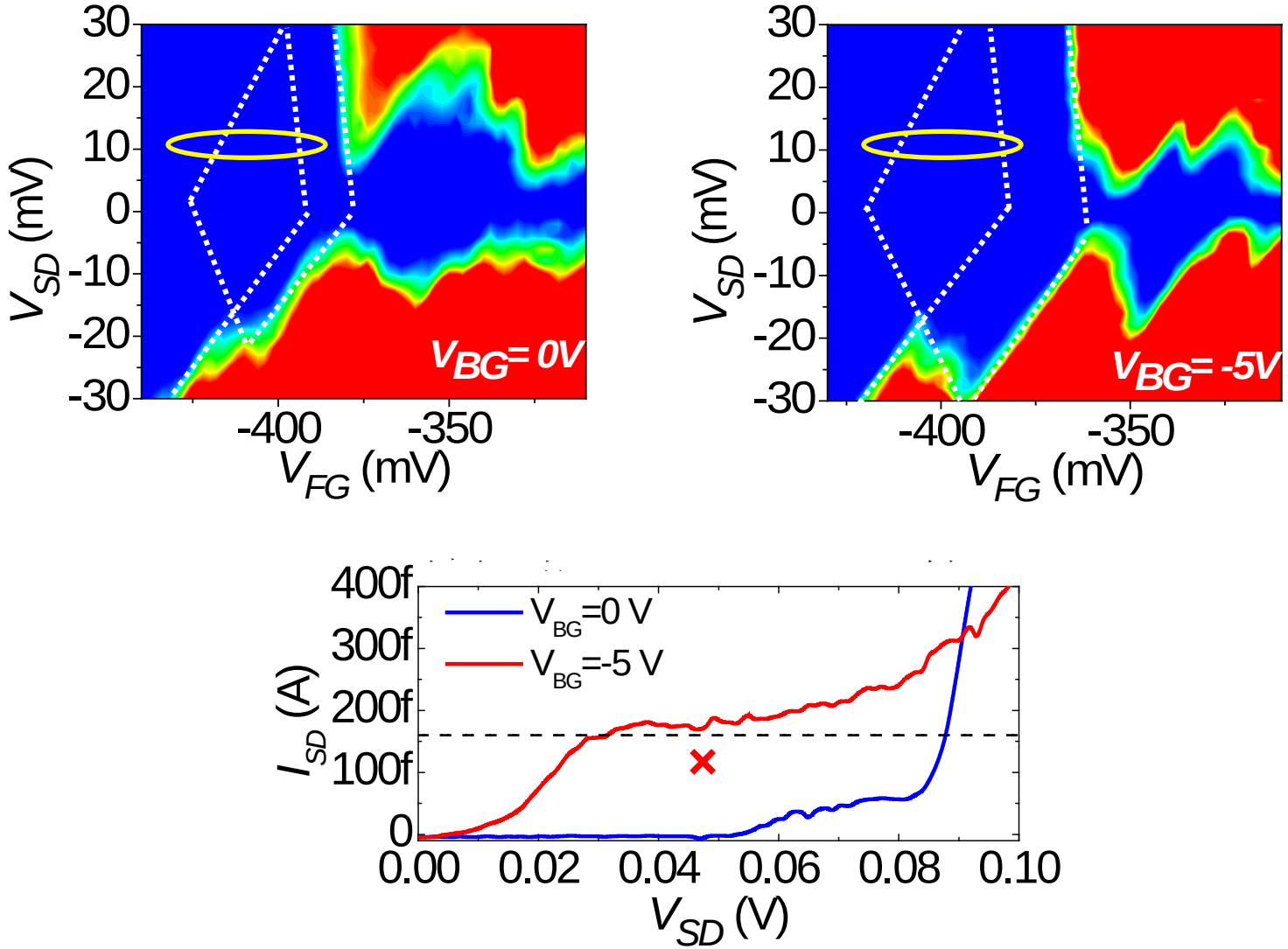

D. Moraru *et al*.., Appl. Phys. Express **2** (2009)

✓

✓

✓

Single photon detection by a-few-donor FETs

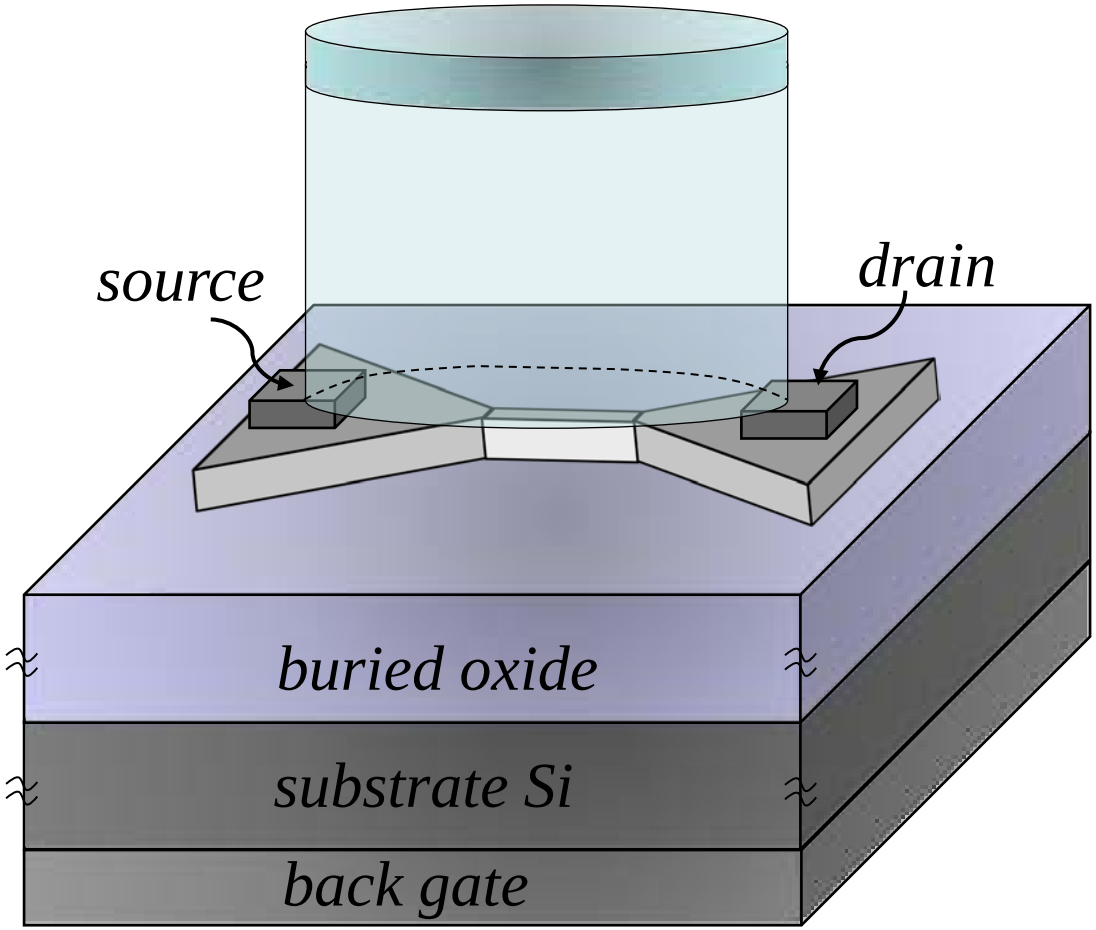
source
drain
buried oxide
substrate Si
back gate

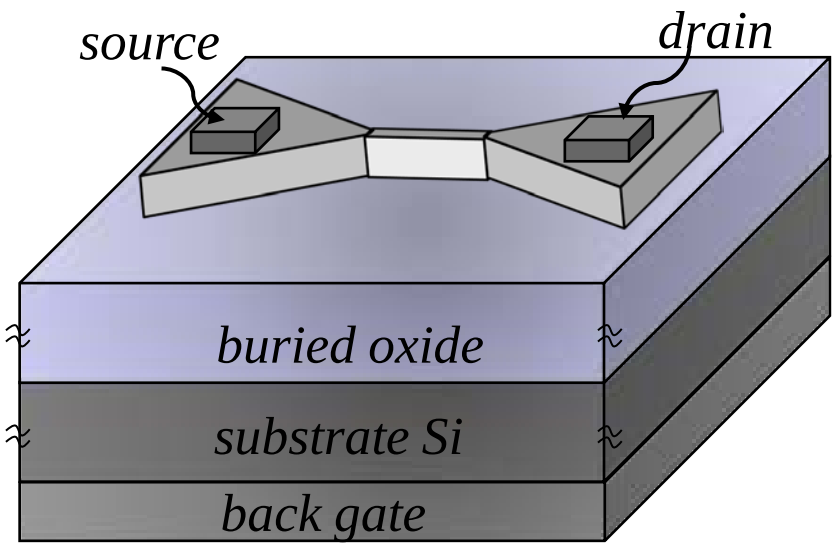
source
drain
buried oxide
substrate Si
back gate

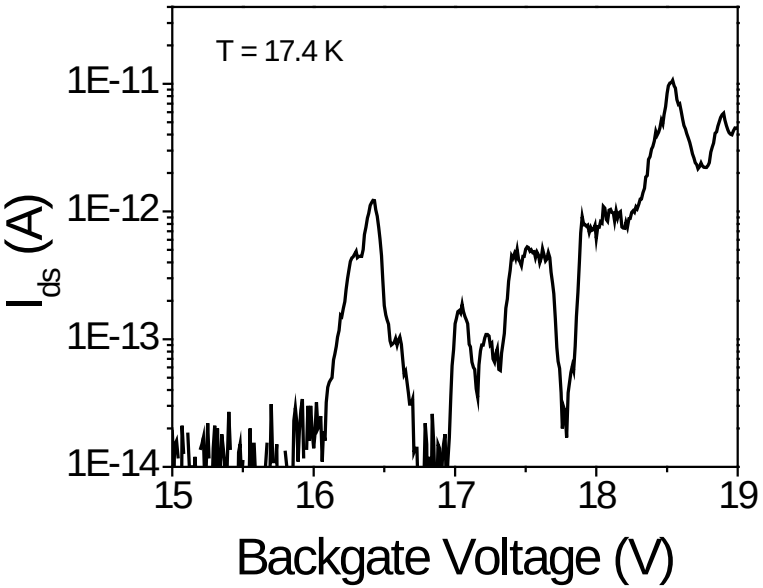
T = 17.4 K
1E-11
1E-12
1E-13
1E-14
I_{ds} (A)
15
16
17
18
19
Backgate Voltage (V)

λ = 525 nm. V_{ds} = 10 mV. V_{bg} = 16.25 V

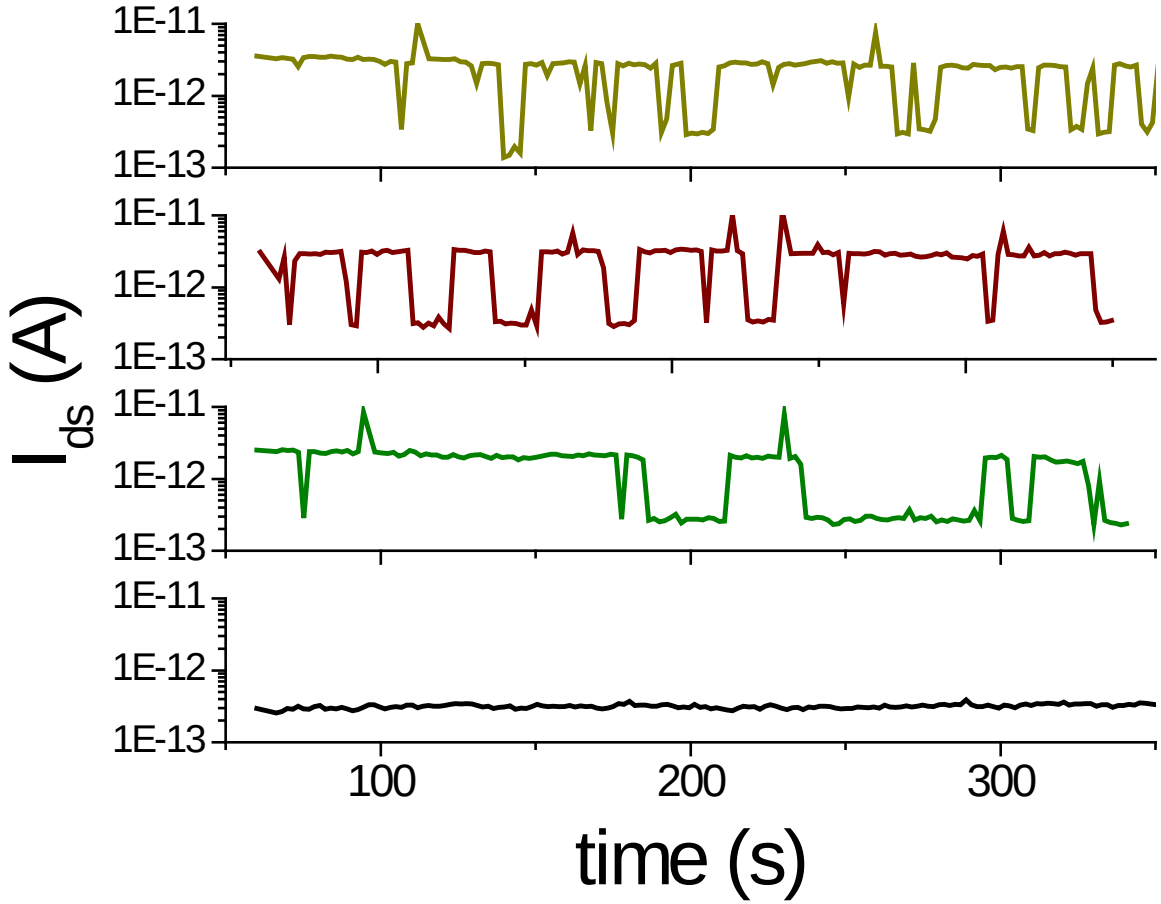

$\Phi_3 = 3 \times \Phi_1$

$\Phi_2 = 2 \times \Phi_1$

$\Phi_1 = 1$
(photons/nm^2.s)

$\Phi_0 = 0$ photon
(dark)

Random telegraph signal → a signature of trapping and detrapping in the dopant near by conduction path.

M. Tabe et al., 2010 E-MRS, *physica status solidi* (to be published)

✓

M. Tabe et al., 2010 E-MRS, *physica status solidi* (to be published)

Observation of dopants by LT-KFM

PHYSICAL REVIEW B **72**, 195323 (2005)

Observation of substitutional and interstitial phosphorus on clean Si(100)-(2×1) with scanning tunneling microscopy

Geoffrey W. Brown,* Blas P. Uberuaga, Holger Grube, and Marilyn E. Hawley
Materials Science and Technology Division, Los Alamos National Laboratory, Los Alamos, New Mexico 87545, USA

Steven R. Schofield,† Neil J. Curson, Michelle Y. Simmons, and Robert G. Clark
Centre for Quantum Computer Technology, School of Physics, University of New South Wales, Sydney, NSW 2052, Australia
(Received 3 June 2005; revised manuscript received 11 August 2005; published 14 November 2005)

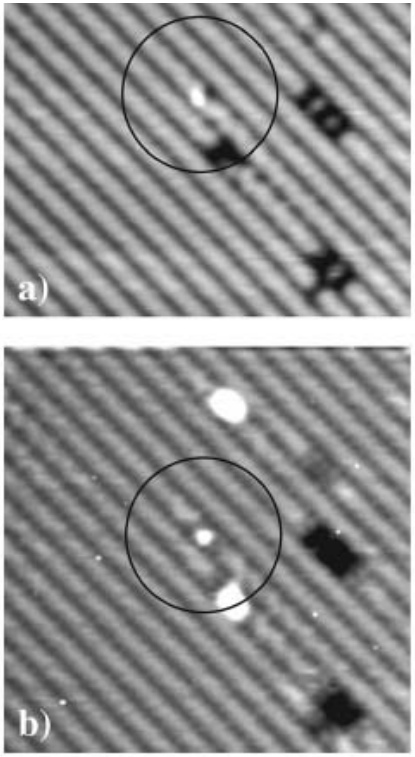

FIG. 3. (a) Filled- and (b) empty-state images from a highly doped sample with one of the "bright" features marked by the circle. A *C* type defect combined with a vacancy is directly below it in the image. The asymmetric dimer and its neighboring structure are consistent with previous observations of Si-P heterodimers. The tunneling conditions were −1.4 V for the filled states, +1.2 V for empty states, and 150 pA tunnel current in both cases. The image area is 120 Å × 120 Å.

by STM (2005)

APPLIED PHYSICS LETTERS **90**, 122118 (2007)

Simultaneous measurement of potential and dopant atom distributions on wet-prepared Si(111):H surfaces by scanning tunneling microscopy

M. Nishizawa,[a] L. Bolotov, and T. Kanayama
MIRAI-Advanced Semiconductor Research Center (ASRC), National Institute of Advanced Industrial Science and Technology (AIST), 1-1-1 Higashi, Tsukuba, Ibaraki 305-8562, Japan

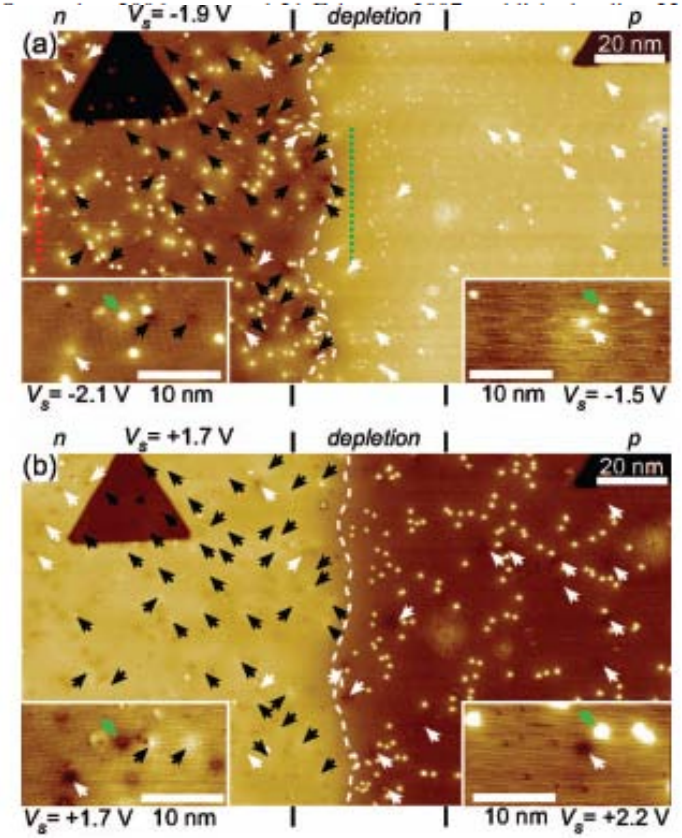

FIG. 2. (Color) STM images of the *p-n* junction region indicated in Fig. 1(b) at (a) V_s=−1.9 V, I_t=6 pA and (b) V_s=+1.7 V, I_t=6 pA. The line markers on the upper and lower edges demarcate the boundaries of the depletion region deduced from the I_t-V_s measurements shown in Fig. 3. The insets show the magnified images of the *n* and *p* regions, where white and black arrows indicate the subsurface acceptor and donor atoms, respectively. A number of bright small dots indicated by green arrows are attributed to the dangling bonds that remain after desorption of hydrogen atoms from the surface (Ref. 2).

by STM (2 0 0 7)

Kelvin Probe Force Microscopy

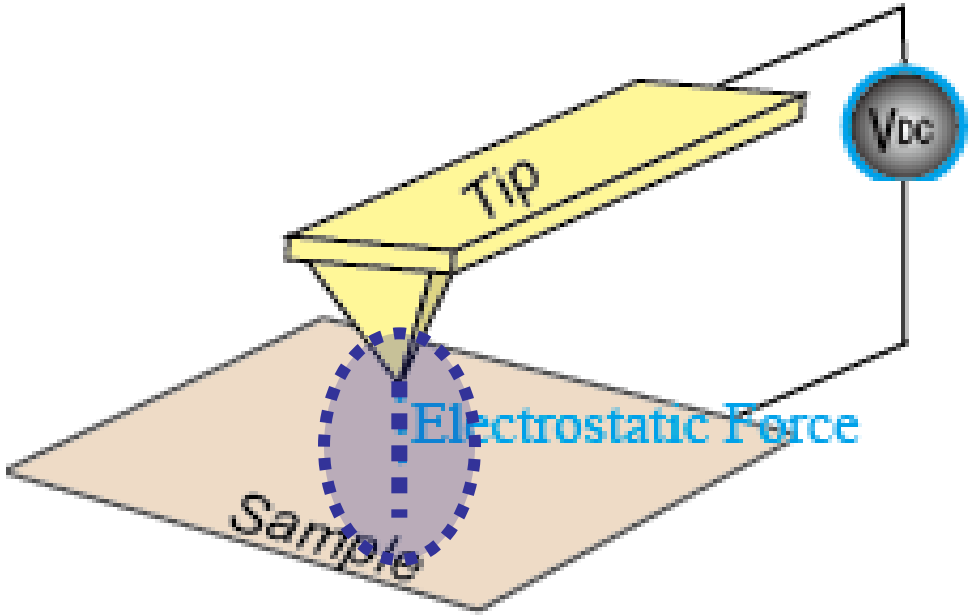

$$F \neq 0$$

Nonnenmacher *et al*. Appl. Phys. Lett. 58, 2921 (1991)

Dopant induced surface potential fluctuations

simulated potential at the surface

ionized
phosphorus atom

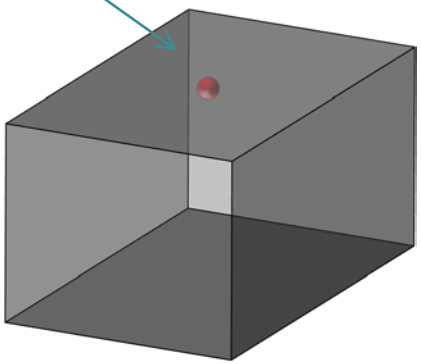

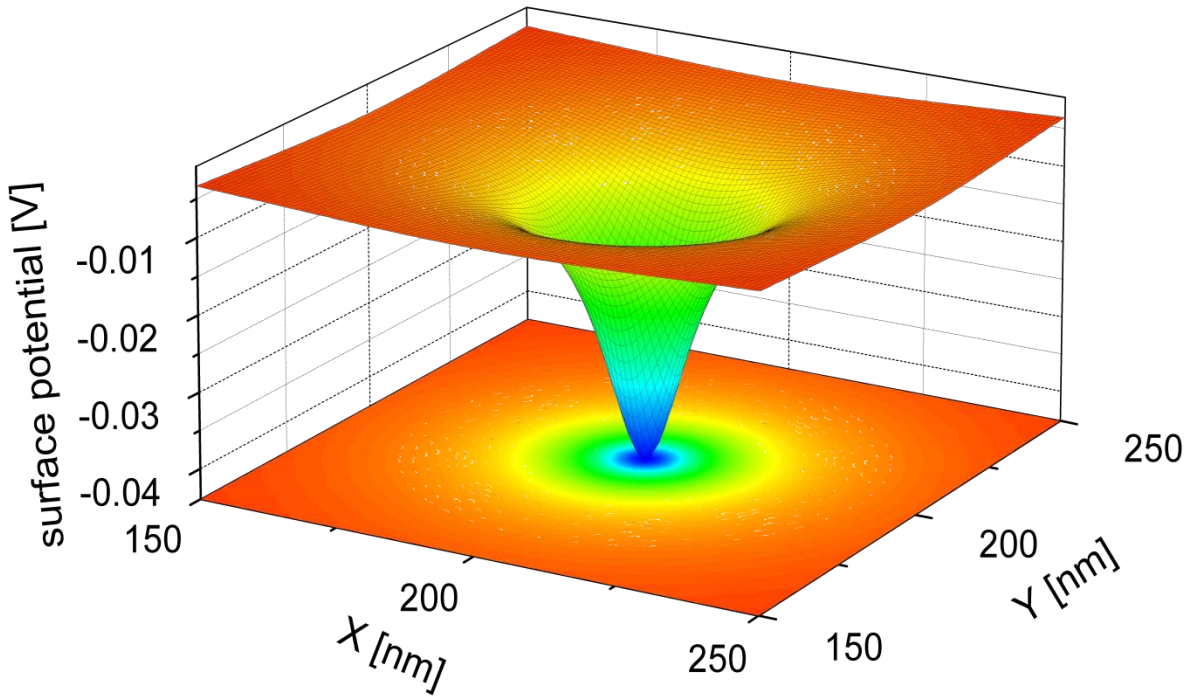

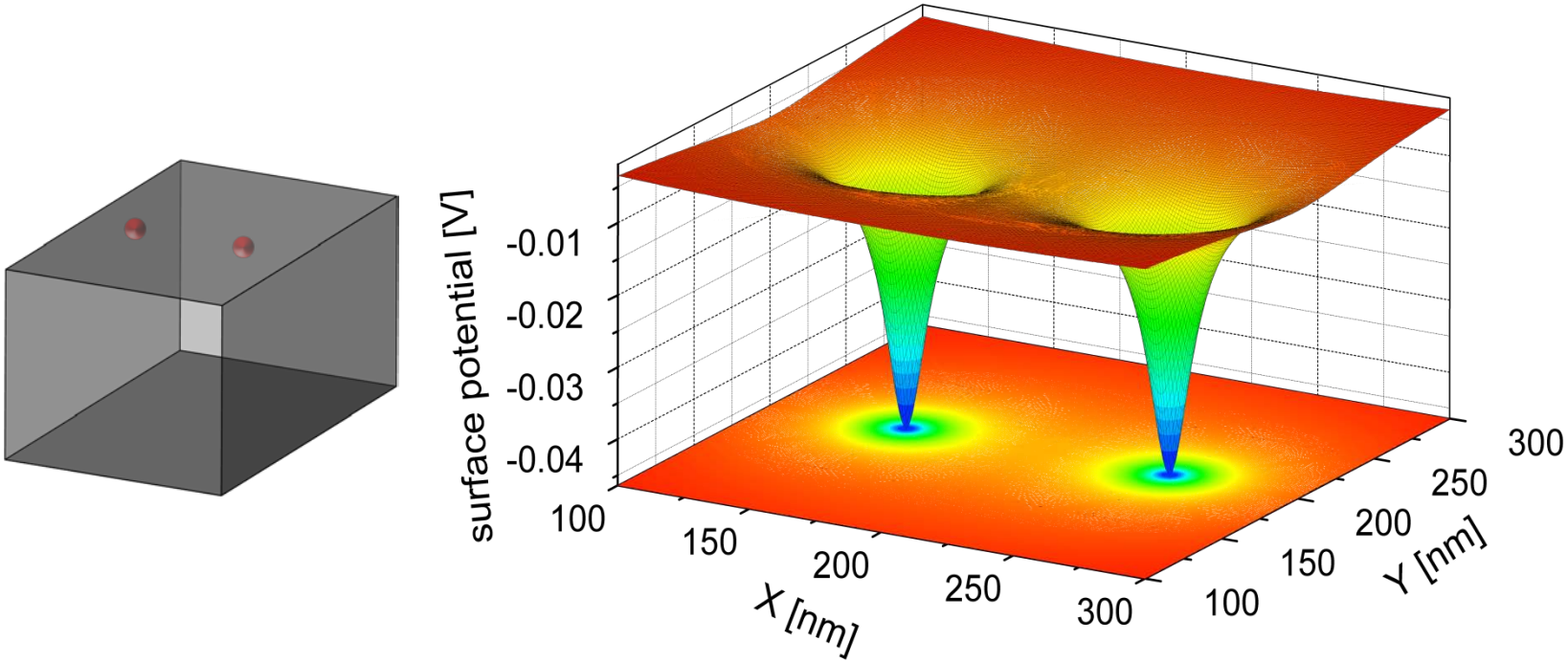
surface potential [V]
-0.01
-0.02
-0.03
-0.04
100
150
200
250
300
X [nm]
100
150
200
250
300
Y [nm]

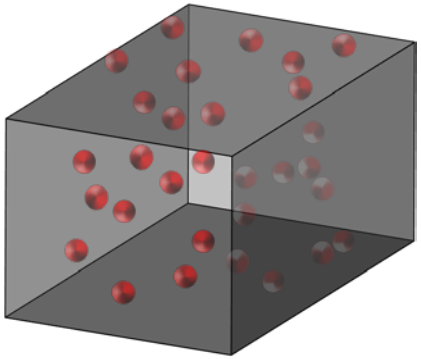

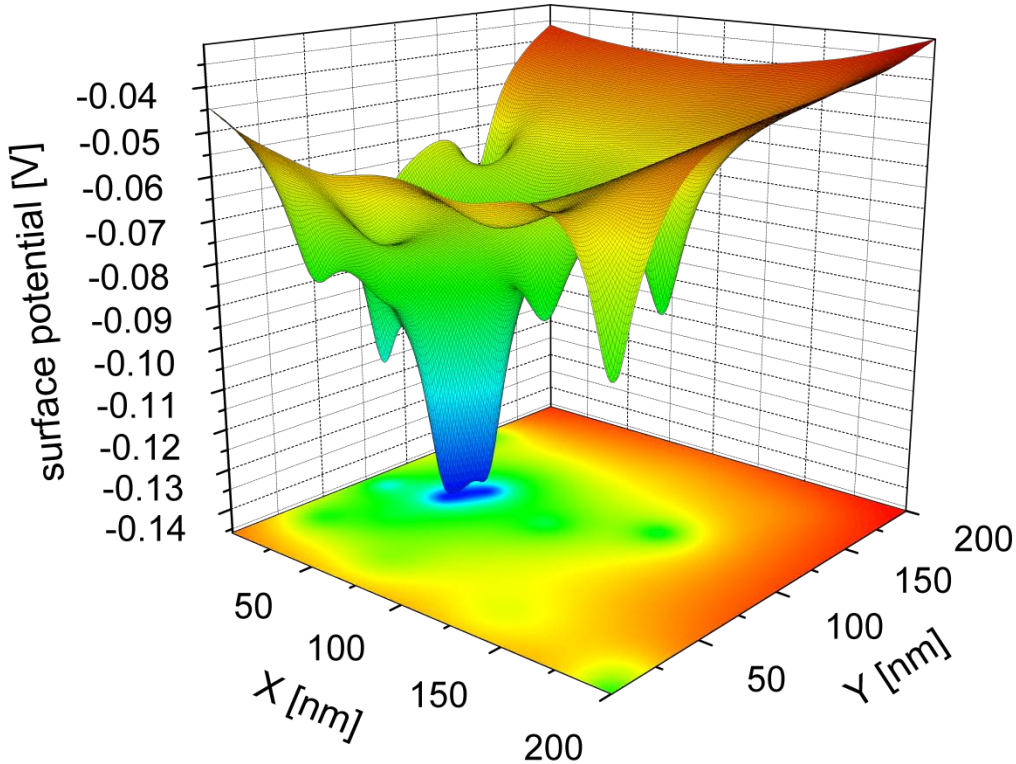
surface potential [V]
-0.04
-0.05
-0.06
-0.07
-0.08
-0.09
-0.10
-0.11
-0.12
-0.13
-0.14
X [nm]
50
100
150
200
Y [nm]
50
100
150
200

Simulated KFM image

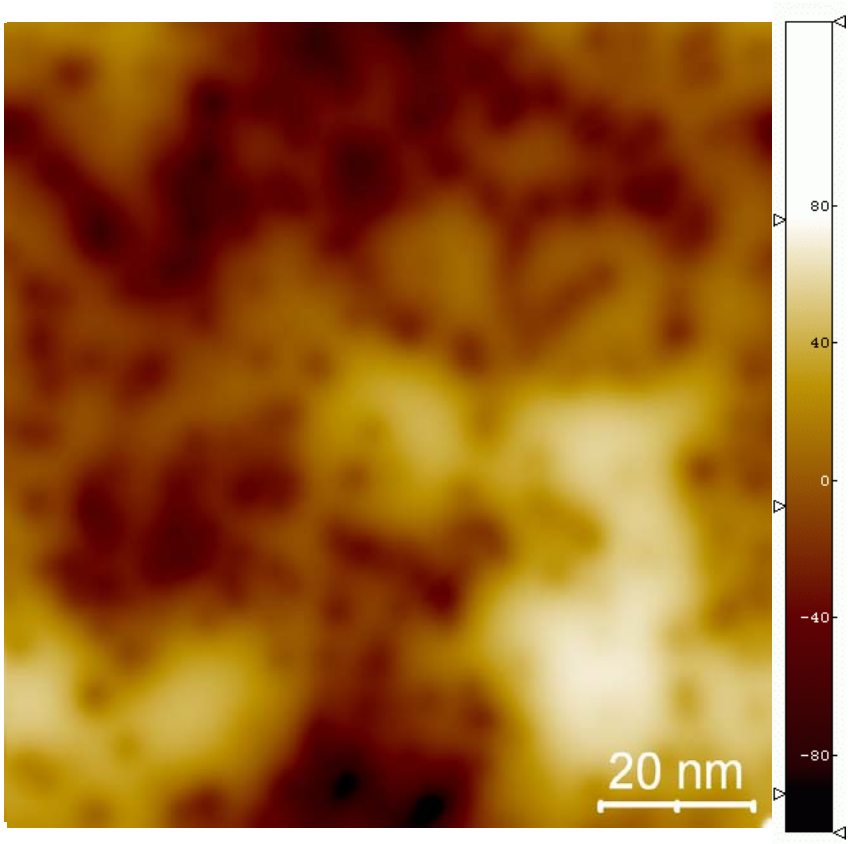

simulated surface potential of
Si cube doped with phosphorus ($1x10^{18}cm^{-3}$)

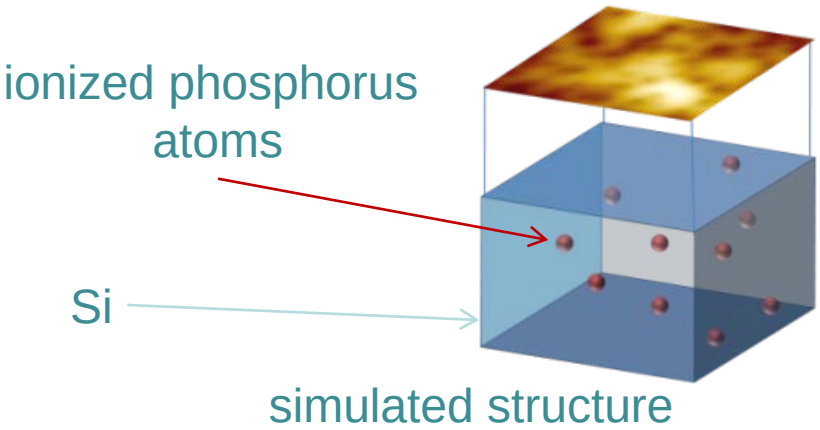

simulated structure

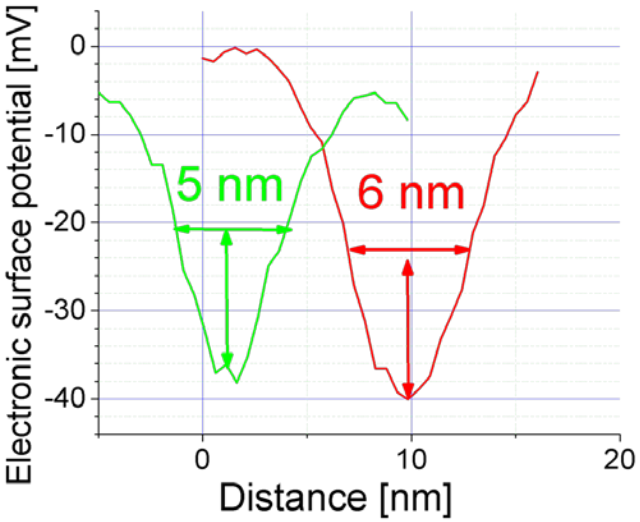

individual profiles

KFM observation of individual phosphorus atoms

KFM image = surface potential map

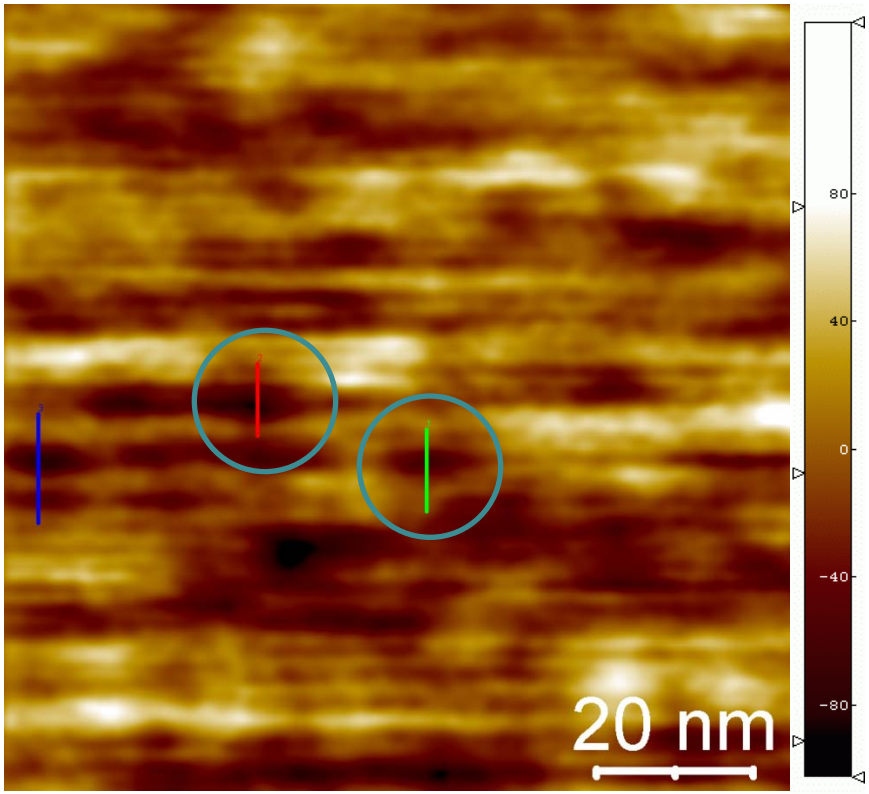

Vg= -3V,
Si layer doped with phosphorus to $1x10^{18}$

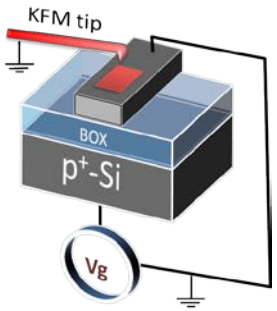

measurement setup

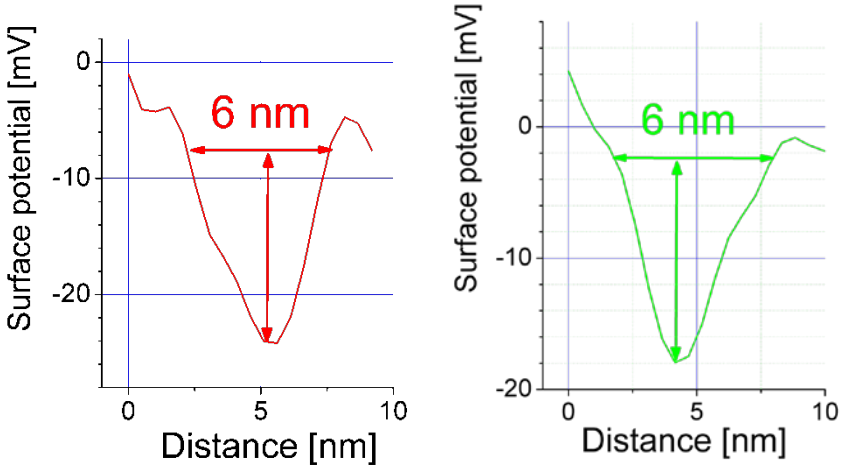

individual profiles

M. Ligowski et.al., APL (2008)

KFM observation of individual boron atoms

surface potential map

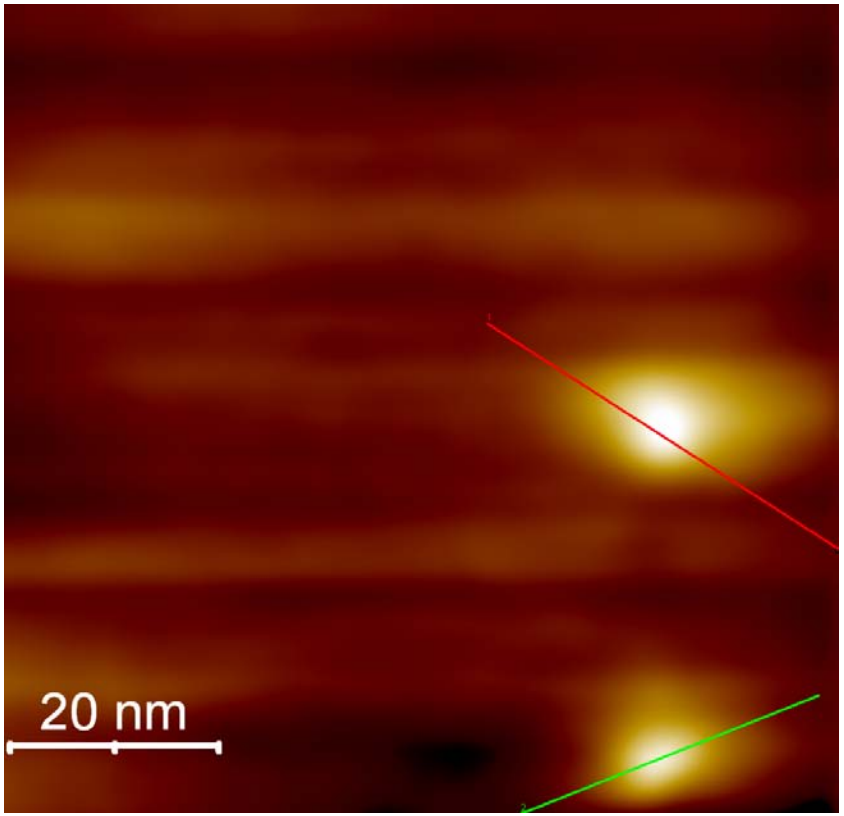

KFM image,
Si layer doped with boron to $1x10^{16}$

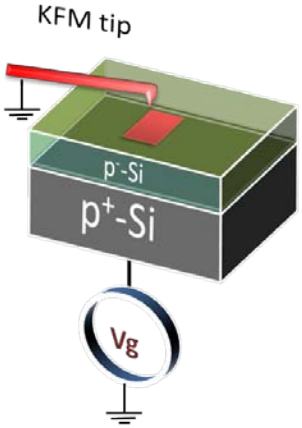

measurement setup

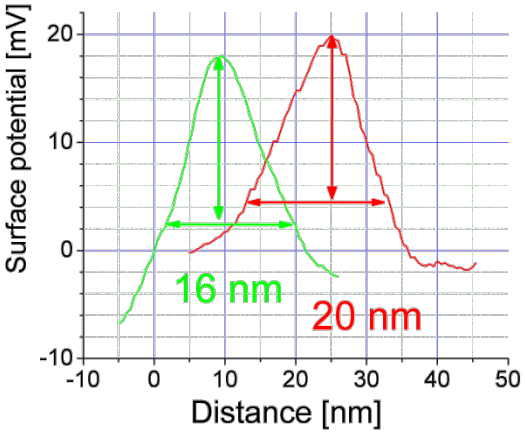

individual profiles

M. Ligowski et.al., APL (2008)

DEVICE STRUCTURE & KFM SETUP

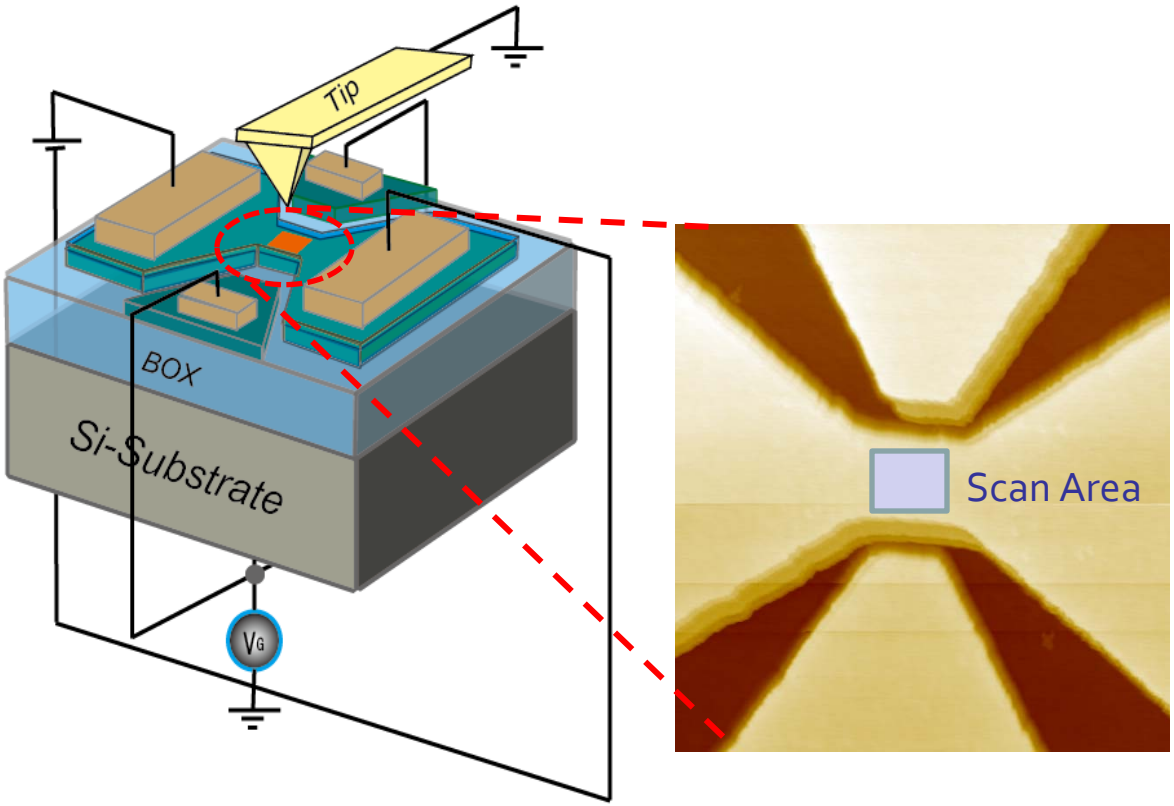

Structure of SOI-FET device

single-electron transport observed by LT-KFM

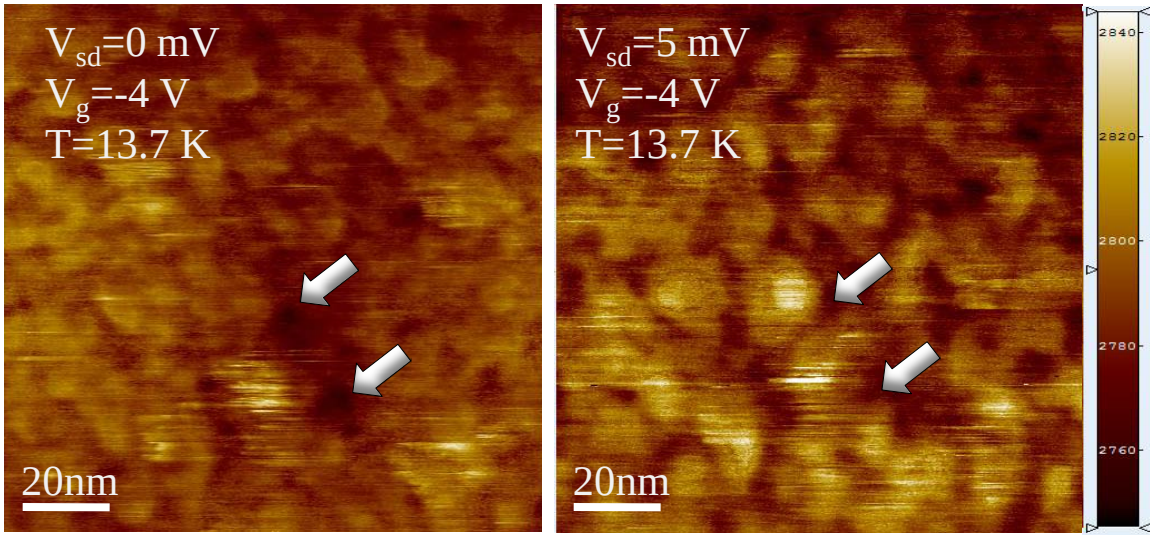

Charging of the lowest potential valleys

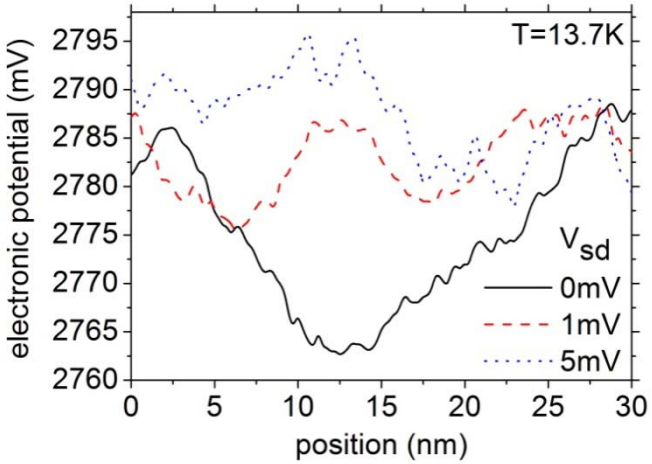

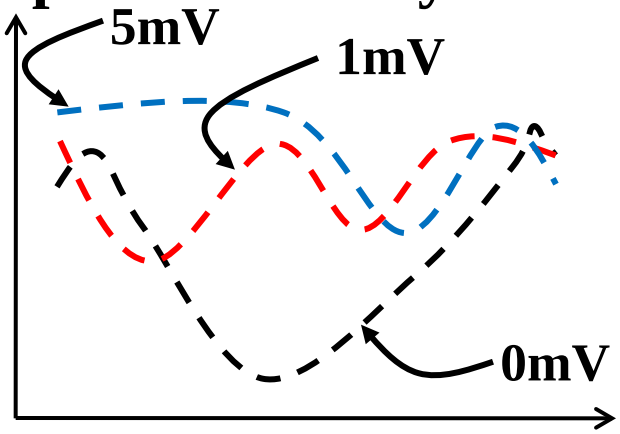

M. Tabe et al., PRL (2010)

OUTLINE

1. Introduction

2. Progress over the past five years
   - 1-donor FET: single-electron transistor
   - 2-donor FET: single-electron memory
   - 3-donor FET: single-electron turnstile
   - Single photon detection
   - Observation of dopants by LT-KFM

3. Challenges for the next ten years

4. Summary

Challenges for the next ten years

•to develop ***deterministic doping process***:
(i) single ion implantation or equivalent doping techniques,
(ii) effect of nanometer-scale channel structures,
(iii) interaction with S/D electrodes,

•to ***increase dopant potential for room temperature operation*** by means of coupled dopants,

•to develop ***devices having immunity from unavoidable fluctuation*** in position of dopants,

•to develop ***single-dopant observation techniques*** as well as ***theoretical work*** on dopant physics.

OUTLINE

1. Introduction

2. Progress over the past five years
   - 1-donor FET: single-electron transistor
   - 2-donor FET: single-electron memory
   - 3-donor FET: single-electron turnstile
   - Single photon detection
   - Observation of dopants by LT-KFM

3. Challenges for the next ten years

4. Summary

Single-dopant memory

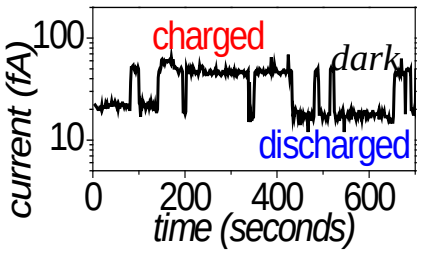

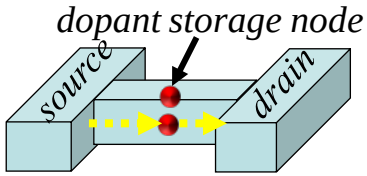

Donor-donor single-electron exchange

Single-dopant transistor

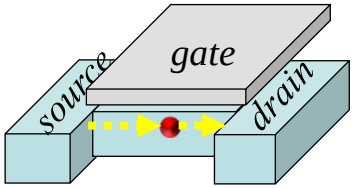

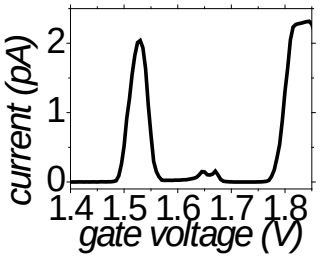

Single-electron tunneling via donor

Dopant-based photon detector

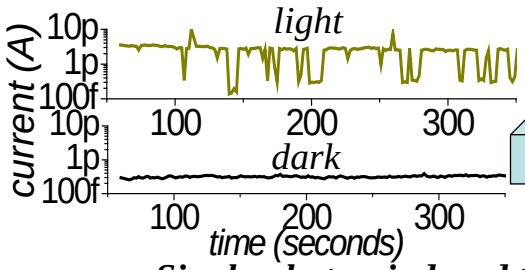

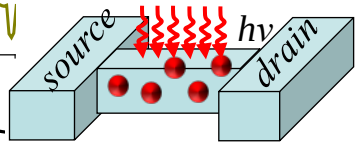

Single-photon-induced trapping

Dopant-based turnstile

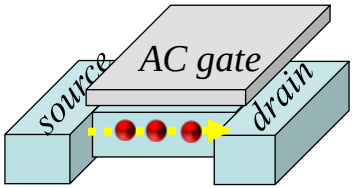

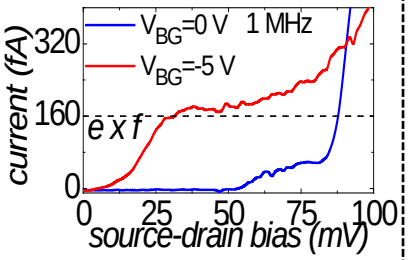

Tunable single-electron turnstile

Dopant observation by LT-KFM

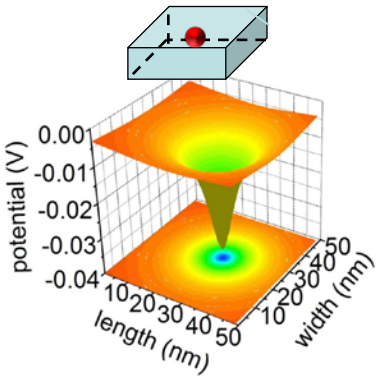

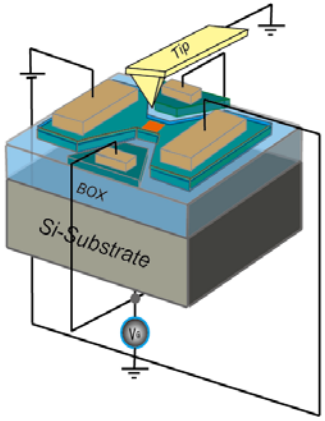

Theoretical analysis

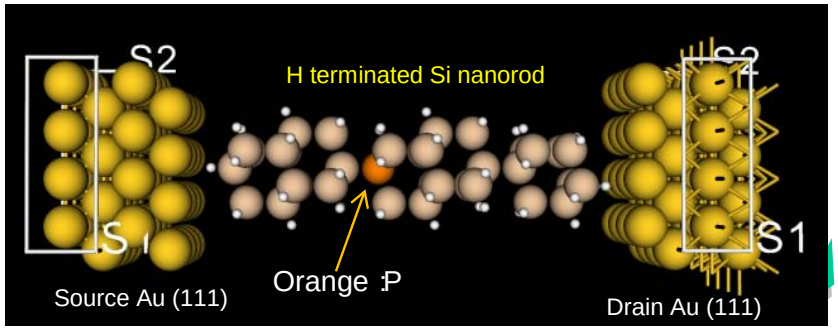

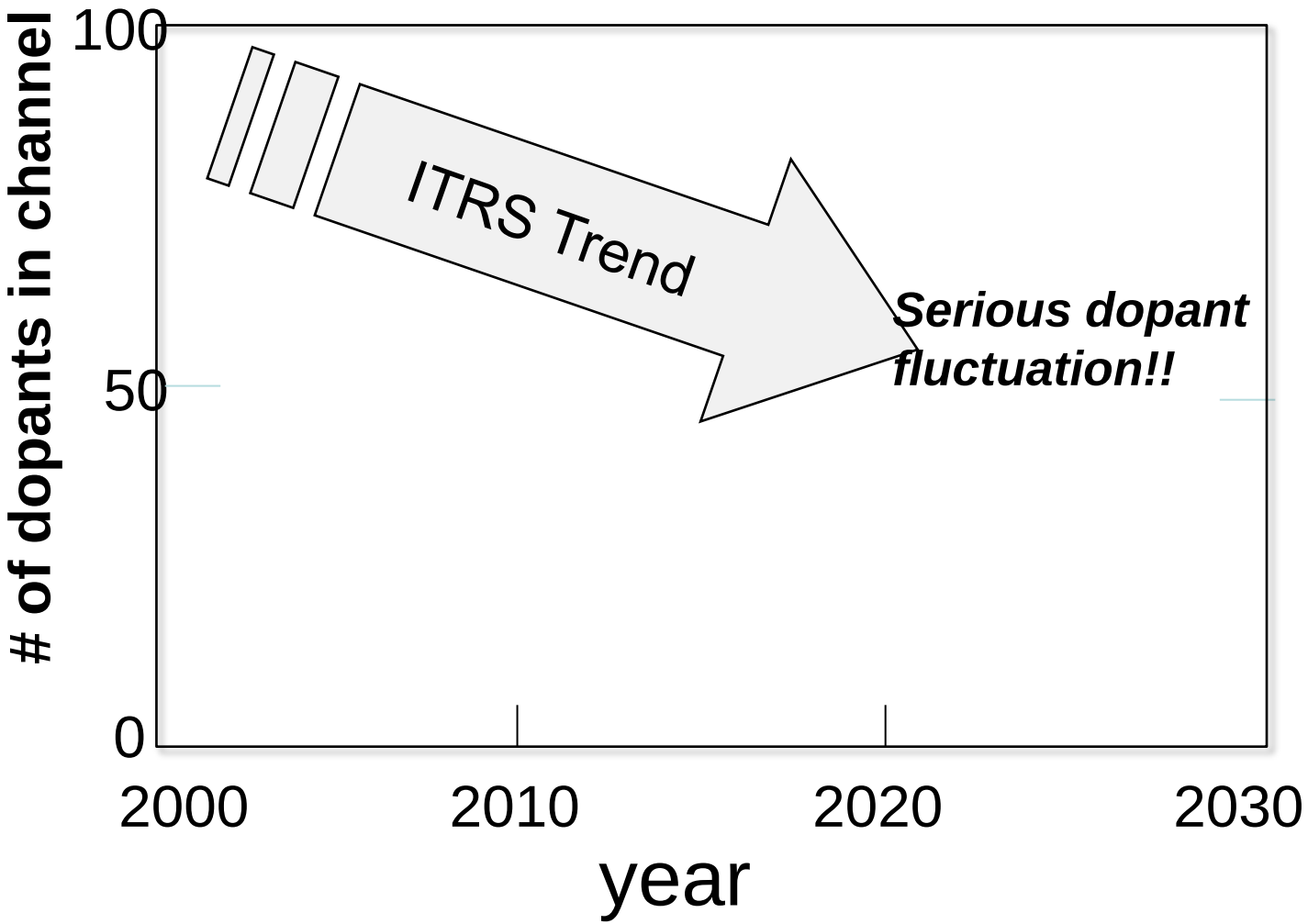
# of dopants in channel
100
50
0
ITRS Trend
Serious dopant fluctuation!!
2000
2010
2020
2030
year

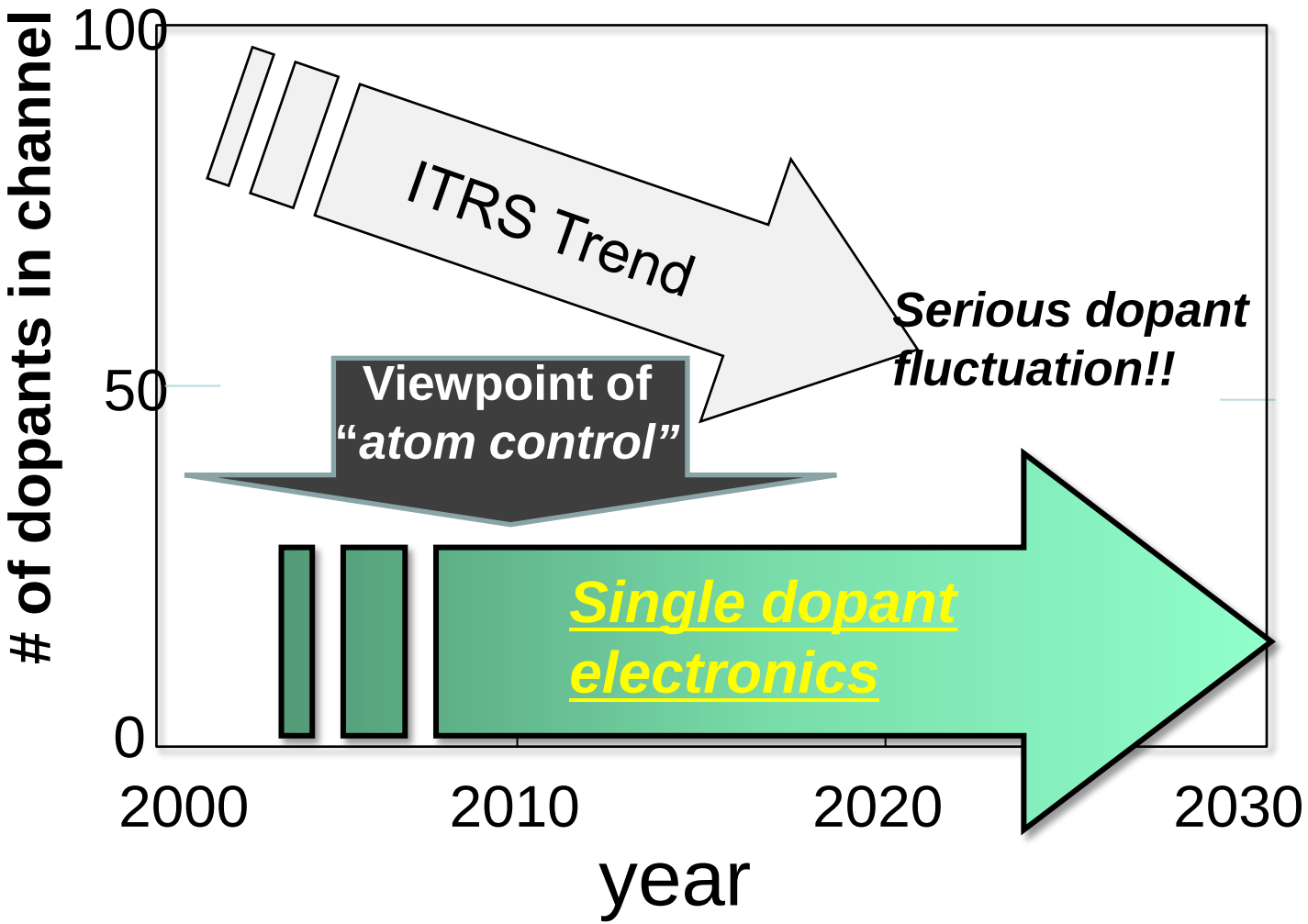
# of dopants in channel
100
50
0
2000
2010
2020
2030
year
ITRS Trend
Serious dopant fluctuation!!
Viewpoint of "atom control"
Single dopant electronics

Thank you for your kind attention!!

Summary

- Background
- Drift-diffusion
- Monte Carlo
- Quantum transport
- First principle approach
- Applications
- Challenges

Summary

- Background
- Drift-diffusion
- Monte Carlo
- Quantum transport
- First principle approach
- Applications
- Challenges

Variability has become a major challenge to scaling and design

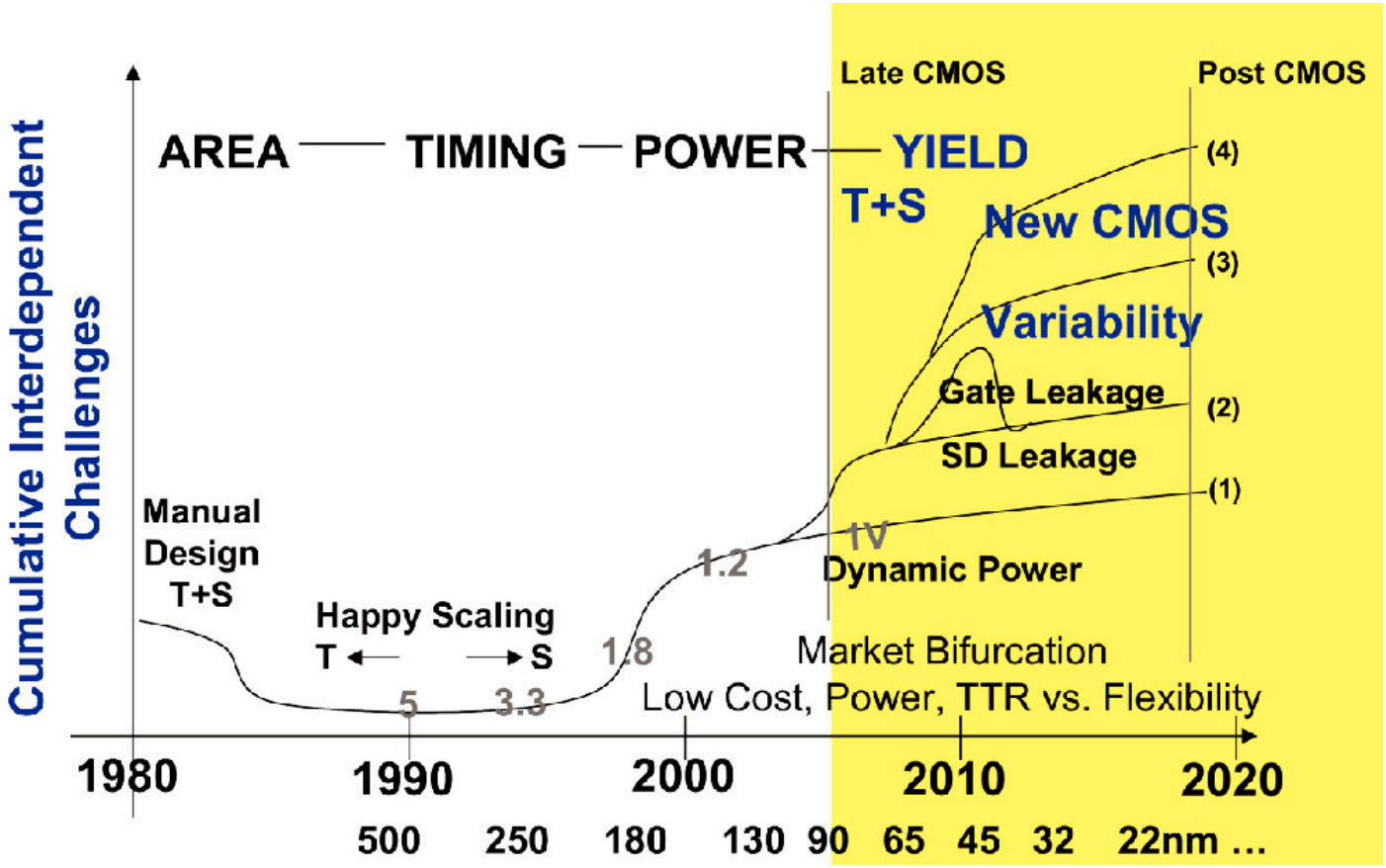

G. Declerck, Keynote talk, VLSI Technol. Symp. 2005

Statistical variability

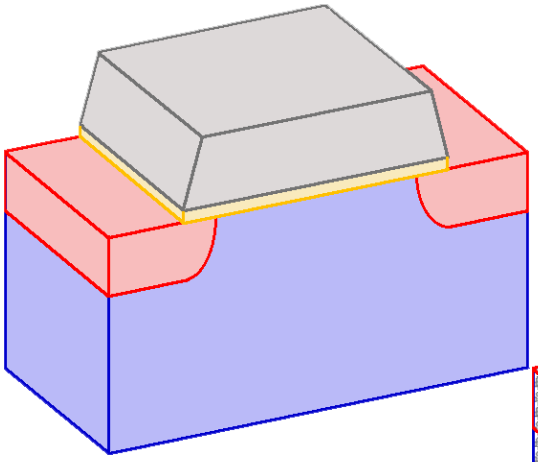

The simulation
Paradigm now

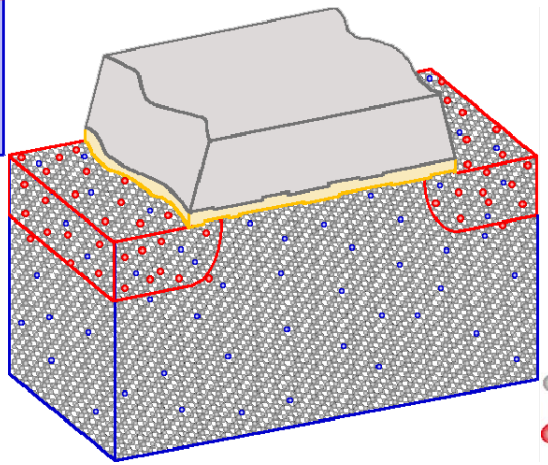

A 22 nm MOSFET
In production 2012

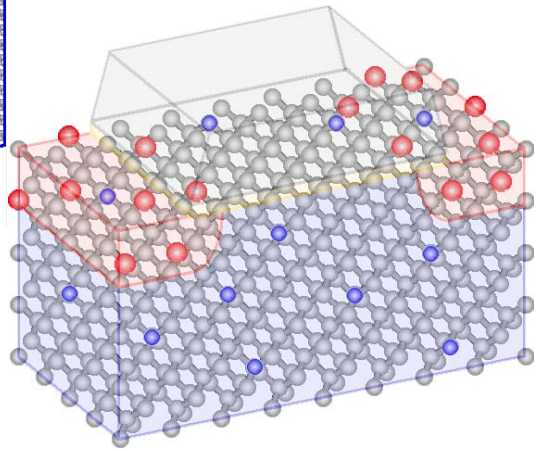

A 4.2 nm MOSFET
In production 2023

Summary

- Background
- Drift-diffusion
- Monte Carlo
- Quantum transport
- First principle approach
- Applications
- Challenges

Resolving individual dopants

M. Hane NEC

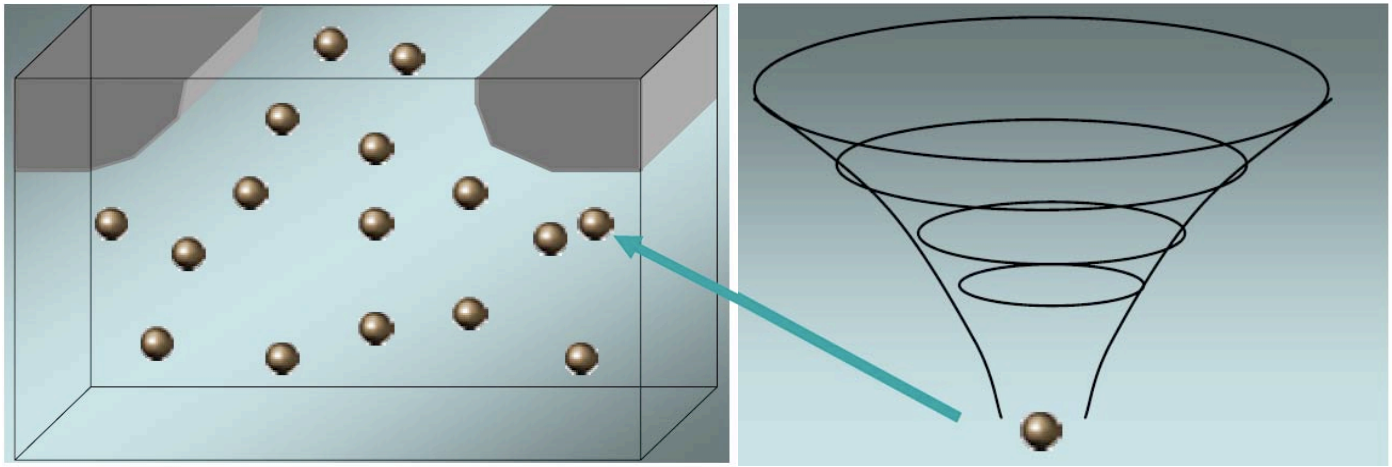

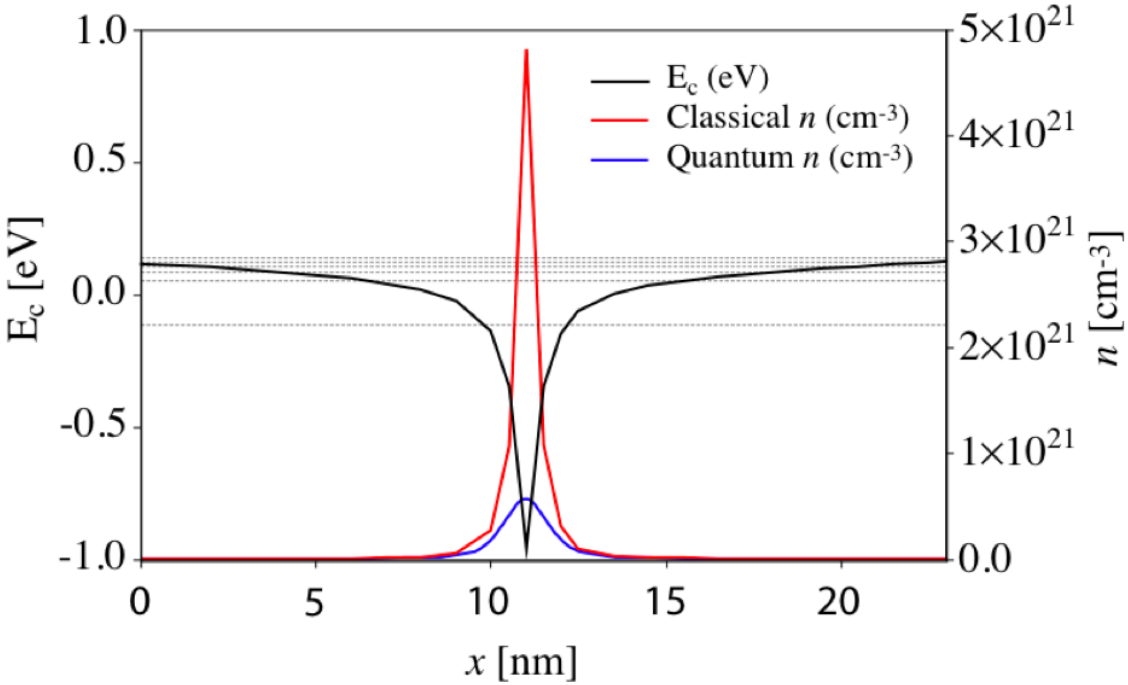

Solution - quantum corrections for electrons and holes using DG

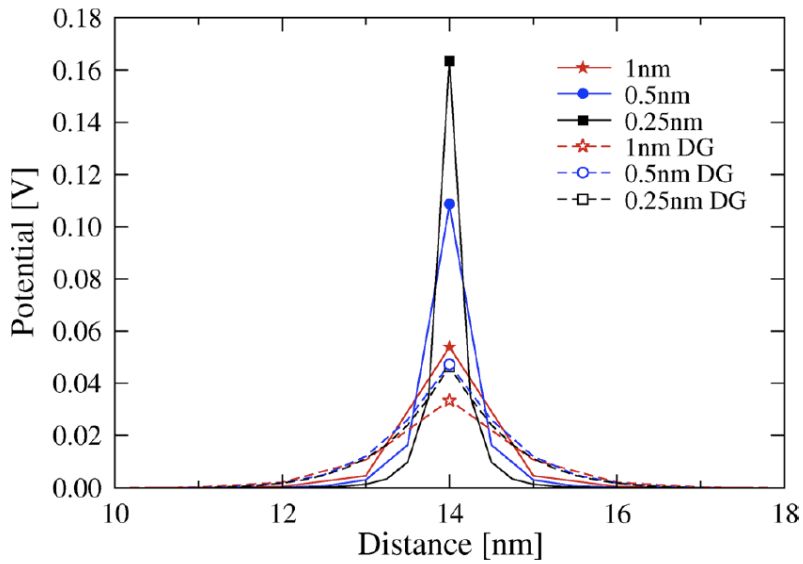

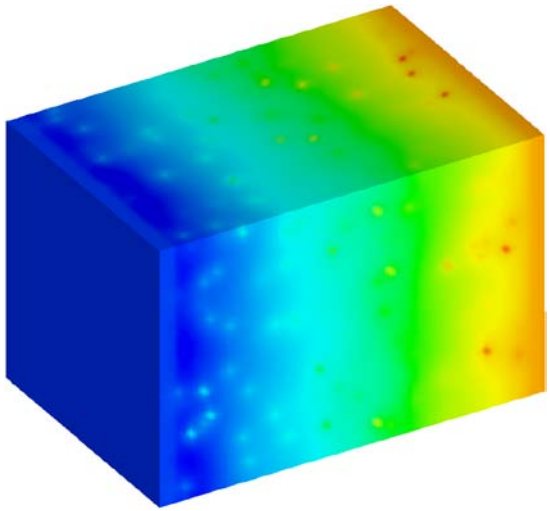

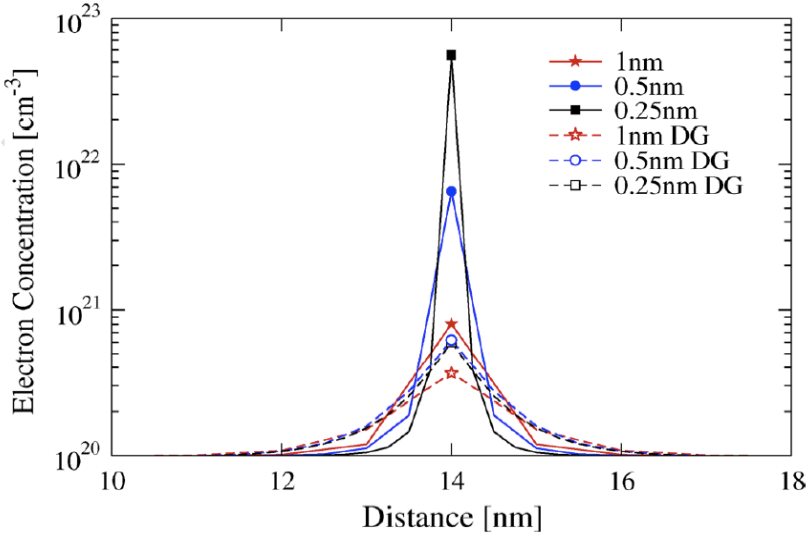

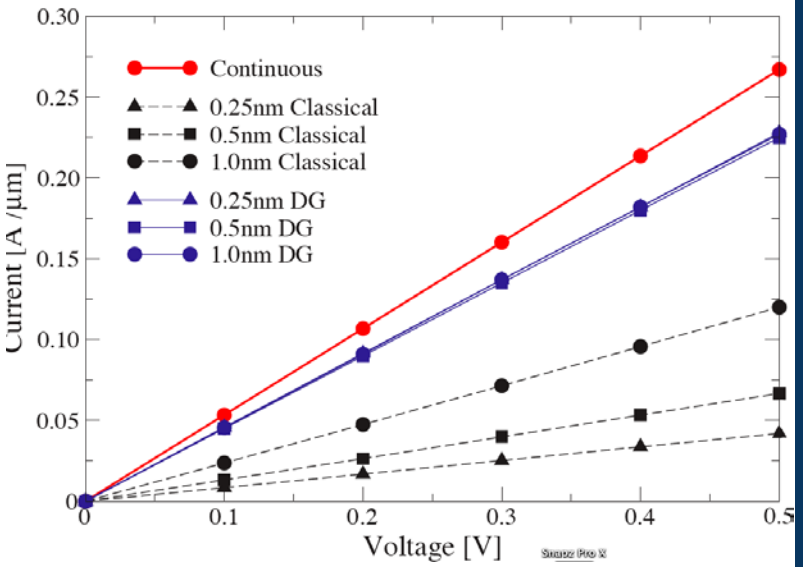

G. Roy et al.

How accurate is the DG solution?

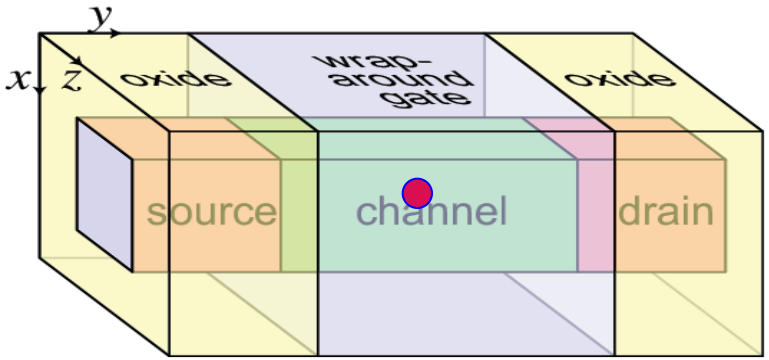

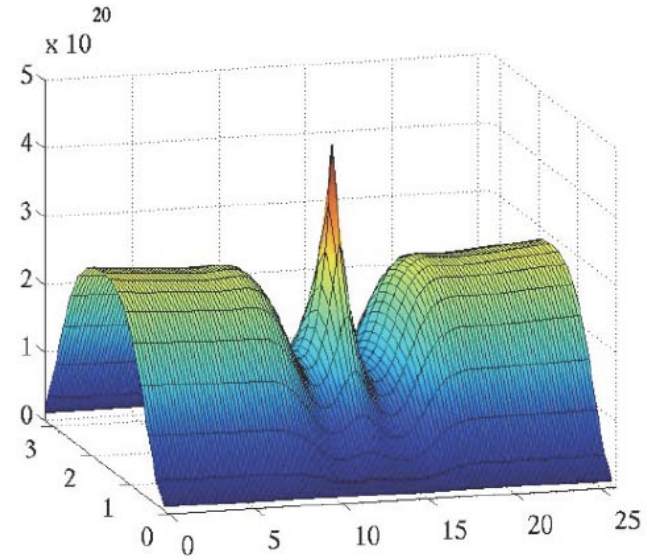

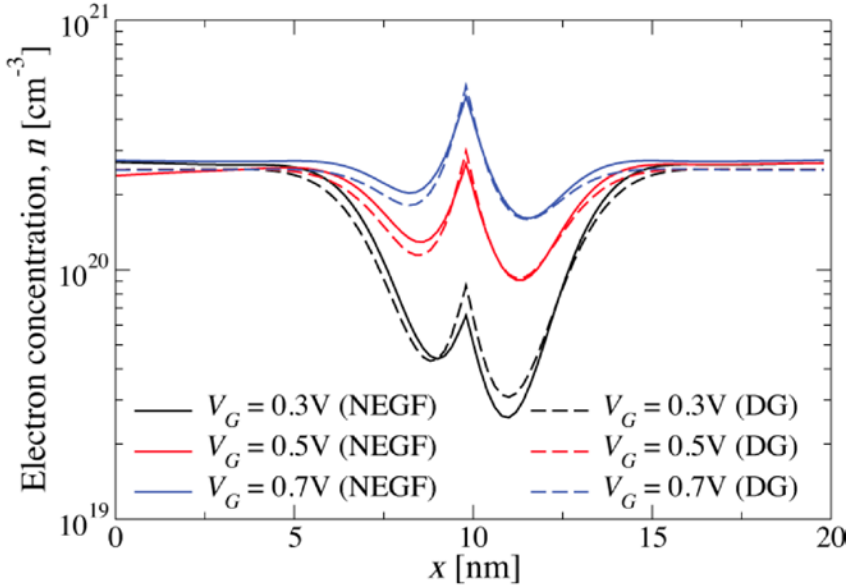

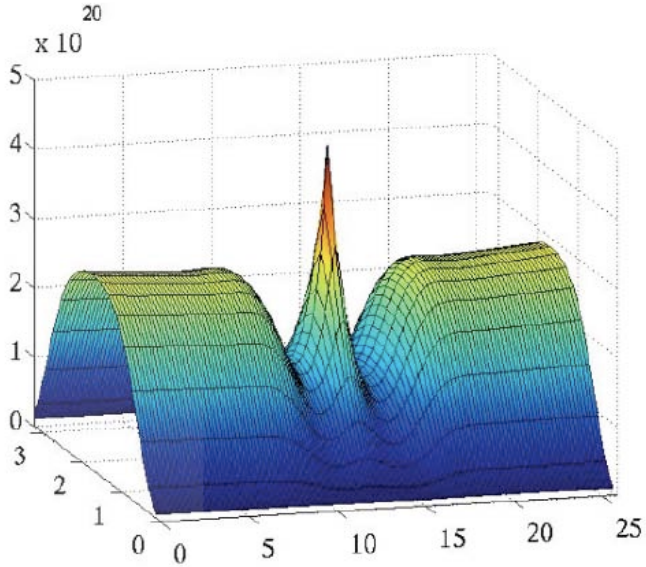

A.R. Brown et al.

Potential remedy short/long range potential

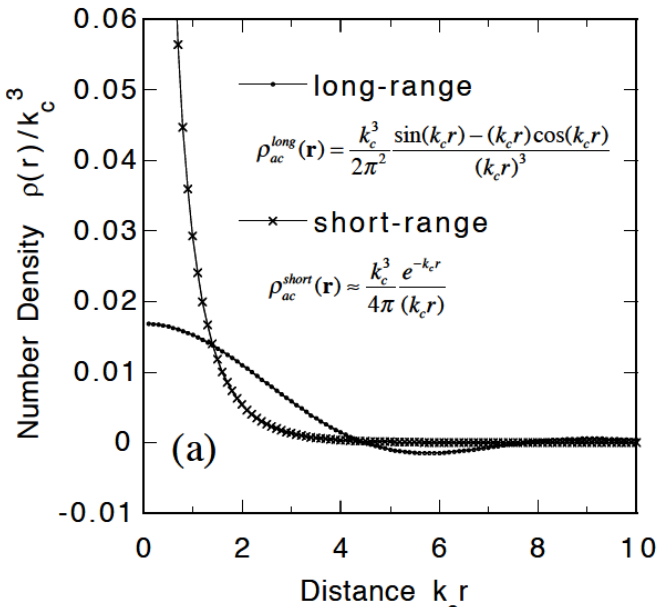

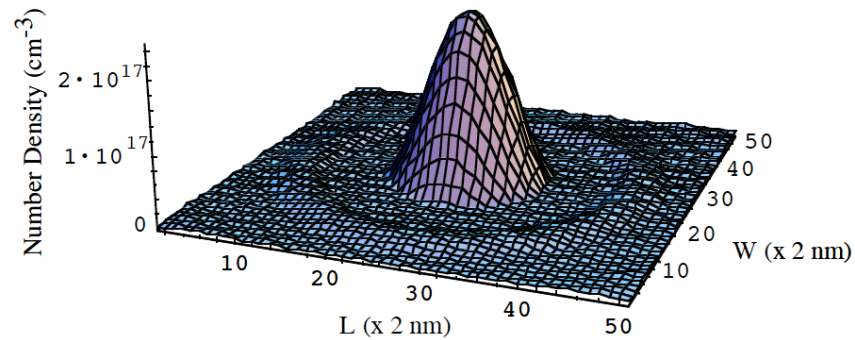

Problems in determining k_c

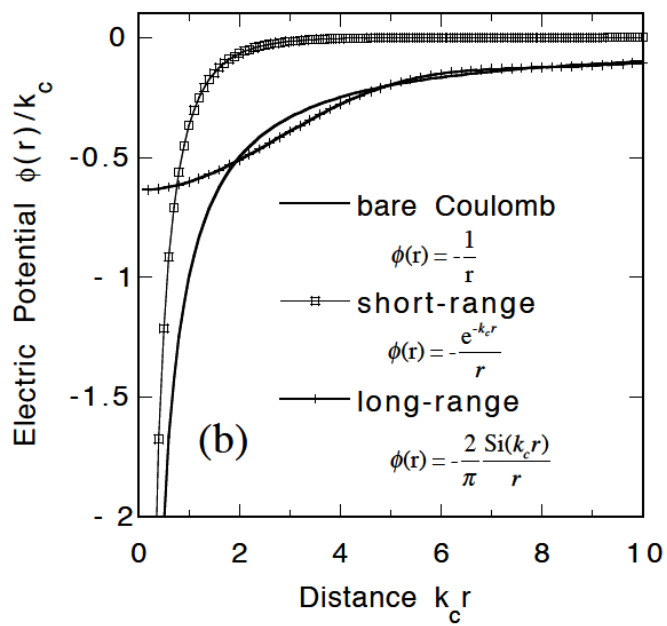

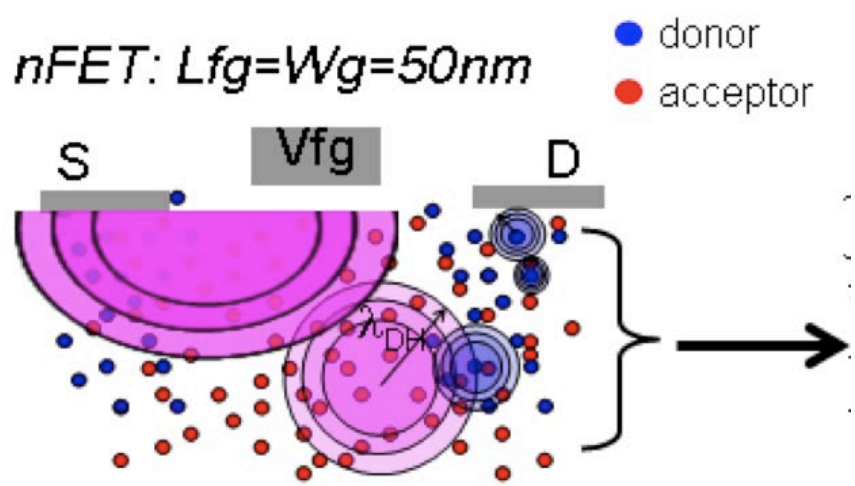

N. Sano, IEDM 2000

S. Toriyama, SISPAD W. 2010

DG vs. the Sano approach

10x10 nm DG MOSFET

DG

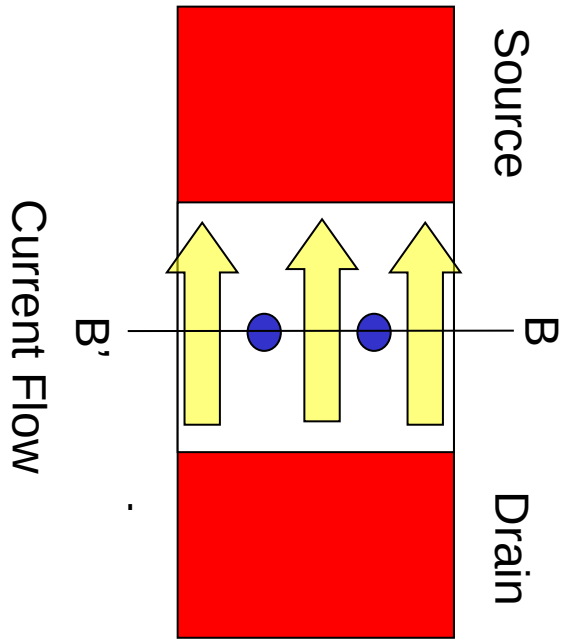

Sano

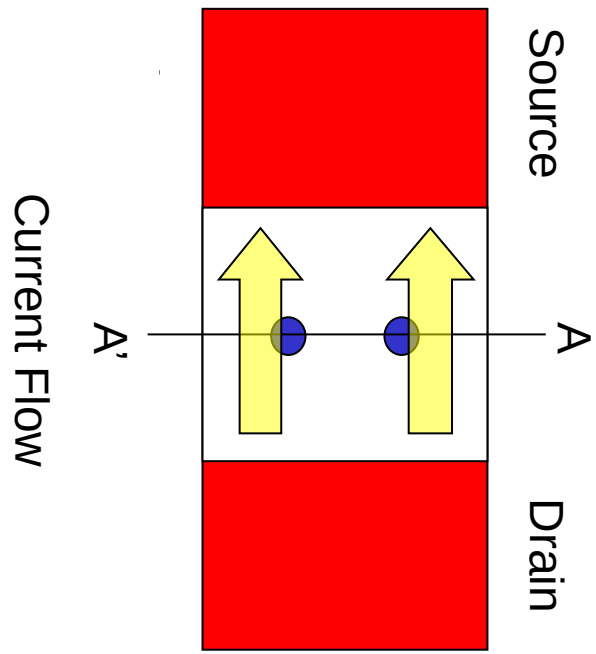

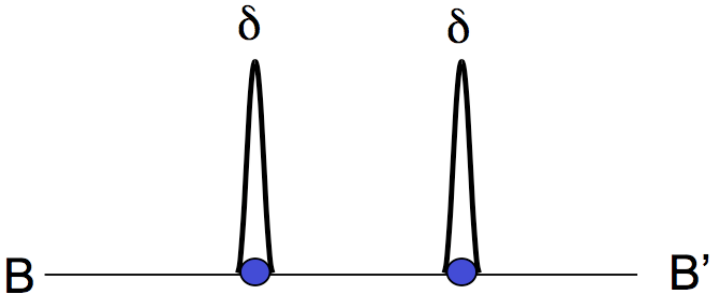

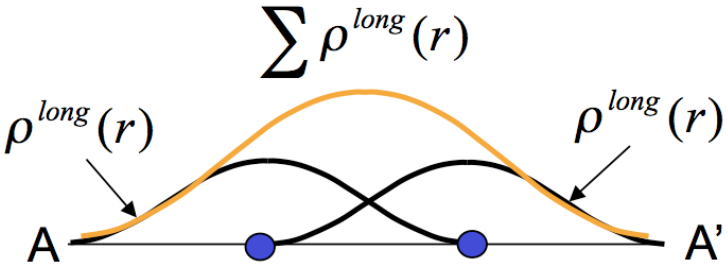

Y. Ashisava (Fujitsu)

DG vs. the Sano approach

10x10 nm DG MOSFET

DG

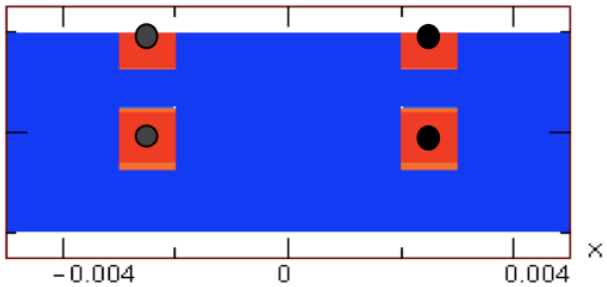

Sano

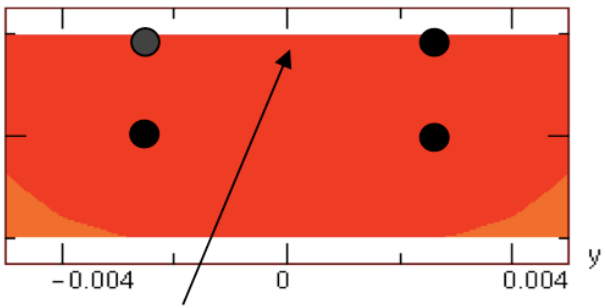

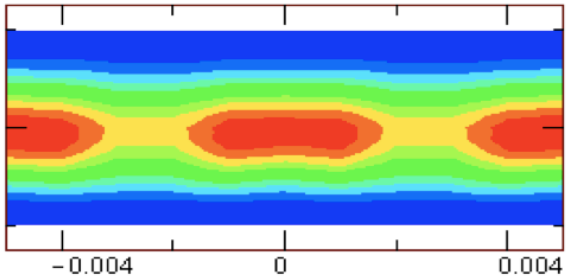

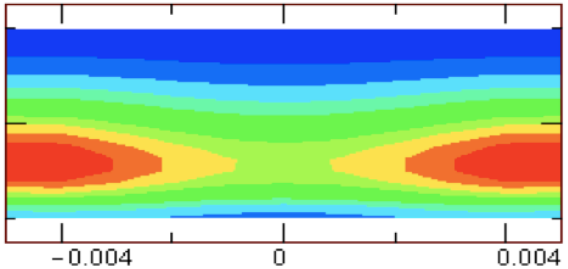

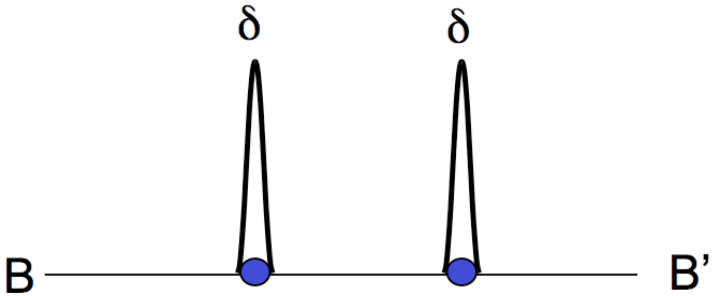

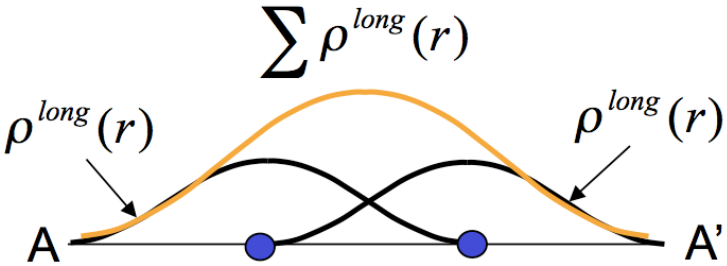

Y. Ashisava (Fujitsu)

The mobility dilemma (1)
Velocity saturation, field dependence

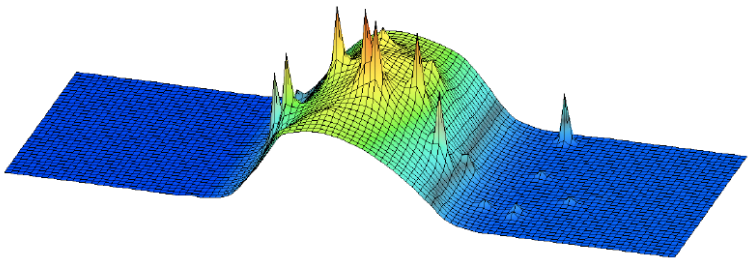

Field distribution in a MOSFET with random dopants

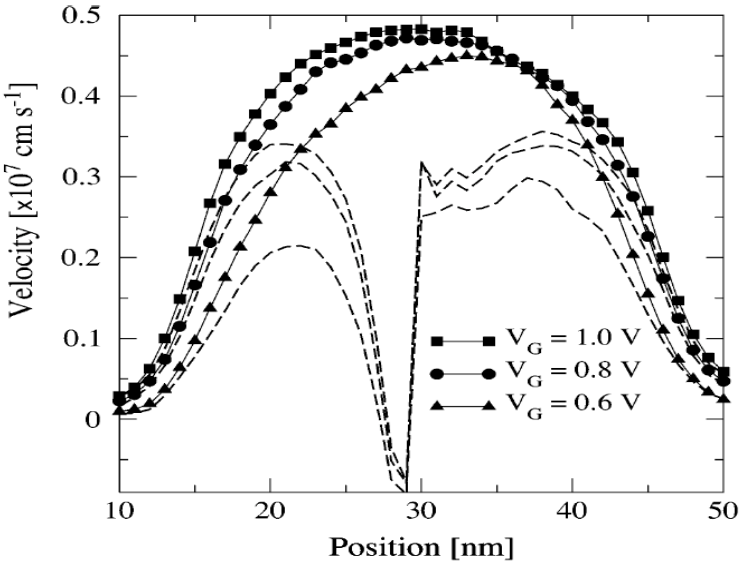

Velocity distribution in a MOSFET with single dopant

- Field dependent mobility have a meaning in ‘adiabatic’ conditions.
- The high electric field around single dopant cannot be used in the field dependent mobility model.
- The velocity saturation is associated with dissipative phonon scattering.
- The reduction of velocity around single dopant is associated with Coulomb scattering.

The calibration dilema

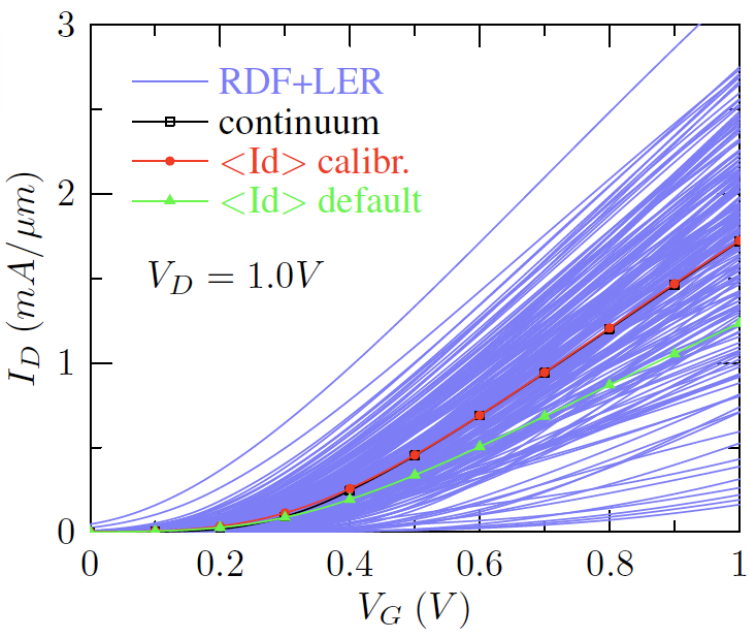

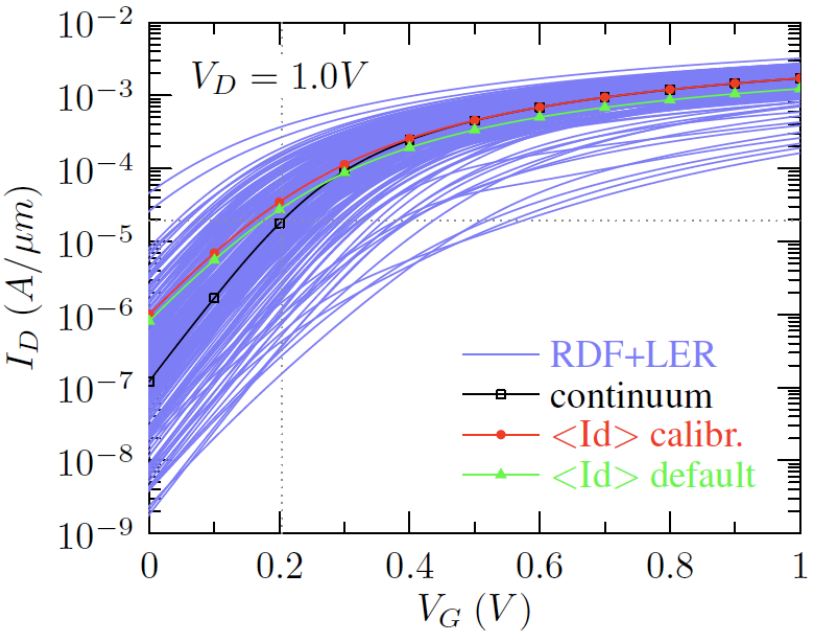

- The shape of the continuous simulation and the average ‘atomistic’ I-V curves are different.
- The calibration of continuous TCAD simulations to measurements which are equivalent to average atomistic simulation results in compensations through the mobility models..

Summary

- Background
- Drift-diffusion
- Monte Carlo
- Quantum transport
- First principle approach
- Applications
- Challenges

Short range force corrections and Rutherford backscattering

$$E(r) = \frac{er}{4\pi\varepsilon_0\varepsilon_r\left(r^2 + 2r_c^2\right)^{3/2}}$$

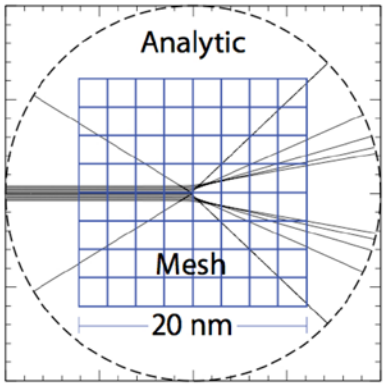

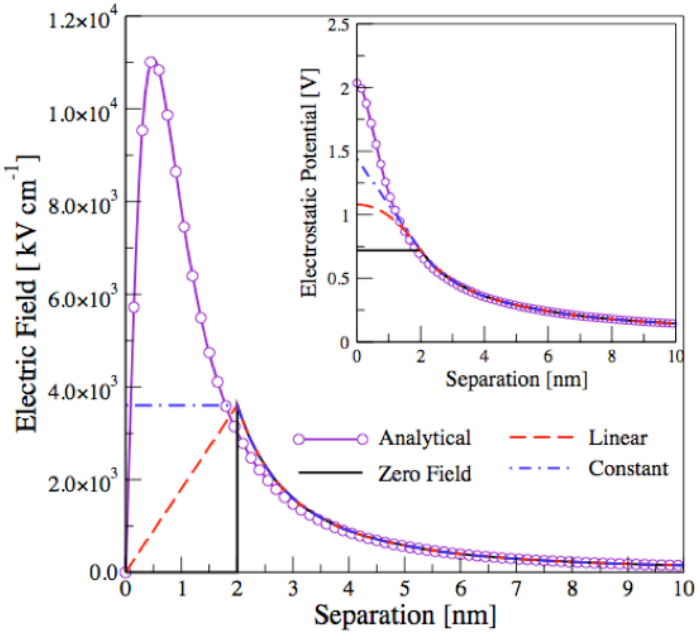

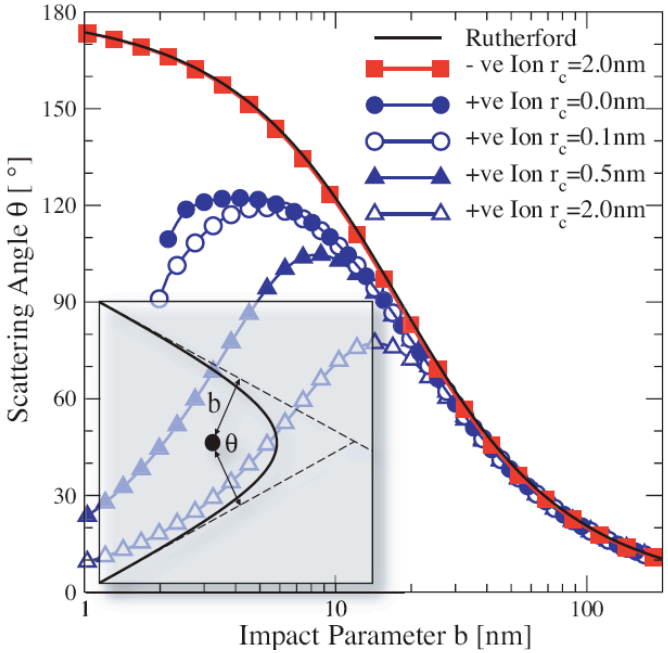

C. Alexander et al.

Reproducing the doping concentration mobility dependence

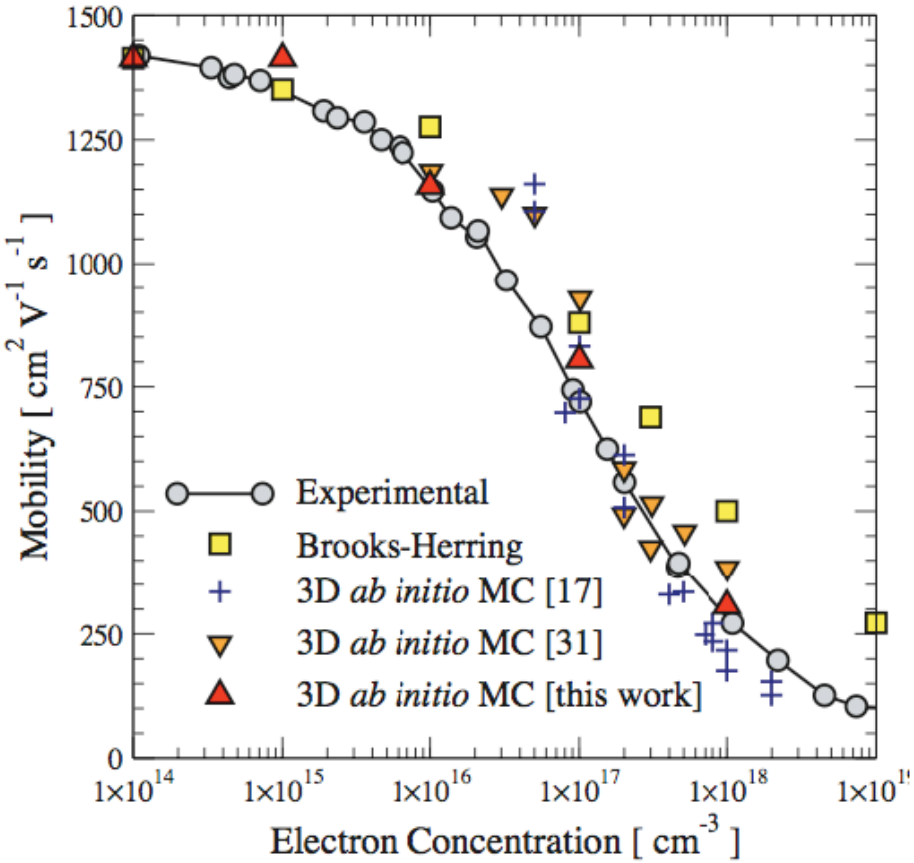

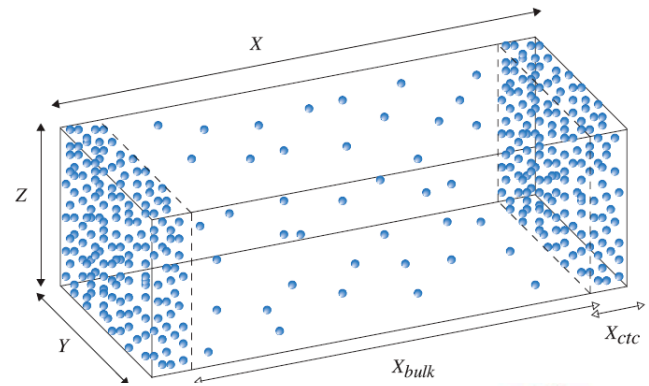

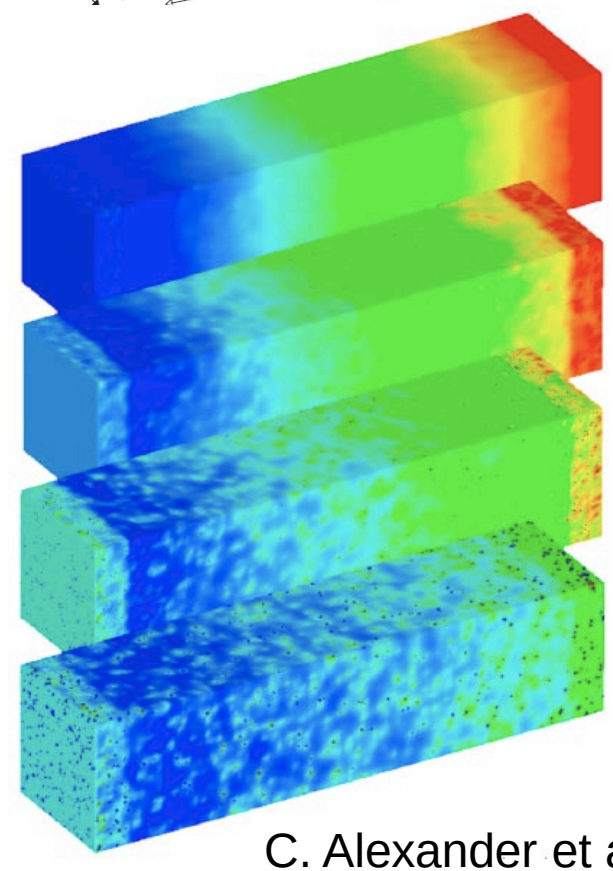

C. Alexander et al.

Statistical reliability: transport

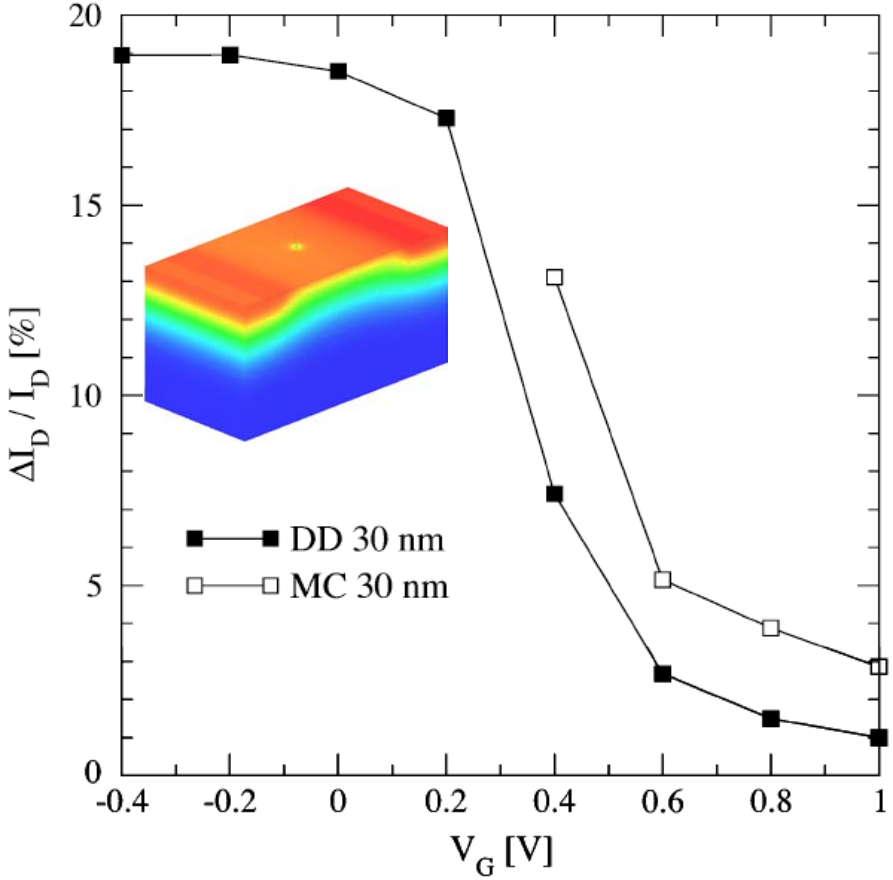

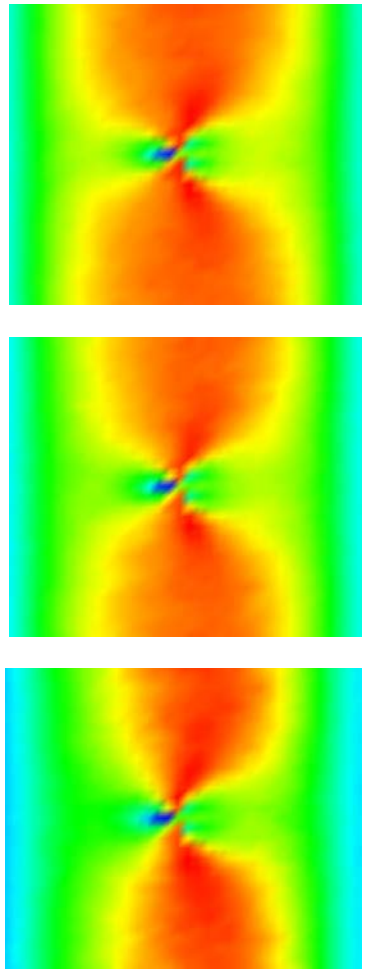

C. Alexander et al.

Transport (scattering) related variability

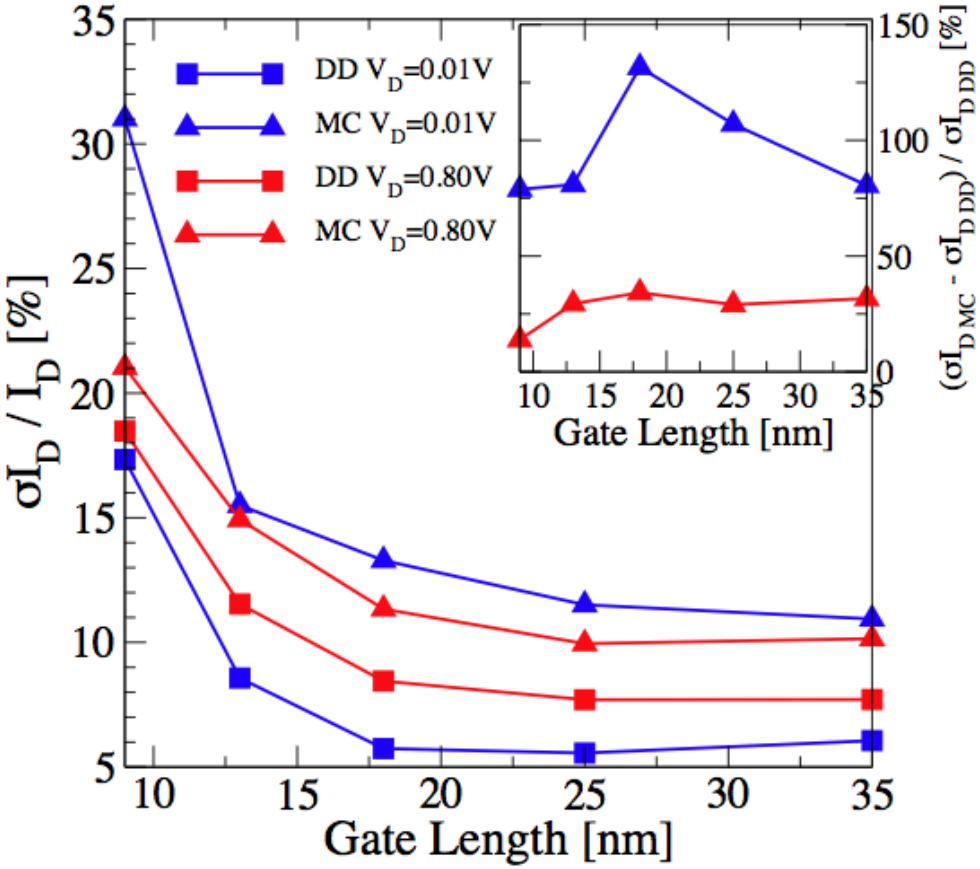

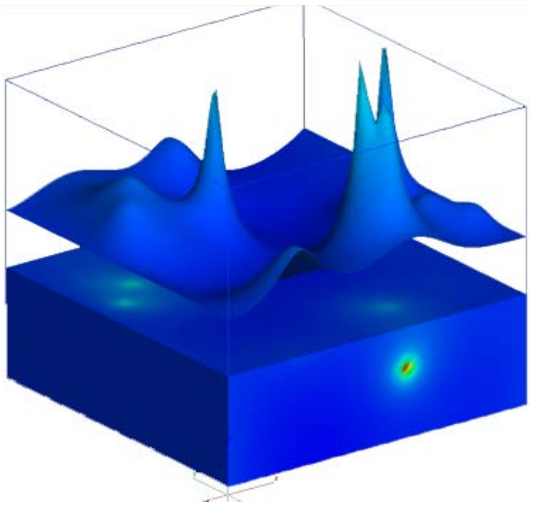

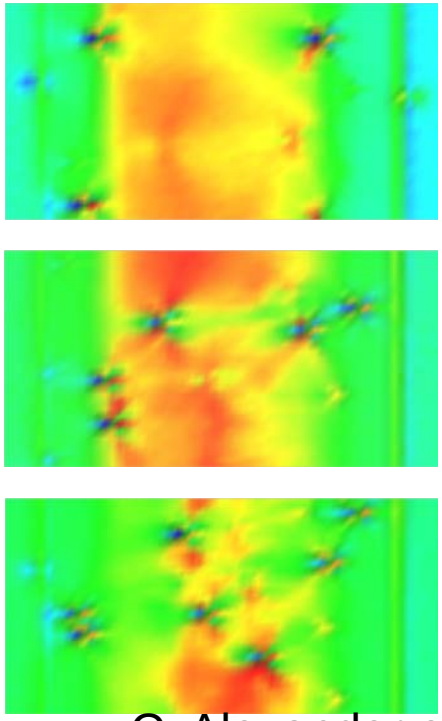

C. Alexander et al.

The impact of the transport related variability

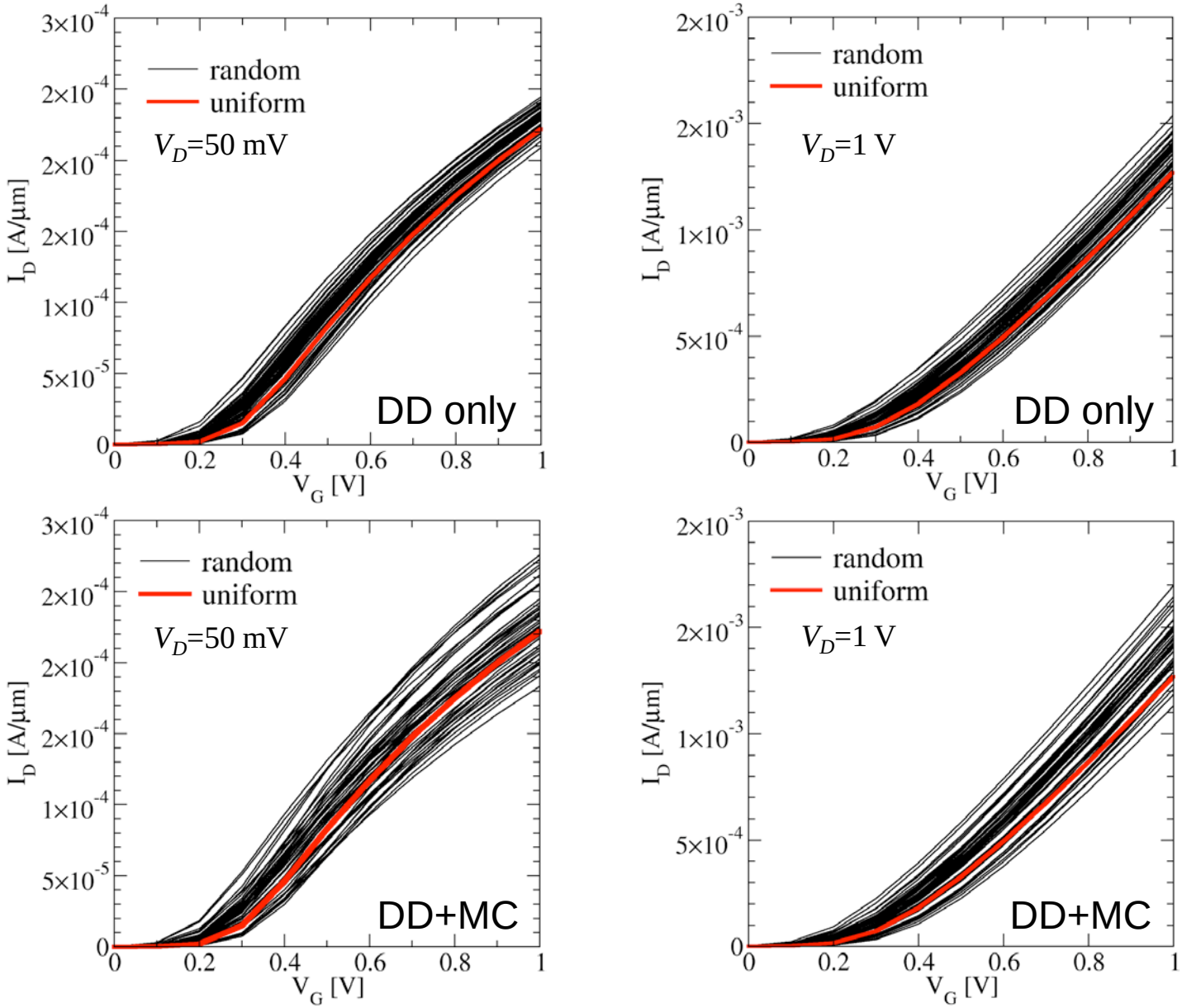

35 nm MOSFET

U. Kováč et al.

Summary

- Background
- Drift-diffusion
- Monte Carlo
- Quantum transport
- First principle approach
- Applications
- Challenges

Single dopants in NEGF simulations

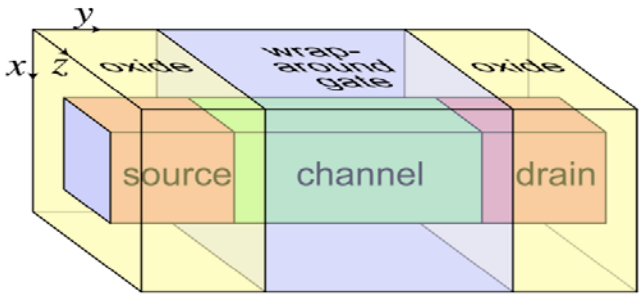

Repulsive potential

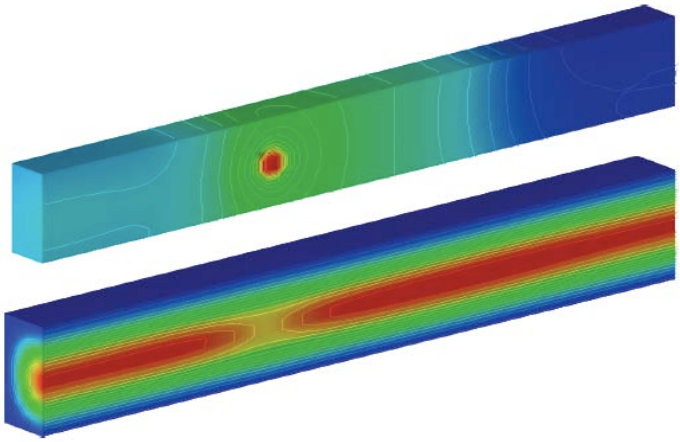

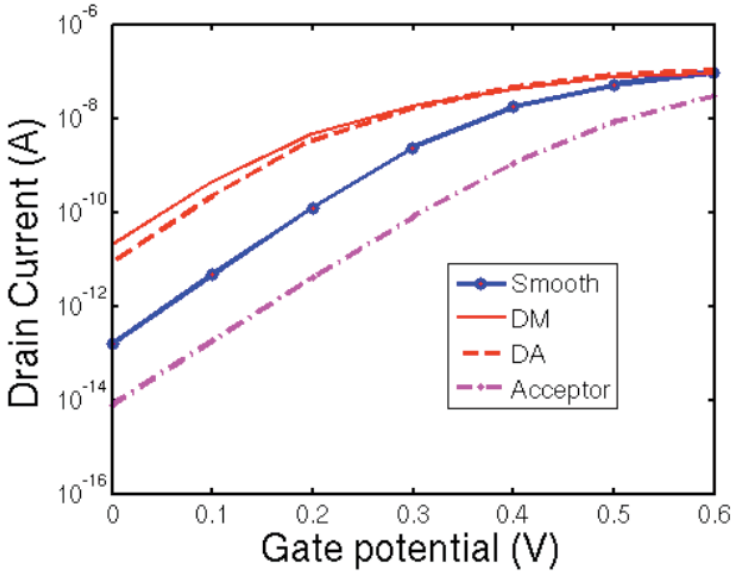

Attractive potential

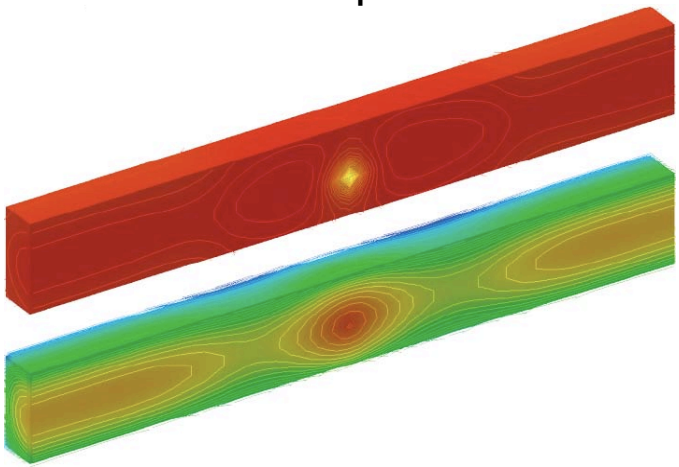

A. Martinez et al.

Single dopants in NEGF simulations

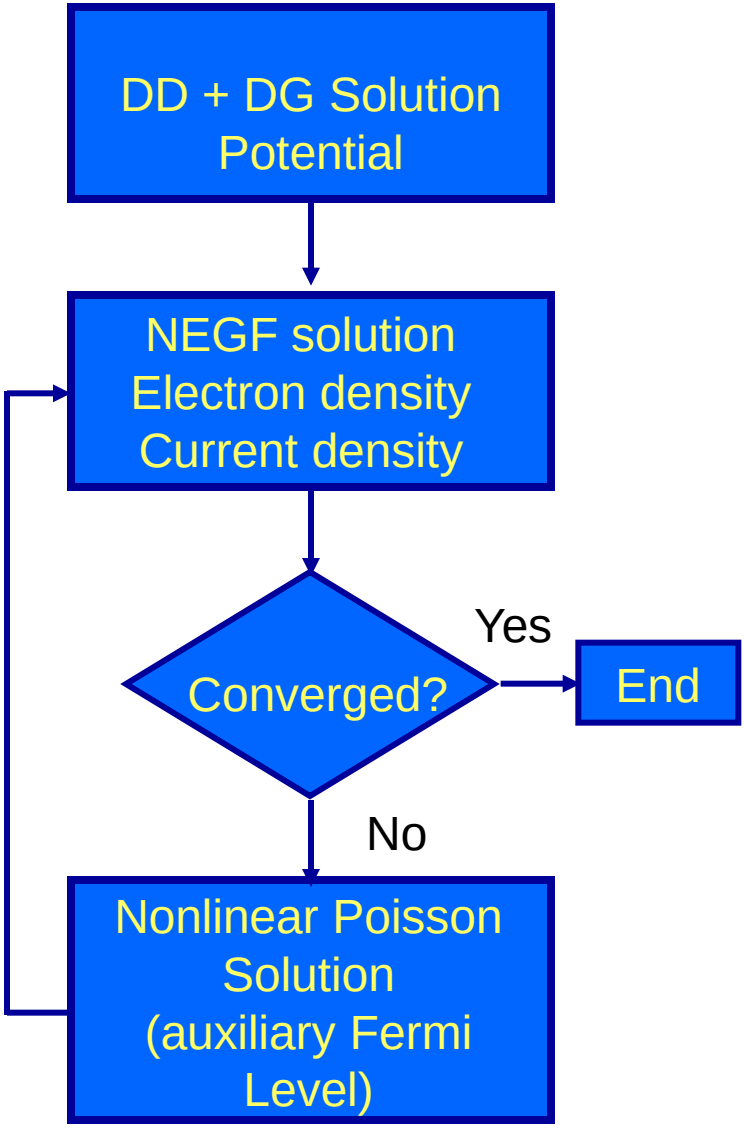

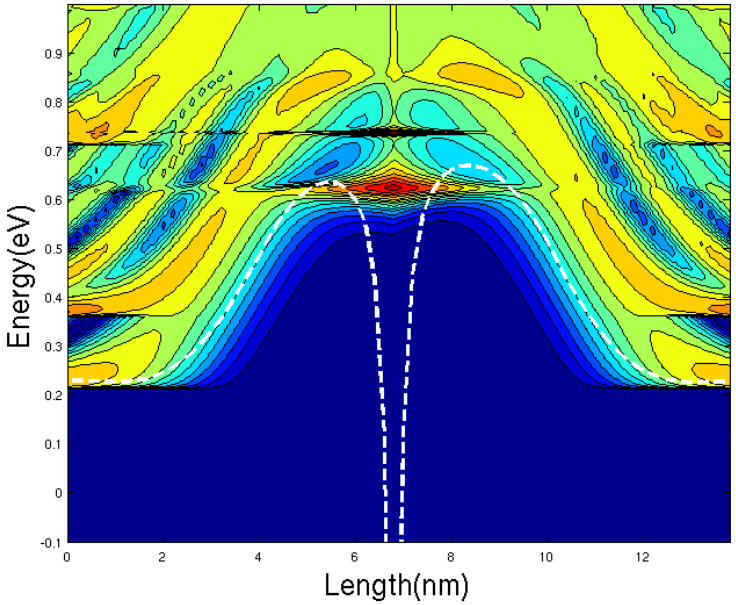

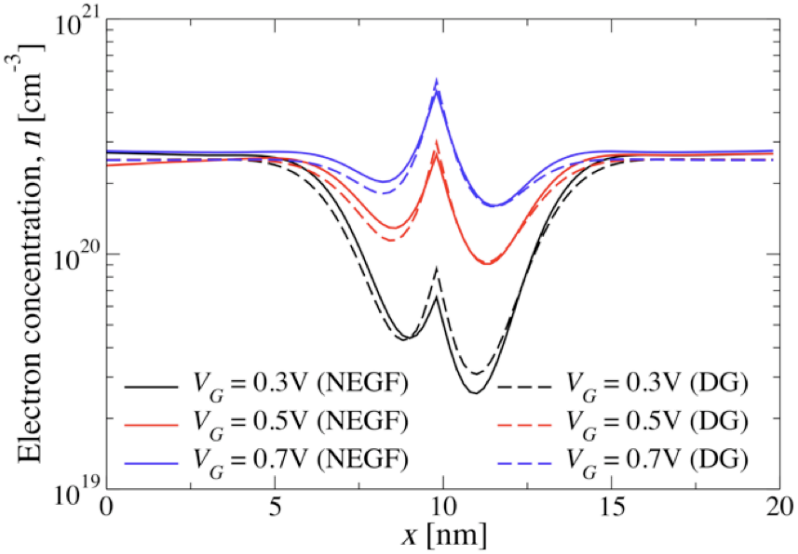

A. Martinez et al.

Single donor in the channel

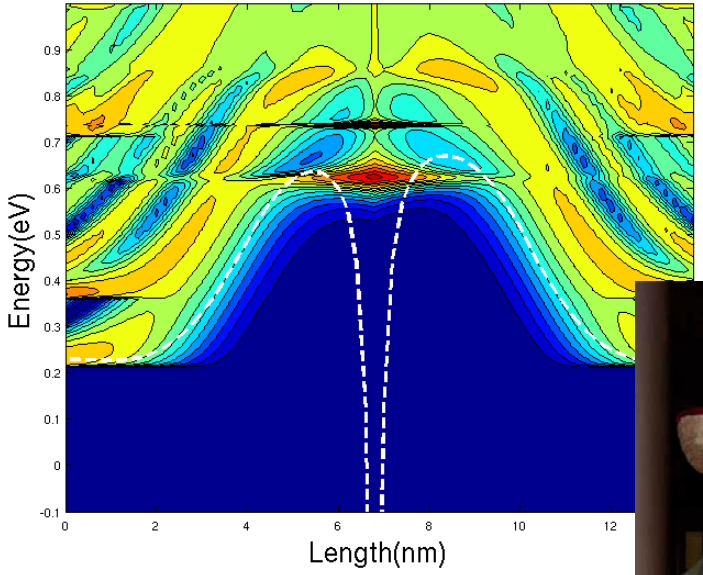

Inverted sombrero potential

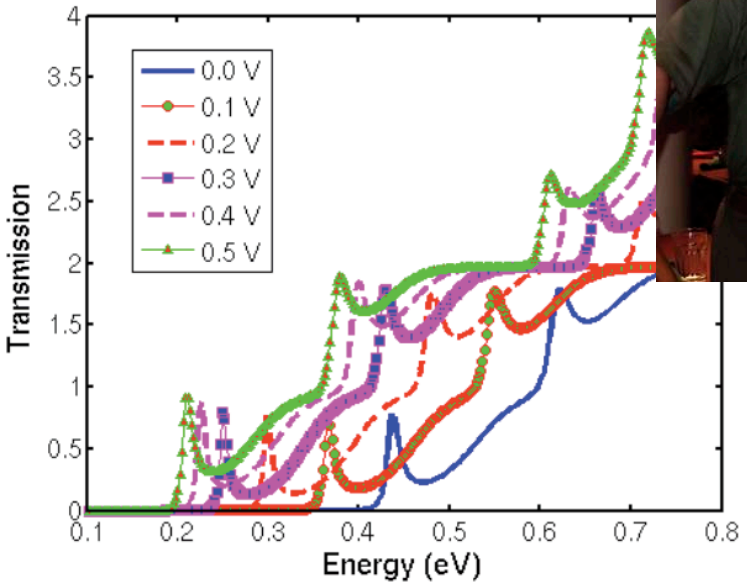

A. Martinez et al.

Summary

- Background
- Drift-diffusion
- Monte Carlo
- Quantum transport
- First principle approach
- Applications
- Challenges

Dopants in UTB structure and at interfaces

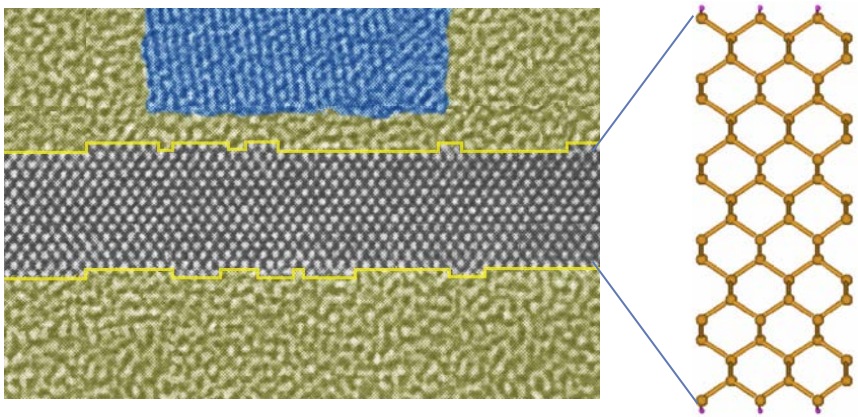

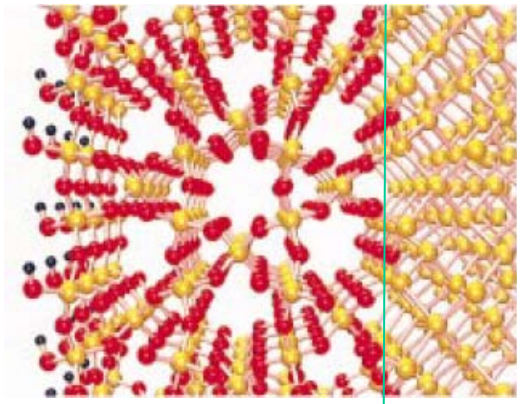

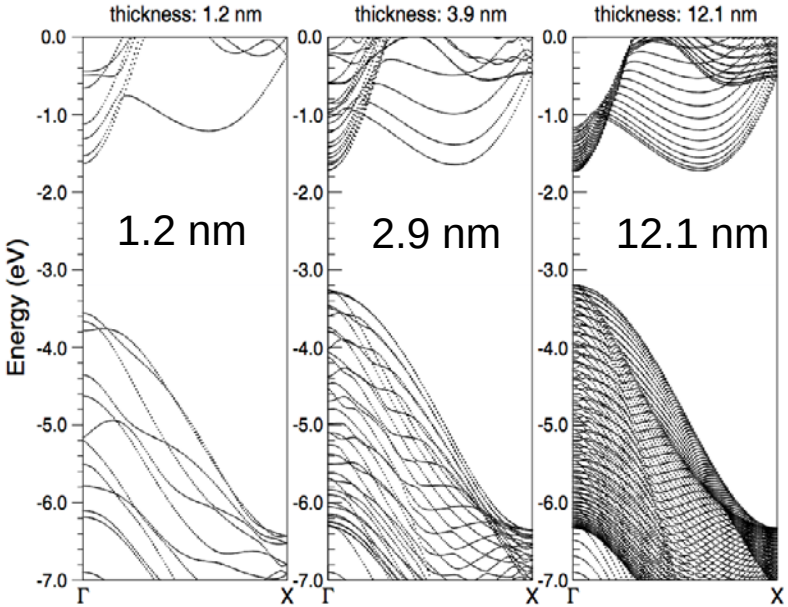

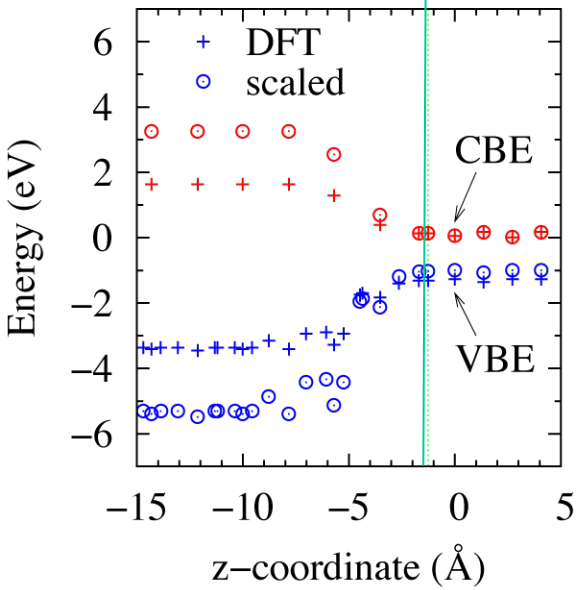

Summary

- Background
- Drift-diffusion
- Monte Carlo
- Quantum transport
- First principle approach
- Applications
- Challenges

Application of precise dopant placemen

- Reducing the variability

  Should consider interactions with other variability sources

  Should consider impact of placement inaccuracy

- Improvement of device performance

  Reduce contact resistance

  Source/drain resistance

  Short channel effects

  Mobility and injection velocity

- Beyond Moore devices

  Quantum computing

  Sensing

Arranging the dopants in the S/D

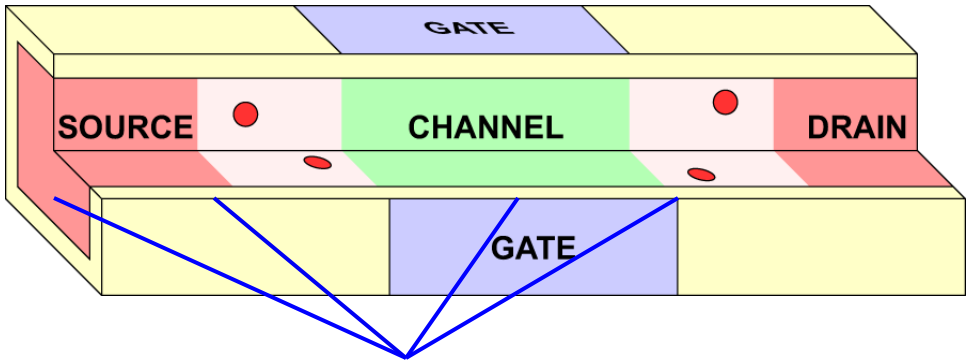

4nm S/D extension with discrete donors

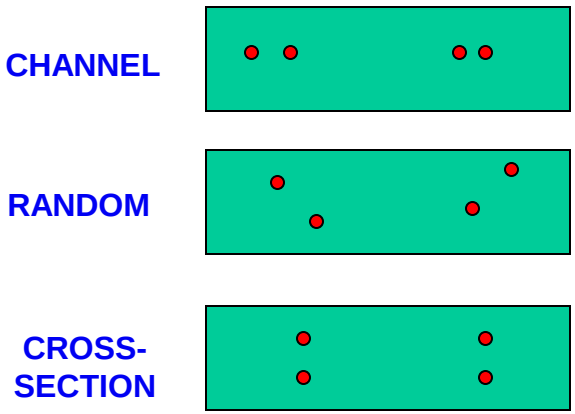

Doipant configurations

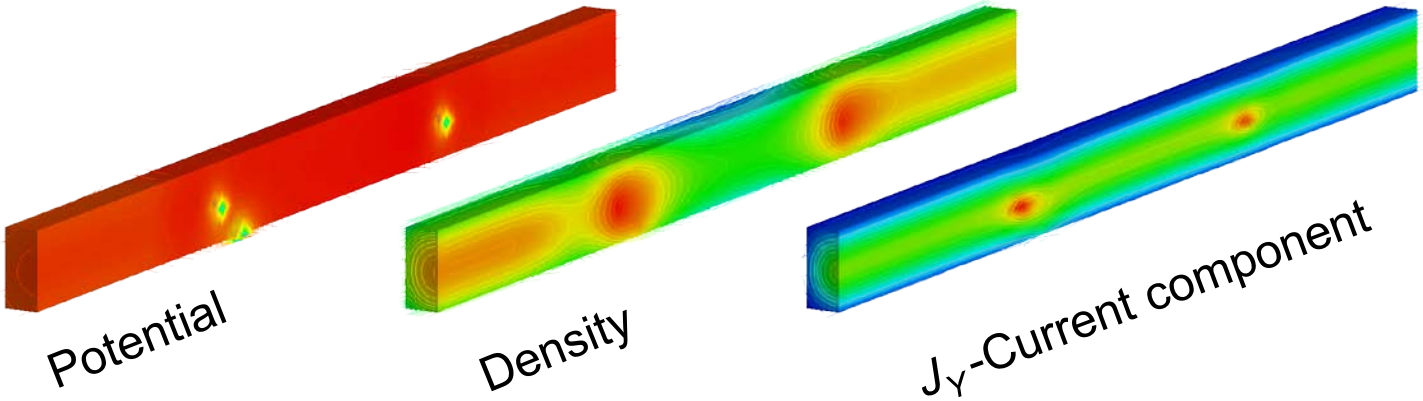

Arranging the dopants in the S/D

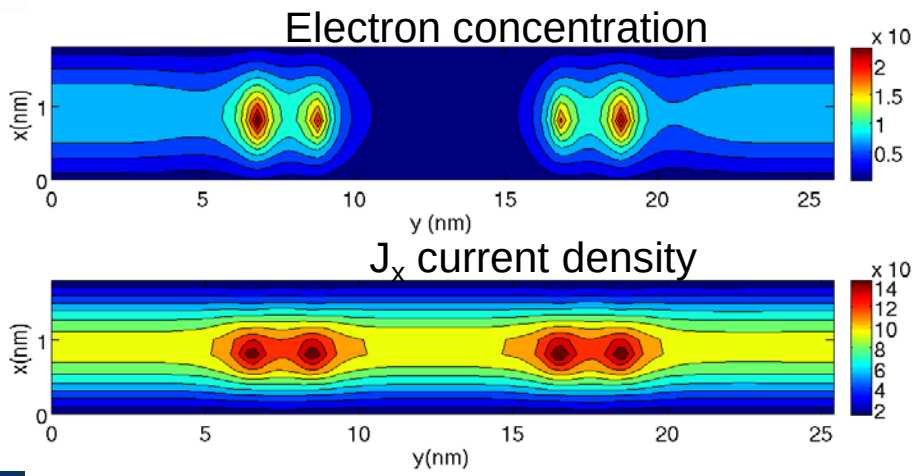

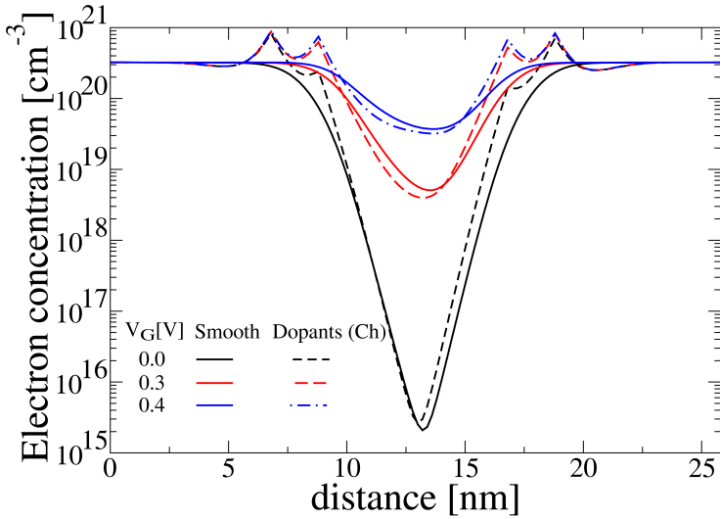

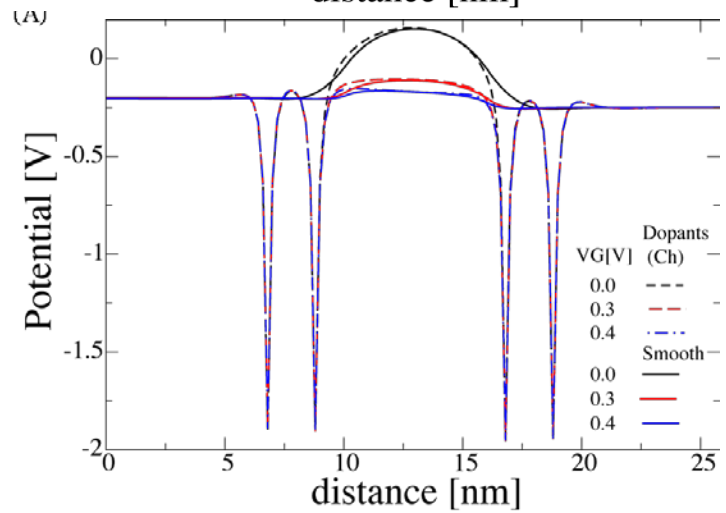

- $v \approx j/n$: Electrons going slower closer to the interface than in the middle of the cross section
- Screening density affected by gate potential at the channel neighboring impurities, strong inhomogeneity of electron density and current density

Arranging the dopants in the S/D

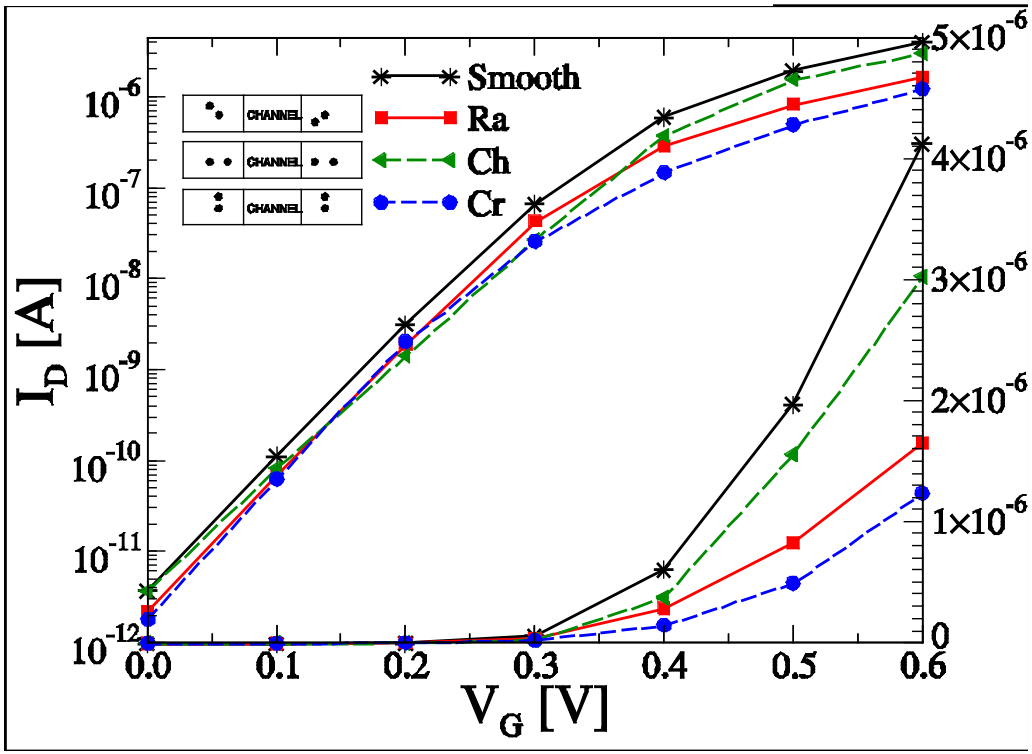

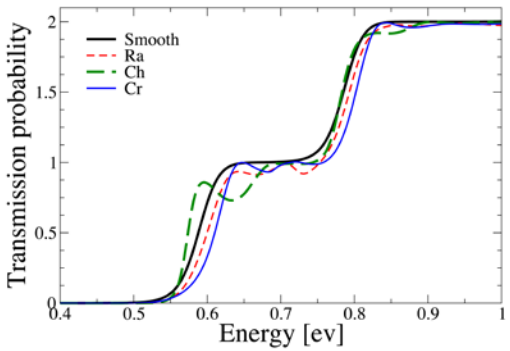

Vg=0V

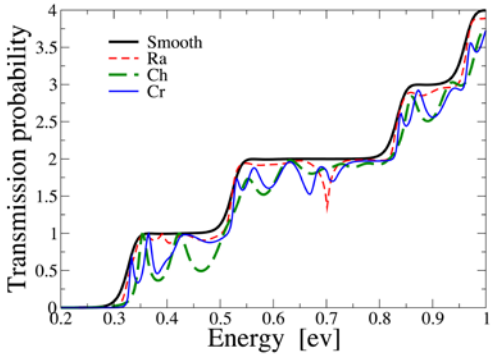

Vg=0.3V

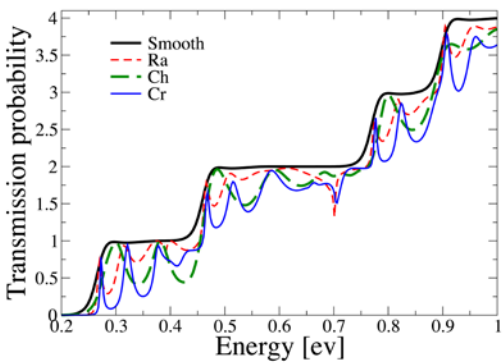

Vg=0.4V

Summary

- Background
- Drift-diffusion
- Monte Carlo
- Quantum transport
- First principle approach
- Applications
- Challenges

Challenges

DD simulations

Computational efficiency.

Mobility models that reflect the impact of individual dopants on the transport and therefore on the on-current and performance.

MC Simulations

Computational efficiency.

Efficient short-range corrections for the impurity potential and the short range driving force.

Impact of the interface on the short-range corrections and driving force.

Efficient techniques for self force avoidance.

QT Simulations

Computational efficiency.

Accurate resolution of the impurity potential.

Efficient introduction of phonon and surface roughness scattering.

Coupling to heat flow.

Coupling to first principle DFT simulations.

Adding phonon scattering to NEGF

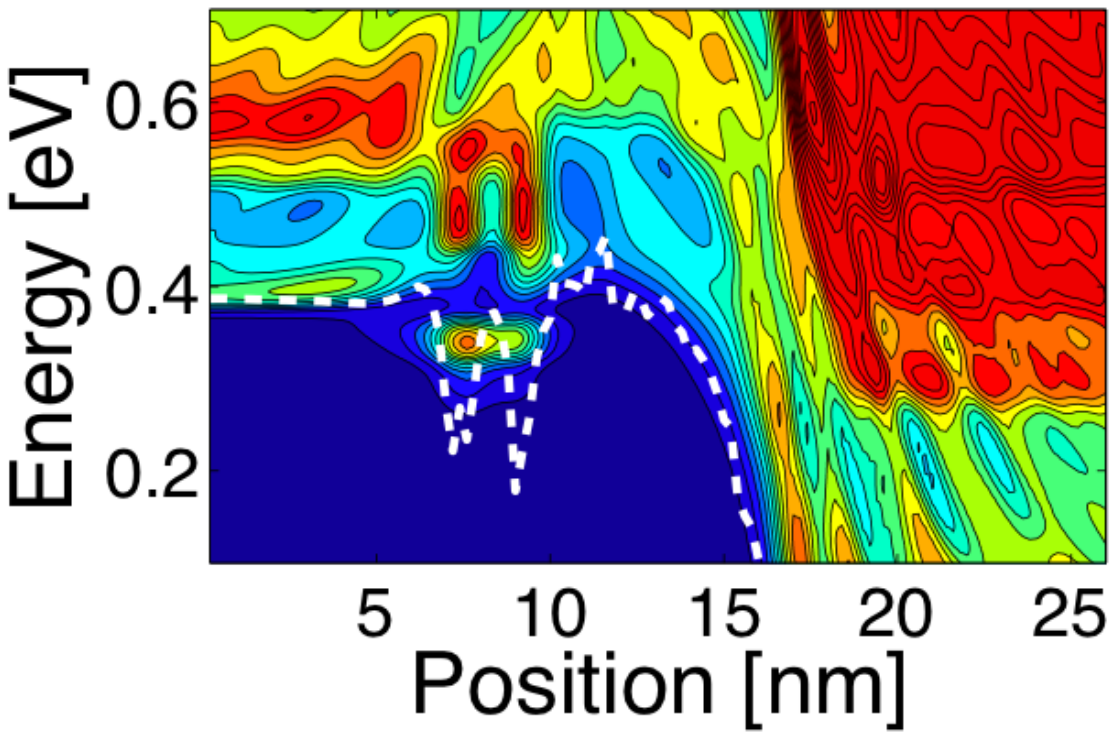

Control and readout of a single dopant spin in silicon

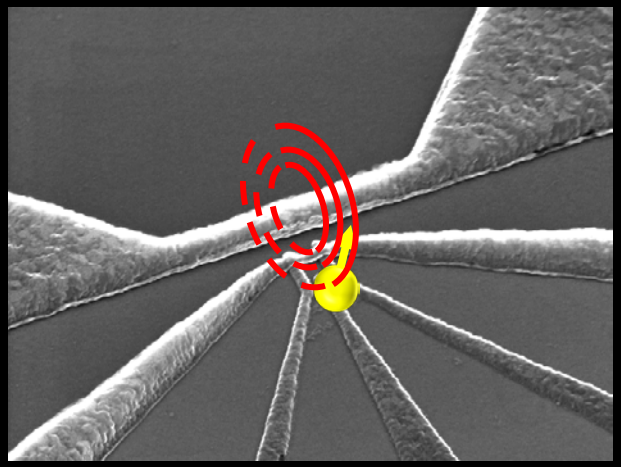

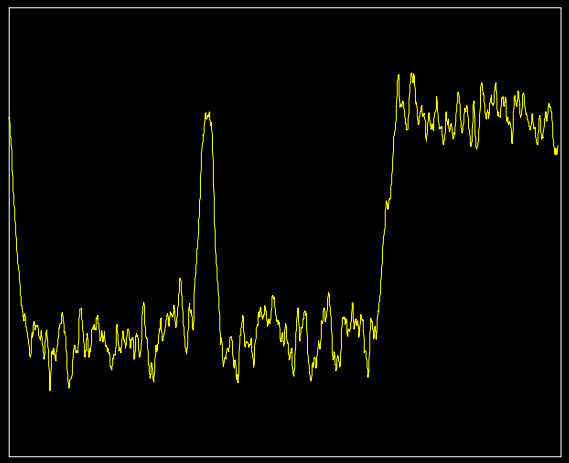

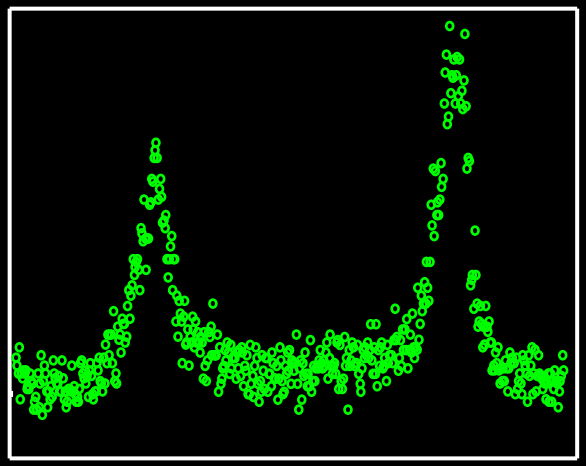

Andrea Morello

CQC²T, Centre for Quantum Computation and Communication Technology
The University of New South Wales
a.morello@unsw.edu.au

Spin-based quantum computers

Spin S = 1/2 ⇒ natural qubit

1 = |↑⟩

0 = |↓⟩

Individual dopants
e.g. in silicon

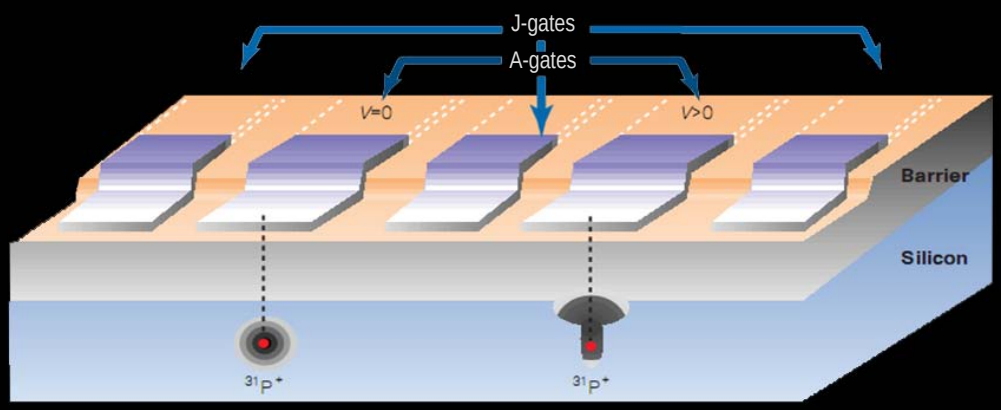

Natural atoms

Kane, Nature **393**, 133 (1998)

Electrostatically defined
quantum dots

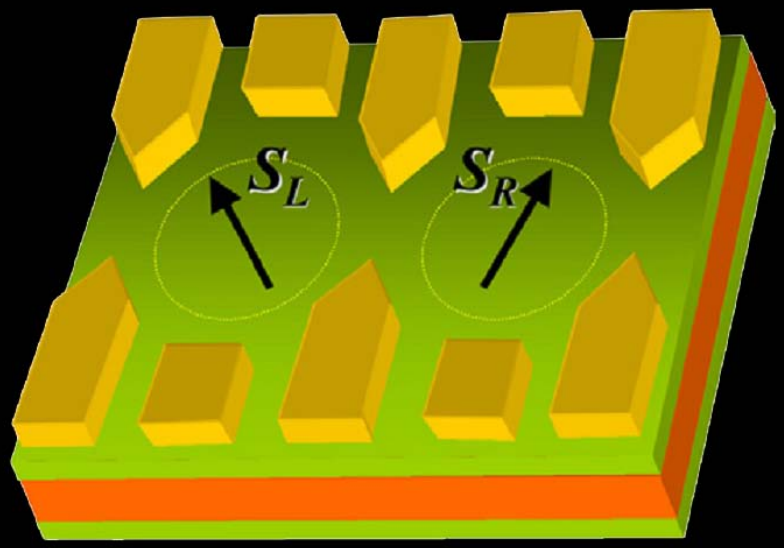

"Artificial atoms"

Loss & DiVincenzo, PRA **57**, 120 (1998)

Scalable QC architecture

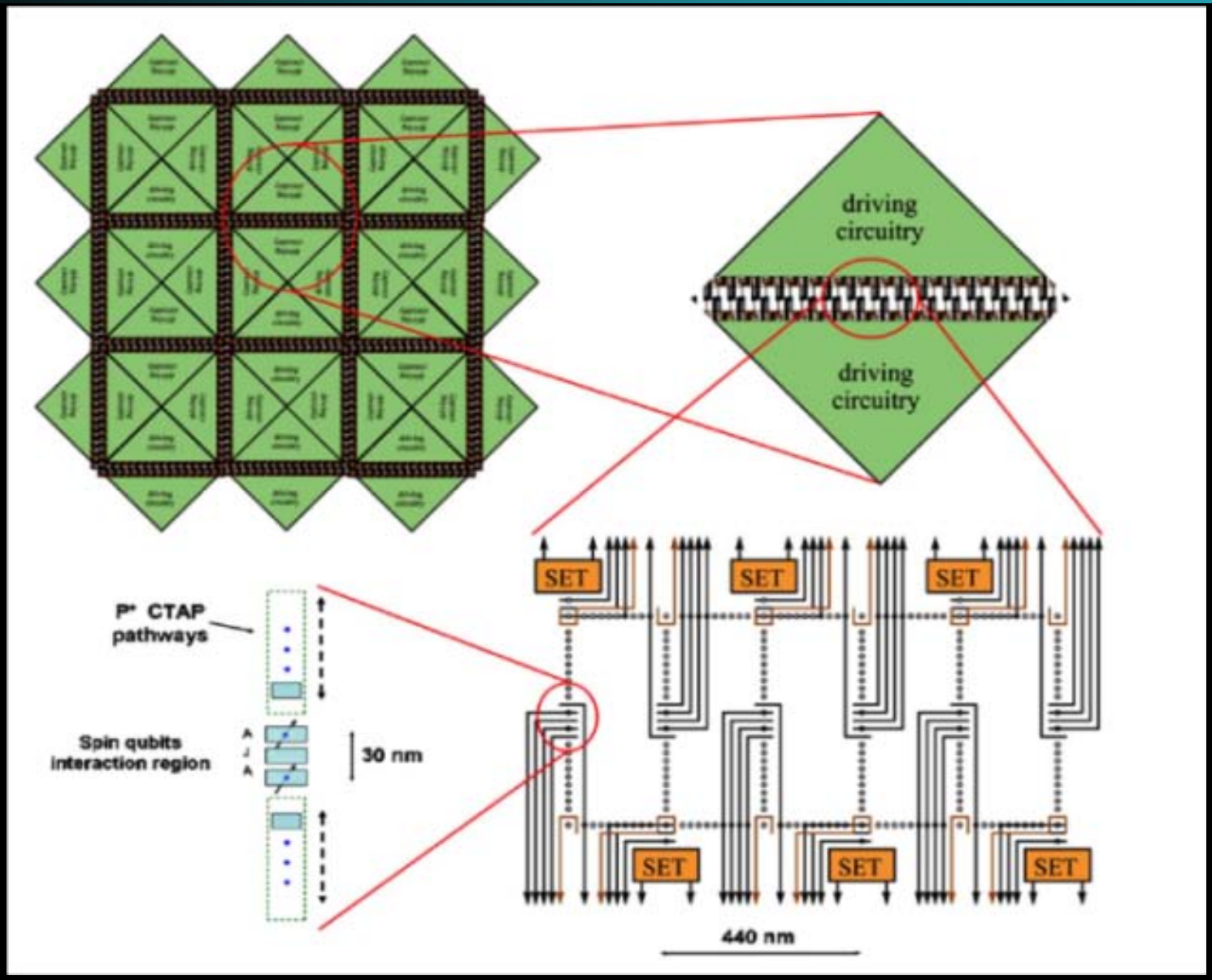

Hollenberg et al., PRB **74**, 045311 (2006)

Components and milestones

1. Read

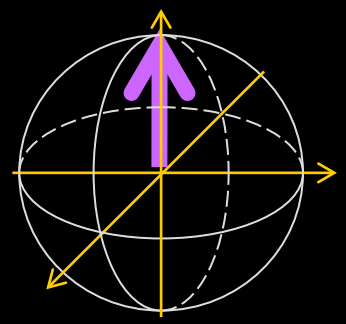

$|1\rangle$

Spin-dependent tunneling

Components and milestones

1. Read

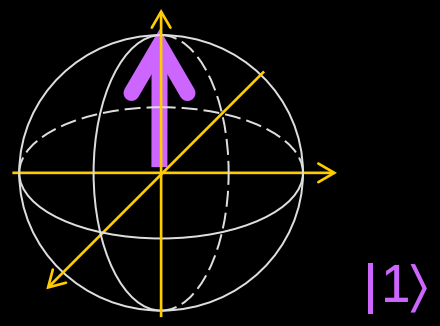

Spin-dependent tunneling

2. Write

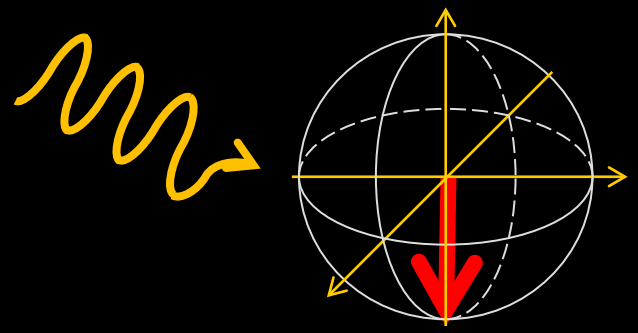

Electron spin resonance

Components and milestones

1. Read

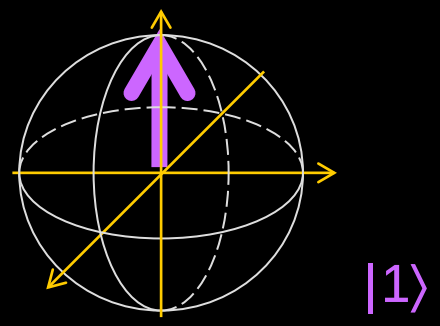

Spin-dependent tunneling

2. Write

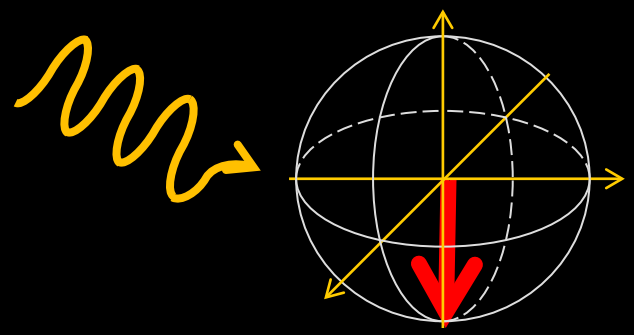

Electron spin resonance

3. Couple

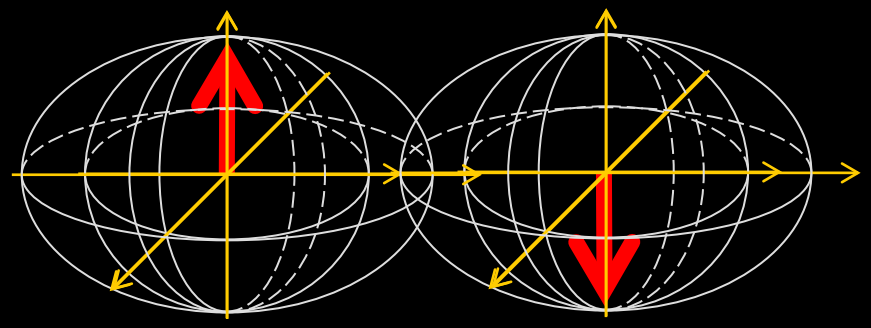

Exchange interaction

Components and milestones

1. Read

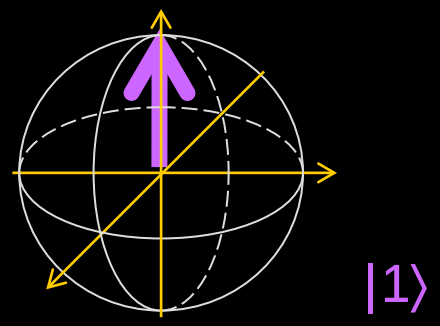

Spin-dependent tunneling

2. Write

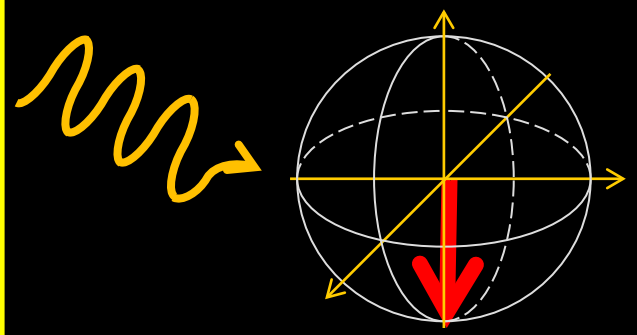

Electron spin resonance

3. Couple

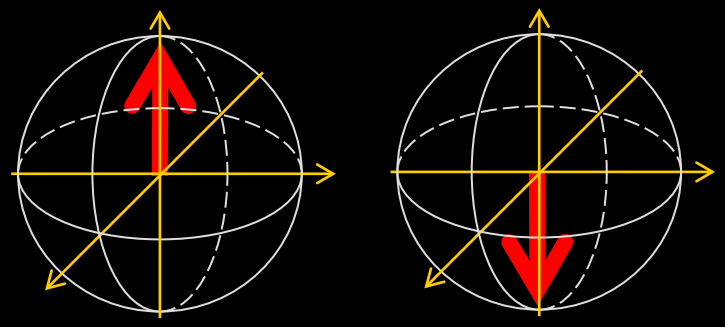

Exchange interaction

4. Transport

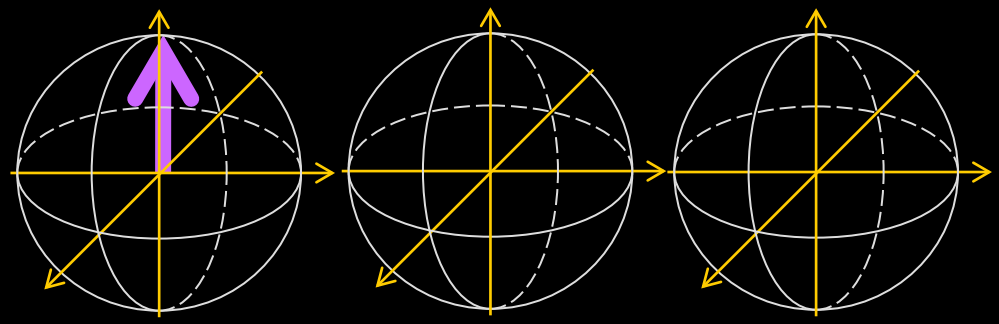

CTAP, shuttle, spin bus, ...

Placing the donors

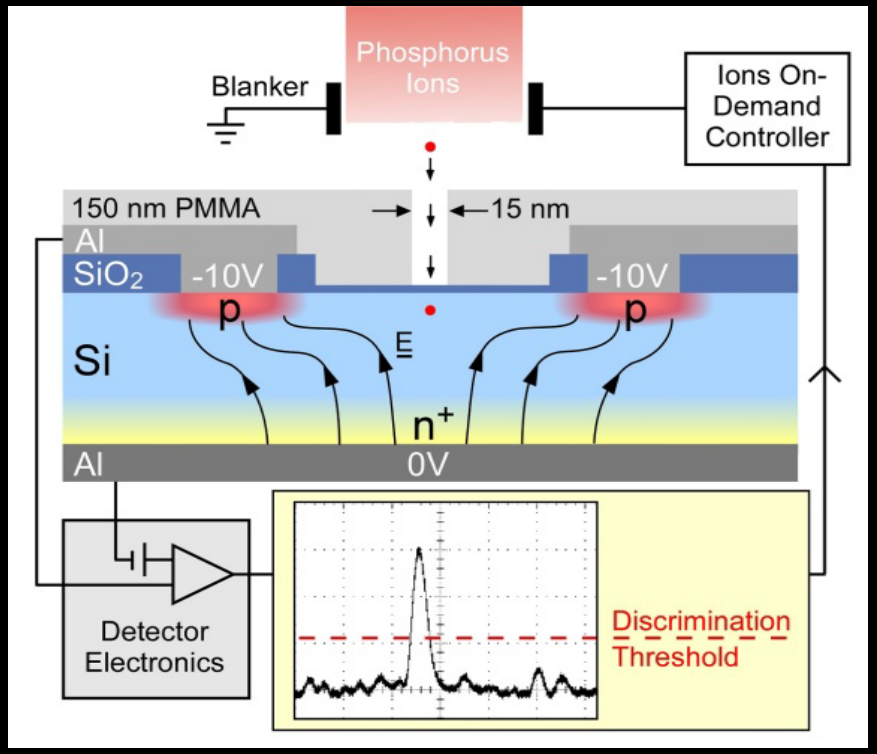

Counted single-ion implantation

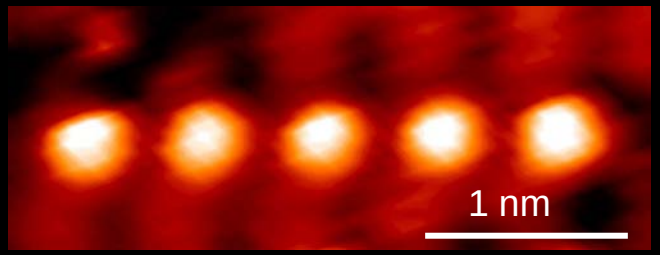

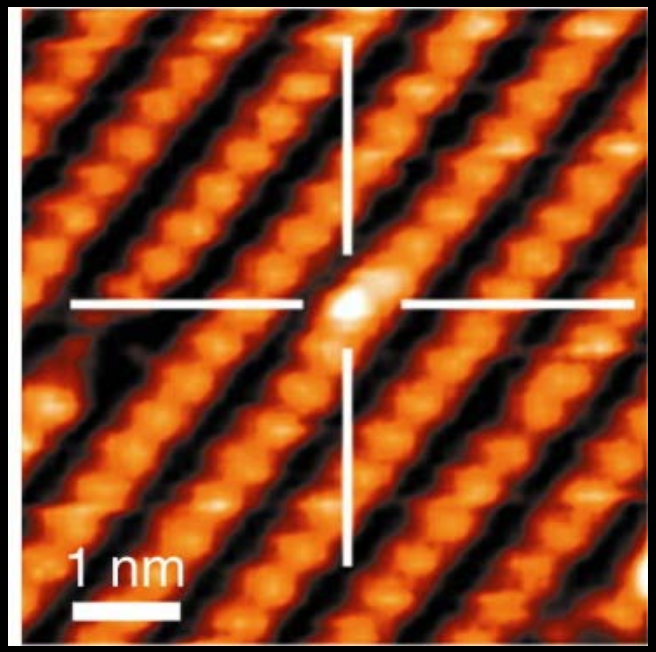

STM patterning

Jamieson et al., APL **86**, 202101 (2005)

Schofield et al., PRL **91**, 136104 (2003)

MOS Si Single Electron Transistor

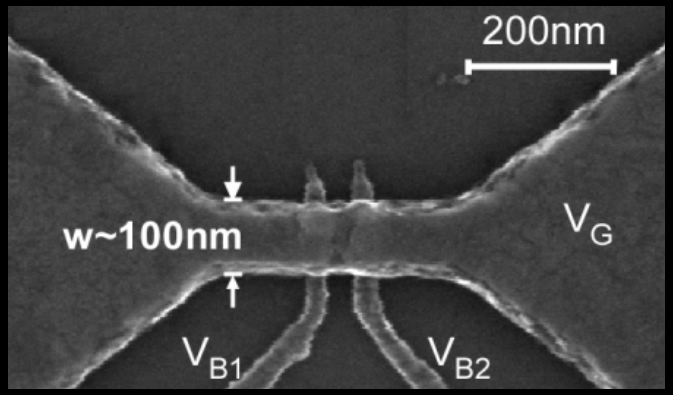

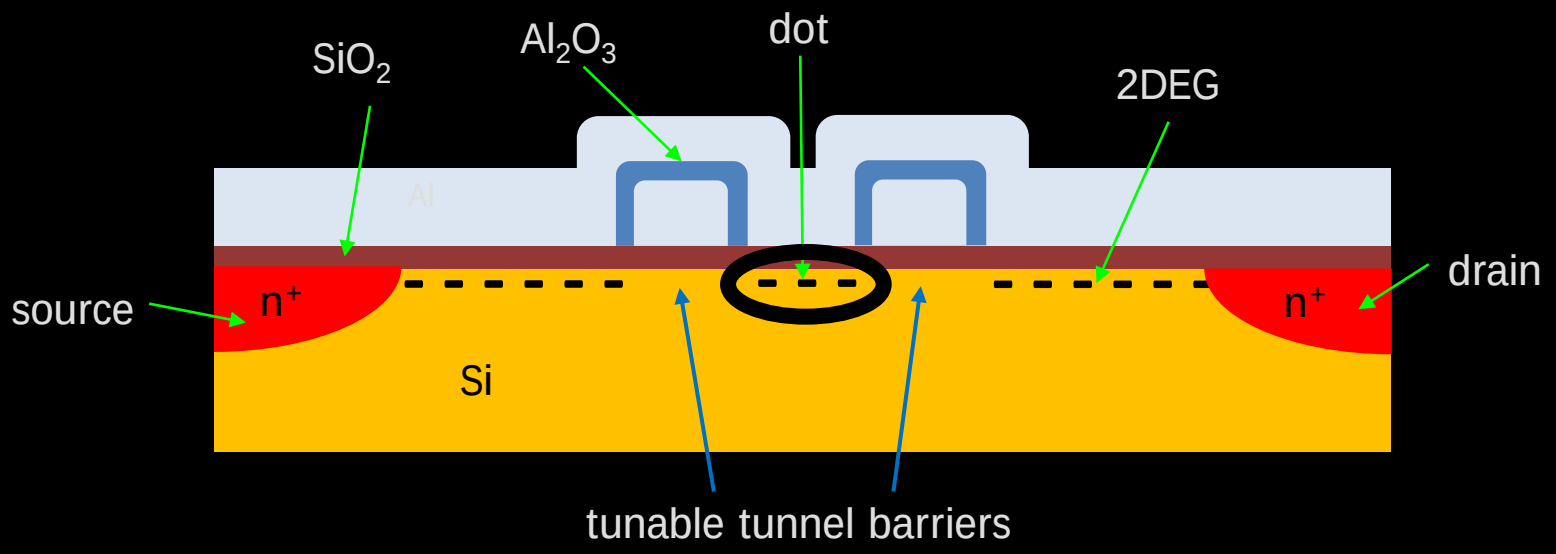

SET island underneath the SiO_2

Angus et al., Nano Lett. **7**, 2051 (2007); APL **92**, 112103 (2008)

Spin readout device for P donors

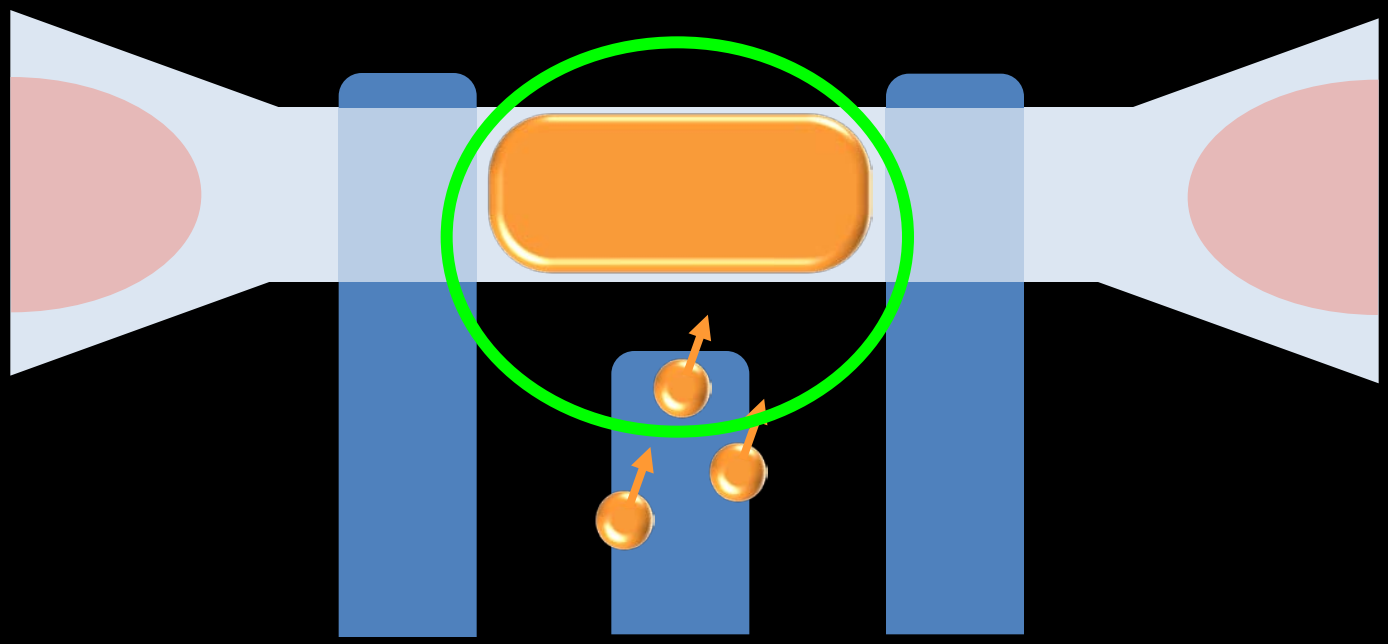

~ 3 donors in the 30×30 nm “active area”
~ 16 in total

Donor and SET island form a tunnel-coupled parallel double dot

MOS-compatible fabrication

AM et al., PRB **80**, 081307(R) (2009)

The “Single Electron Reader”

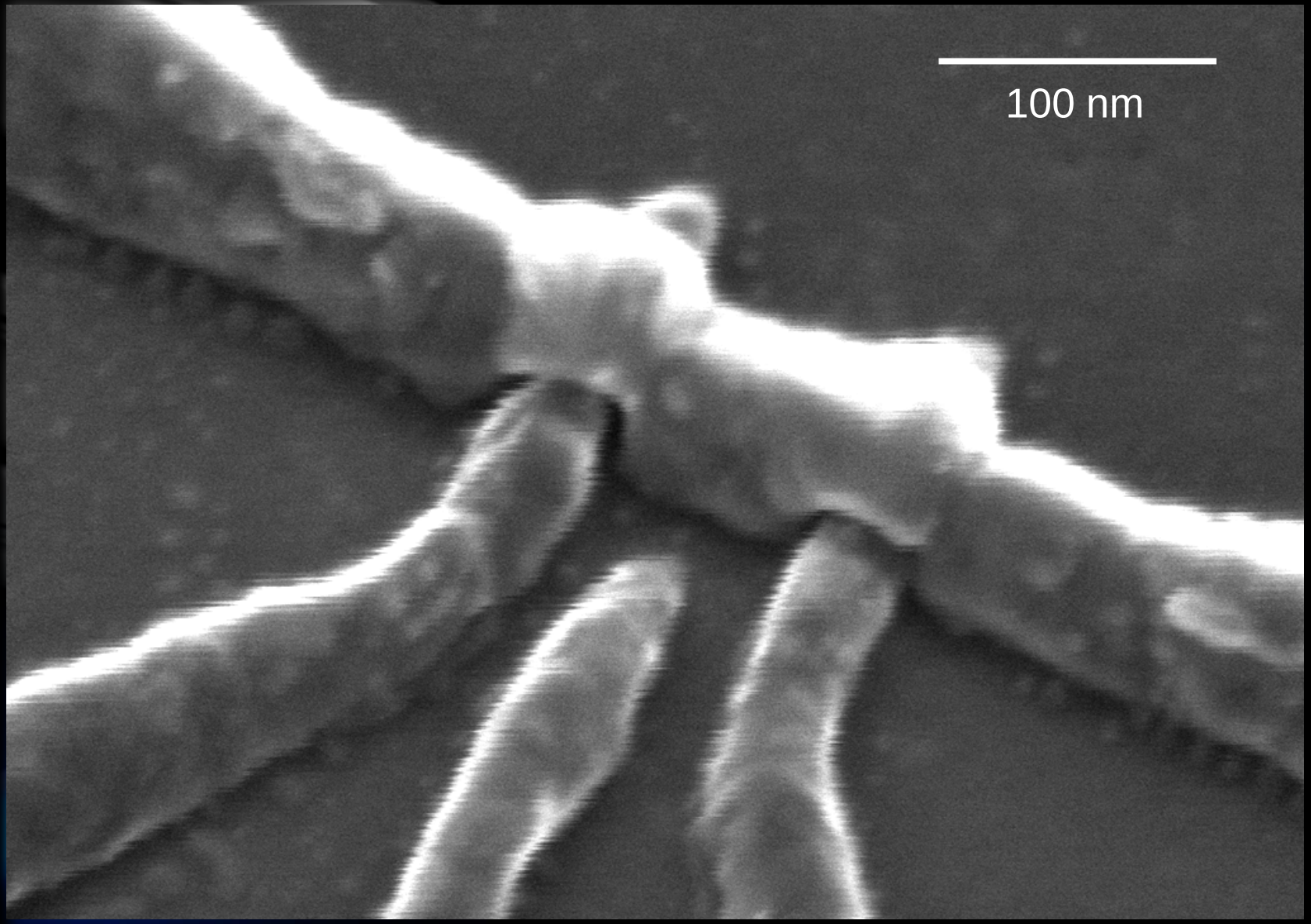

Spin to charge conversion

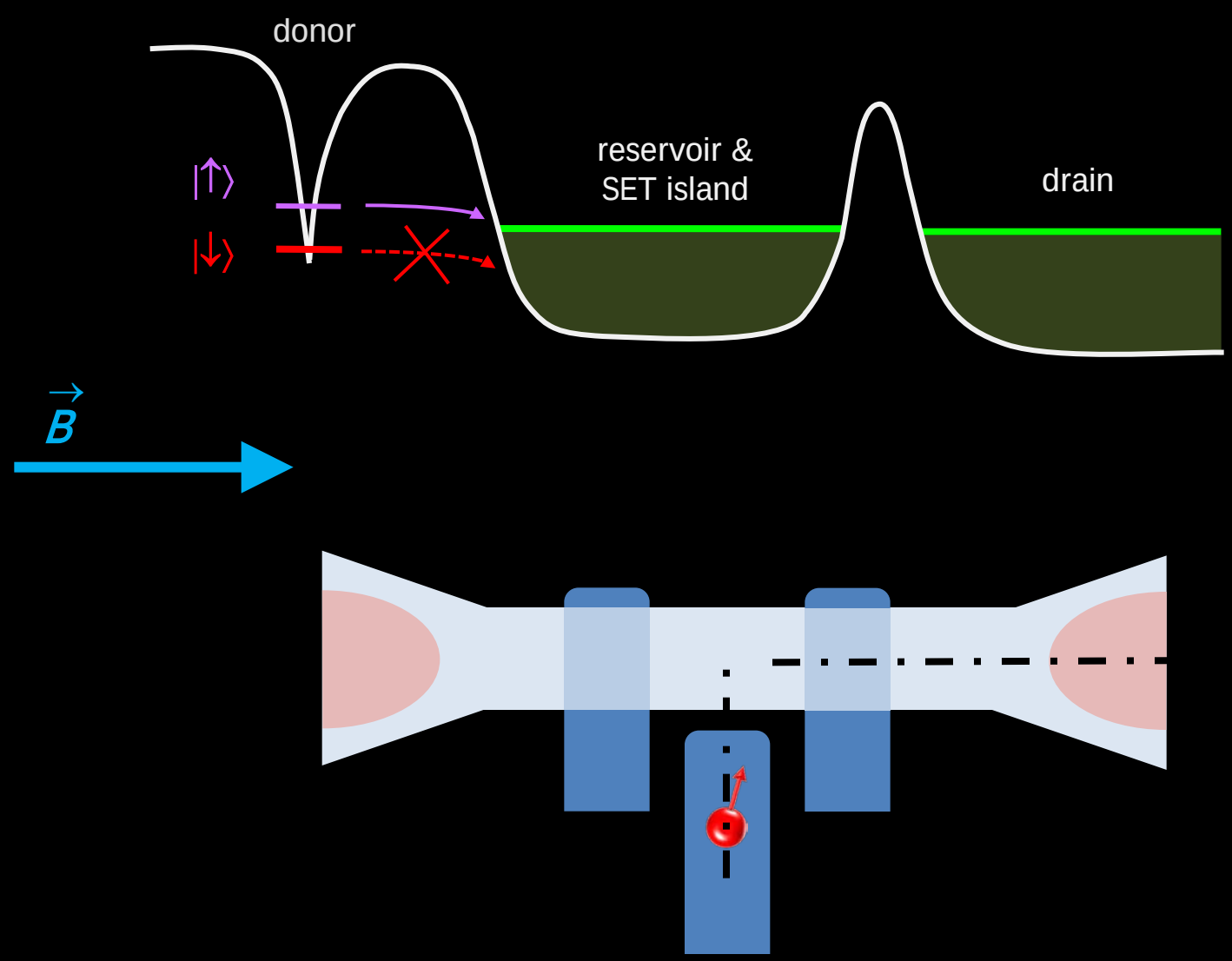

Spin readout protocol

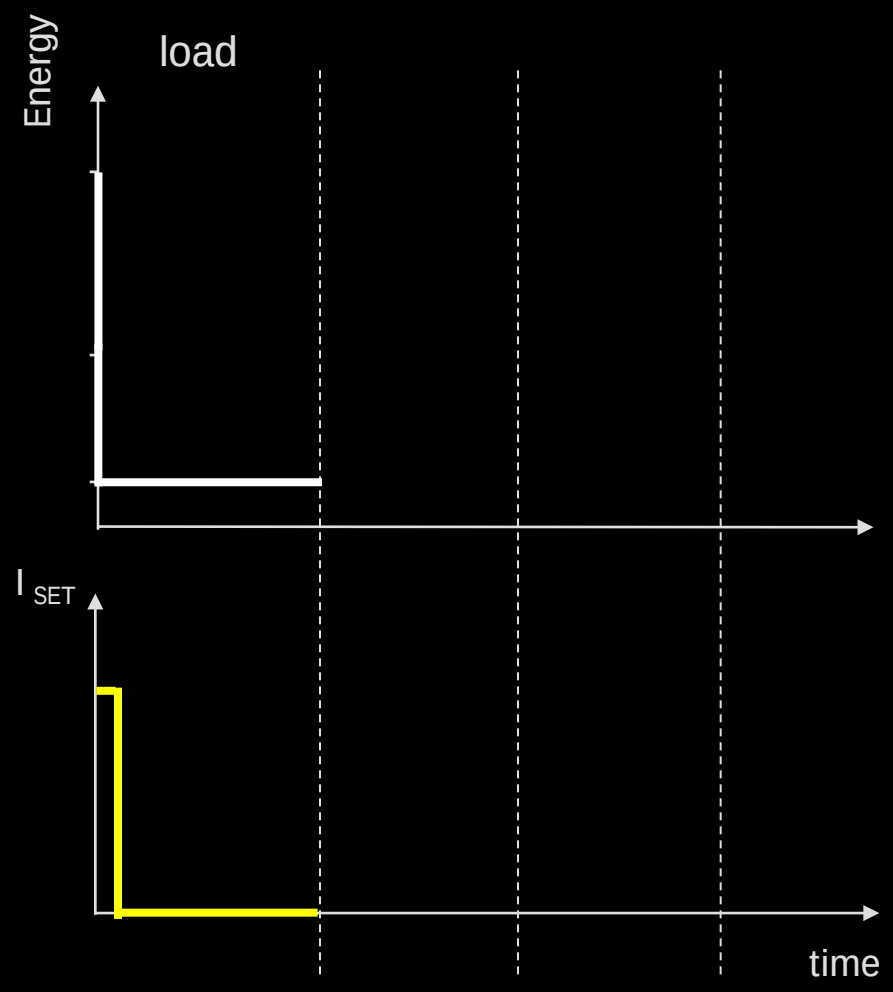

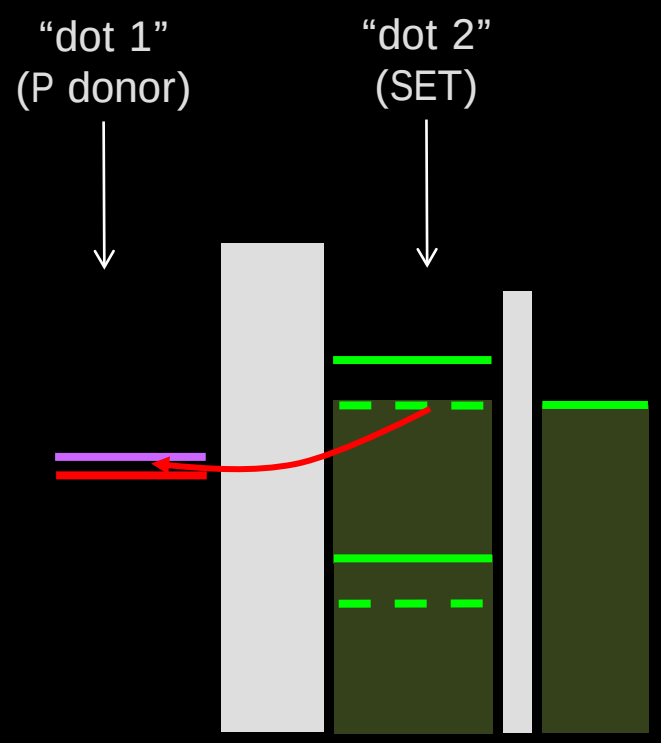

Spin readout protocol

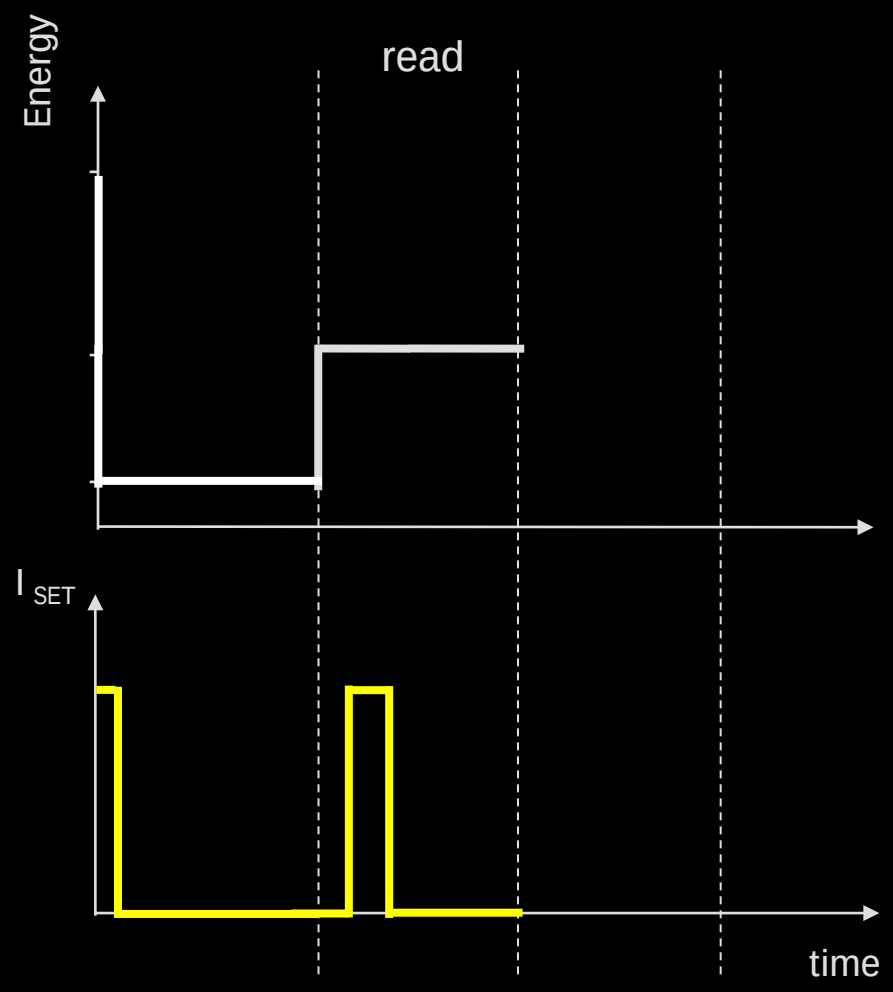

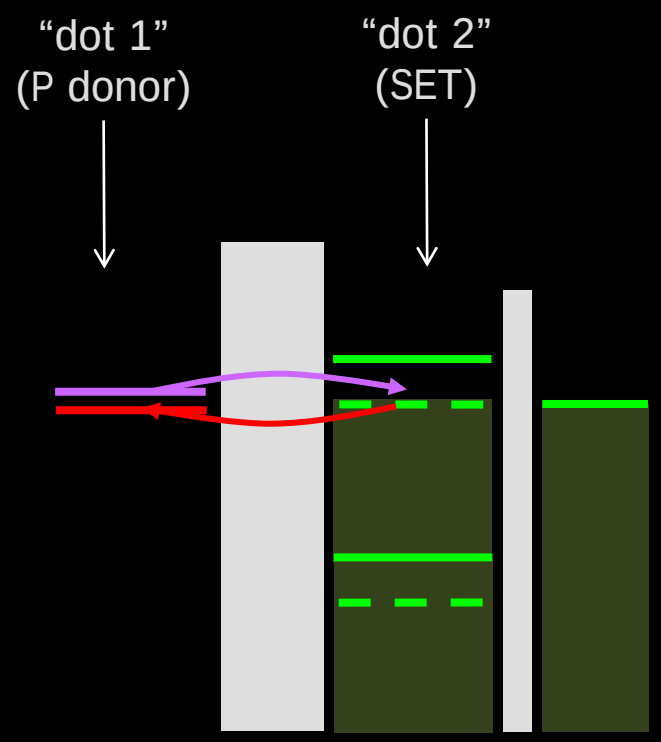

Spin readout protocol

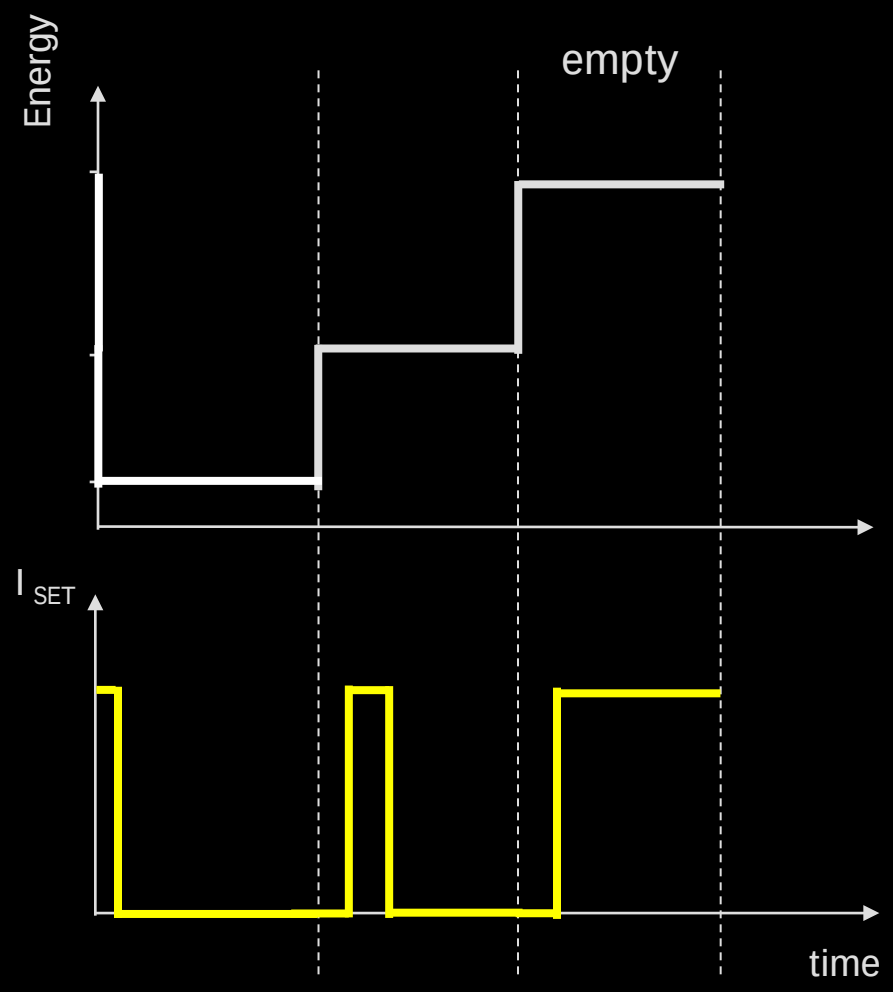

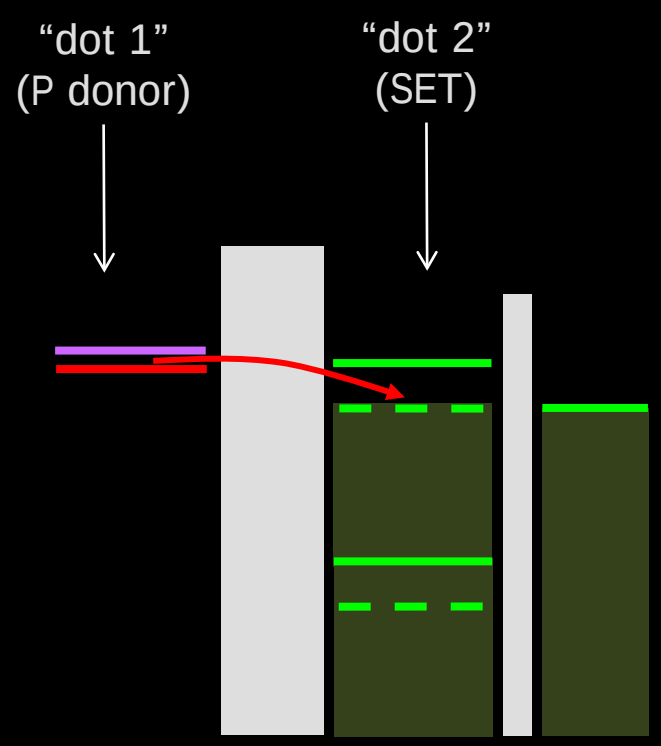

Single-shot spin readout

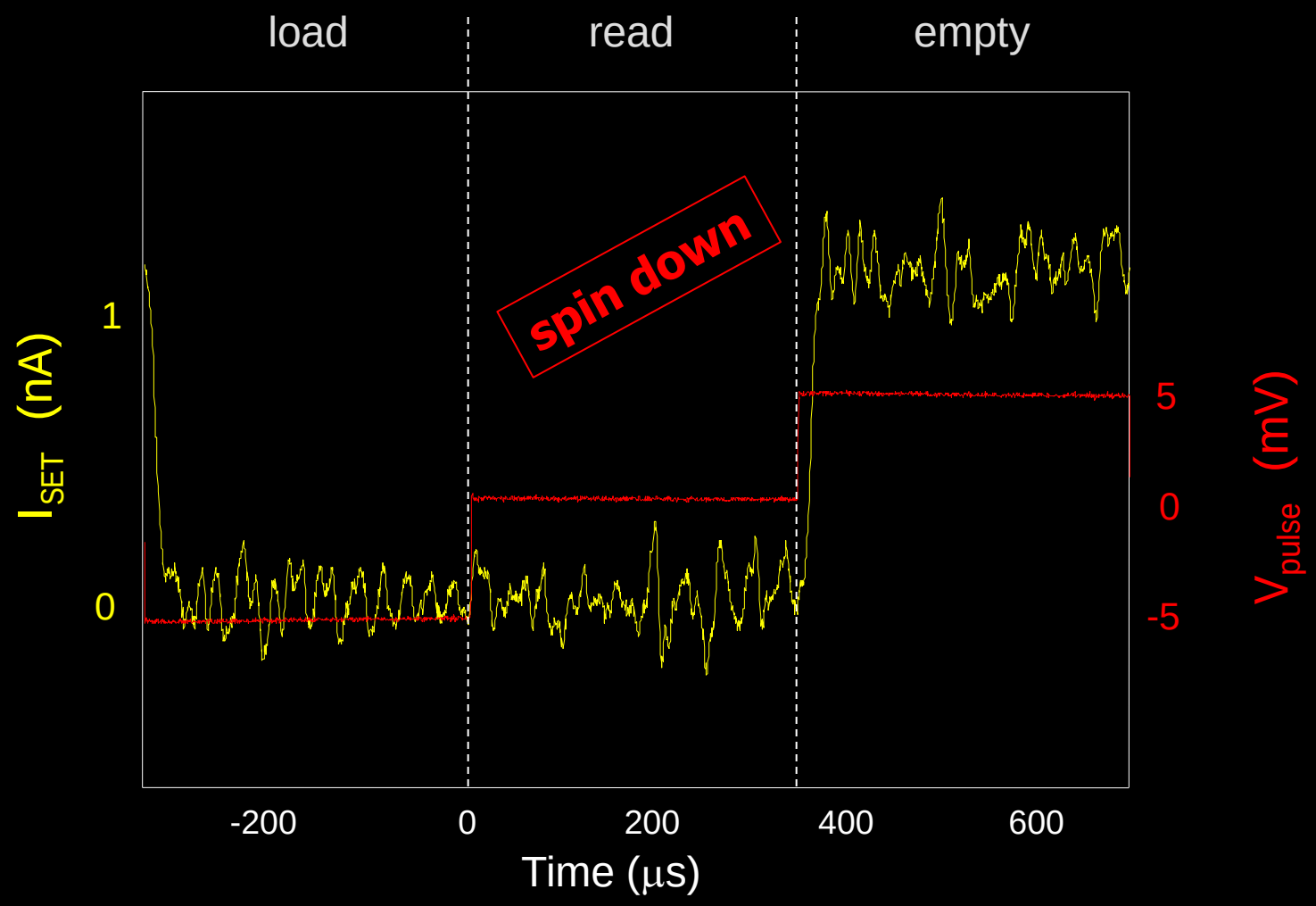

AM et al., Nature **467**, 687 (2010)

Single-shot spin readout

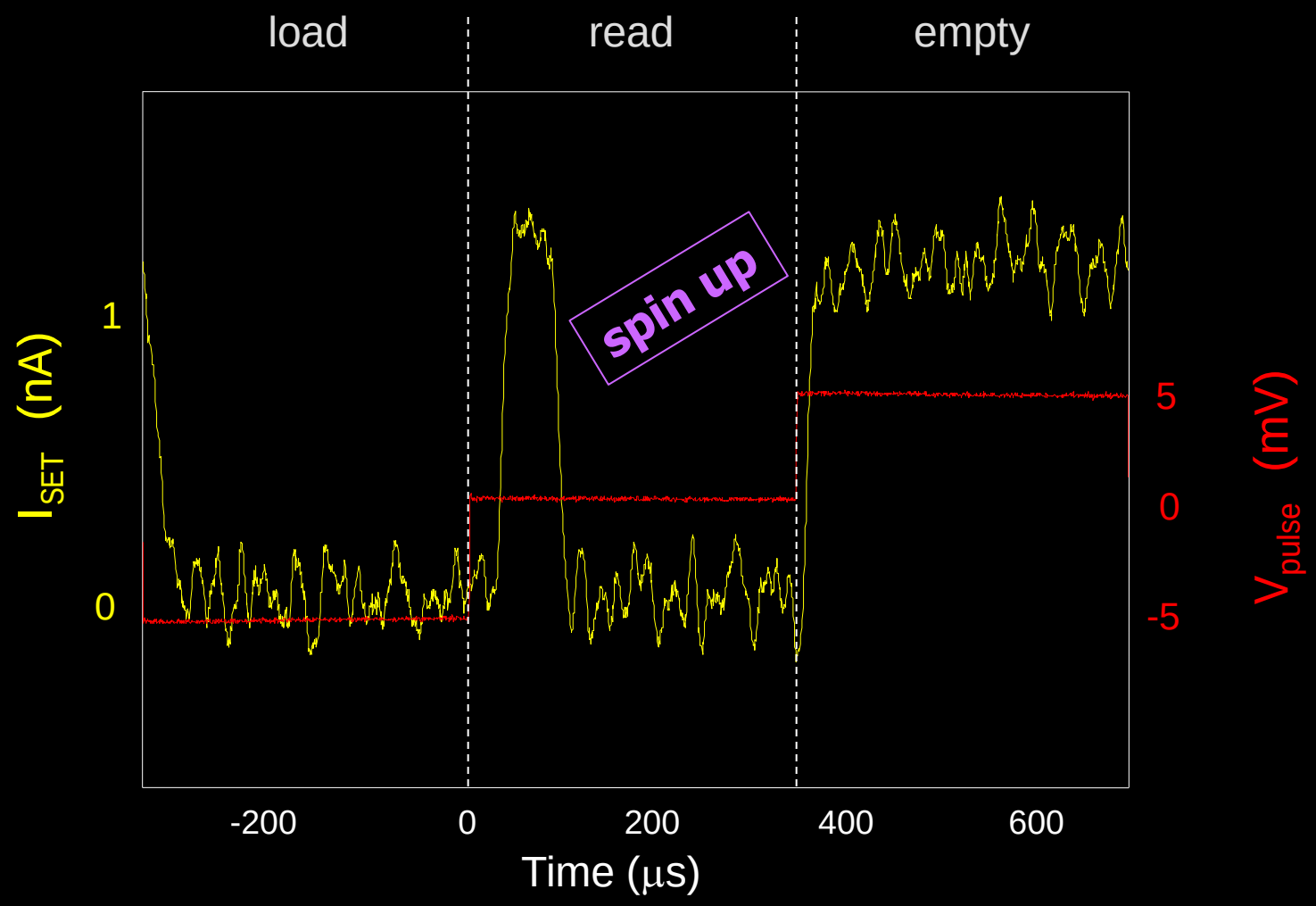

AM et al., Nature **467**, 687 (2010)

Spin lifetime T_1

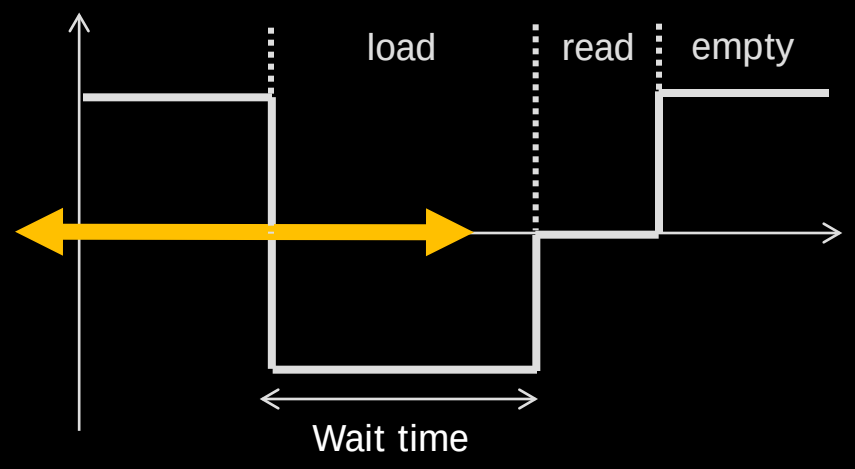

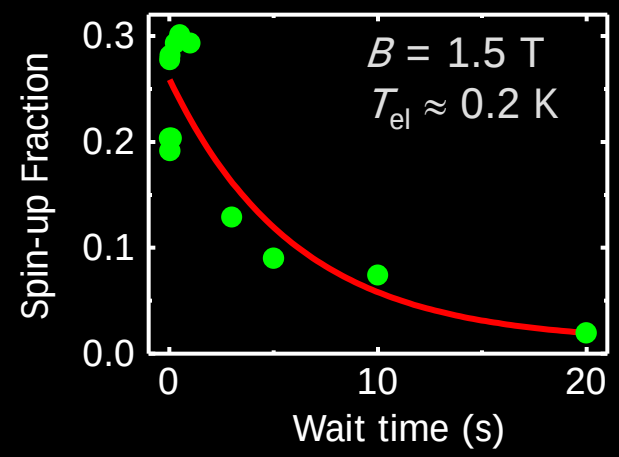

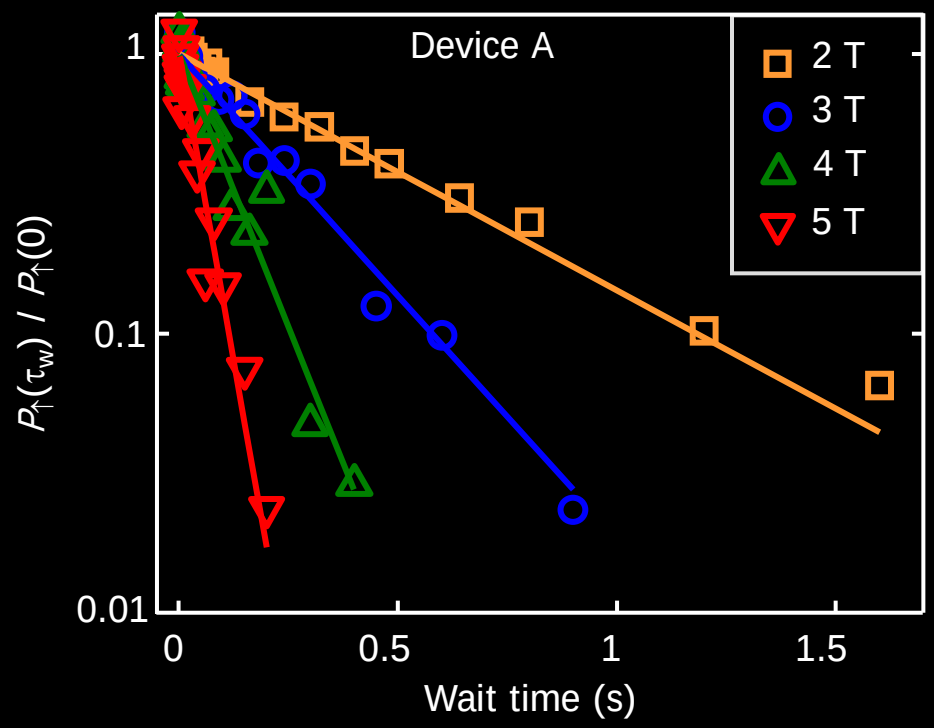

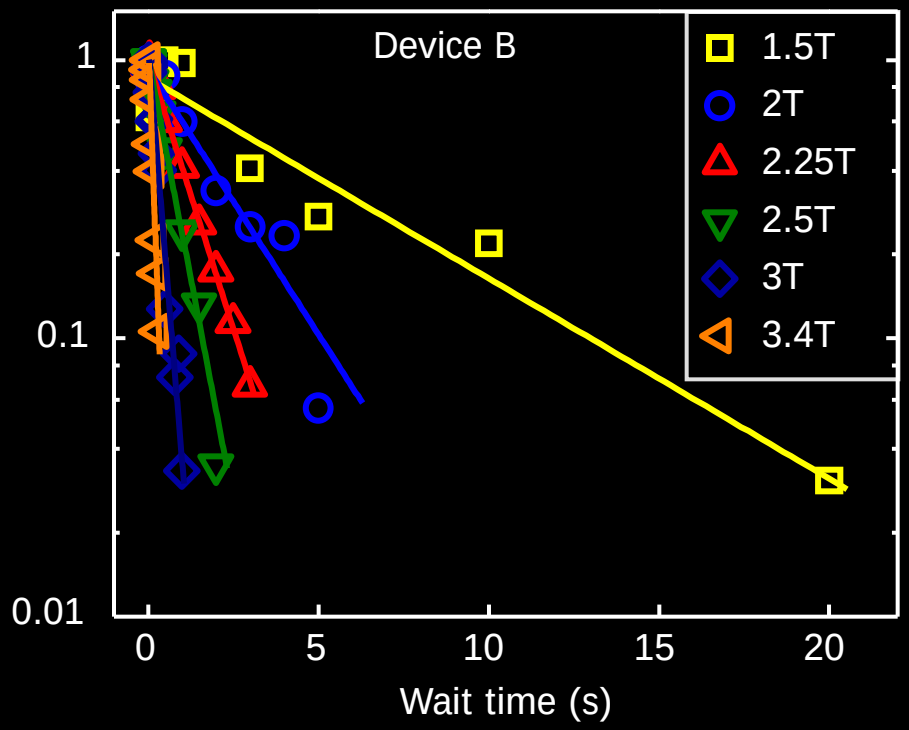

Field dependence of spin lifetime

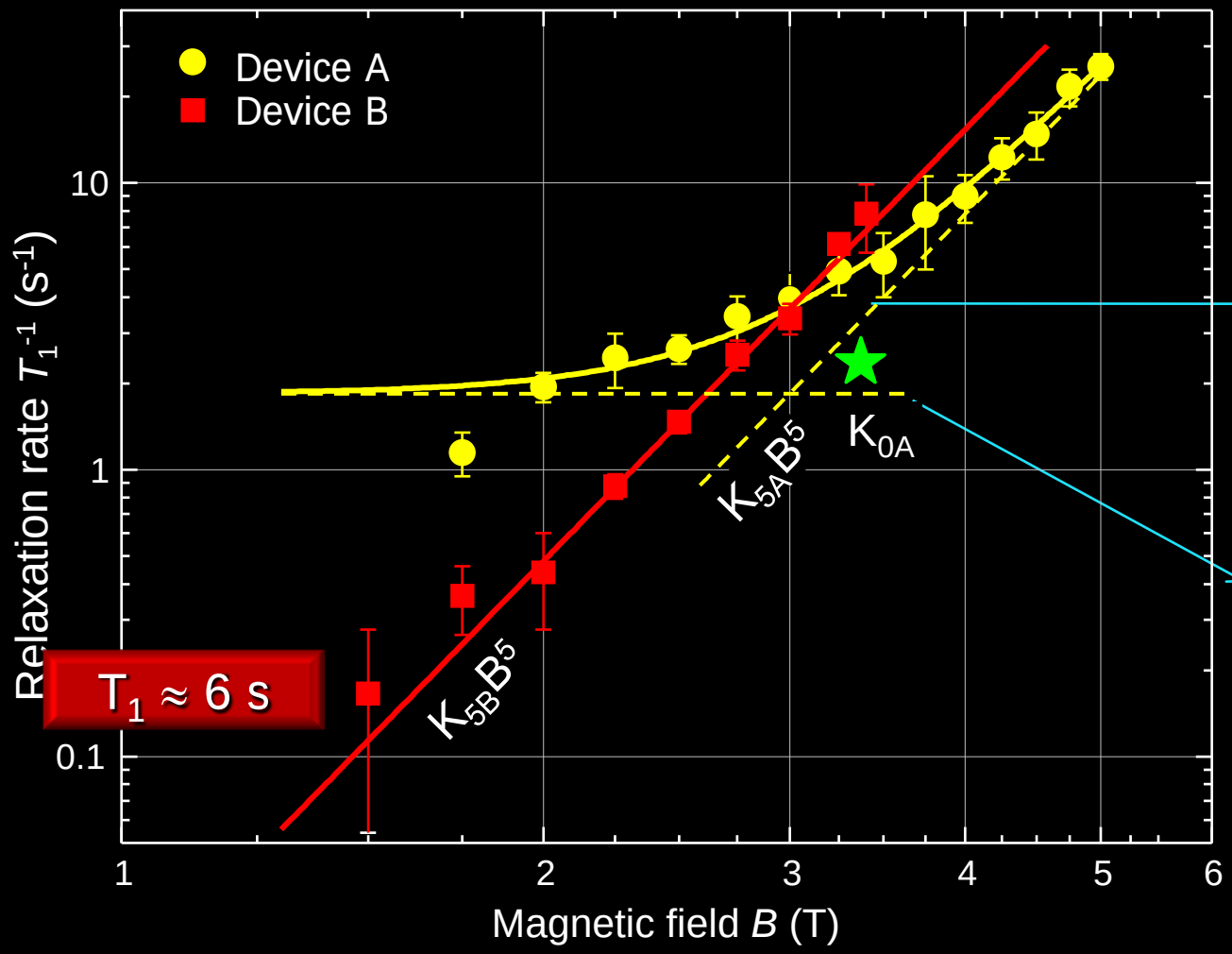

Valley repopulation $T_1^{-1} \propto B^5$

Dipolar flip-flops ~ 2 s^{-1}

Bulk Si:P data point: within factor 2

AM et al., Nature **467**, 687 (2010)

J.J.L. Morton, private communication

Readout fidelity

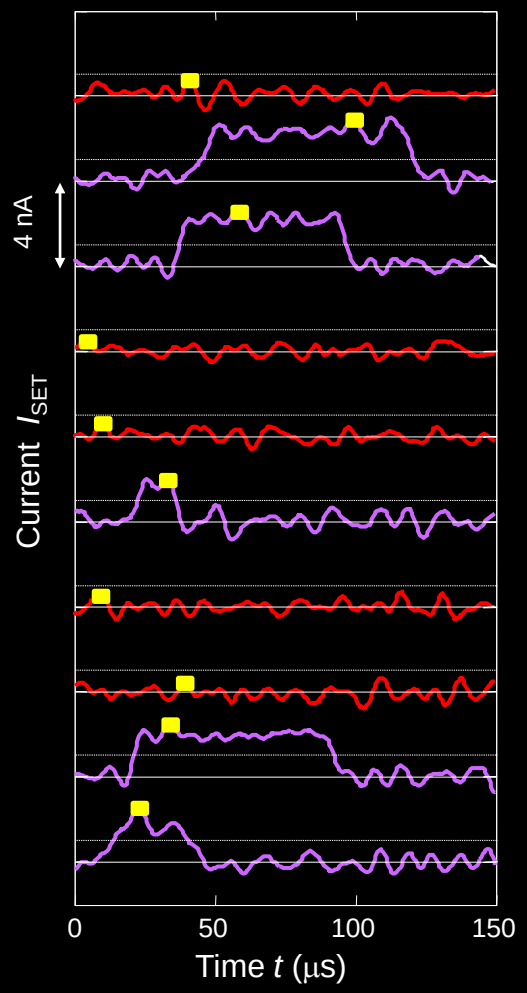

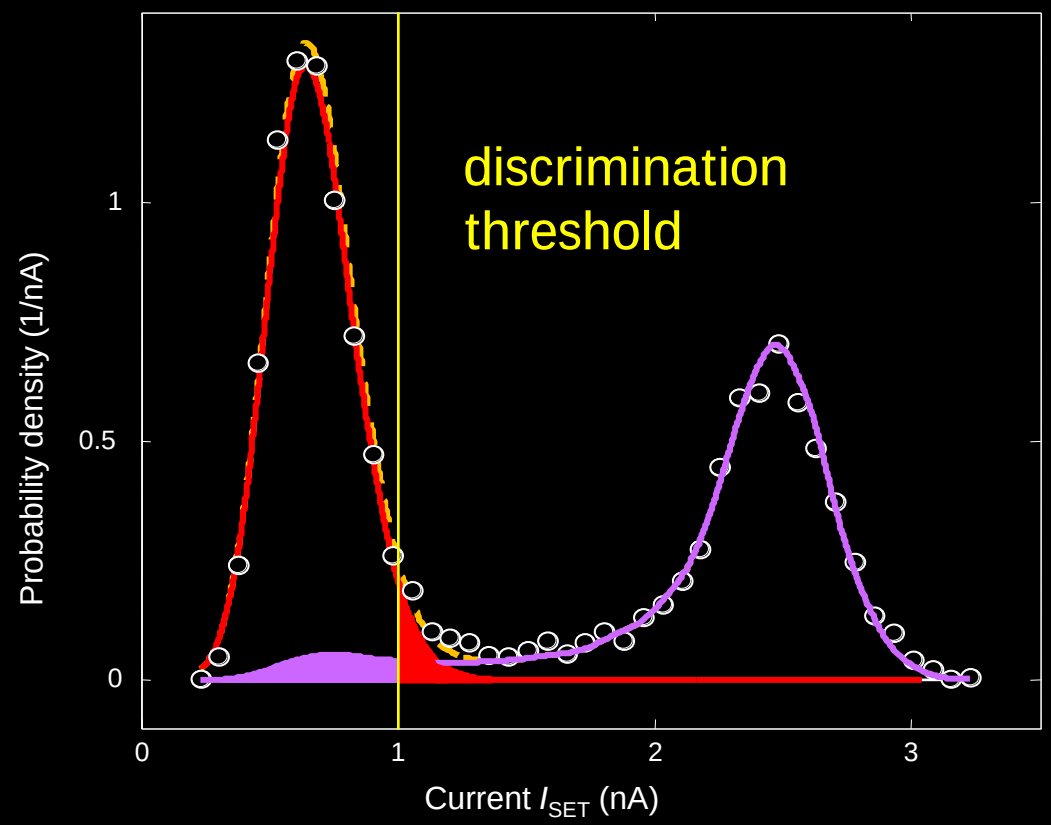

BW = 120 kHz
rise/fall time ≈ 3 μs

$$\int_{I_T}^{\infty} N_{\downarrow}(I)\, dI \rightarrow \text{spin-down error}$$

$$\int_{-\infty}^{I_T} N_{\uparrow}(I)\, dI \rightarrow \text{spin-up error}$$

Fidelity and visibility

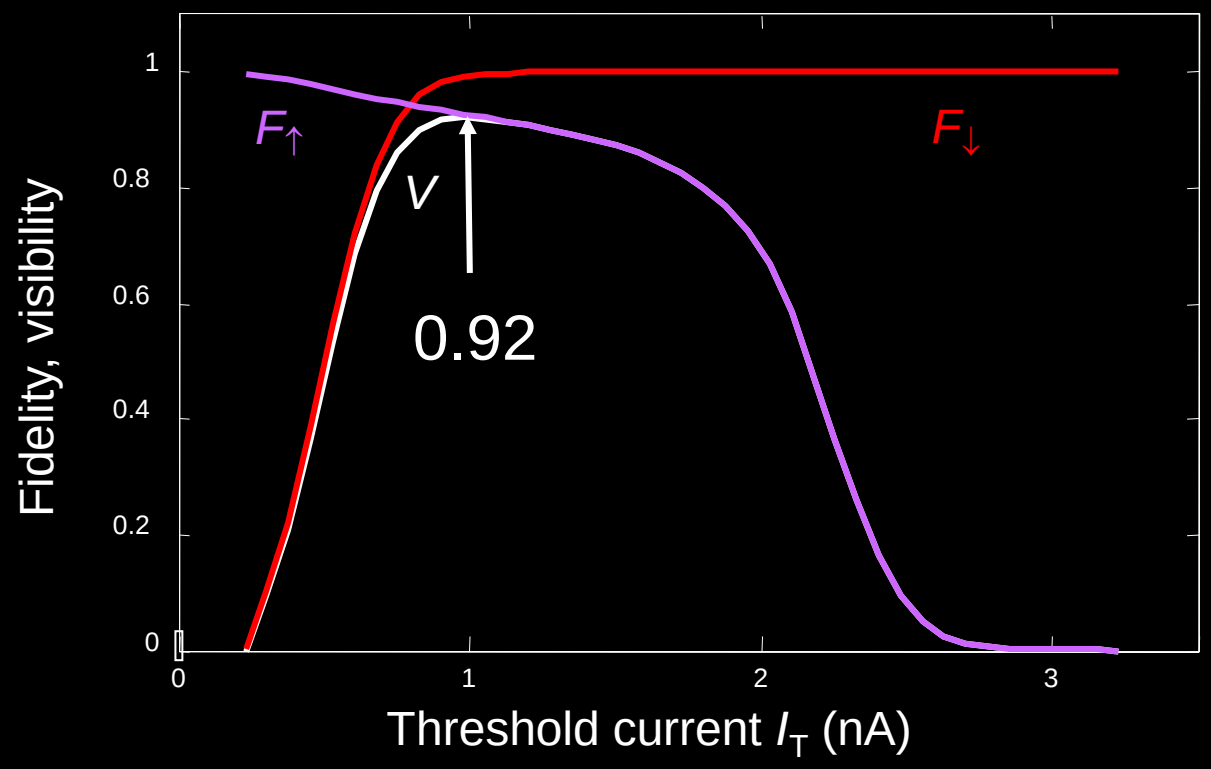

$$F_\downarrow = 1 - \int_{I_T}^{\infty} N_\downarrow(I)\, dI \qquad F_\uparrow = 1 - \int_{-\infty}^{I_T} N_\uparrow(I)\, dI \qquad V = F_\downarrow + F_\uparrow - 1$$

92% visibility with 3 μs rise/fall time

AM et al., Nature **467**, 687 (2010)

Microwave control

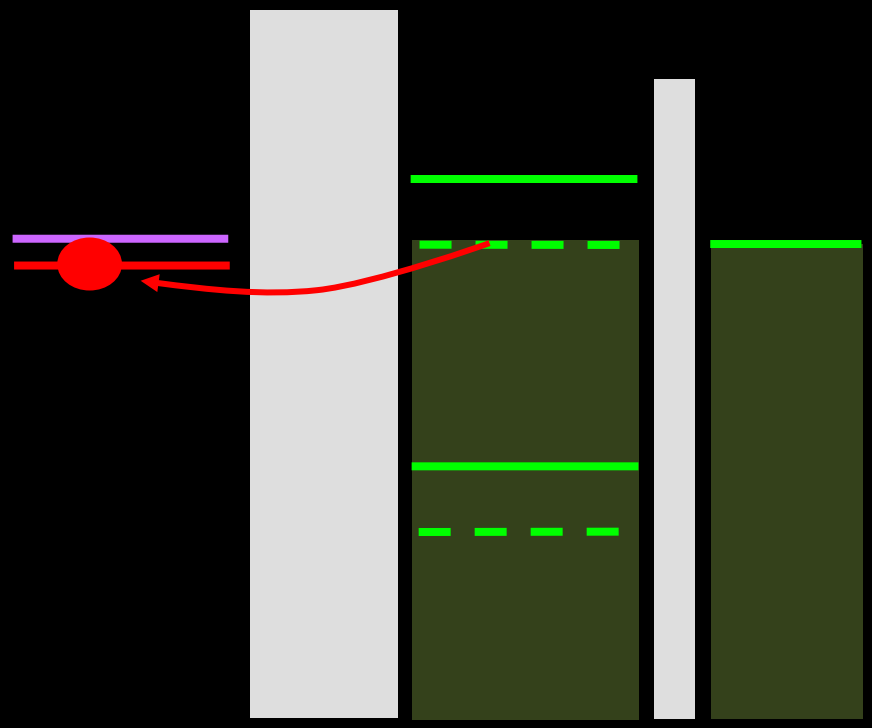

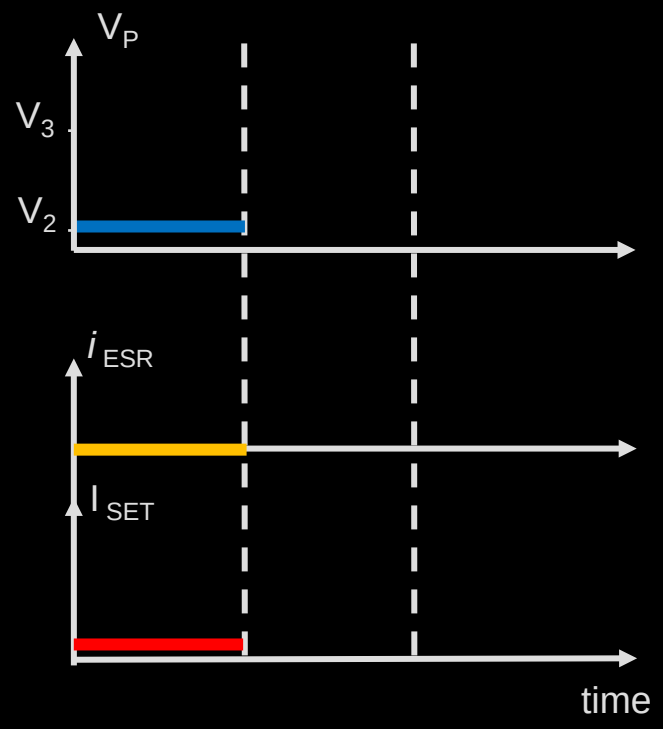

Initialize spin-down state

Microwave control

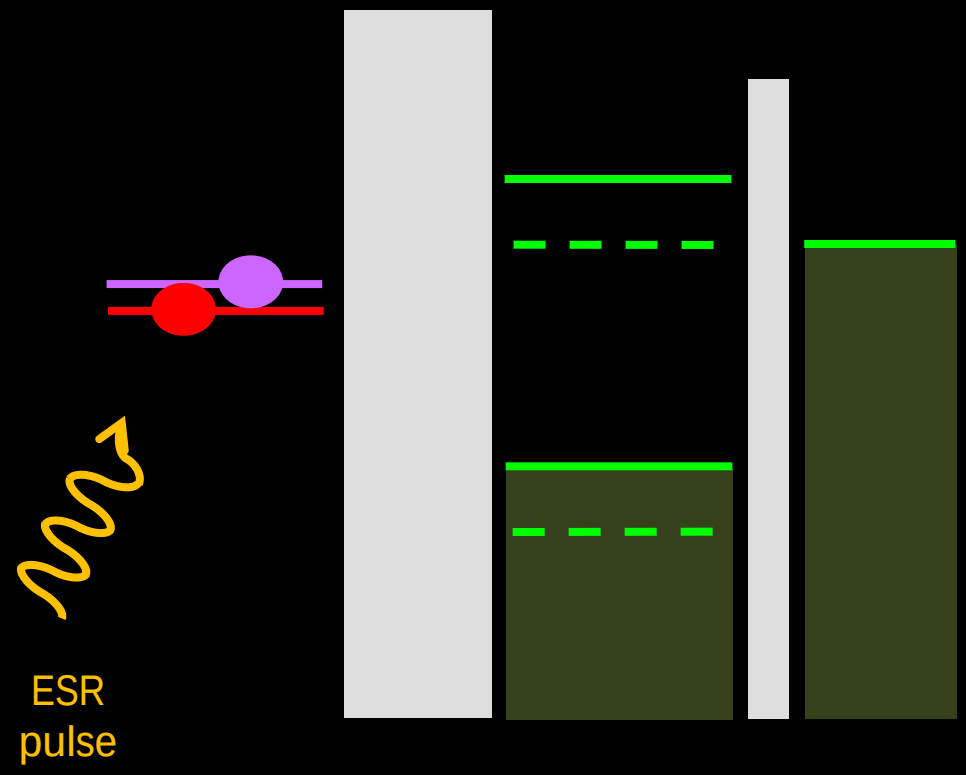

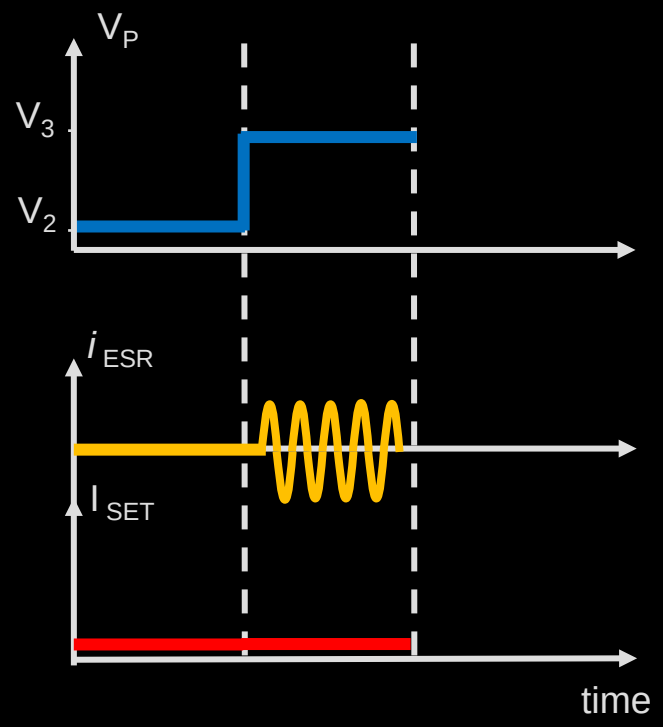

Excite the spin with resonant microwaves

Microwave control

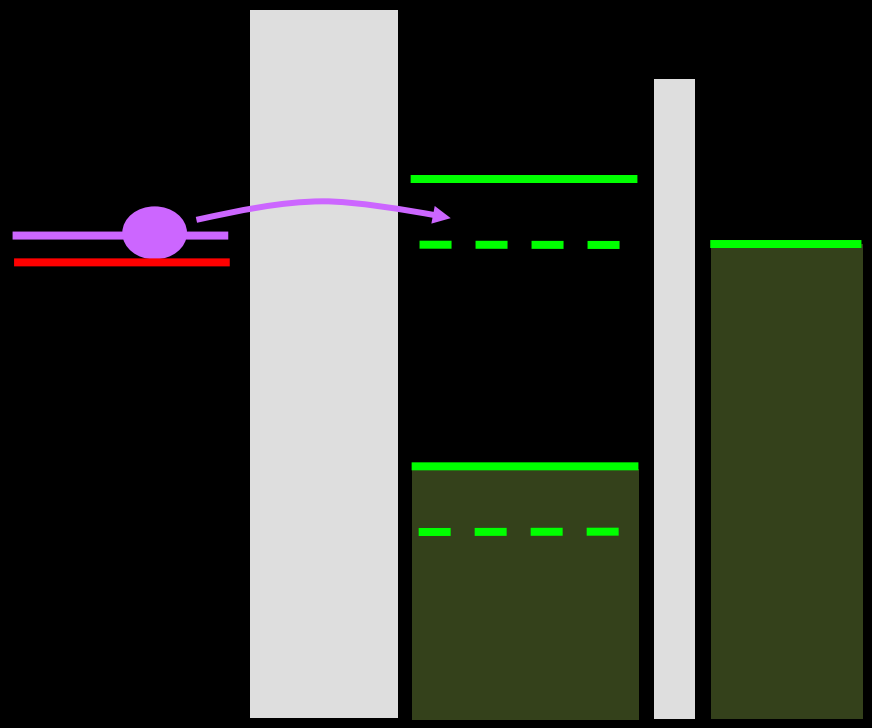

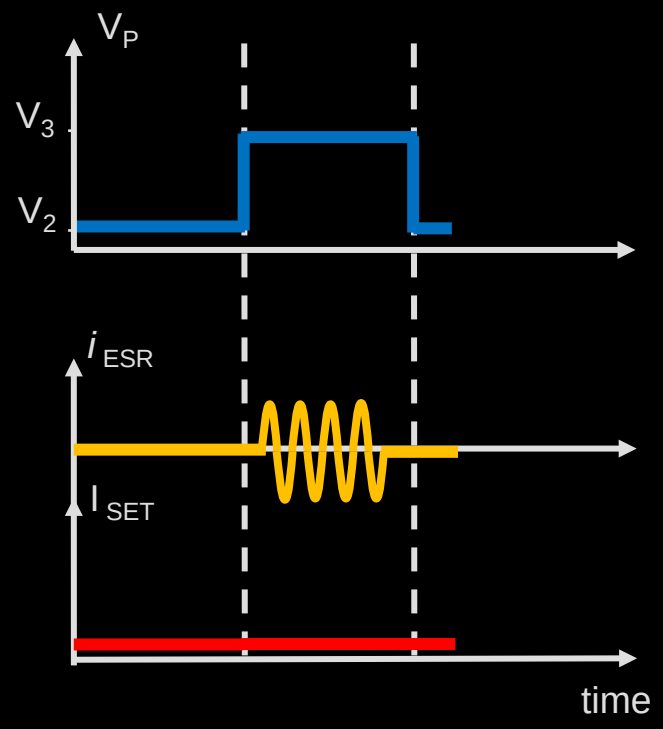

Pulse to the readout position

Microwave control

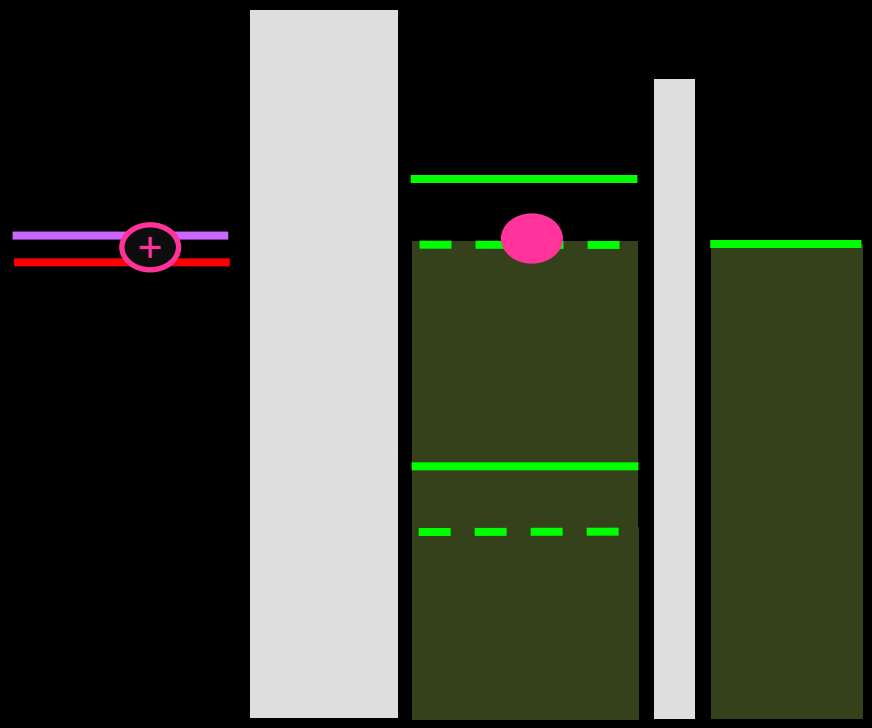

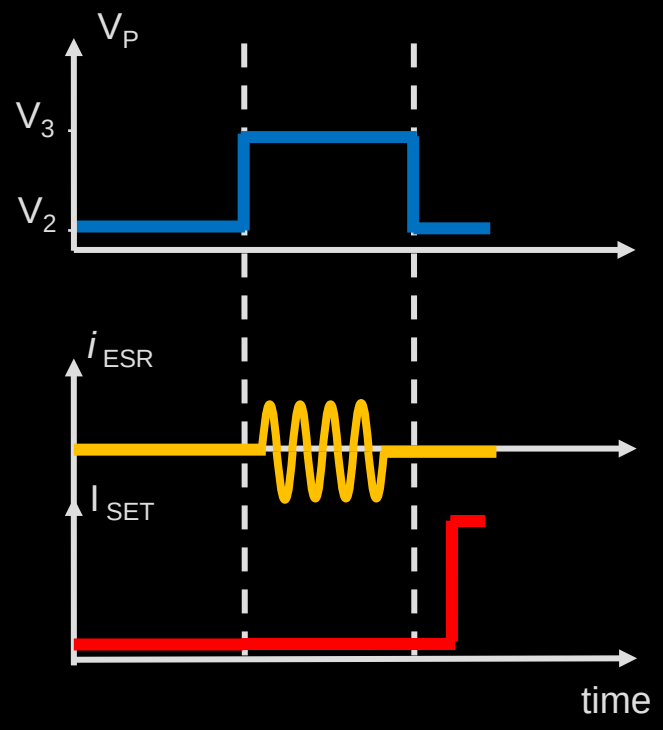

Detect spin-up current pulse

Microwave control

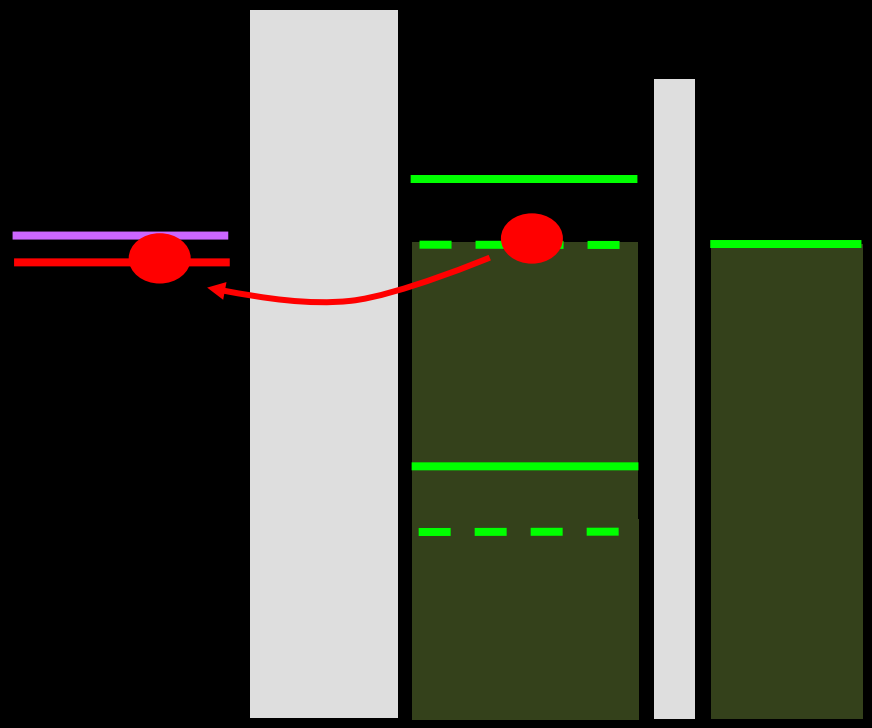

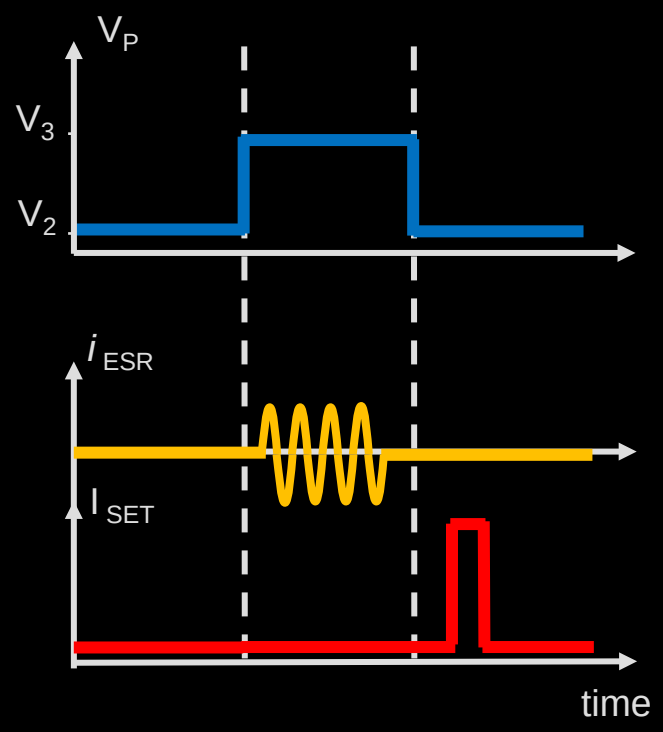

Start over: the qubit is already initialized!

On-chip microwave line

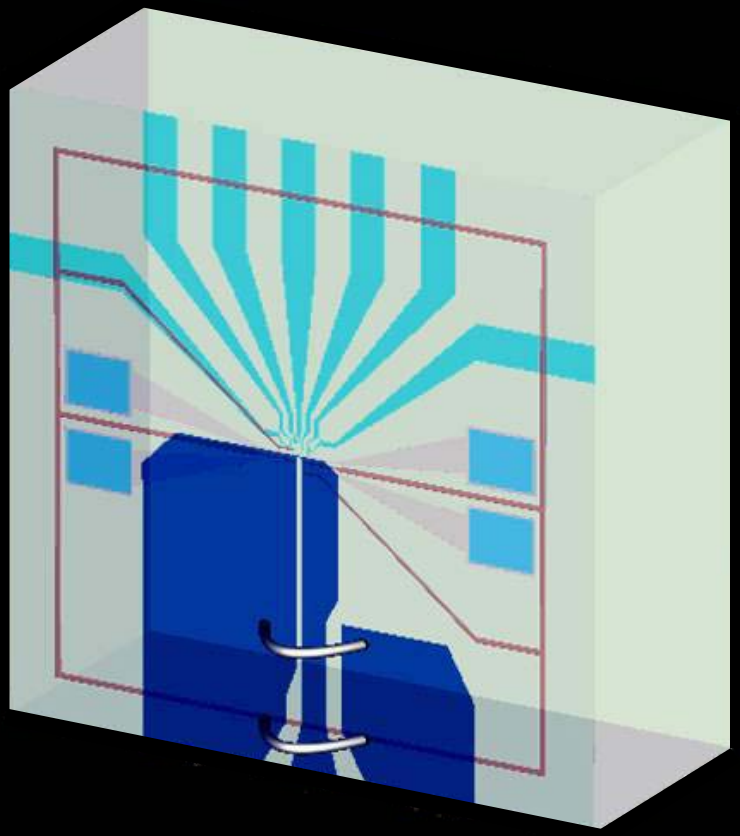

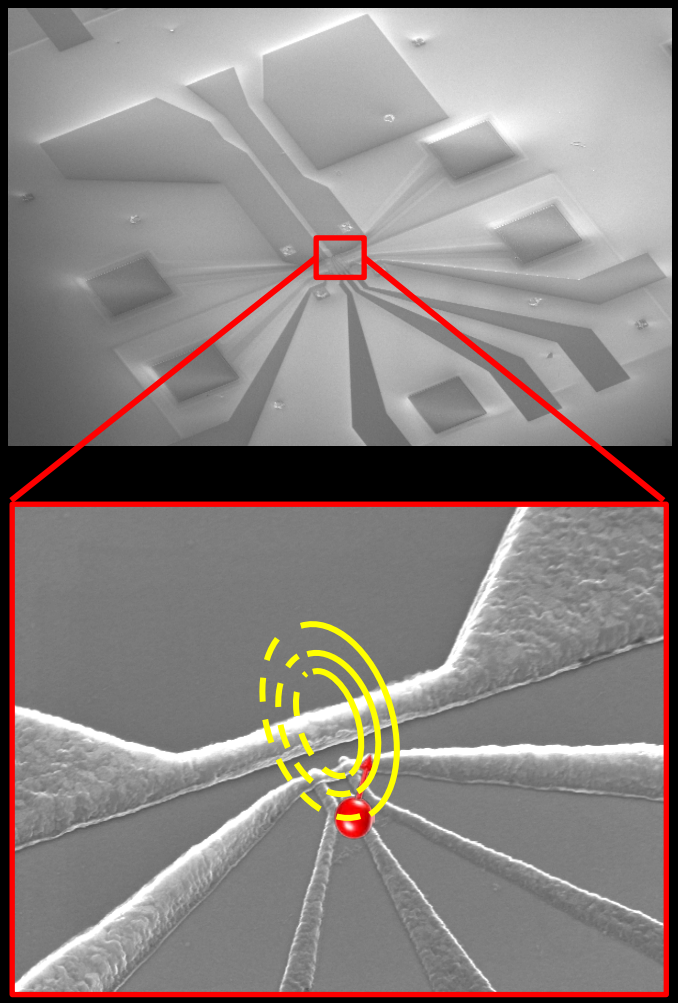

No resonator $\Rightarrow$ Broadband up to 50 GHz
On-chip balun $\Rightarrow$
lithographic transition CPW $\rightarrow$ CPS

Local spin resonance integrated with single-shot readout

Single-donor Spin Resonance

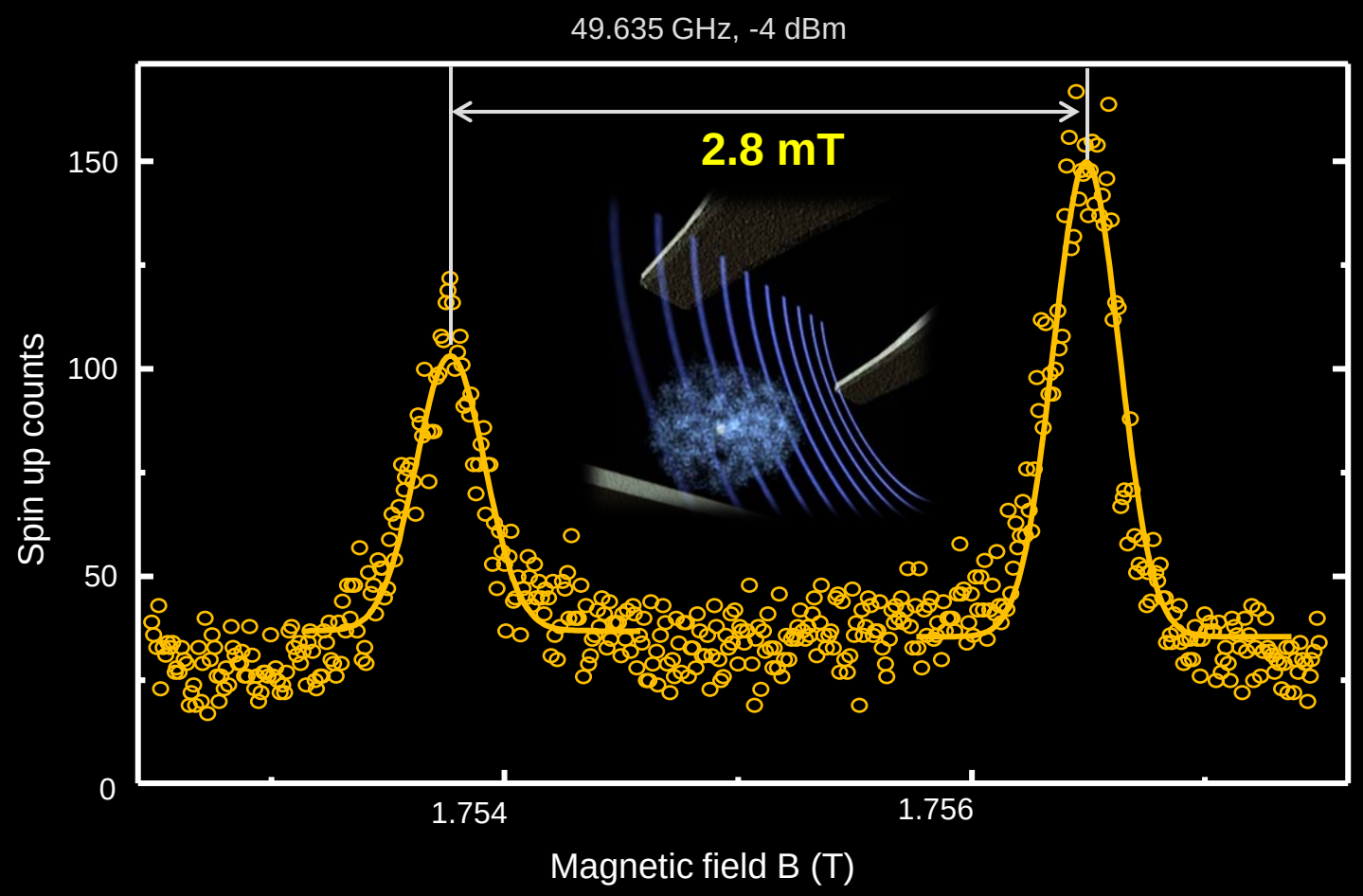

First-time spin resonance on a single P donor

ESR combined with single-shot spin readout

TCAD model → electric field

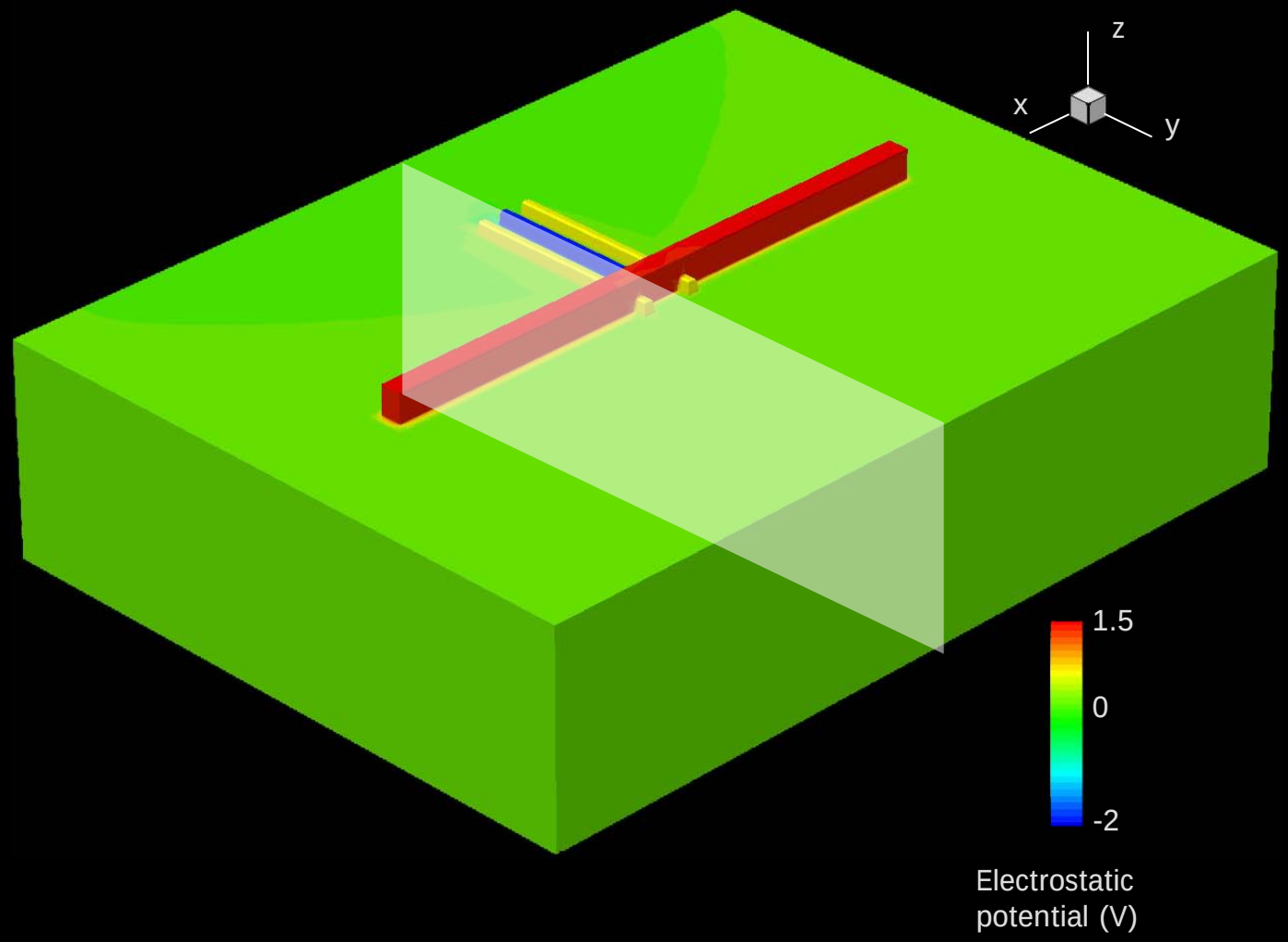

→ Electric field map in the y-z plane

Stark shift of the hyperfine

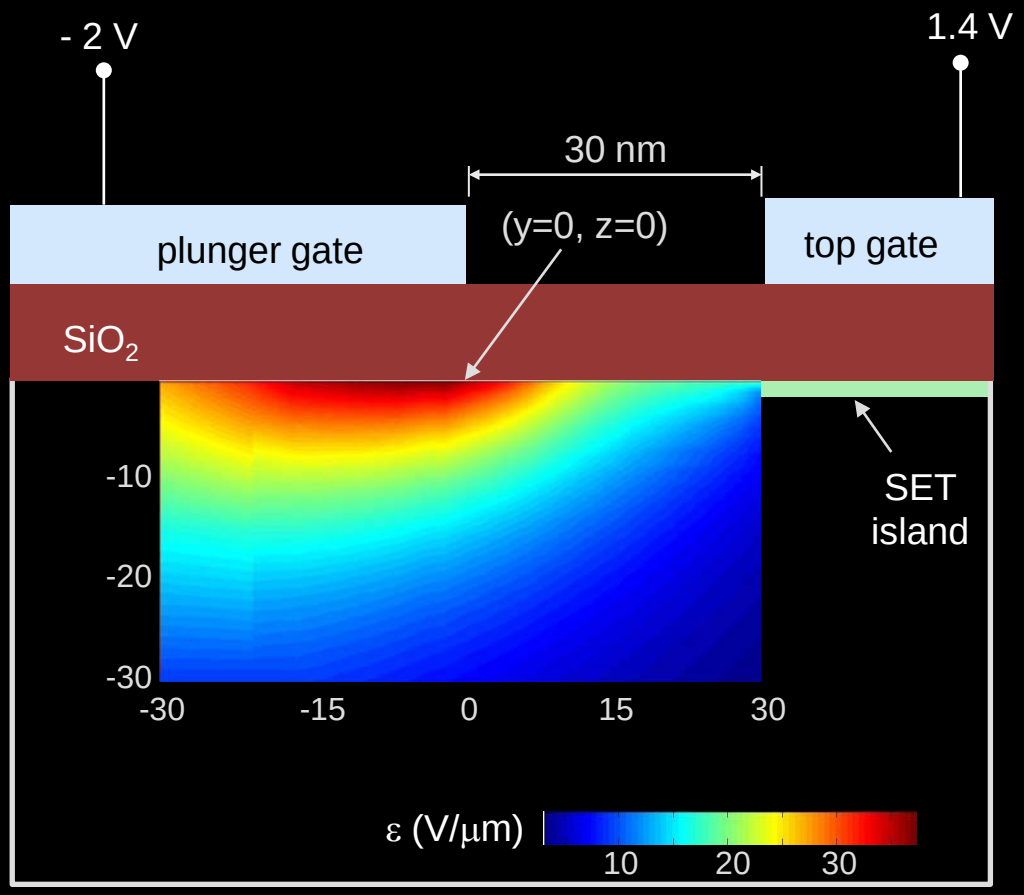

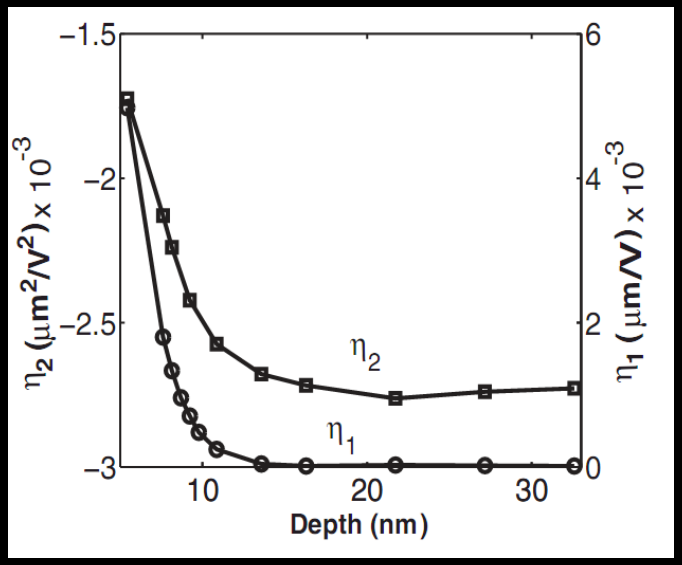

$$A(\varepsilon) = A(0)\,(1 + \eta_1\varepsilon + \eta_2\varepsilon^2)$$

Rahman et al., PRL 99, 036403 (2007)

Stark shift of the hyperfine

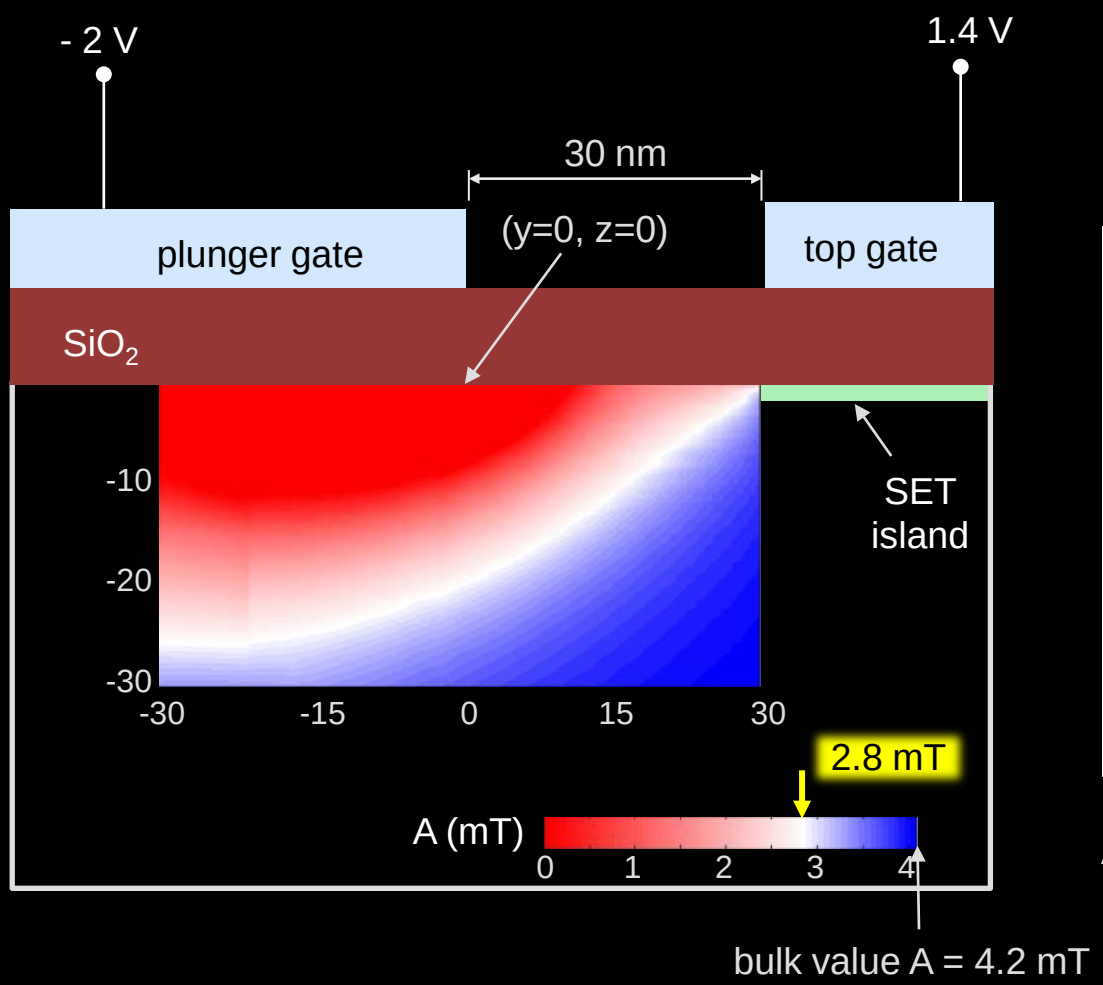

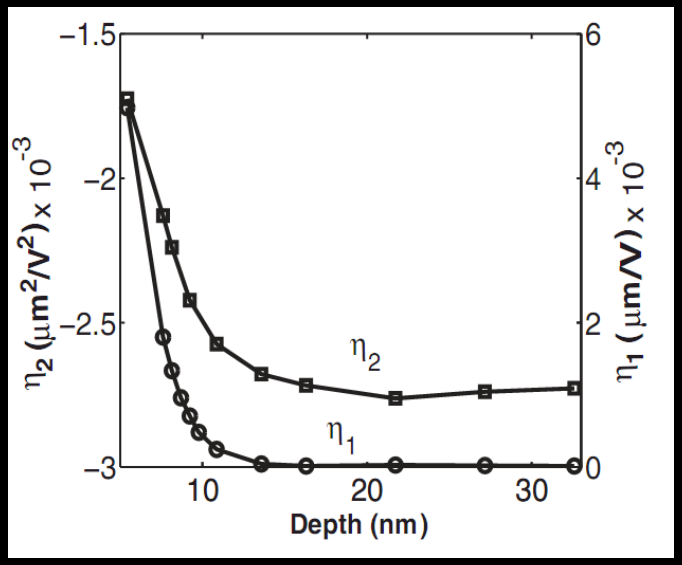

$$A(\varepsilon) = A(0)\,(1 + \eta_1\varepsilon + \eta_2\varepsilon^2)$$

The donor is a local electric field probe

Rahman et al., PRL 99, 036403 (2007)

Stark shift of the hyperfine

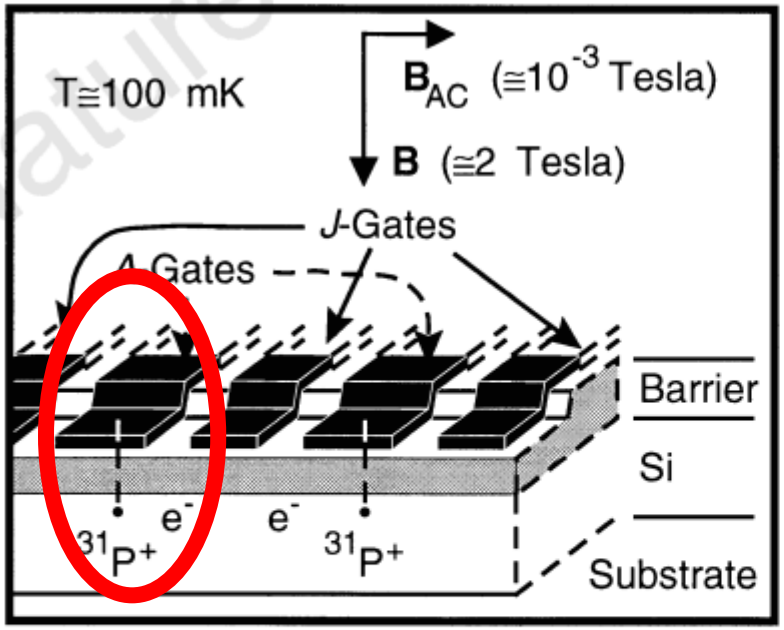

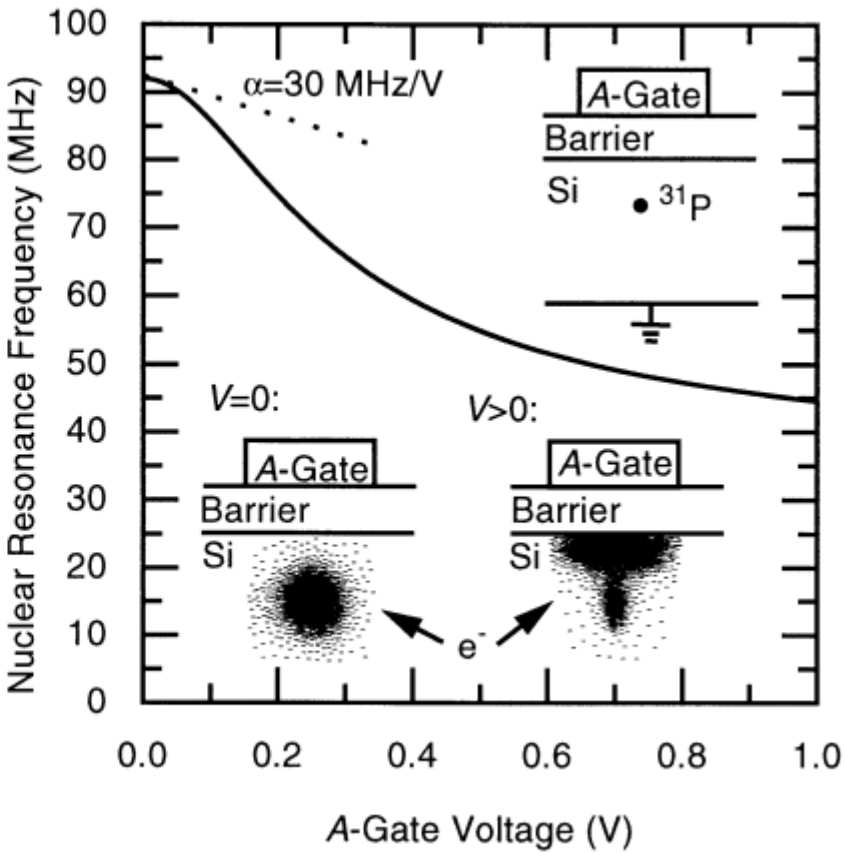

Essential ingredient of the Kane QC scheme

Kane, Nature **393**, 133 (1998)

Single-spin ESR in a MOSFET

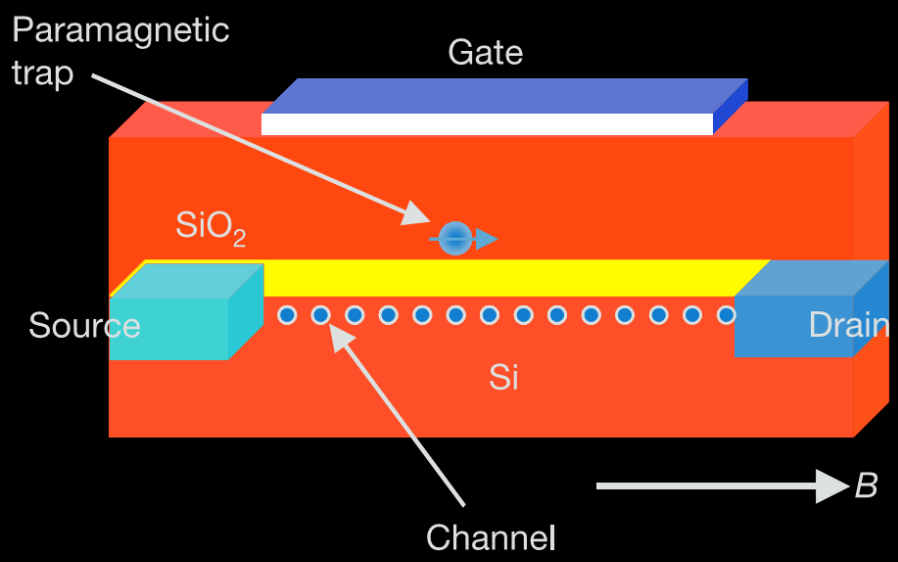

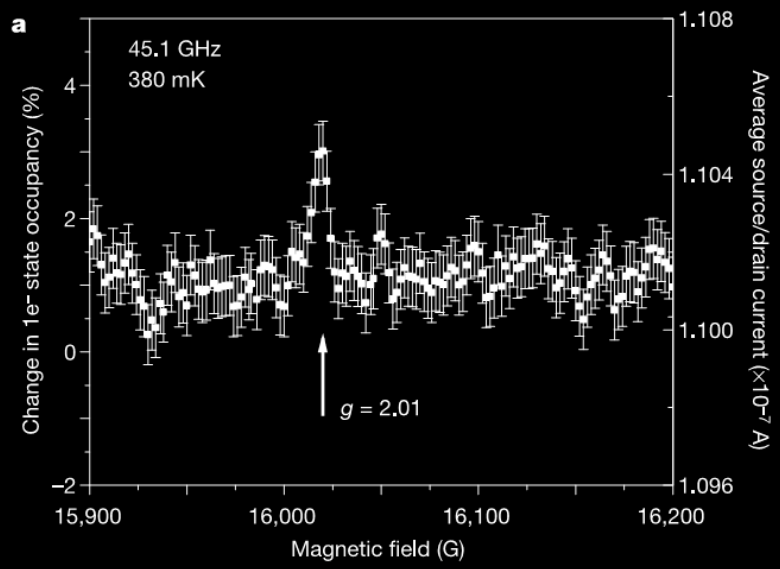

The SET can be replaced by a MOSFET channel

Single dopants coupled to a nanoelectronic device can be used as sensitive local electric field probes, by measuring their spin

Xiao et al., Nature **430**, 435 (2004)

Transport through implanted donors

timed P-implant
<n> = 3
in 50×30 nm

barrier/donor gate

P-implant area

$V_{barrier}$

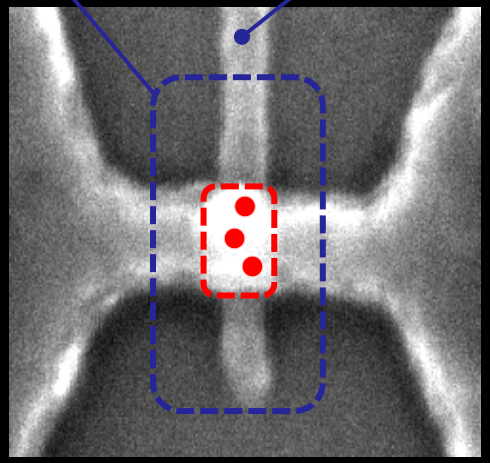

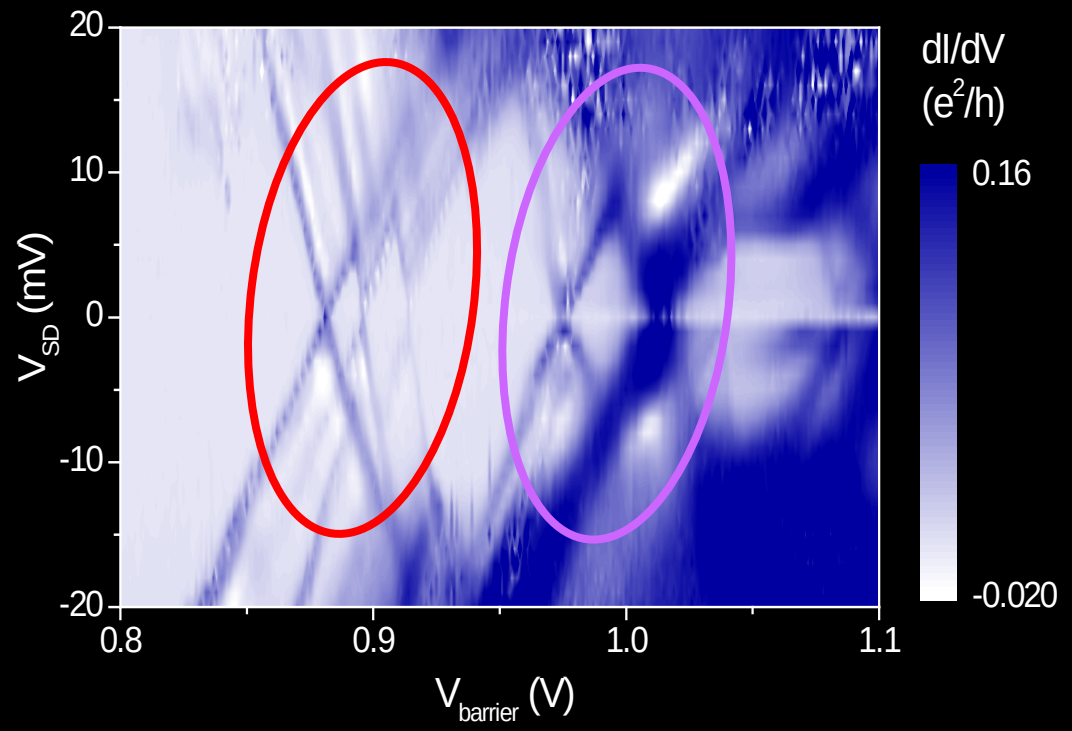

<n> = 3 ↔ 3 sharp resonant features...

...plus the related peaks for the addition of a second electron (D^- states) forming 3 overlapping Coulomb diamonds

Tan et al., Nano Letters **10**, 11 (2010)

Future work: 2-qubit devices

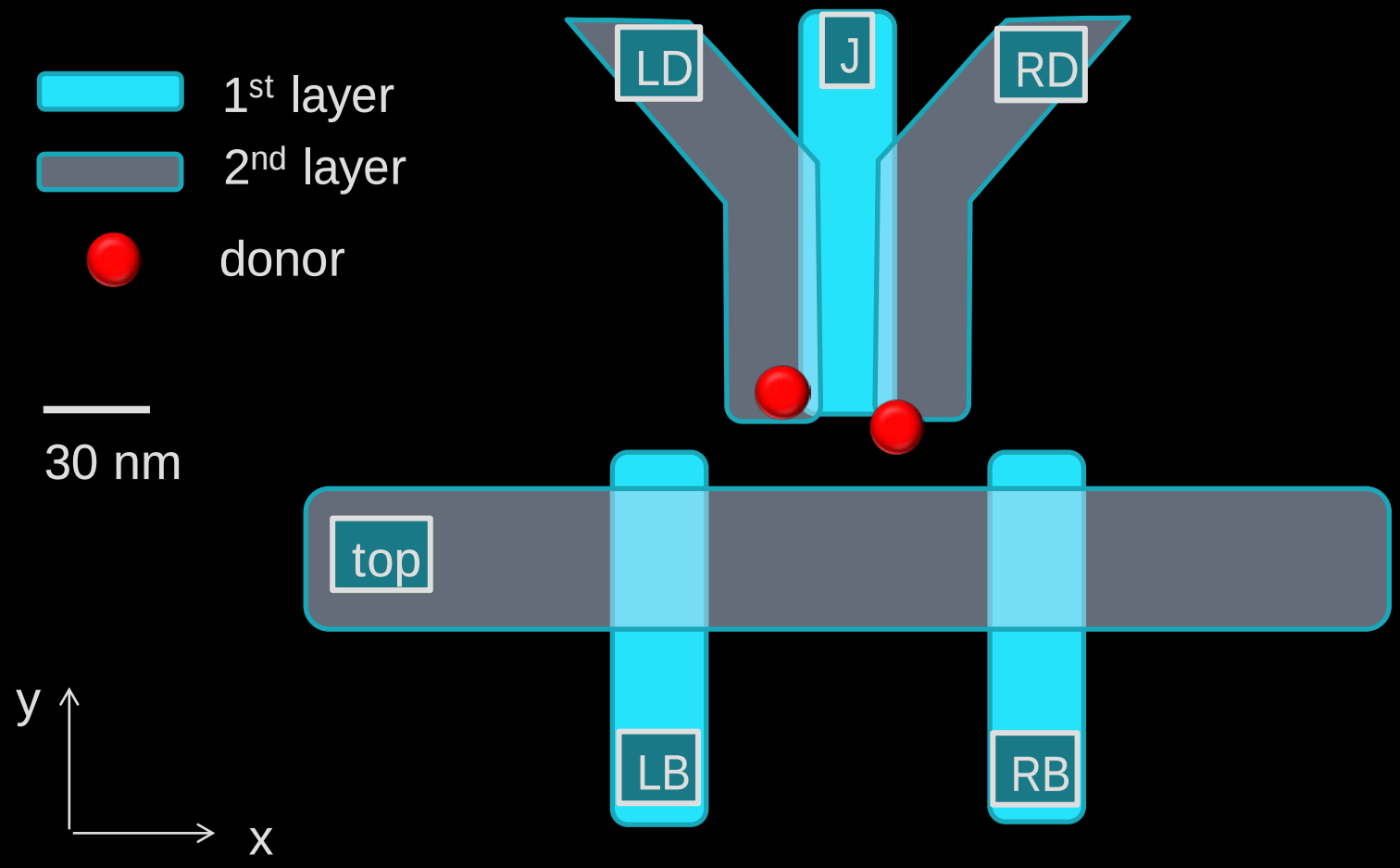

Future work: 2-qubit devices

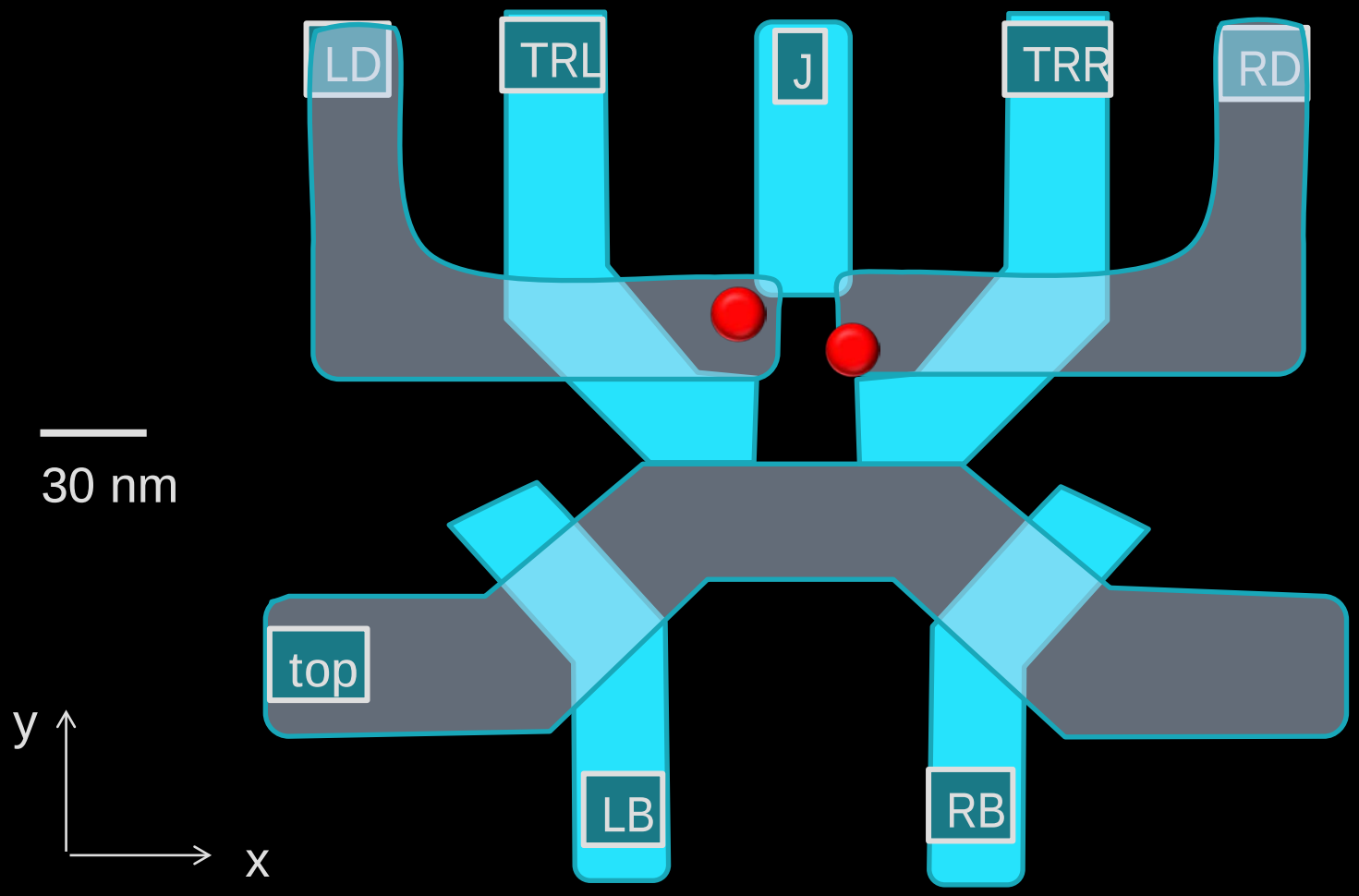

Future work: 2-qubit devices

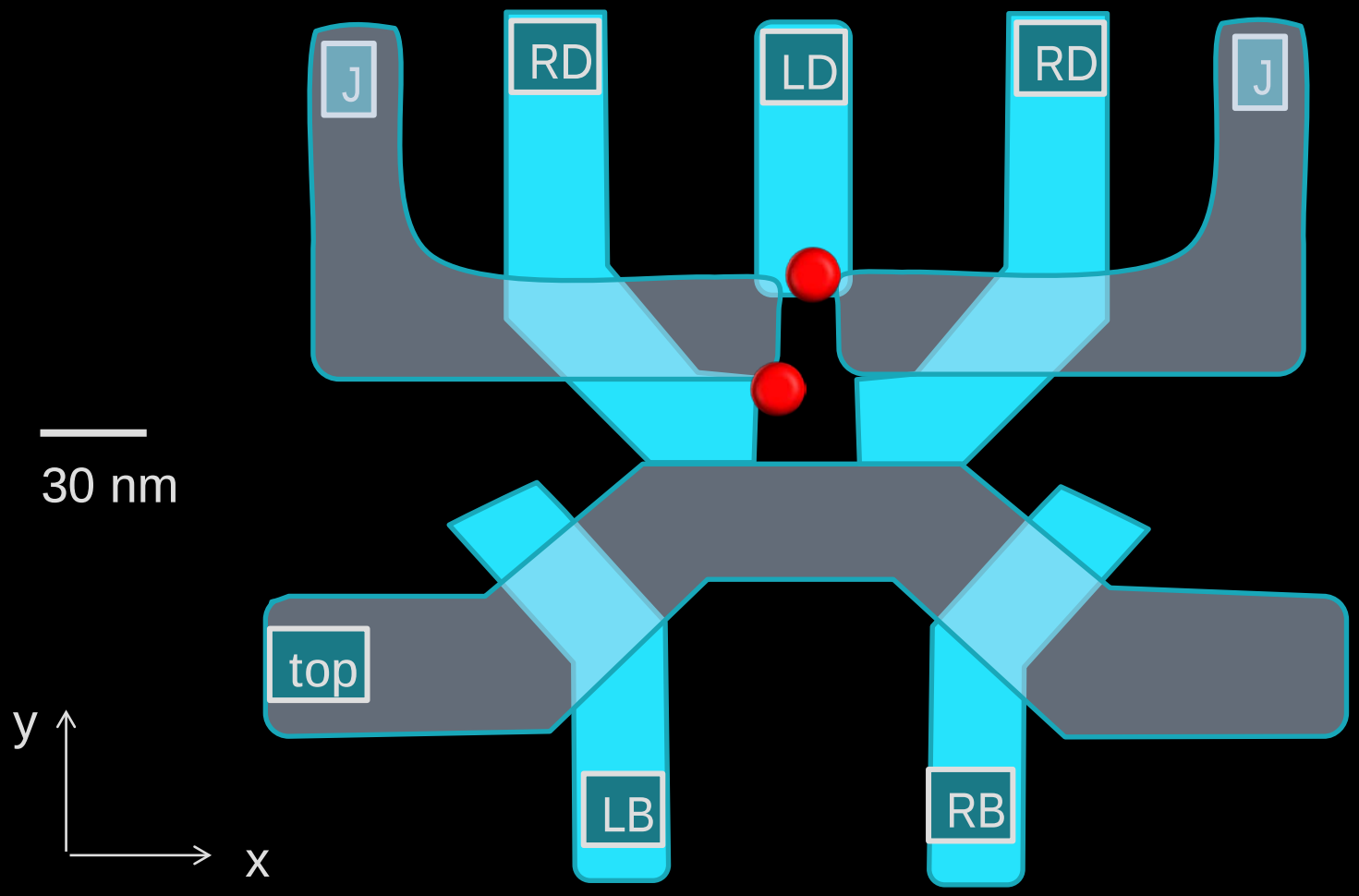

Highly tunable and robust architecture

Summary & Outlook

MOSFET donor-based spin qubit architecture

Single-shot spin readout

Fast qubit initialization

Measured T_1 (up to ~ 6 s) consistent with P donors in Si

92% readout visibility with 3 μs rise time

Local spin resonance of a single P donor

Single dopant as local electric field probe?

Rabi oscillations – single-spin coherence

2-donor devices → logic gates

The Team

Classical vs. Quantum Computers

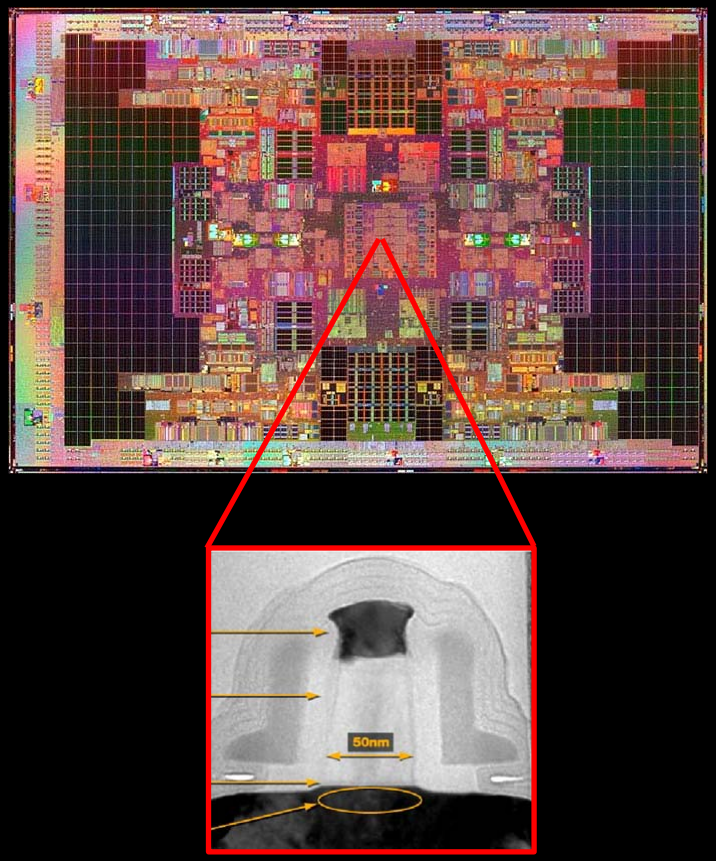

- Established technology
- Highly scaled and cost-effective
- Almost universal
- Uncertainty on future progress

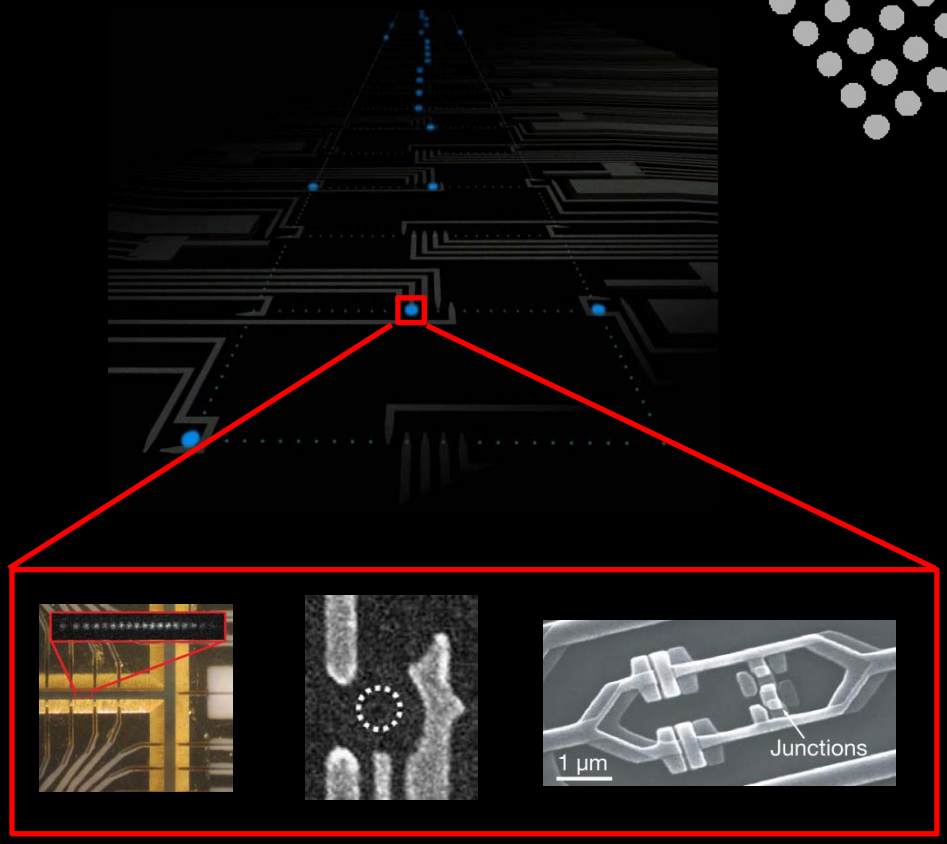

- Still in infancy,
  only small “proofs of principle”
- Not universal, few algorithms
- Truly revolutionary

Nitrogen-Vacancy “Defect” Centers in Diamond

Boris Naydenov, F. Jelezko, J. Wrachtrup
University of Stuttgart

quantum computing

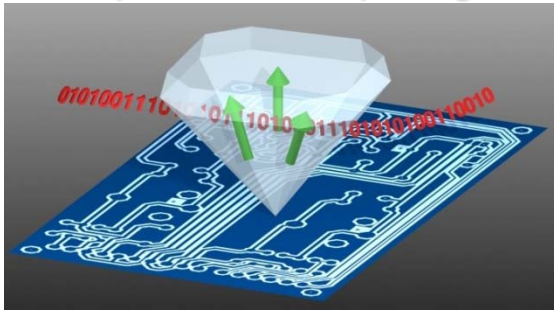

Neumann P. et al., *Science* 320, 1326 (2008)
Neumann P. et al., *Science* *329, 542 (2010)*

Scanning probe magnetometer

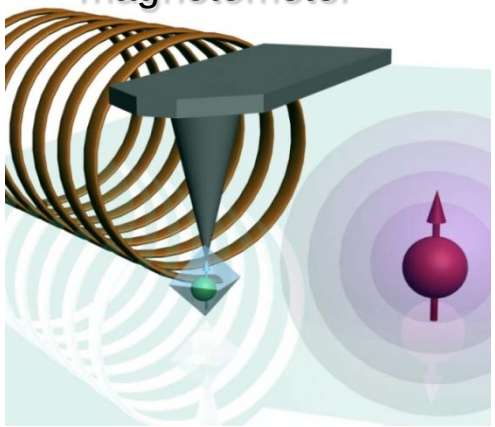

G. Balasubramanian, et al. *Nature* 455, 648 (2008)

Quantum devices

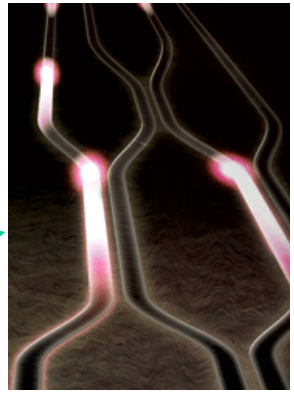

R. Kolesov et al. *Nat. Phys.* 5, 470 (2009)

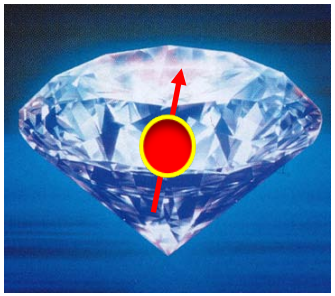

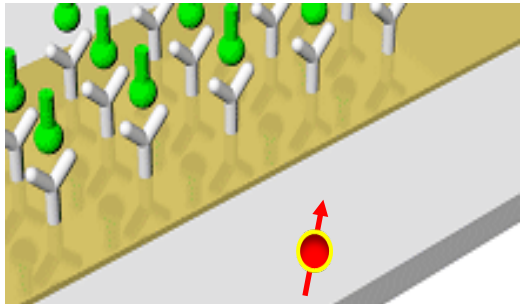

Biosensor technology & Molecular Spin sensors

NV in diamond

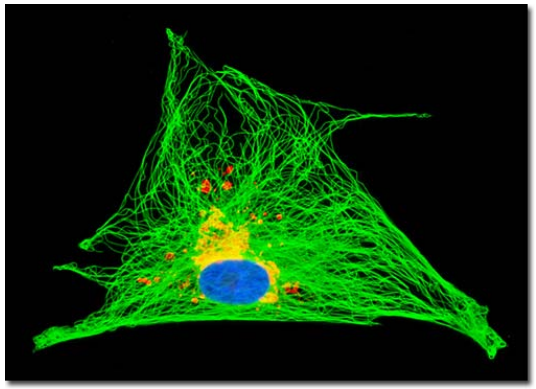

Sub µm cellular imaging
F. Neugart et al., *Nano Lett.*, 7, 3588 (2010)

Outline

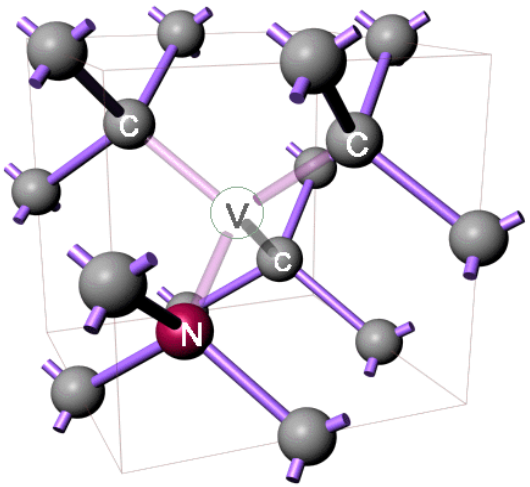

- Nitrogen-Vacancy (NV) Quantun Computer
- What is an NV center
- NV as a magnetic field sensor
- Coherence time of NV
- Quantum register based on two NVs

NV Quantum Computer

Array of implanted NV with controllable coupling

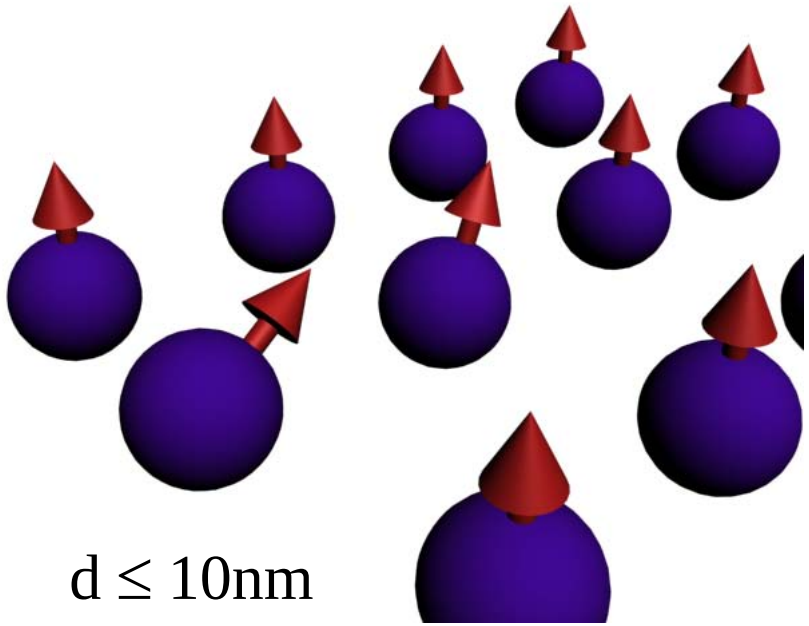

$d \leq 10nm$

Coupling of many NVs via magnetic dipolar interaction

$$E_d \sim 1/d^3$$

Long coherence times

Spin manipulation with MW pulses

Optical read-out

Nano-scale positioning and high yield of NV production

NV production

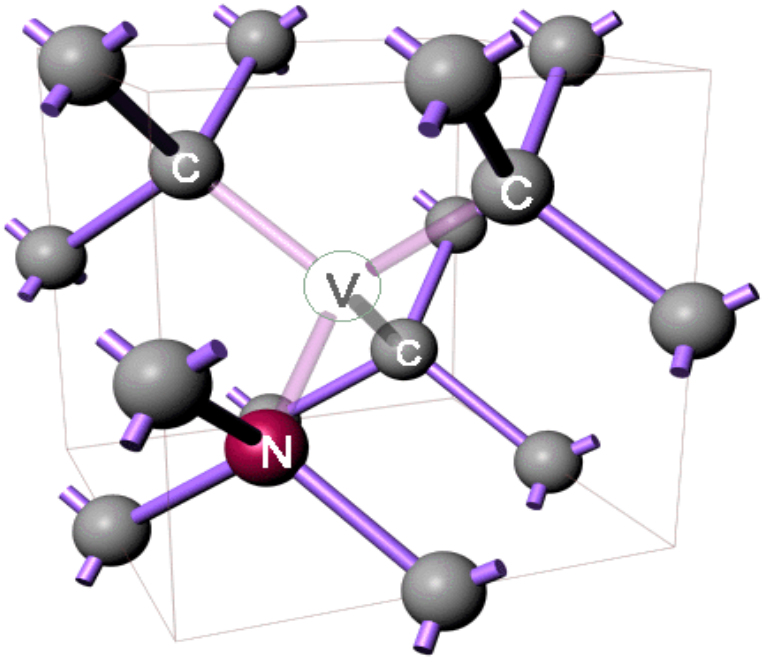

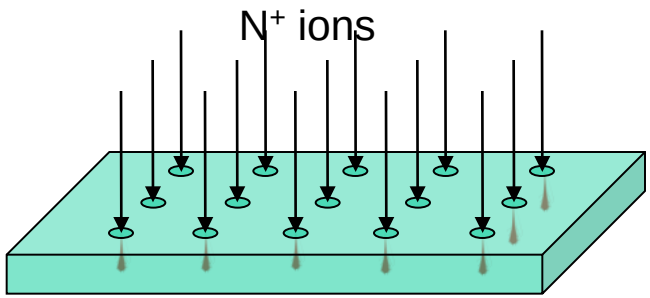

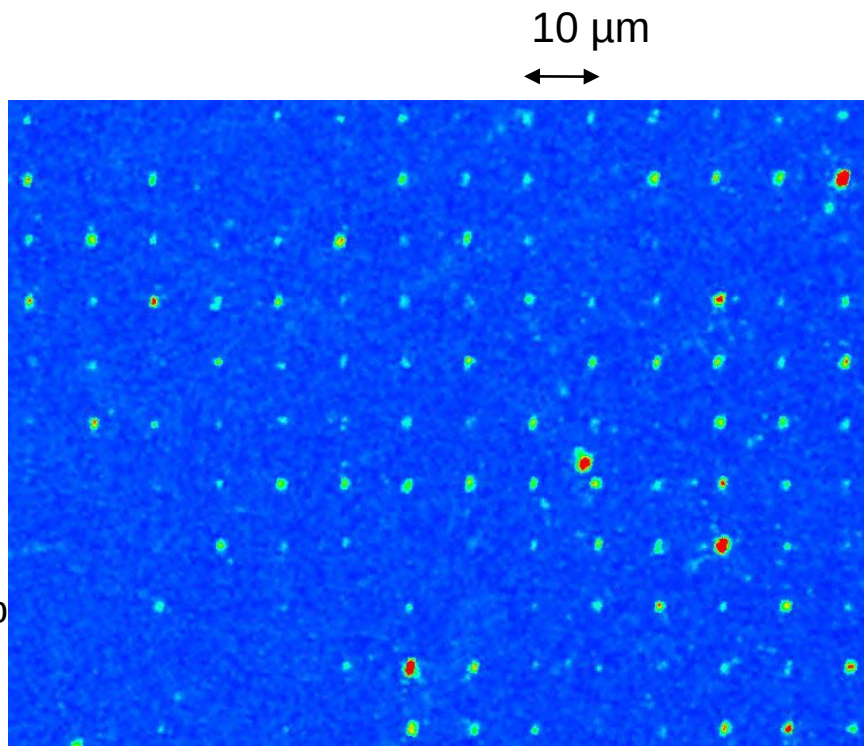

Implantation of nitrogen ions

Annealing at T > 700 °C

Cleaning the surface in acid

Yield depends on the impl. energy 1 to 60 %

J. Meijer et. al., APL 87, 261909 (2005).
J. R. Rabeau, et al. APL 88, 023113 (2006)

Single center signature: photon antibunching

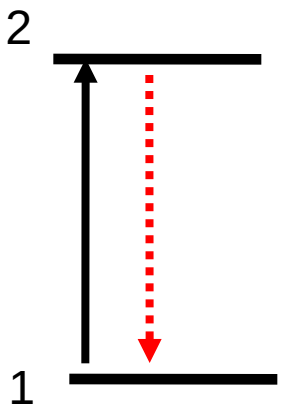

<u>Single photon source:</u>
H. Weinfurter et al. PRL 85 (2000)
P. Grangier et al. PRL 89 (2003)

Estimating number of defect centers

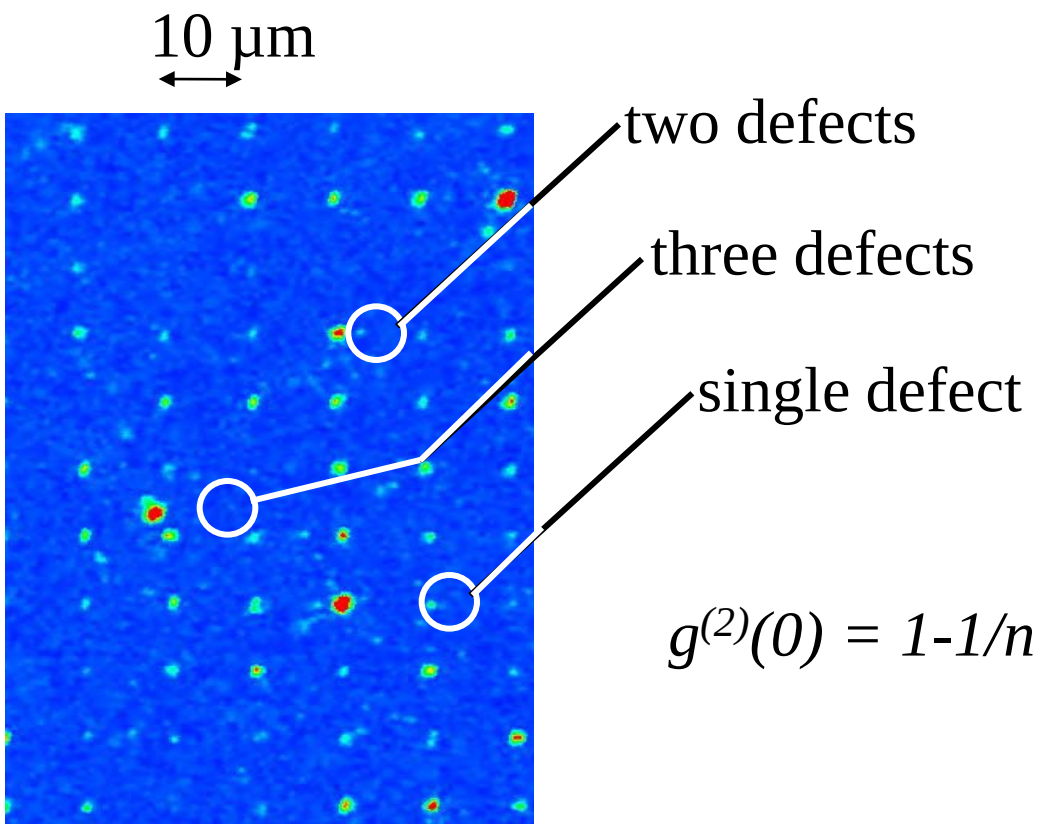

$$g^{(2)}(0) = 1-1/n$$

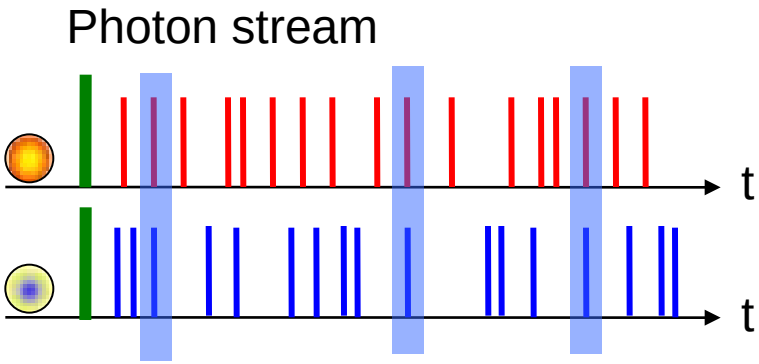

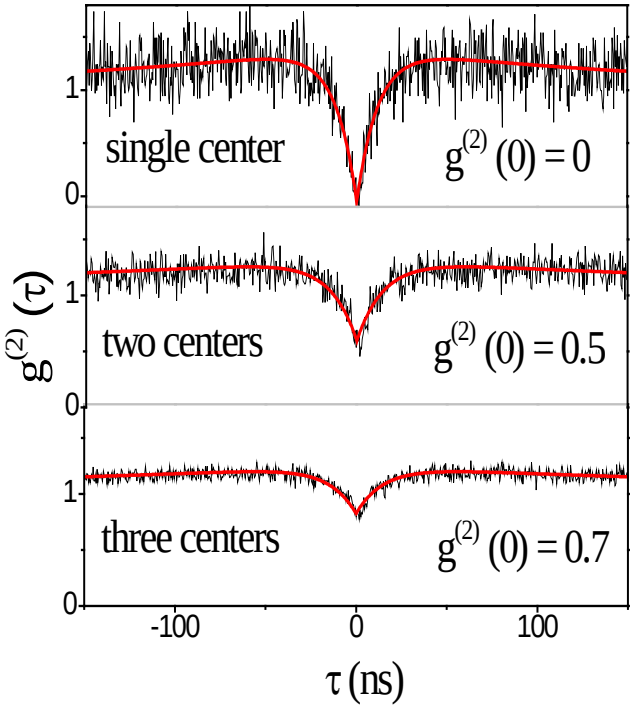

Spin properties of NV-center

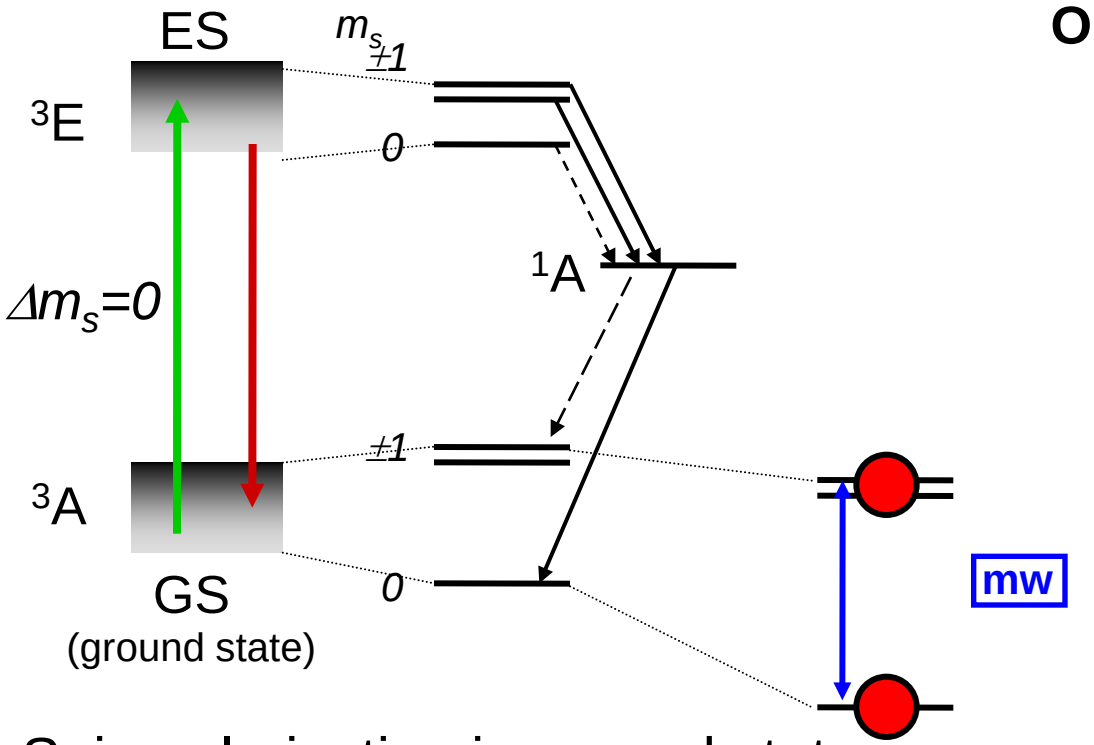

Optically **D**etected **M**agnetic **R**esonance

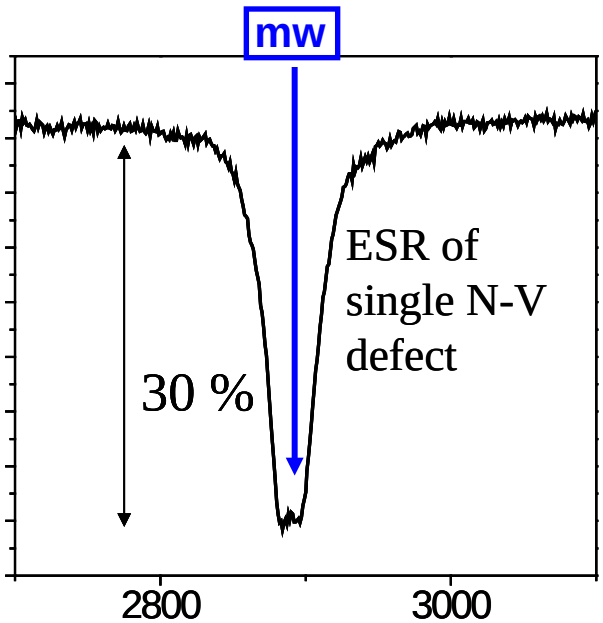

- Spin polarization in ground state $m_s=0$ by optical pumping
- Encoding $m_s=0$ and $m_s=\pm1$ in bright and dark state
- Optical read out of spin state
- Spin manipulation with MW

Single spin manipulation and read out at room temperature!

A. Gruber et al., Science 276, 2012 (1997)
F. Jelezko, et .al , Phys. Rev. Lett. 92, 76401 (2004)

NV – Atomic magnetometer

- Zeeman effect on single spin
- Atomic vector magnetometer.
- Absolute - No calibration.
- Sensitivity depends on the line width.

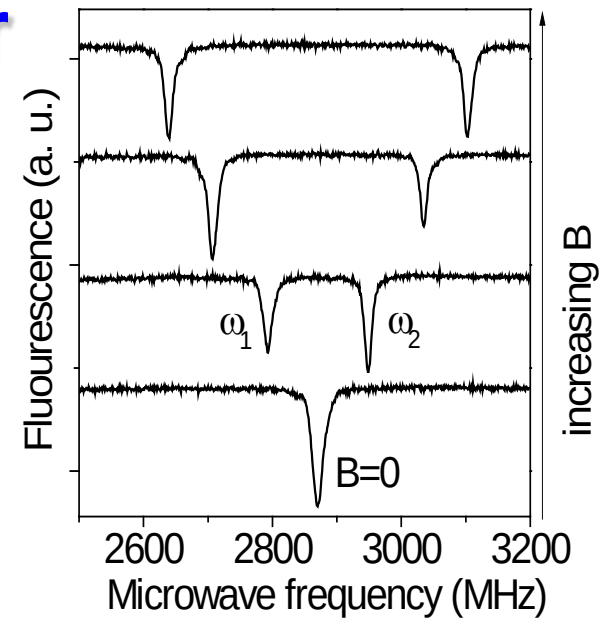

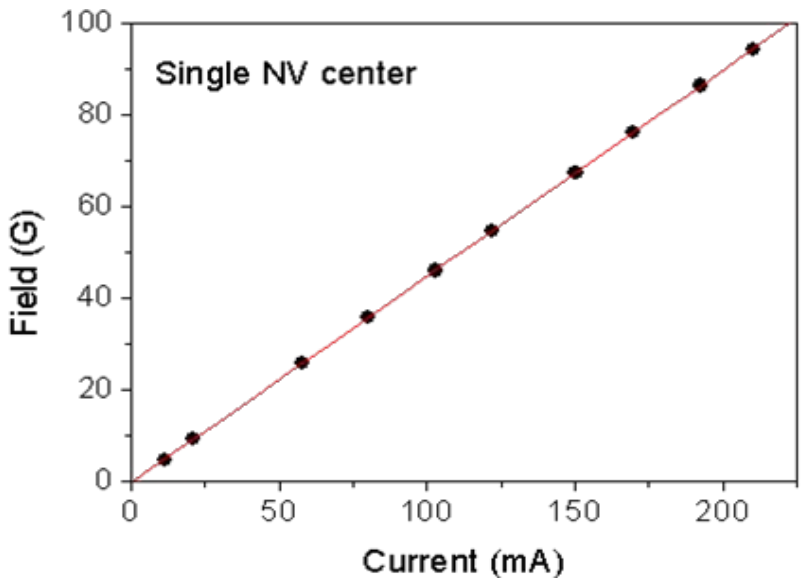

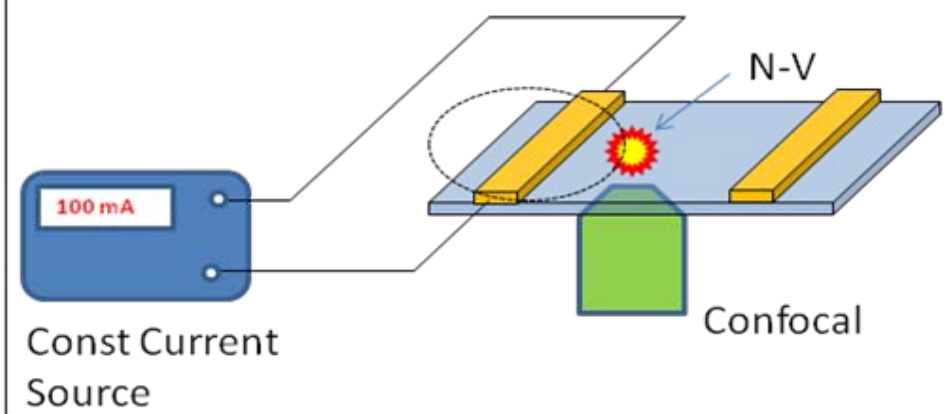

G. Balasubramanian et. al, *Nature* ,455, 648 (2008)
Maze, J. et. al., *Nature*, 455, 644 (2008)

Single electron spin Rabi oscillations

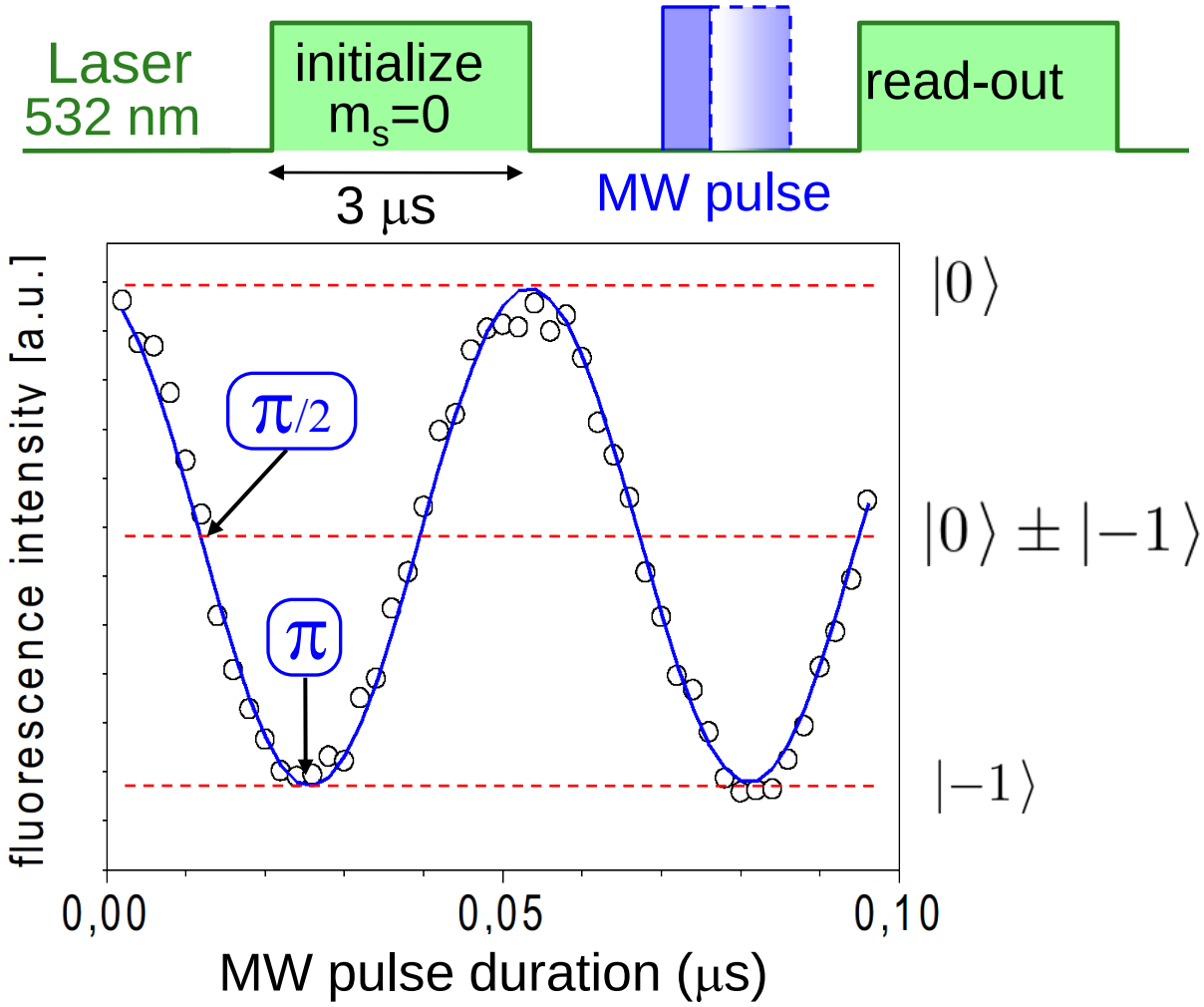

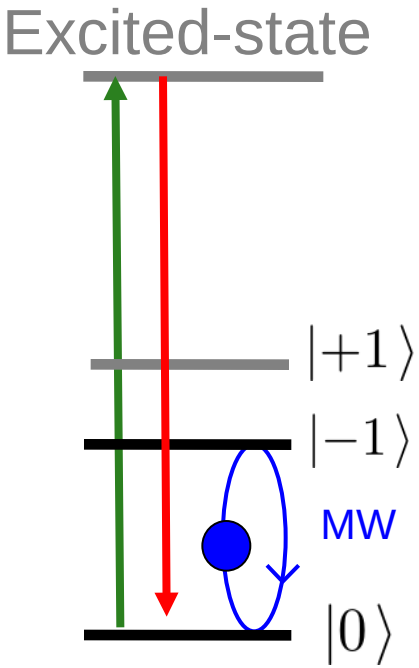

effective 2-level system
by Zeeman splitting

R. Hanson et al. Science 320, 352 (2008).
P. Neumann et al. Science 320, 1326 (2008).

F. Jelezko et .al , PRL 92, 76401 (2004)
G. D. Fuchs et al., Science 326, 1520 (2009)

Single Spin Hahn Echo at RT

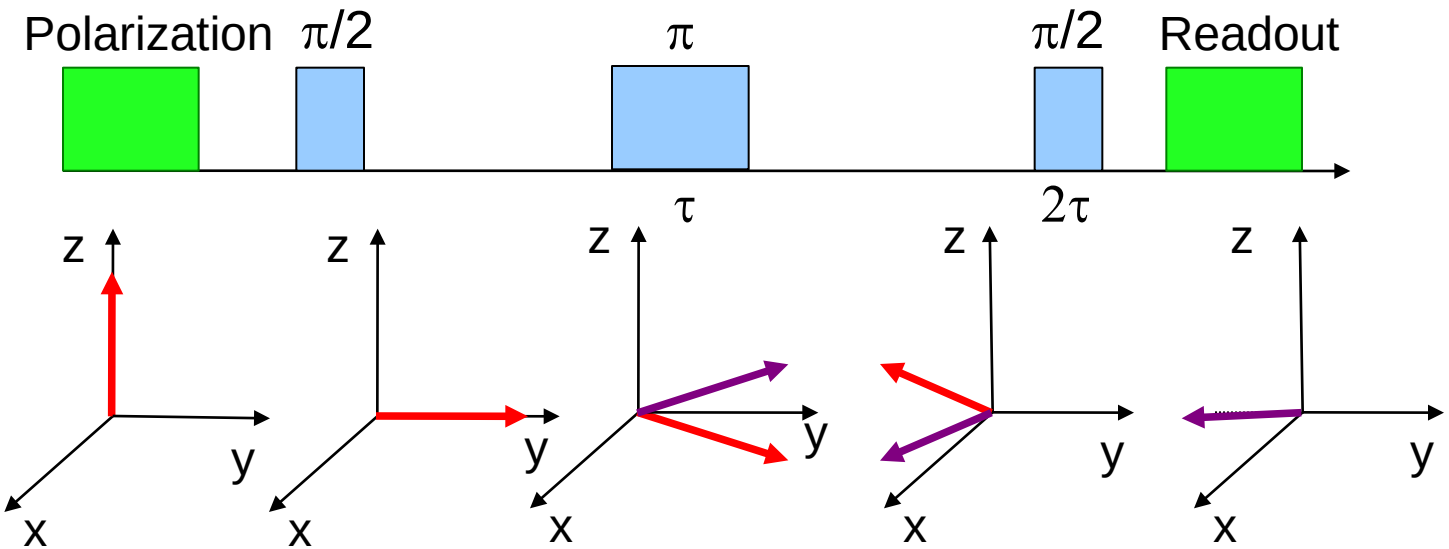

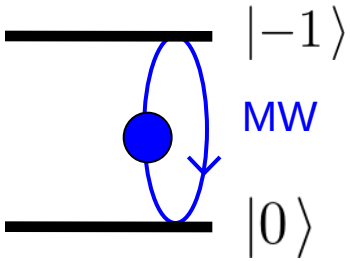

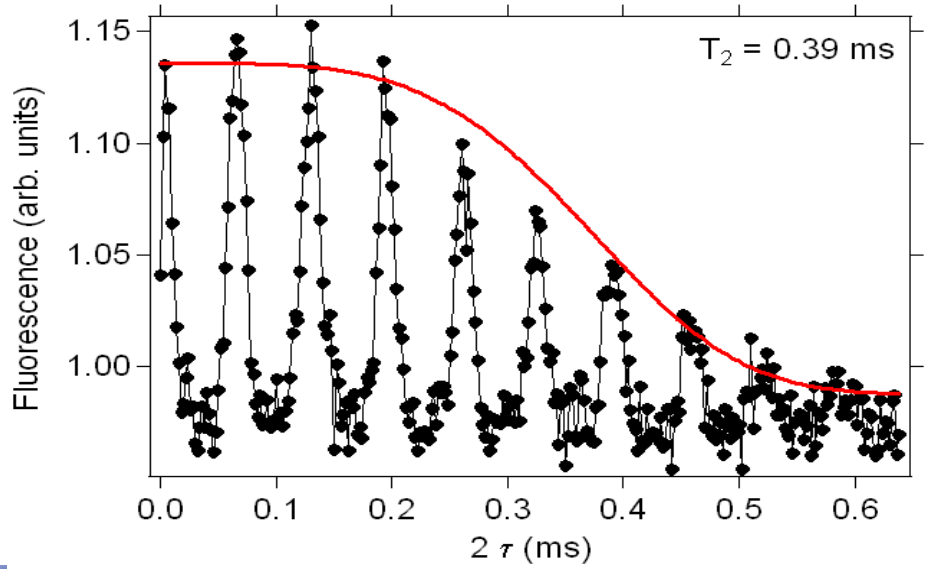

Main source of decoherence

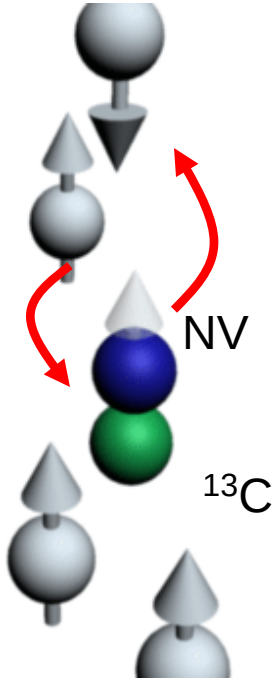

F. Jelezko et al PRL,92, 076401 (2004)
L. Childress, et al. Science 314, 281 (2006)

Coherence time in engineered diamond

Diamond with 0.3 % ^{13}C

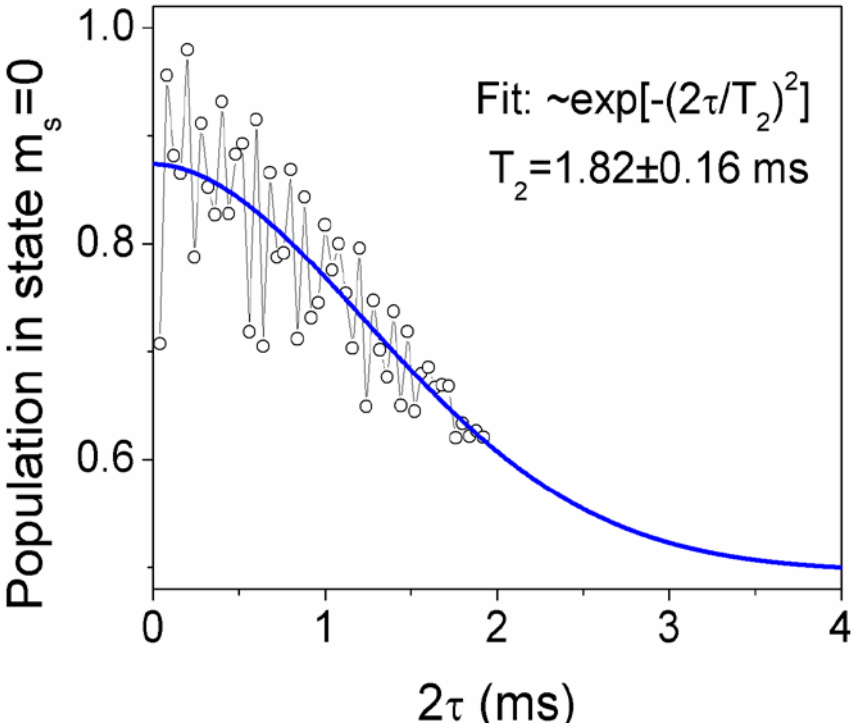

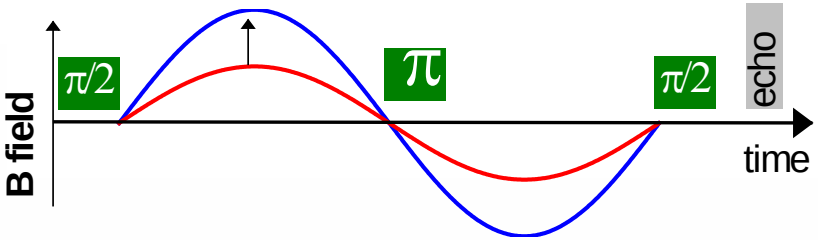

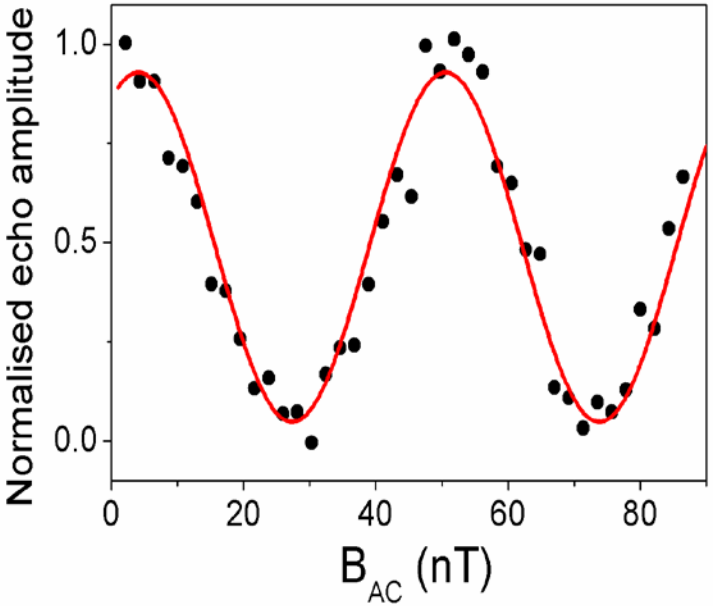

The magnetic field synchronized with the Hahn echo sequence, achieved sensitivity 4nT/√Hz

G. Balasubramanian et.al Nature Materials, 8, 383 (2009)

Improving the coherence time by using dynamical decoupling

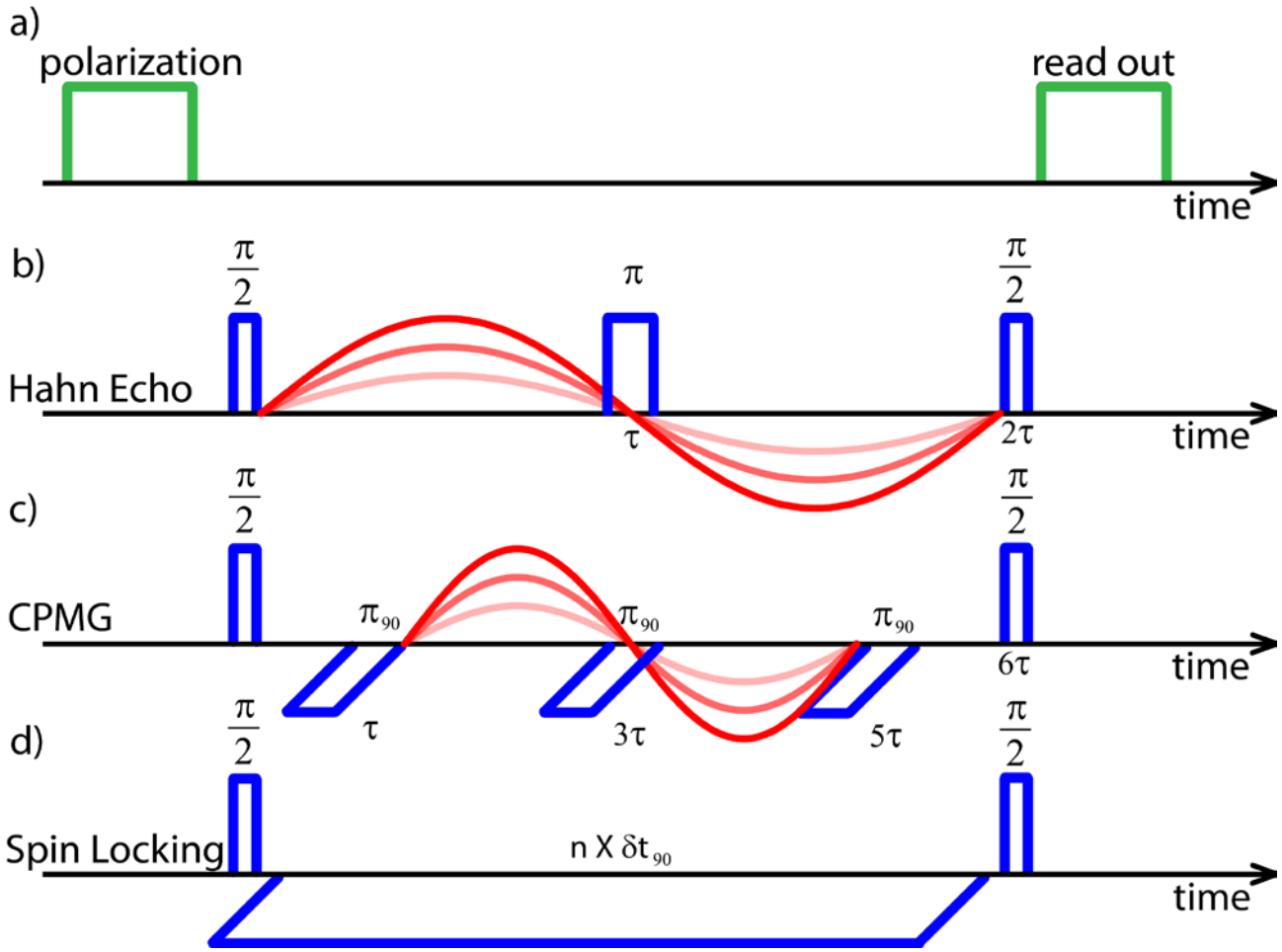

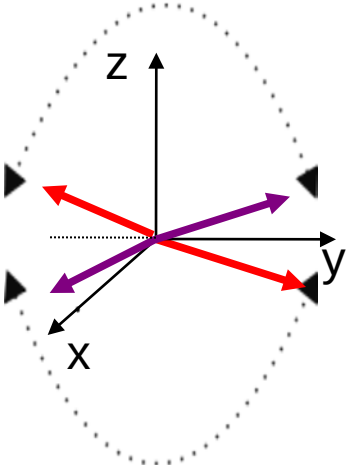

Dynamical decoupling with NV

Increasing the coherence time up to 2.4 ms

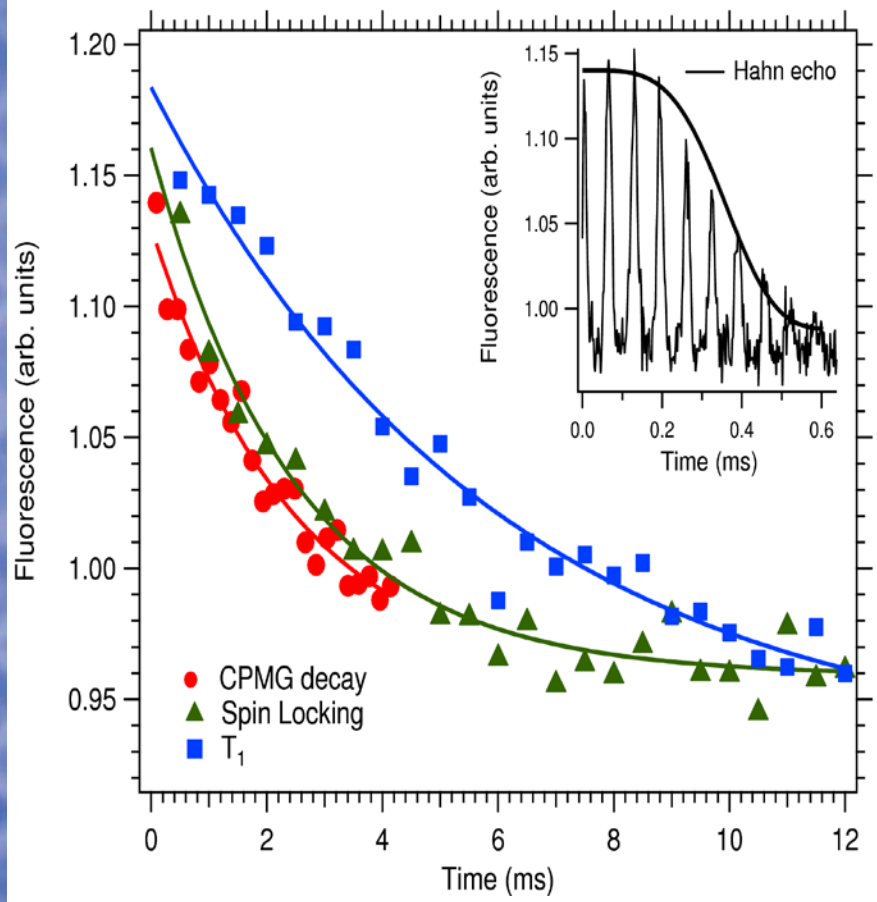

Limited by the thermal relaxation

Max. magnetic field sensitivity of 3.5 nT/√Hz

B. Naydenov et al., *arXiv1008:1953v2* (2010)
G. de Lange et al., *Science*, 330, 60 (2010)
C. A. Ryan et al., *arXiv:1008.2197v2 (2010)*

How to increase the yield of NV?

Just add more vacancies

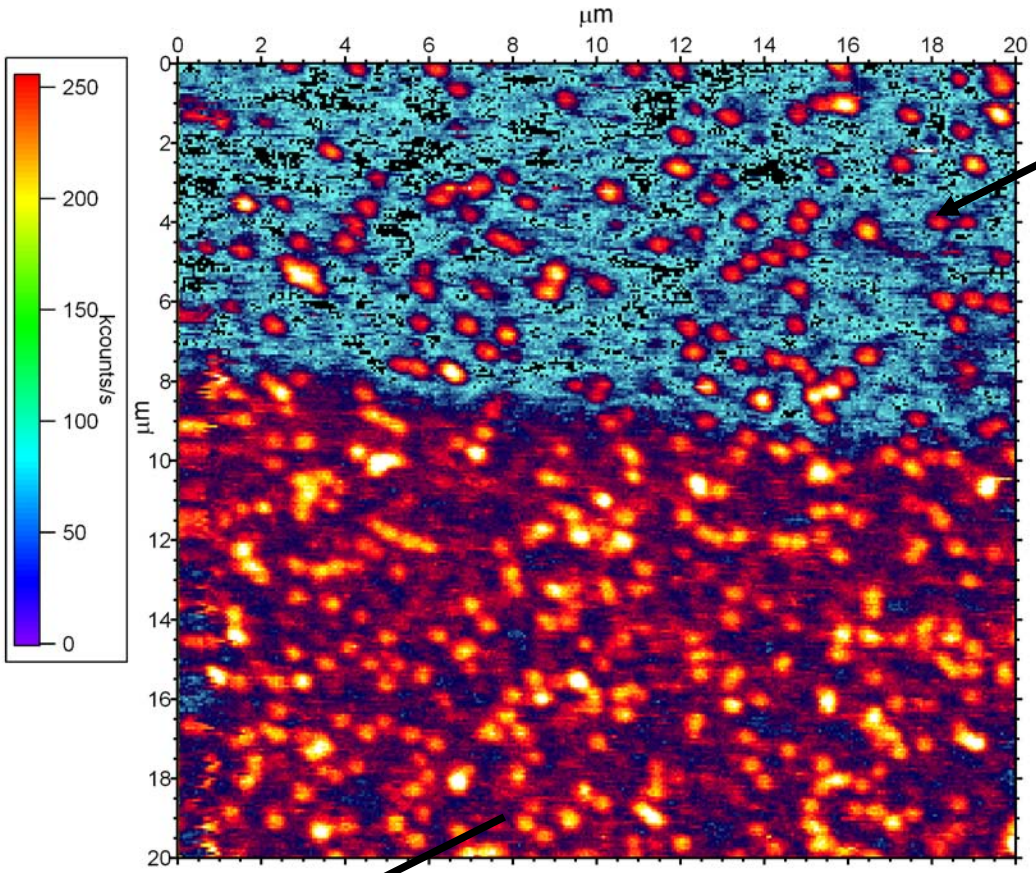

$^{15}N_2^+$ ions 60 keV, 1 ion/µm^2

The yield increased from 20 % to above 50%

However many of the NVs are from ^{14}N

$^{15}N_2^{+z}$ ions 60 keV and C^+ 40 keV, 10^4 ions/µm^2

How does it work?

Matching the vacancy profile with the nitrogen implantation distribution

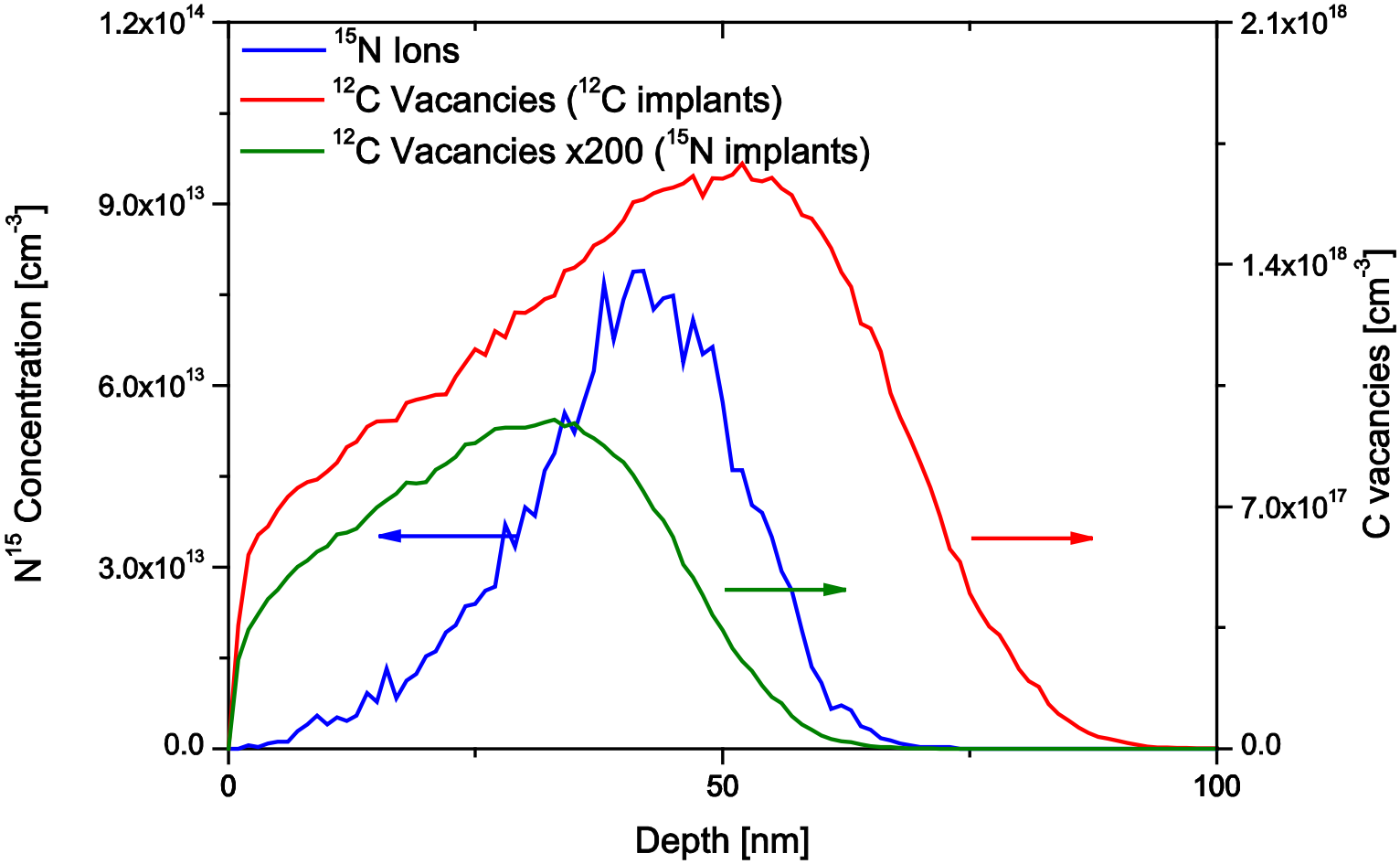

B. Naydenov et al. *APL*, 96, 163108 (2010)

Detection of low N concentration

Maximum ^{15}NV yield 33 %

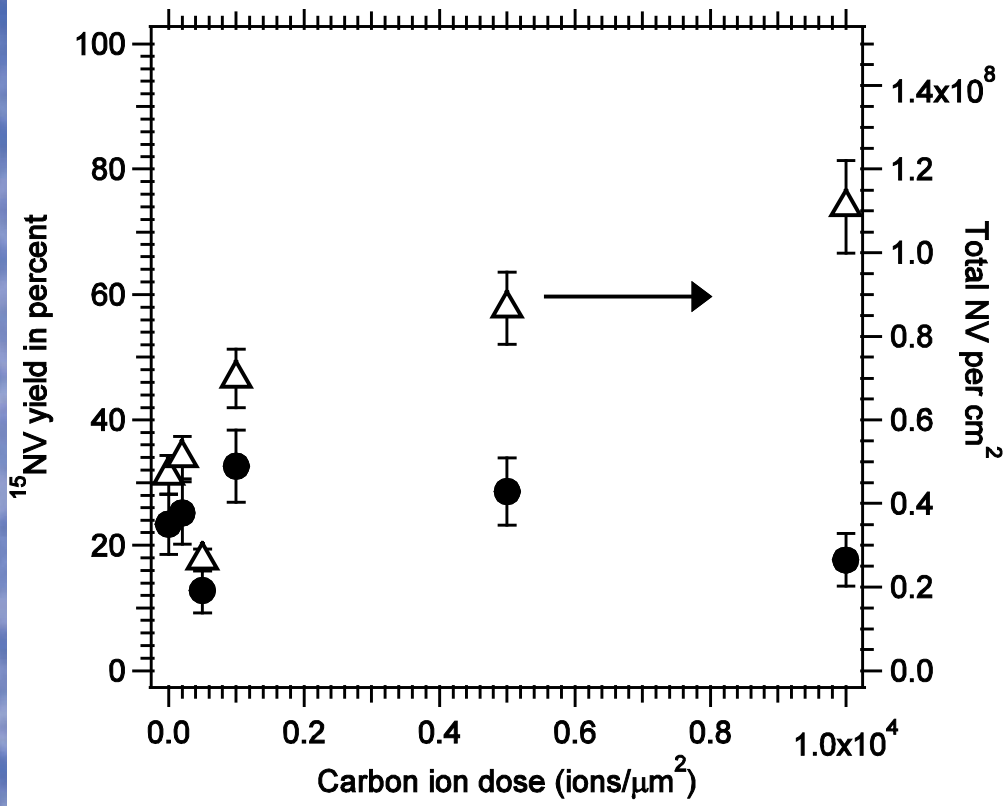

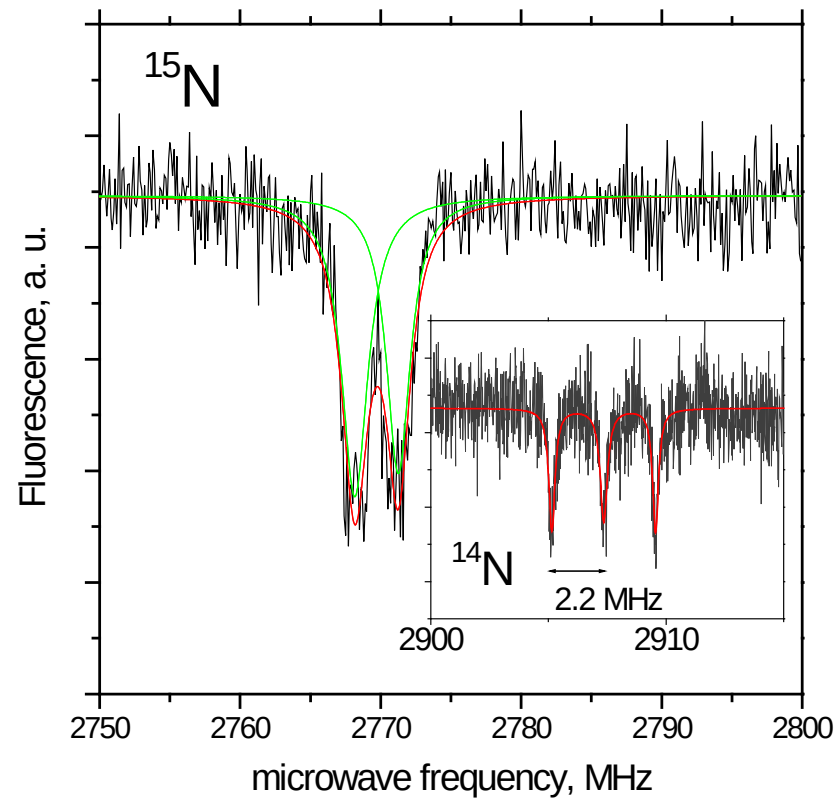

Detected nitrogen concentration < 0.07 ppb

B. Naydenov et al. *APL*, 96, 163108 (2010)

NV – NV pair

Implanting with high energy (13 MeV) and good focus

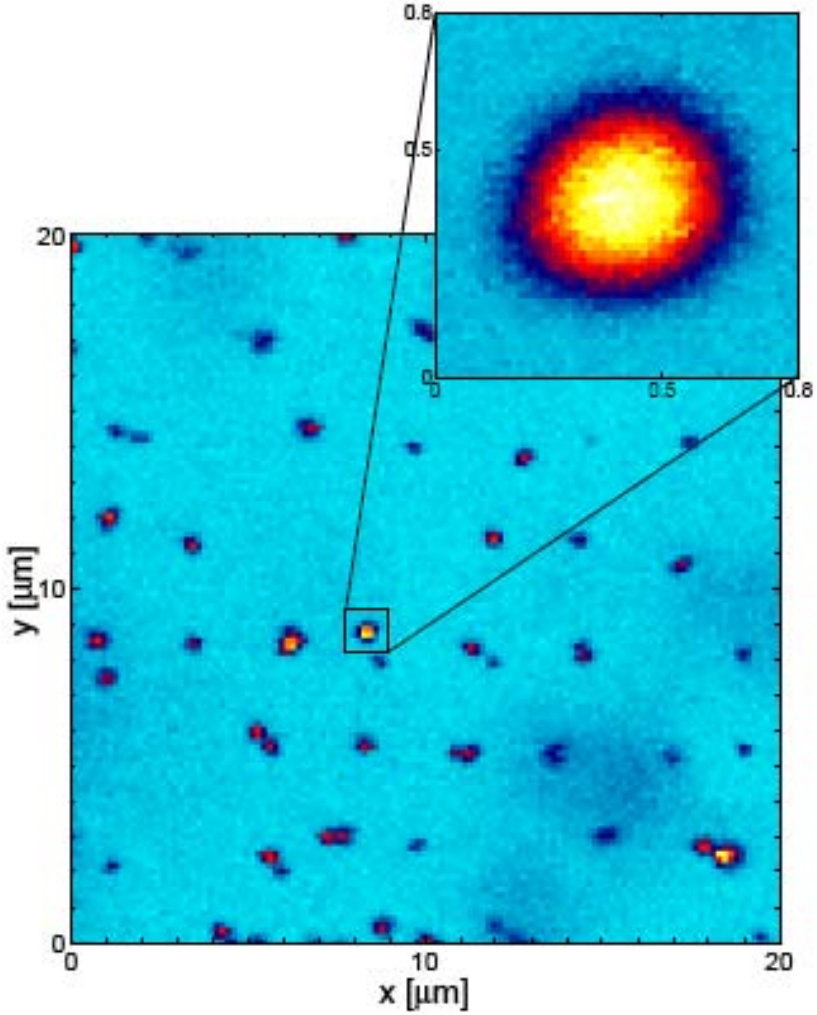

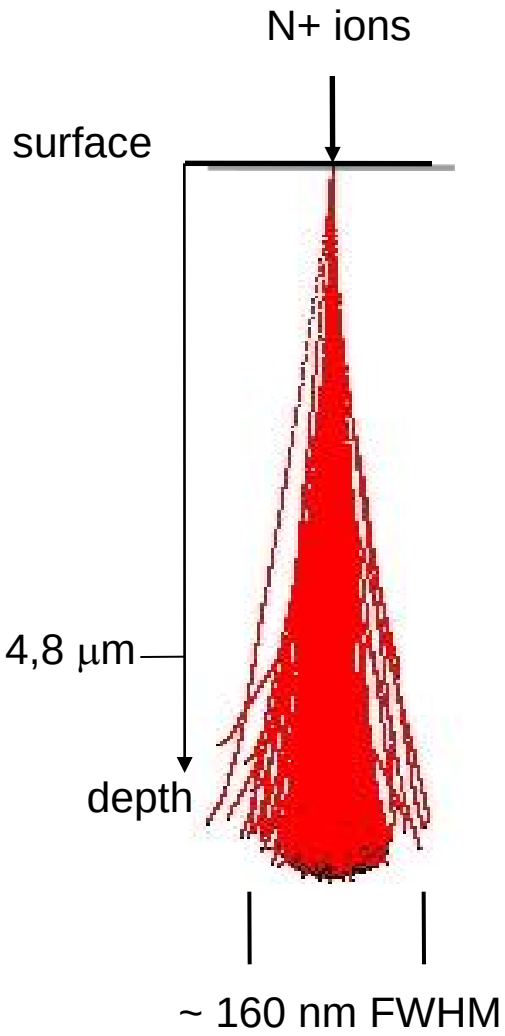

P. Neumann et al. *Nat. Phys.*, 6, 249 (2010)

NV Quantum Register

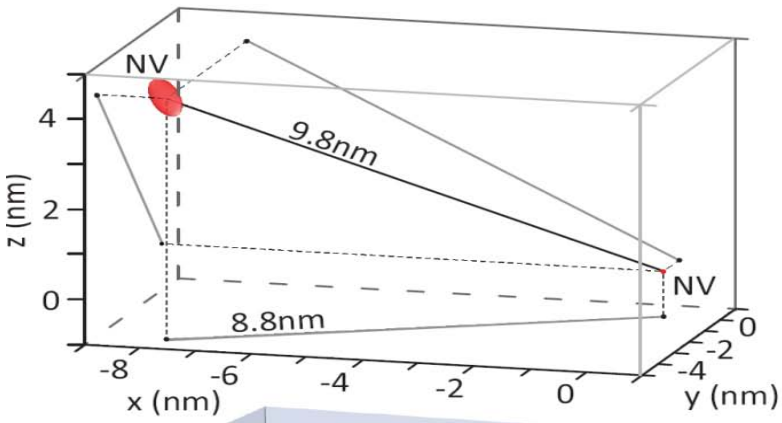

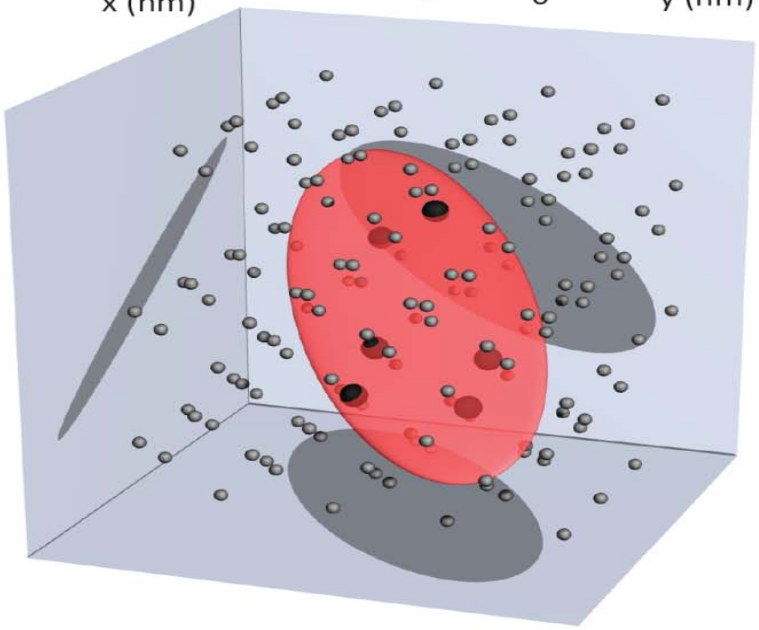

Coupling 40 kHz

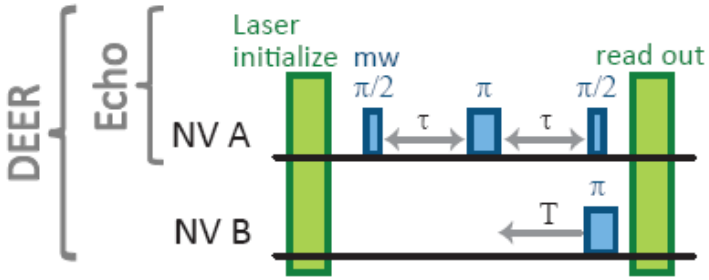

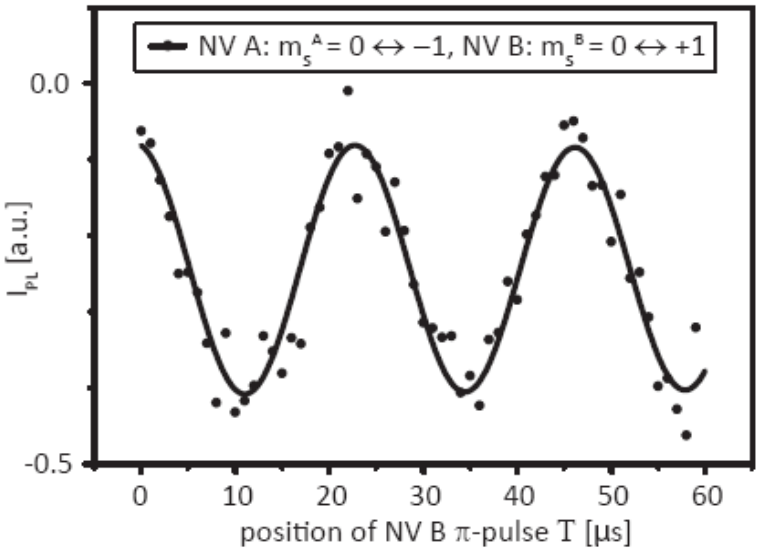

P. Neumann et al. *Nat. Phys.*, 6, 249 (2010)

Conclusions

- NV is a unique “defect” center in diamond
- Ultra low magnetic field sensing at nano-scale
- Very long electron spin coherence time
- Quantum register based on two couple NVs

Outlook

- Improve the lateral resolution of the ion implantation
- Push the yield close to 100 %
- Entanglement and QC algorithms with several NVs

Thank you !

P. Neumann G. Balasubramanian F. Jelezko J. Tisler F. Dolde

In collaboration with:

S. Pezzagna, D. Rogalla, J. Meier (Bochum)

D. Twitchen (Element 6)

V. Richter, R. Kalish (Haifa, Israel)

VolkswagenStiftung
Deutsche Forschungsgemeinschaft DFG
LANDESSTIFTUNG Baden-Württemberg

Dependence of T_2 on the depth of NV

NV depth varies from 40 to 300 nm (Ion energy 30 – 300 keV)

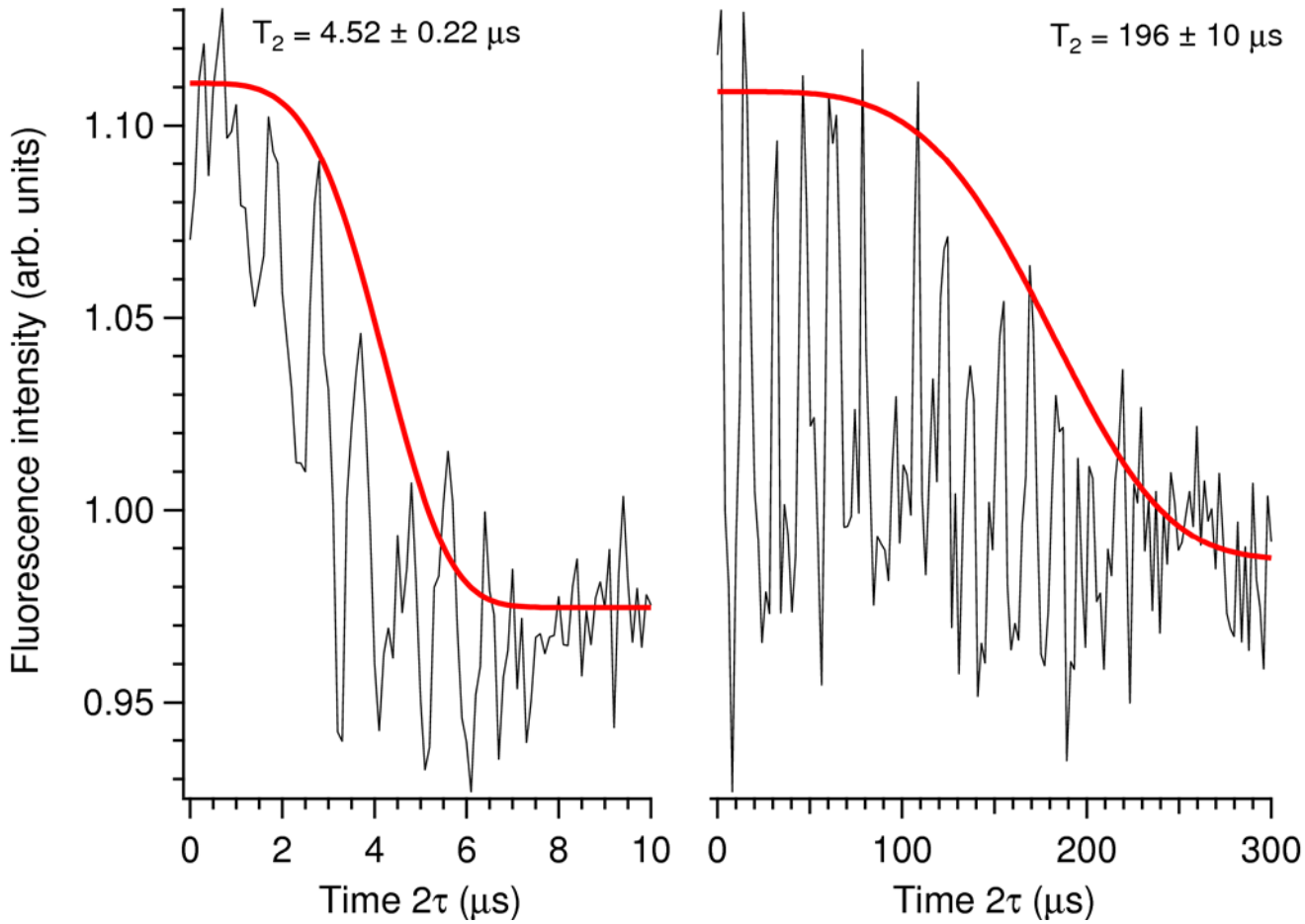

About 20 % discharge to NV^0

Removing the defects surround the NV

After annealing at T = 1200 C

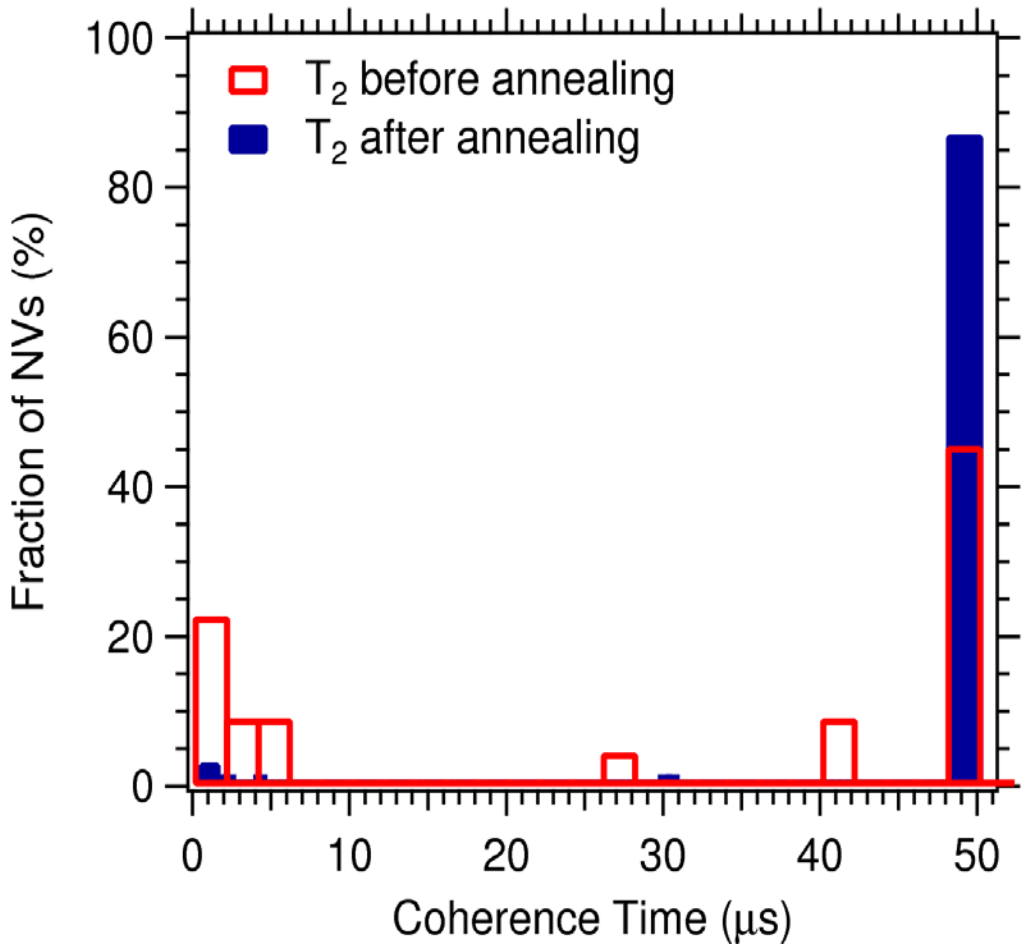

Now only 6 % show discharging

Directed Self-Assembly: Patterning

Christopher K. Ober
Cornell University

Deterministic Doping Workshop, Berkeley, CA 2010

Overview

- Assume all know how polymers driven to phase separate by large size
- Classically form spheres, cylinders and lamellae
- Size range typically 20 nm, not much smaller than good resist
- Some systems capable of <5 nm spacings

Block copolymers

- Block copolymers are two or more chemically distinct polymers linked together with covalent bonding
- Sum of entropic and enthalpic effects within polymer are minimized by microphase separation

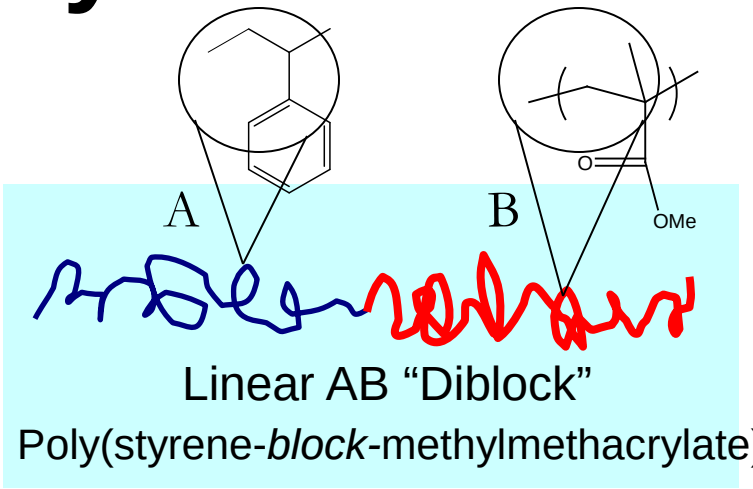

$$F_m = k_i \left[\underbrace{\frac{\phi}{N} \ln \phi + (1-\phi) \ln (1-\phi)}_{\textbf{Entropy} \propto \frac{1}{N}} + \underbrace{\chi (1-\phi)\phi}_{\textbf{Enthalpy} \propto \chi} \right]$$

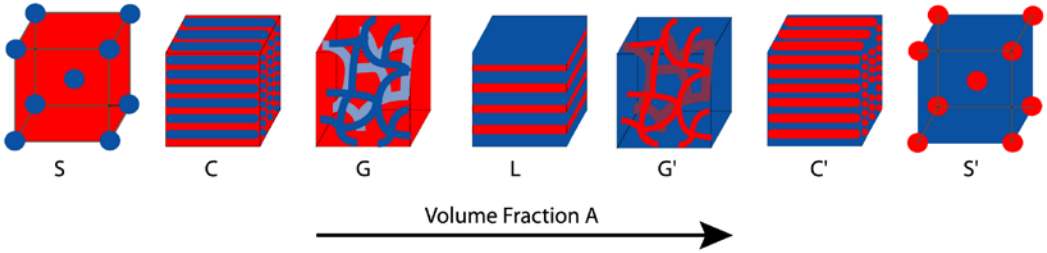

Bates, Frederickson, Phys. Today, Feb. 1999, 32-38.

Where are we today?

- Bcps studied largely limited to diblocks and classical phases – sphere, cylinder, layers
- Bcps used to pattern today are largely at weak segregation limit
- What about triblocks?
- Cubic instead of hexagonal – otherwise similar today – future?
- Increasing use of inorganic additives

Long Range Order

- Great progress in this area
- Thermal and solvent annealing
- Surface topography
- Surface energy and homopolymer enable bends and turns
- Small size (< 5 nm) when controlled interactions used to force phase separation

Metal Nanodot Memory by Self-Assembled Block Copolymer Lift-Off

poly(styrene-*b*-methyl methacrylate)

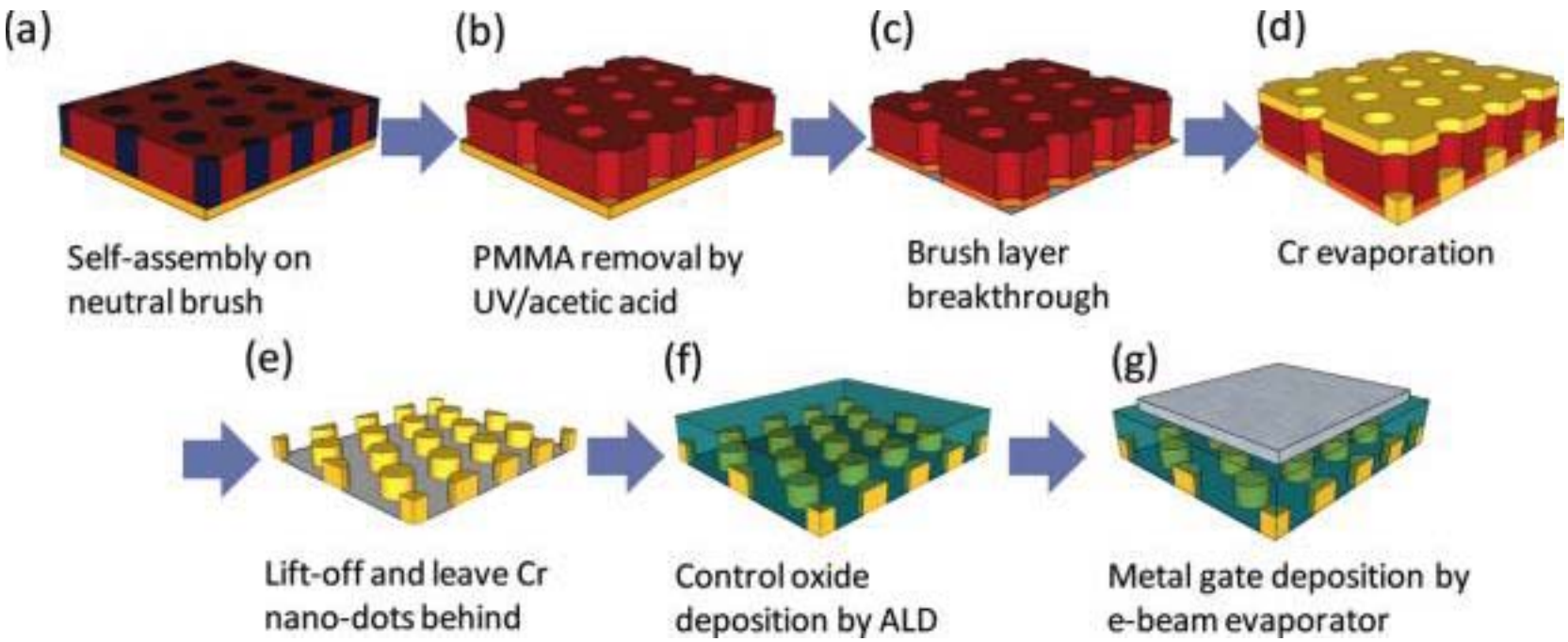

Schematic process flow of the proposed metal nanodot memory fabrication using a self-assembled block copolymer lift-off

A. J. Hong, C. C. Liu, Y. Wang ,J. Kim, F. Xiu, S. Ji, J. Zou, P. F. Nealey, and K. L. Wang, *Nano Lett.* 2010, *10*, 224-229

Metal Nanodot Memory by Self-Assembled Block Copolymer Lift-Off

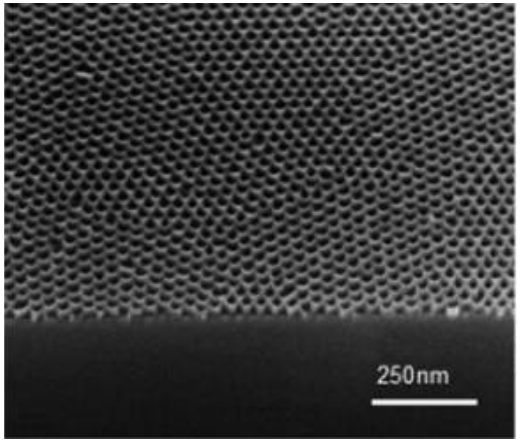

The polymer template before Cr evaporation
Dimensions are ~20 nm in diameter, ~40 nm in spacing, and ~35 nm in height

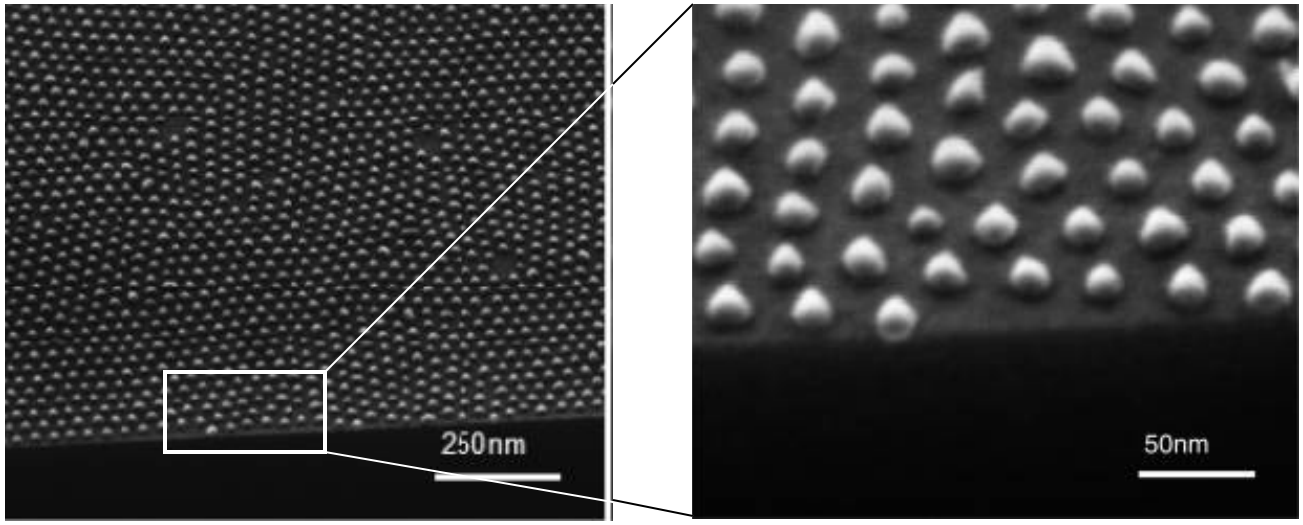

Cr nanodots after lift-off

A. J. Hong, C. C. Liu, Y. Wang ,J. Kim, F. Xiu, S. Ji, J. Zou, P. F. Nealey, and K. L. Wang, *Nano Lett.* 2010, *10*, 224-229

Templated Self-Assembly of Square Symmetry Arrays from an ABC Triblock Terpolymer

polyisoprene-*b*-polystyrene-*b*-polyferrocenylsilane

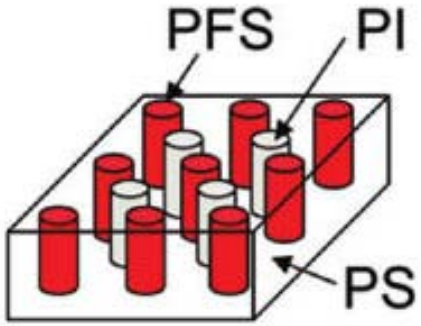

Bulk morphology sketch of PI-*b*-PS-*b*-PFS

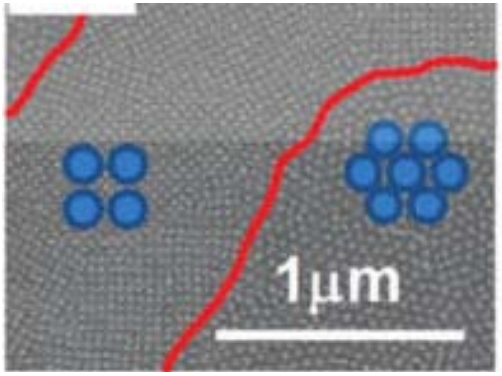

pure ISF_{82} triblock terpolymer

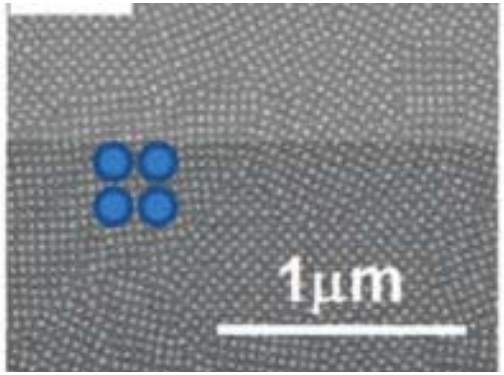

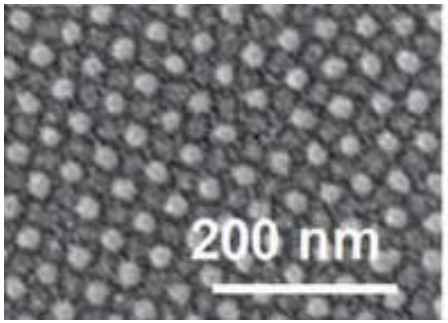

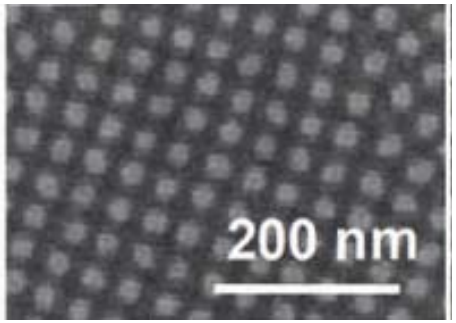

ISF_{82}/PS blend on oxidized Si after spin-coating, annealing in chloroform vapor and RIE etch

V. P. Chuang, J. Gwyther, R. A. Mickiewicz, I. Manners and C. A. Ross, *Nano Lett.,* Vol. 9, No. 12, 2009

Templated Self-Assembly of Square Symmetry Arrays from an ABC Triblock Terpolymer

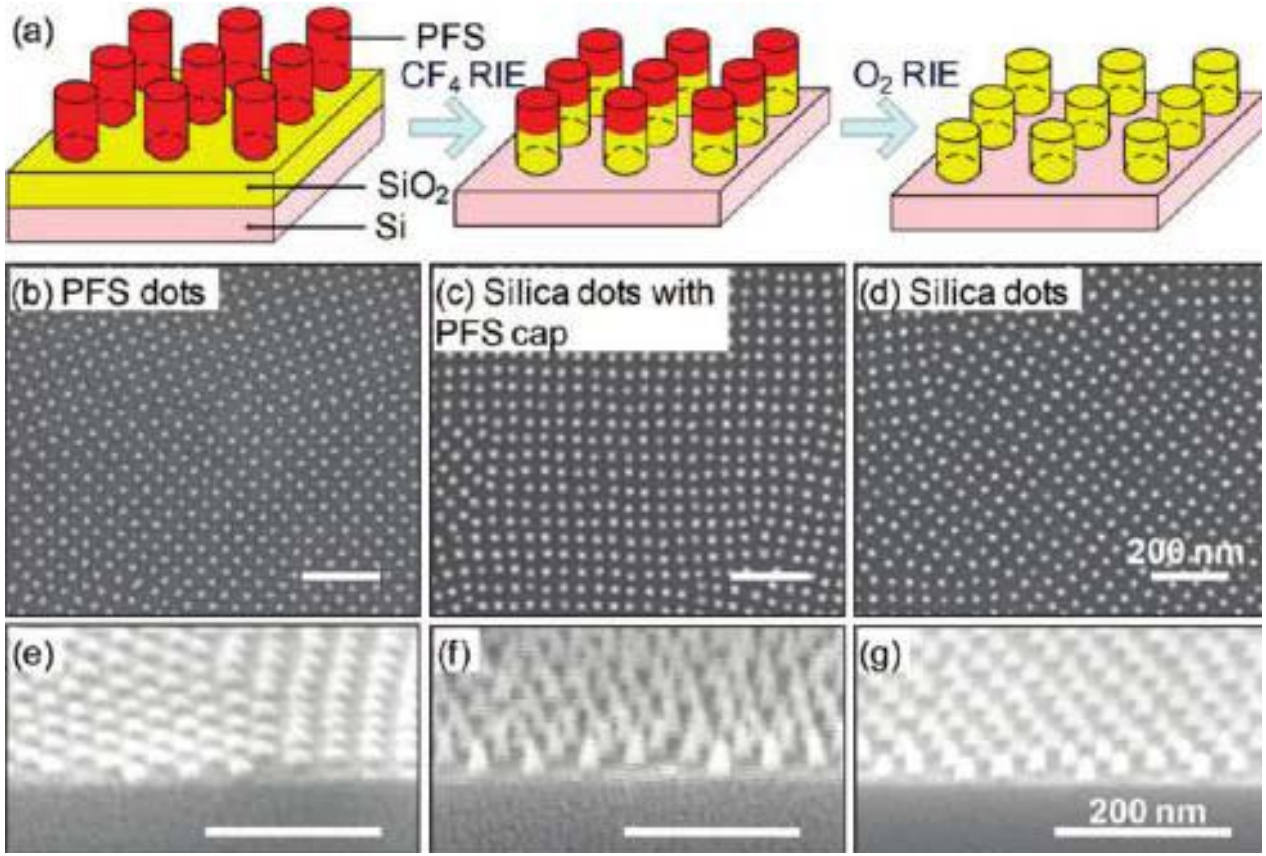

Pattern transfer to form square arrays of posts

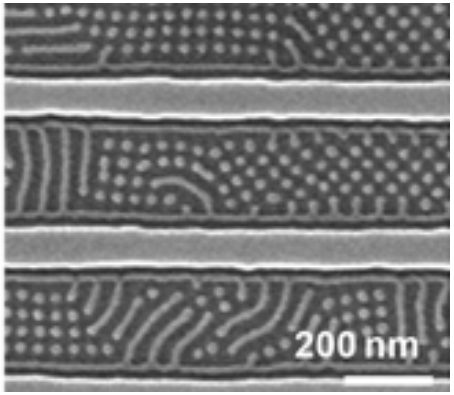

Templated in-plane cylinders parallel to the trench walls, surrounding a mix of inplane cylinders and 45°-oriented and 90°-oriented out of-plane cylinder arrays.

V. P. Chuang, J. Gwyther, R. A. Mickiewicz, I. Manners and C. A. Ross, *Nano Lett.,* Vol. 9, No. 12, 2009

Self-Assembly of Metallo-Supramolecular Block Copolymers in Thin Films

terpyridine-functionalized poly(ethyleneoxide) and polystyrene was mixed with this ruthenium complex to create a PS-[Ru]-PEO metallo-supramolecular copolymer

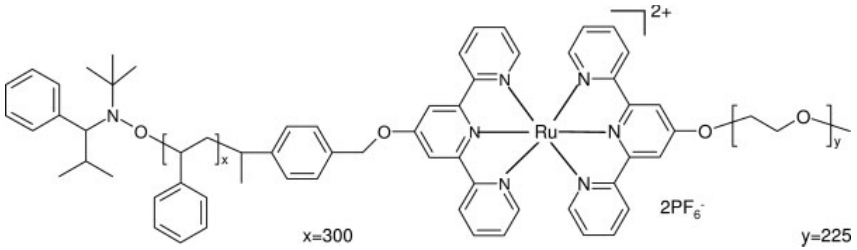

SFM phase image of a 250 nm thick film of PS300-[Ru]-PEO225 spin-coated from a THF solution that was floated and flipped to show the bottom of the original film.

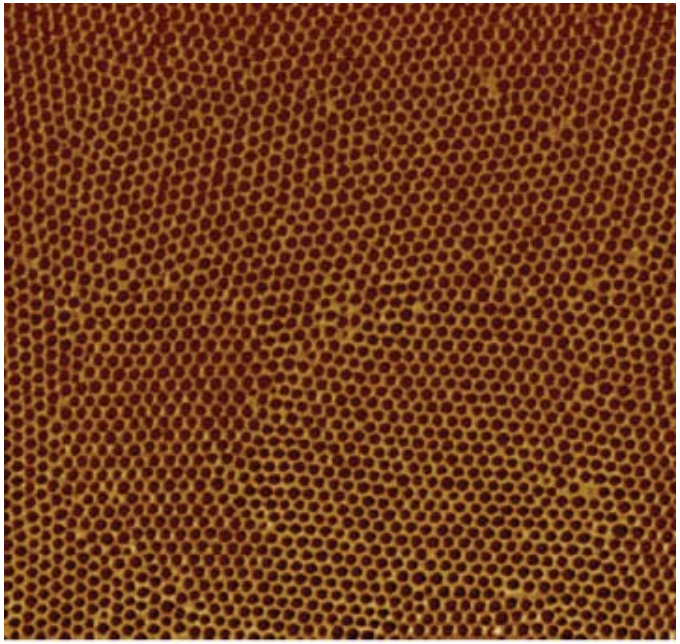

SFM phase image of a film of PS300-[Ru]-PEO225 spin-coated from a THF solution and annealed 24 h in THF vapor.

C.-A. Fustin, P. Guillet, M. J. Misner, T. P. Russell, U. S. Schubert, J.-F. Gohy, J. Polym. Sci. Part A: Poly. Chem., 46,*14*, 4719–4724, 2008

Rapid directed self assembly of lamellar microdomains from a block copolymer containing hybrid

PS-b-PEO, OS1, OS2 (copolymers of methyltrimethoxysilane and tetraethoxysilane)

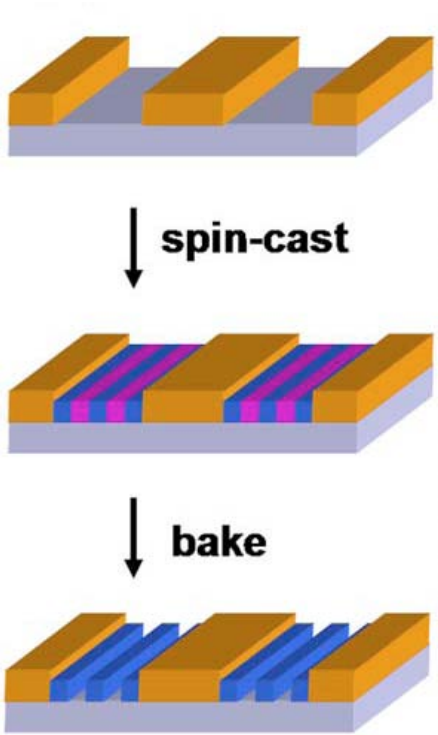

addition of OS provides an additional control over the persistence length of lamellae and DSA behavior

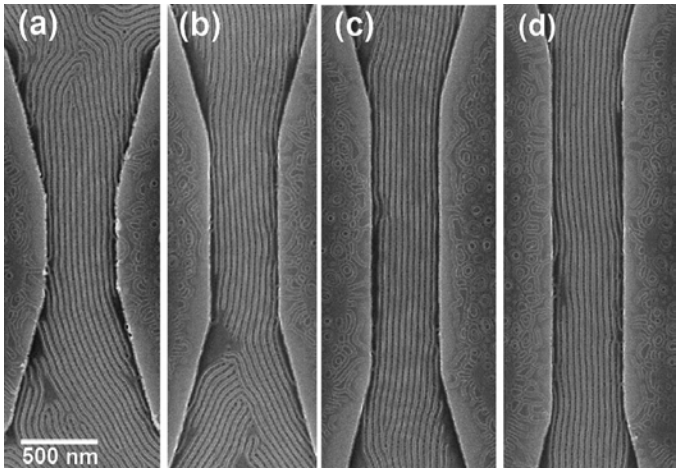

directed self-assembly of the PS-*b*-PEO/OS2 system in a trench with width of 480 nm and length of a) 0.5, b) 1, c) 1.5, and d) 2 µm.

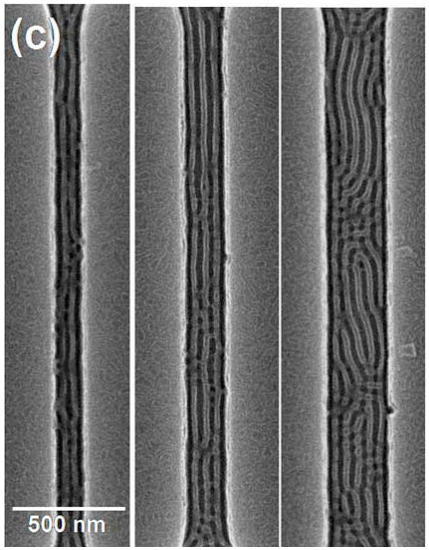

PS-*b*-PEO/OS1 in trenches of various widths

J. Y. Cheng, J. Pitera, O. H. Park, M. Flickner, R. Ruiza, C. T. Black and H. C. Kim, Appl. Phys. Lett. 91, 143106 2007

Fabrication of Diverse Metallic Nanowire Arrays Based on Block Copolymer Self-Assembly

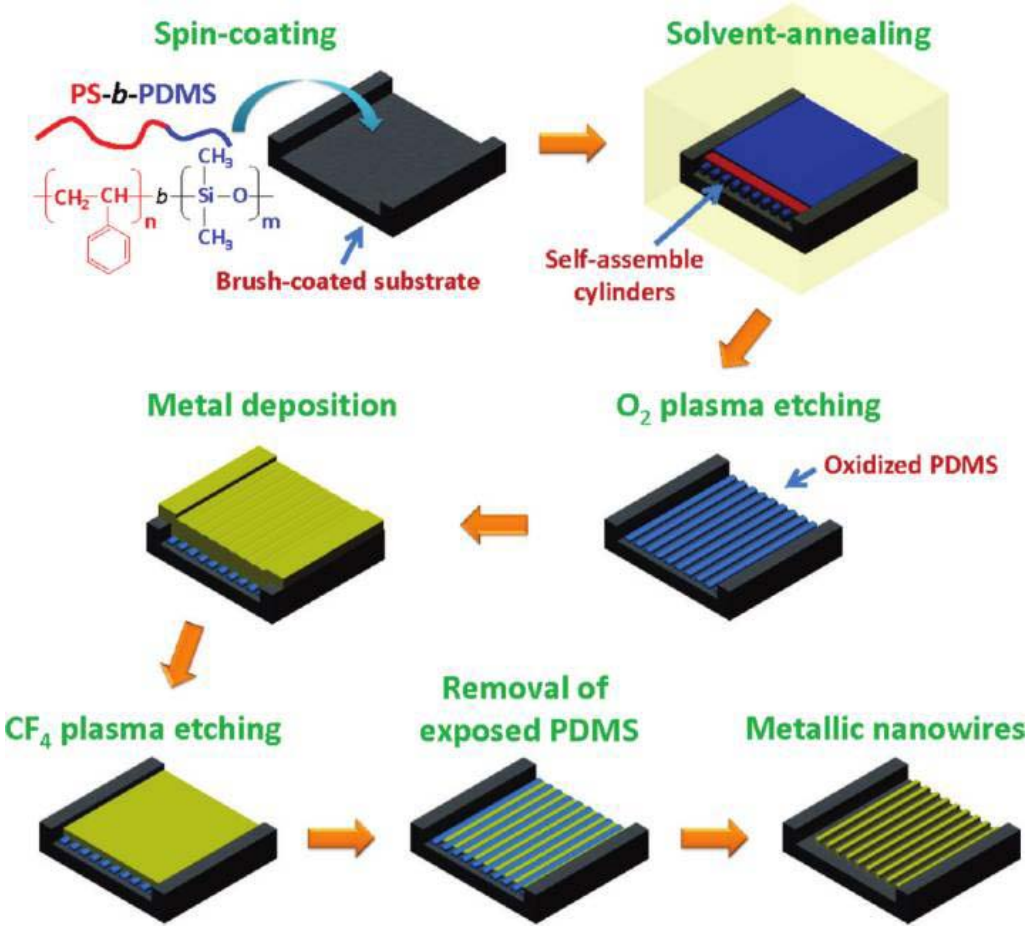

Schematic for fabrication of metallic nanowires via bcp self-assembly

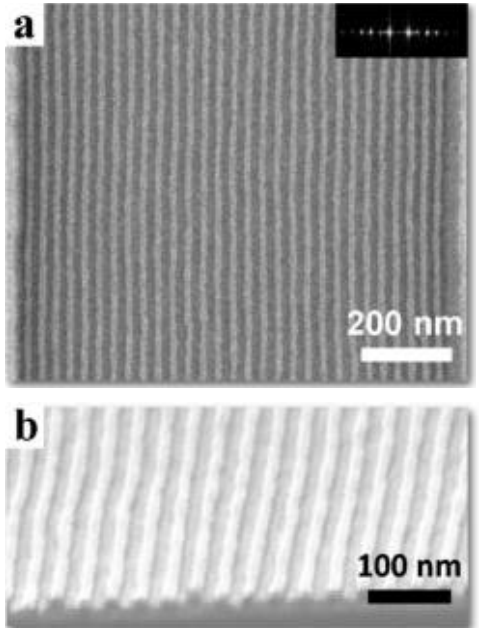

Oxidized self-assembled PDMS pattern after reactive ion etching

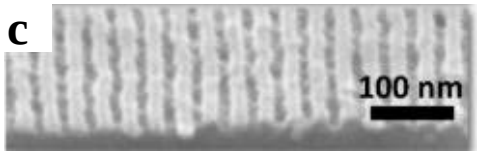

Tungsten nanowires

Y. S. Jung, J. H. Lee, J. Y. Lee, and C. A. Ross, *Nano Lett.* 2010, *10*, 3722-–3726

Fabrication of Diverse Metallic Nanowire Arrays Based on Block Copolymer Self-Assembly

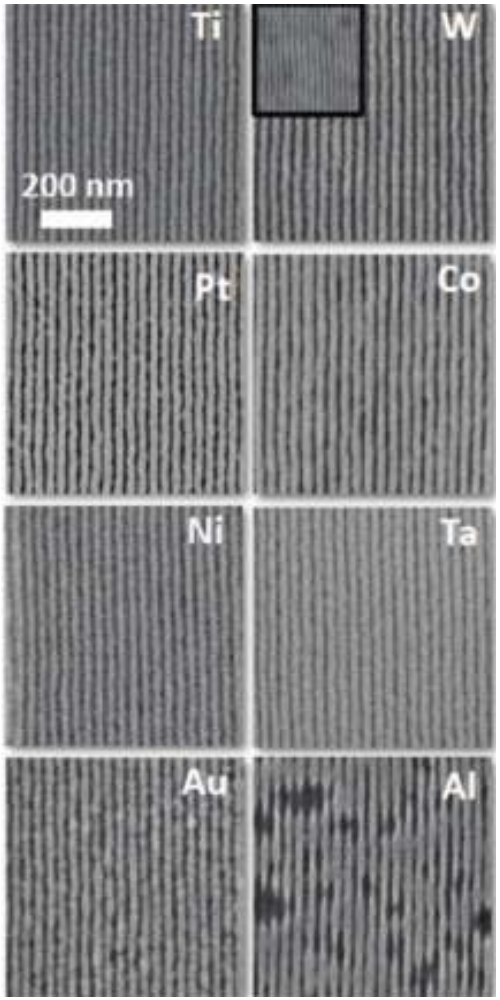

Various metal nanowires

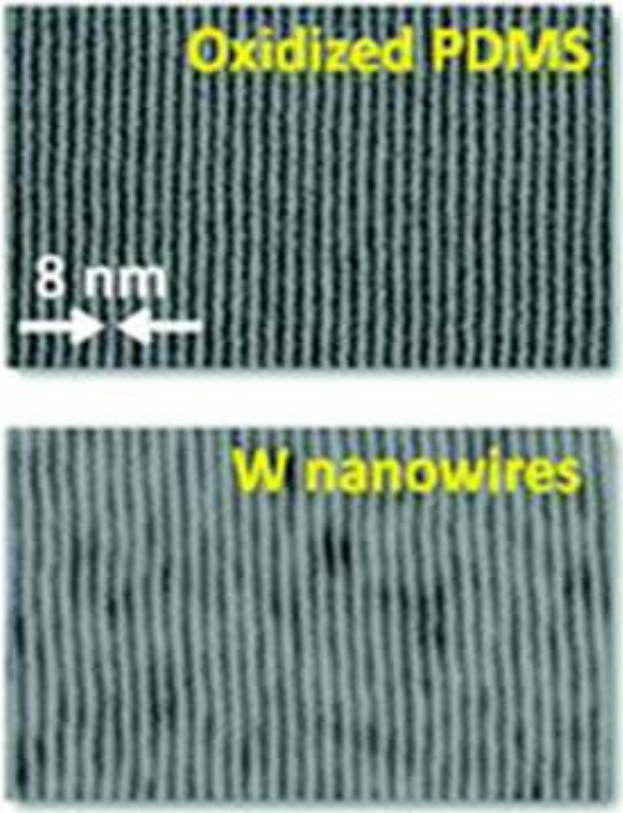

a) Sub-10 nm self-assembled patterns

b) Tungsten nanowires

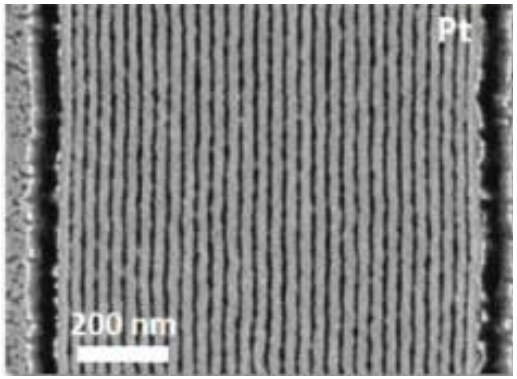

Platinum nanowires adjacent to step edges

Y. S. Jung, J. H. Lee, J. Y. Lee, and C. A. Ross, *Nano Lett.* 2010, *10*, 3722-–3726

Remediation of Line Edge Roughness in Chemical Nanopatterns by the Directed Assembly of Overlying Block Copolymer Films

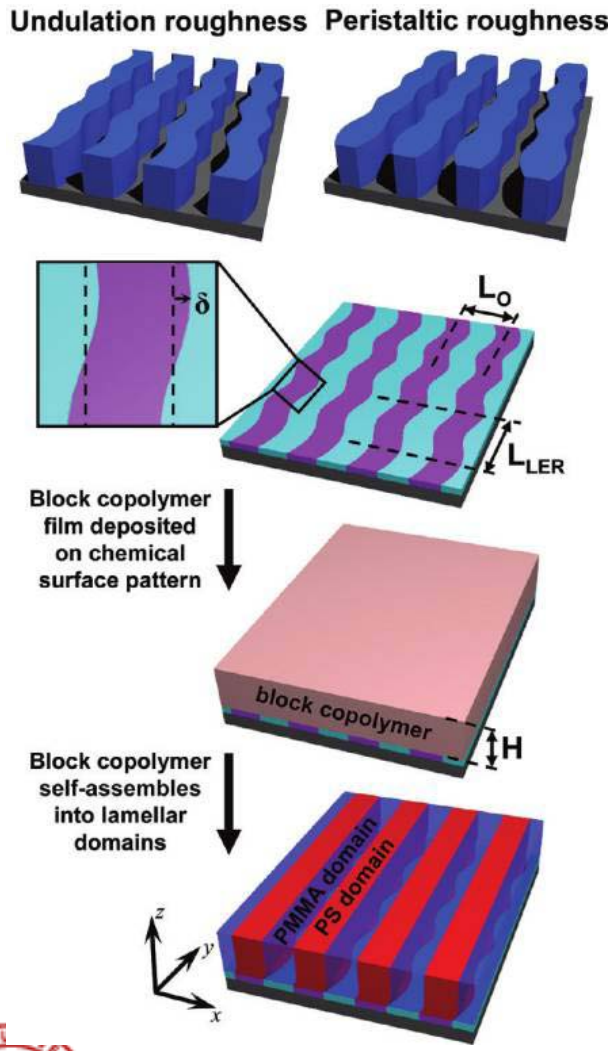

Characterization of PS-b-PMMA lamellae directed to assemble on chemical surface patterns with undulation roughness

L_{LER} = 140 nm

L_{LER} = 70 nm

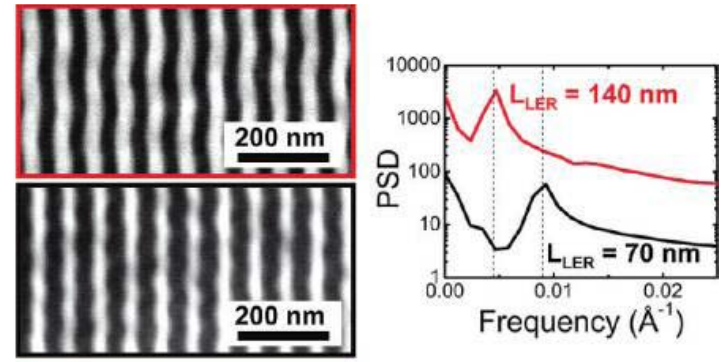

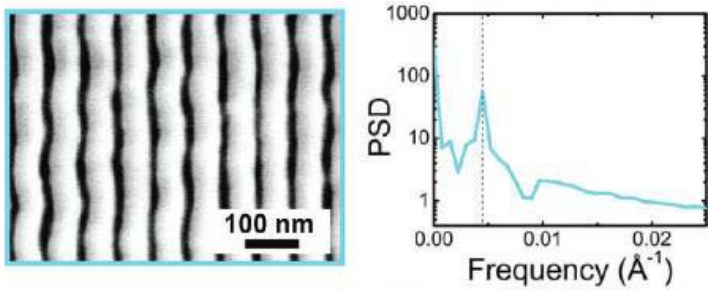

L_{LER} = 140 nm

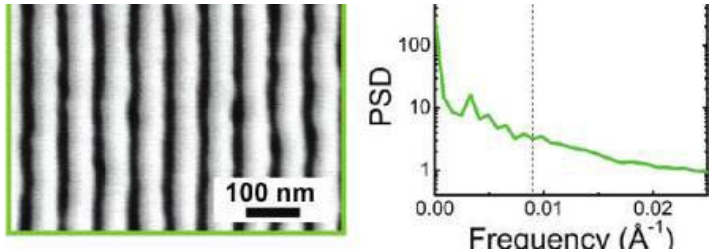

bcp lamellae assembled on surface patterns

M. P. Stoykovich, K. Ch. Daoulas, M. Muller, H. Kang, J. J. de Pablo, and P. F. Nealey, Macromolecules, Vol. 43, No. 5, 2010

Molecular Transfer Printing Using Block Copolymers

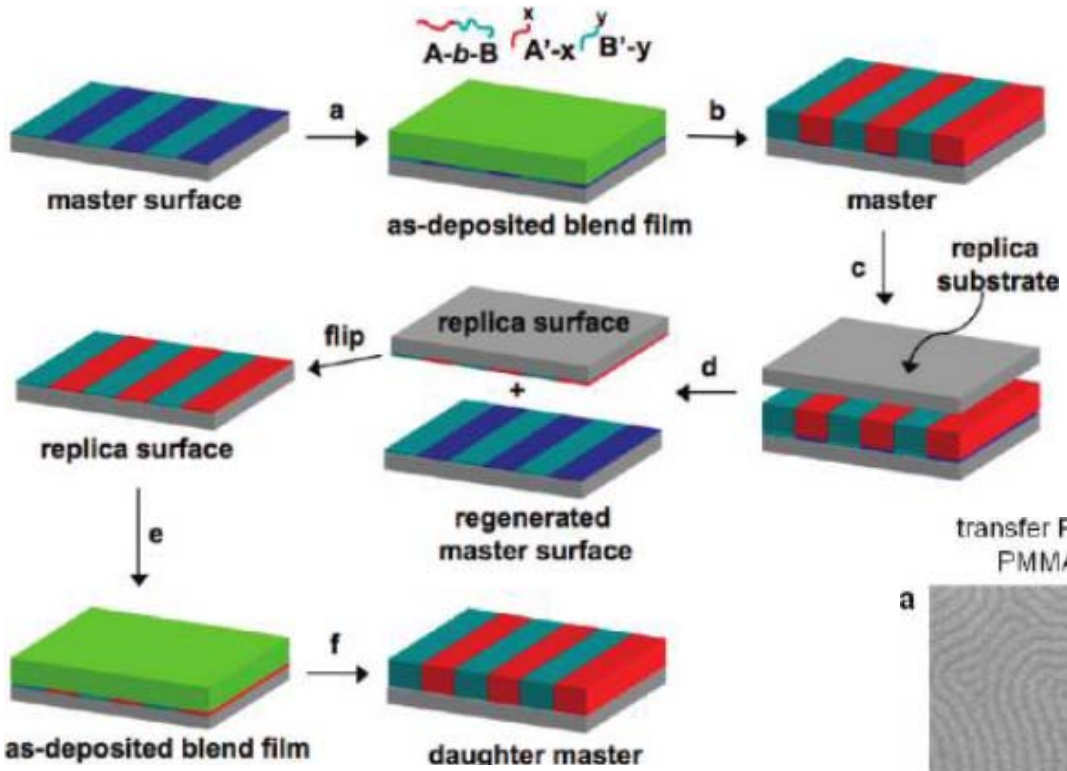

Schematic of molecular transfer printing (MTP)

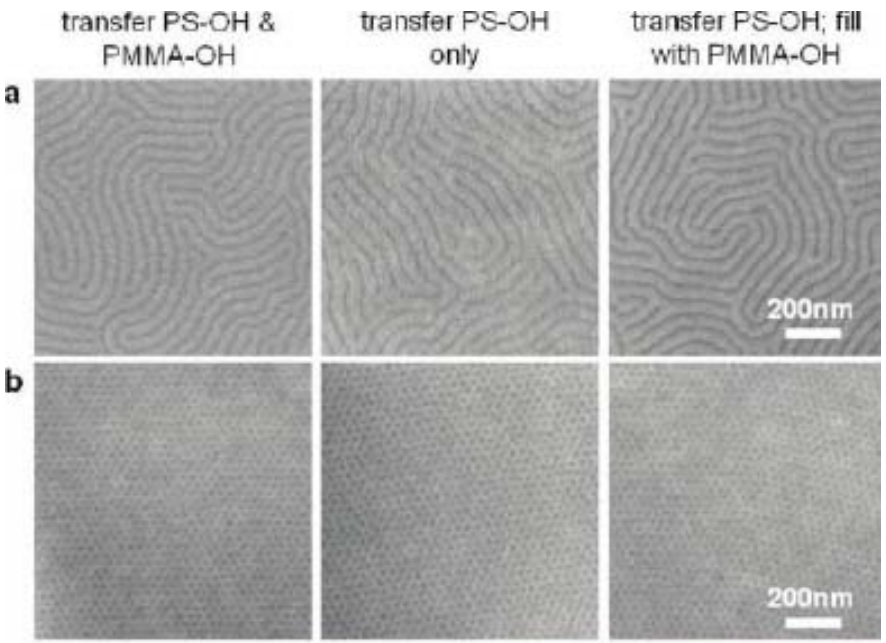

S. Ji, C. C. Liu, G. Liu, and P. F. Nealey, *Nano Lett.* 2010, *10*, 3722-–3726

Molecular Transfer Printing Using Block Copolymers

Demonstration of MTP of different pattern geometries using ternary blends of block copolymers

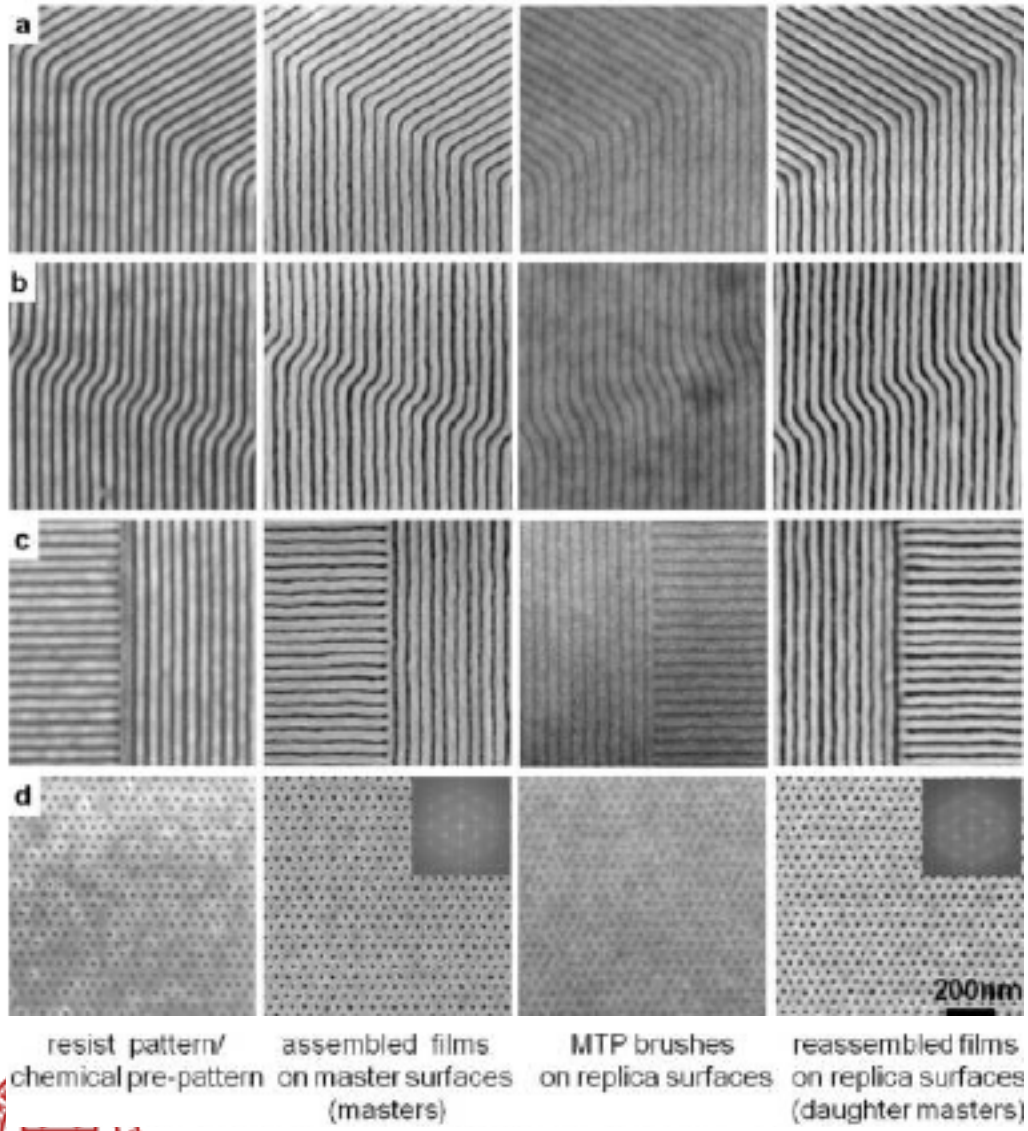

SEM images of the photoresist pattern, indicative of chemical prepatterns, blend films assembled on the master surfaces (masters), transferred brushes on replica surfaces, and reassembled blend films on replica surfaces (daughter masters).

S. Ji, C. C. Liu, G. Liu, and P. F. Nealey, *Nano Lett.* 2010, *10*, 3722-–3726

Controlling Orientation and Order in Block Copolymer Thin Films

hydroxyl-terminated polystyrene (PS-OH) added to the bcp solution to induce ordering

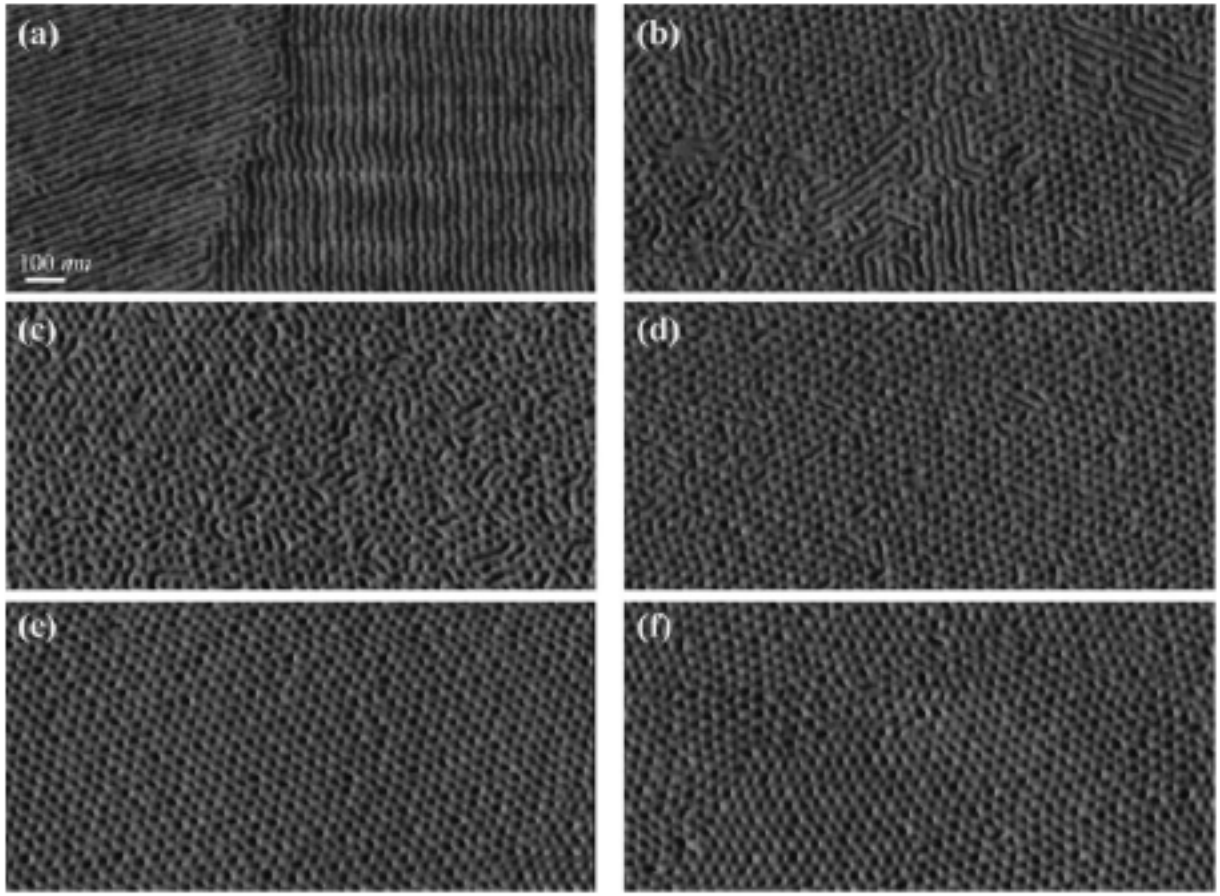

SFM images of copolymer films without (a) and with (b) added PS-OH (2.5 wt%) before solvent annealing, and of solvent-annealed films without (c) and with added PS-OH1 of 0.5 wt% (d), 2.5 wt% (e) and 4 wt% (f).

S. H. Kim, M. J. Misner, and T. P. Russell, Adv. Mater. 2008, 20, 4851–4856

Small scale structures: Salt Complexation in Block Copolymer Thin Films

polystyrene-*block*-poly(ethylene oxide) mixed with KI salt to induce ordering

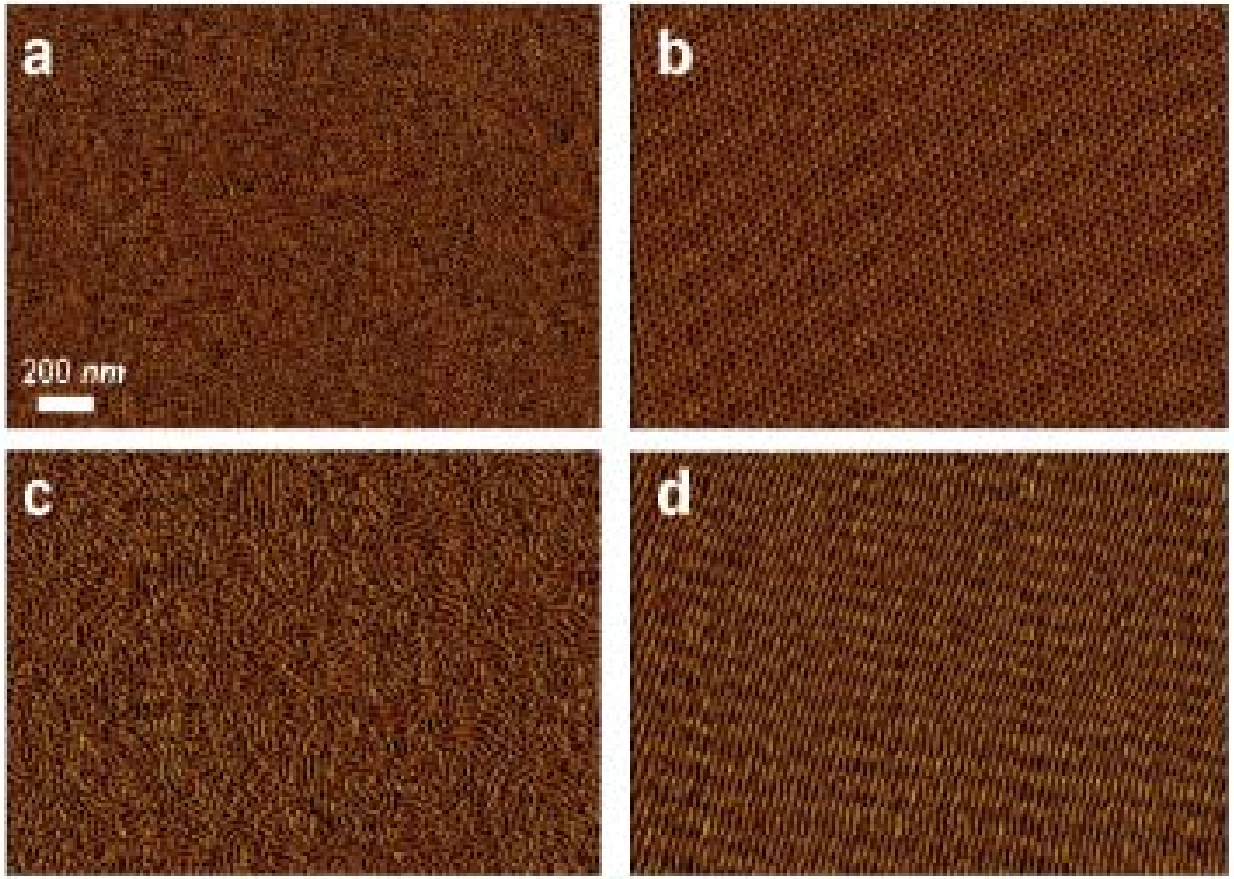

PS-*b*-PEO with KI (a) as spun and (b) after solvent annealing and copolymer films without added KI (c) as spun and (d) after solvent annealing.

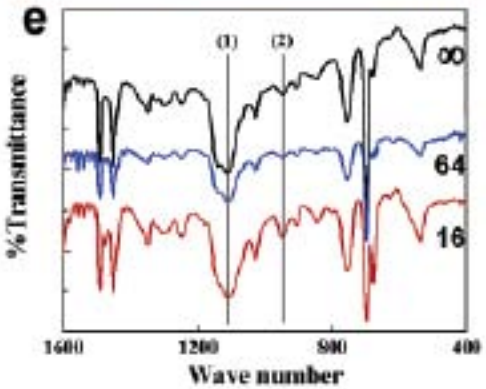

Shifts in the IR spectroscopy of the copolymer with varying monomer-to-salt ratios ([O]/[K]) indicate complexation of the salt with the PEO

S. H. Kim, M. J. Misner, L. Yang, O. Gang, B. M. Ocko, and T. P. Russell, *Macromolecules, Vol. 39, No. 24, 2006*

P⟨MS-b-PHOST

Combined Patterning System

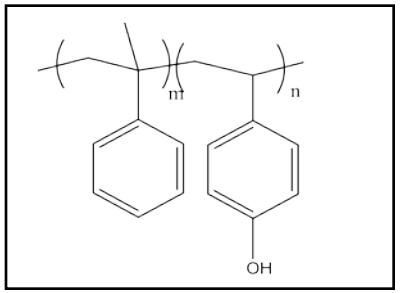

P⟨MS has low Tc:

Remove with h

For long range order, thermal annealing will not work!

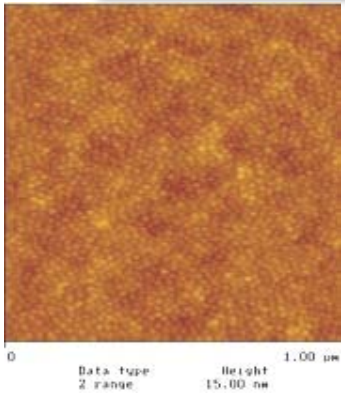

Standing cylinders of P⟨MS

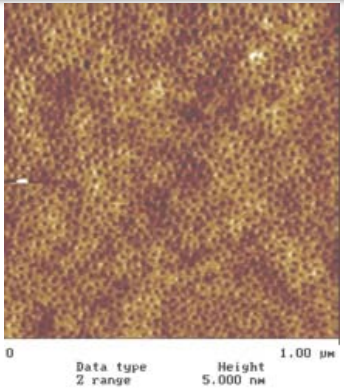

Pores after P⟨MS removal

PHOST is a Negative-Tone Photoresist

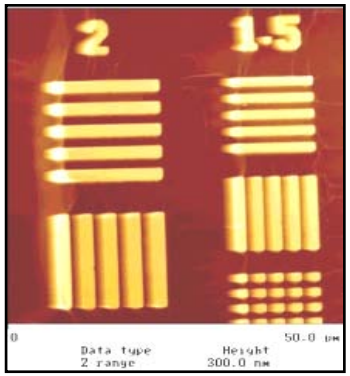

Resolution: 450nm

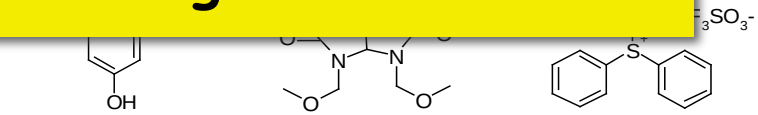

PHOST

TMMGU, Crosslinker

TPST, PAG

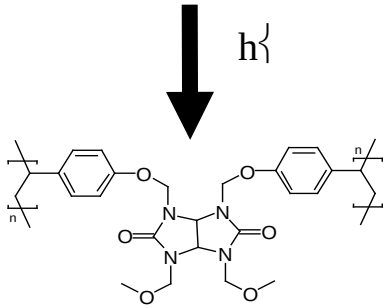

Li, M., et al. Chem. Mater 2004 16 3800.

Switching Orientation using Solvent:

Last anneal erases previous treatment

Katy Bosworth

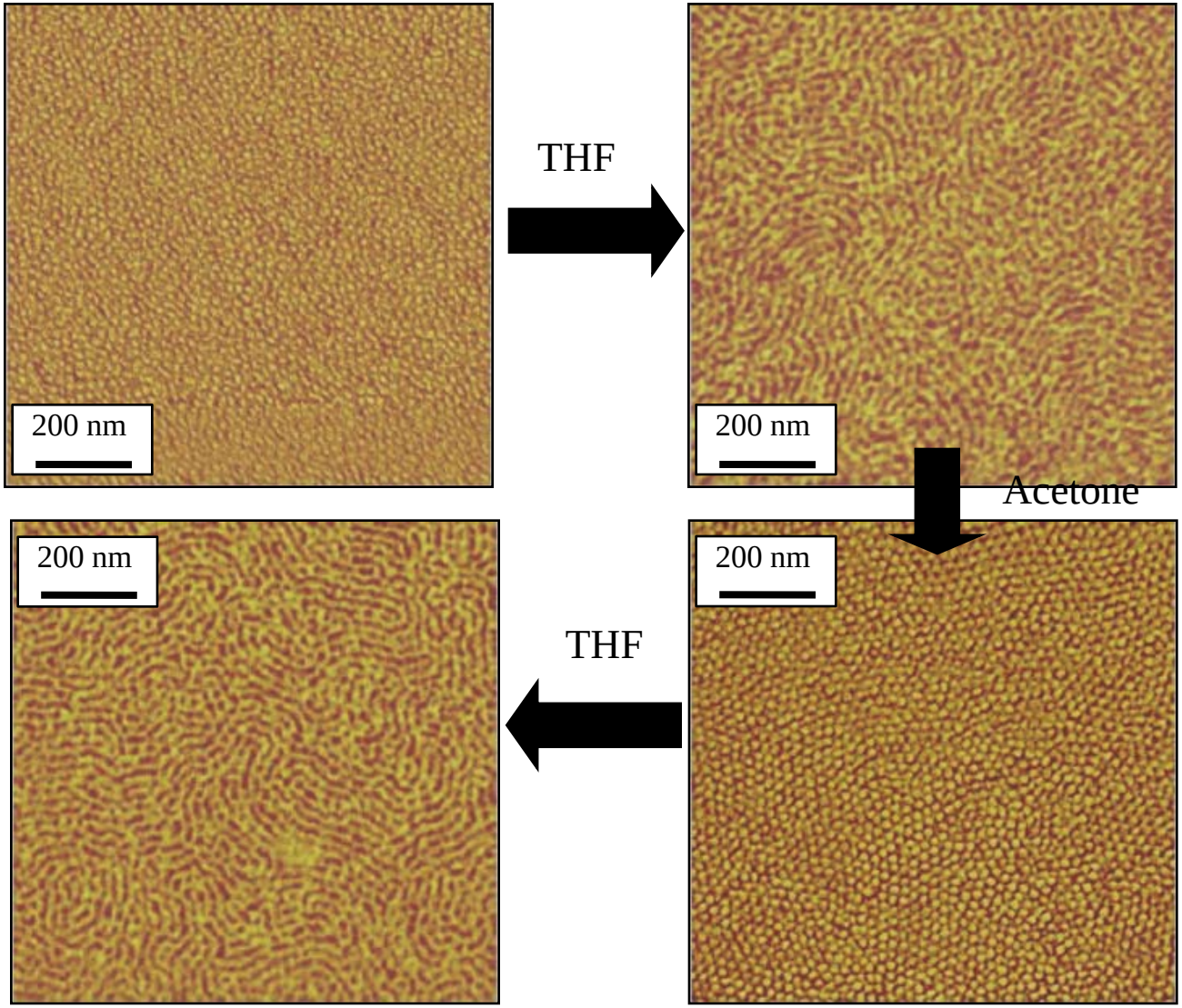

Marvin Y. Paik, Joan K. Bosworth, Detlef-M. Smilges, Evan L. Schwartz, Xavier André, Christopher K. Ober, "Reversible Morphology Control in Block Copolymer Films via Solvent Vapor Processing: An In-Situ GISAXS Study", *Macromolecules*, (2010), 43(9), 4253-4260.

Double Morphology

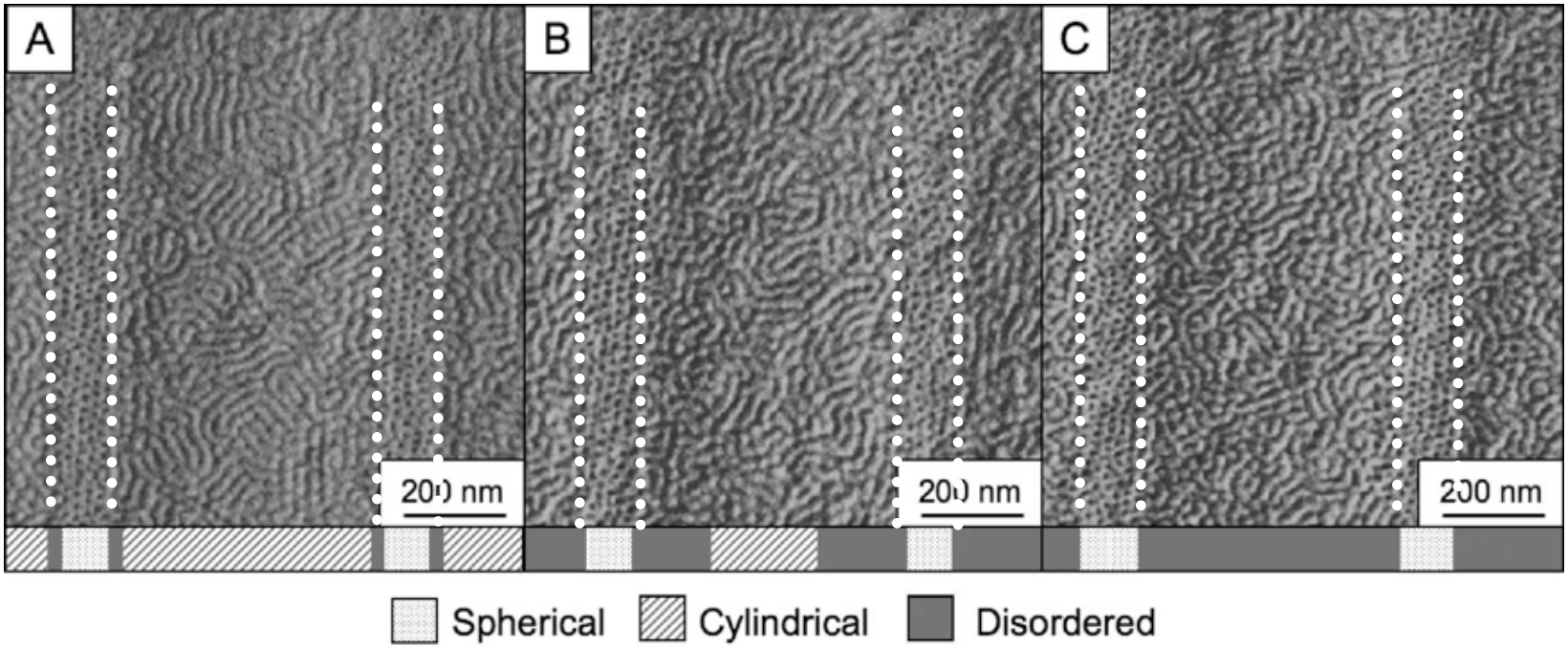

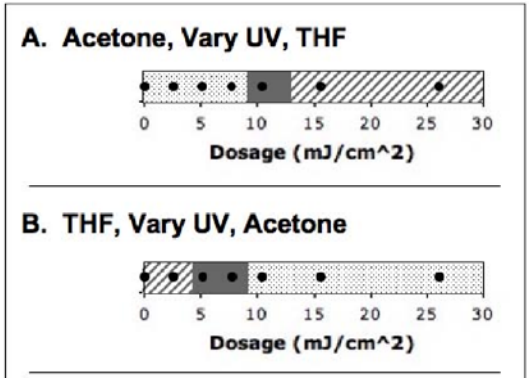

Electron-beam exposure doses are:
a) 100 $\mu C/cm^2$
b) 200 $\mu C/cm^2$
c) 400 $\mu C/cm^2$.

Joan K. Bosworth, Jing Sha, Charles T. Black, Christopher K. Ober, "Multiple Block Copolymer Morphologies on a Single Wafer: The Intersection of Lithography and Solvent Anneal Morphology Switching", *ACS Nano*, 2009, 3(7), pp 1761–1766.

What can we do?

- Make periodic patterns – dot, line
- Can load with inorganic and increase etch resistance
- Can improve LER
- Can make replicas
- Can pattern and control microstructure in single system

How to inject dopant

- Ion implantation through pores cut in bcp will work
- But this approach limits options for placement and leaves process subject to some statistics
- Can we develop method for direct placement?
- And drive dopant into silicon?

Neglected Microstructures

- Using rod-coil polymers
- Form crystalline monolayers

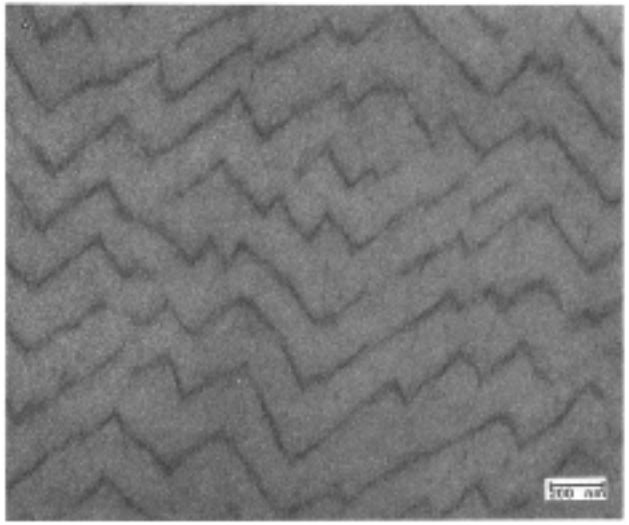

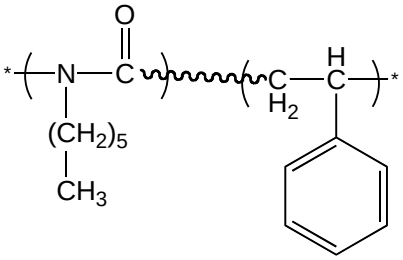

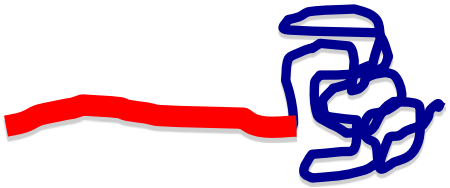

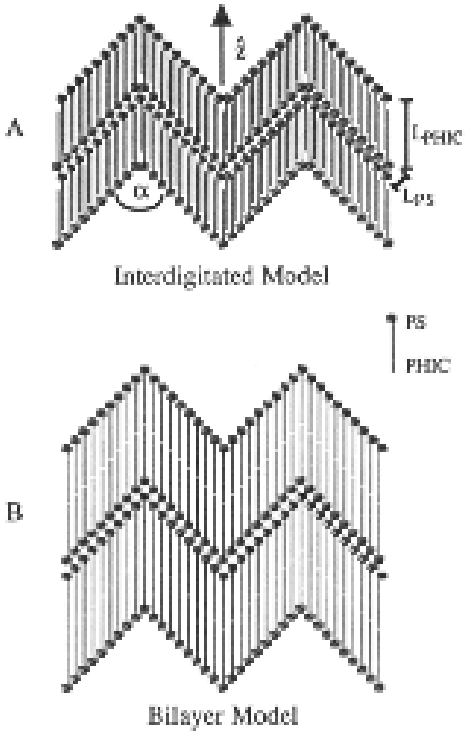

Figure 9. (A) Schematic diagram depicting the packing arrangement of the chains in the zigzag morphology in which the PHIC rods interdigitate. (B) Schematic diagram depicting the packing arrangement of the chains in the zigzag morphology in which the block copolymer molecules order in a bilayer.

J. T. Chen, E. L. Thomas, S. S. Hwang and C. K. Ober, "The Zig-Zag Morphology of a Poly(styrene-b-hexyl isocyanate) Rod-Coil Block Copolymer", *Macromolecules,* 28 (5), 1688-1697 (1995).

Rod-coil for dopant placement

- Can we use the precision synthesis of biomaterials with the placement of self-assembly?

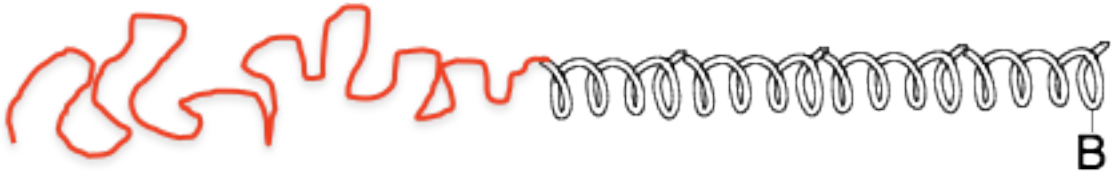

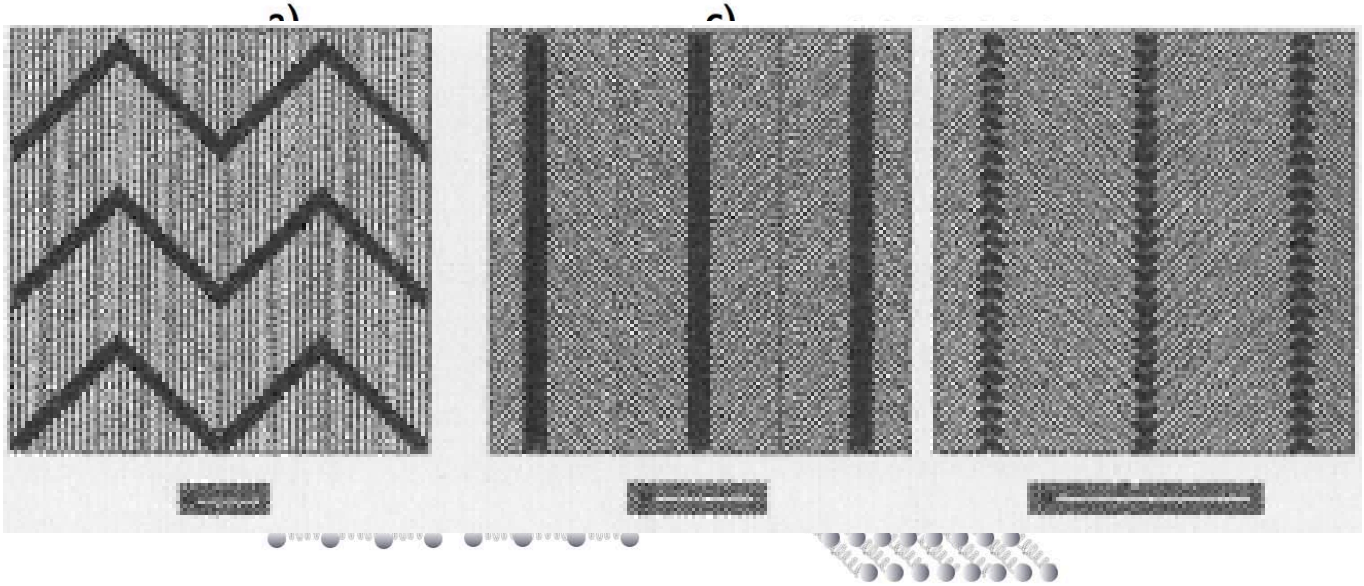

J. T. Chen, E.L. Thomas, C.K.Ober and G.-P. Mao, “Novel Self-Assembled Smectic Phases in Rod-Coil Block Copolymers”, *Science*, 273, 343-346 (1996).

Molecular Origami

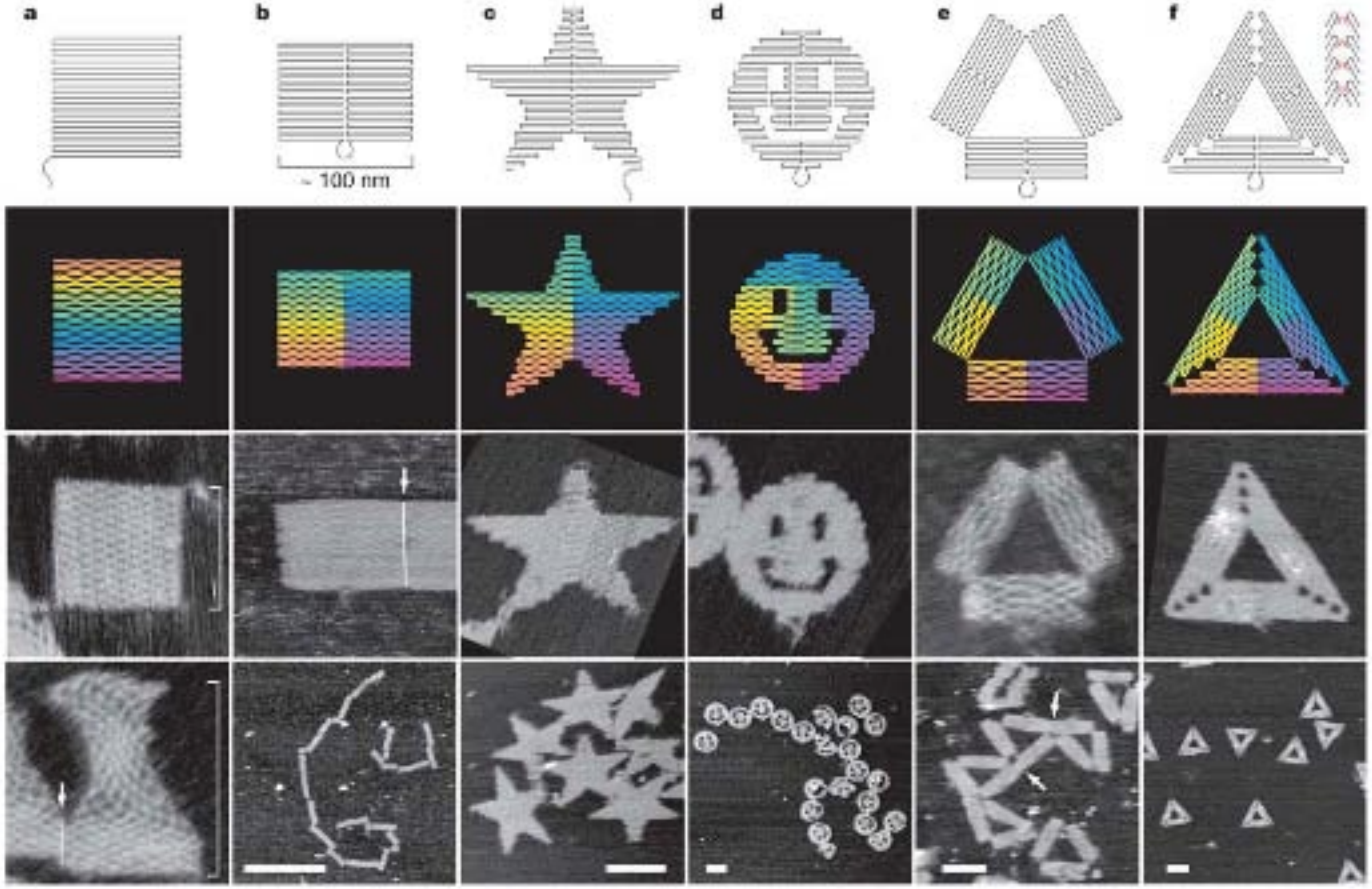

P. Rothemund, Nature, 440, 297 (2006)

Issues

- DNA is loaded with P
- Molecular size is enormous
- But structure is programmable
- Arbitrary shapes possible – even 3D structures
- Is there alternative with good characteristics and without bad?

Molecular Origami

- Could we use PNA?
- PNA is a DNA analog with a protein backbone
- Can use peptide synthesis to create sequence and spacing
- Use assembly to make tailored pattern

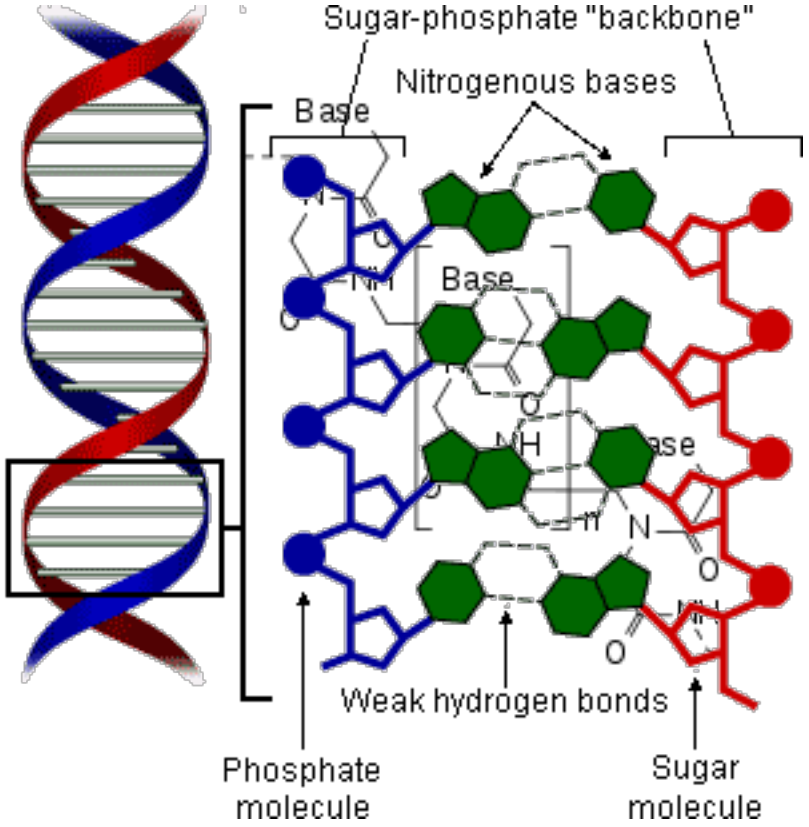

BCPs in Doping

- Today bcp templates for targeted doping within reach
- Length scale can be down to a few nm's
- Dopants can in principle be injected through pores in bcp film – blocked by other regions
- Synthetic methods exist for precise tailoring of bioinspired polymers with placement of dopant on exact place on chain
- In future tailored polymer monolayers that carry dopant may enable exact placement on semiconductor

Assembly of essential shapes and dimensions

Design Driven Set of Shapes

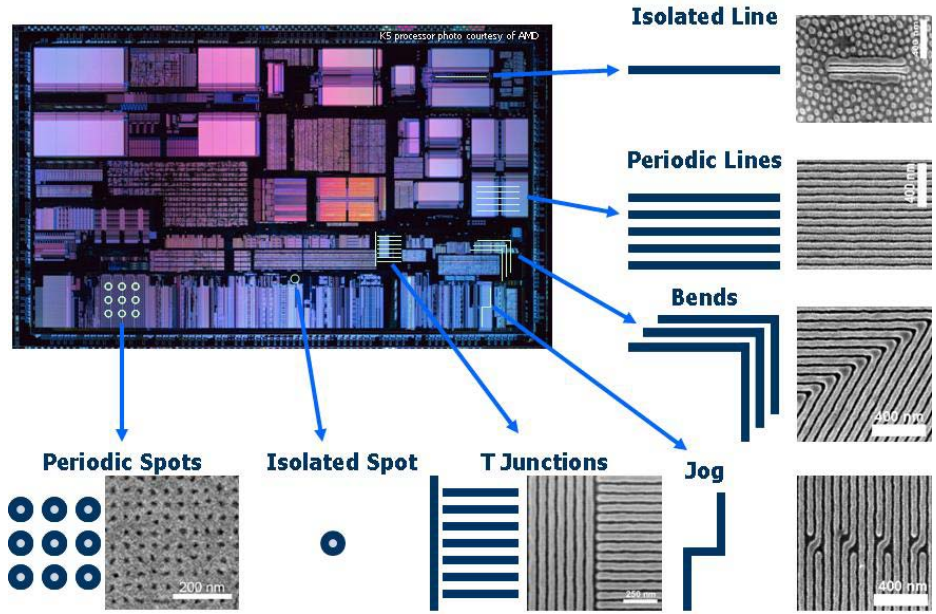

2007 ITRS, ERM, pp. 18-22

Size of Molecular Scaffolds

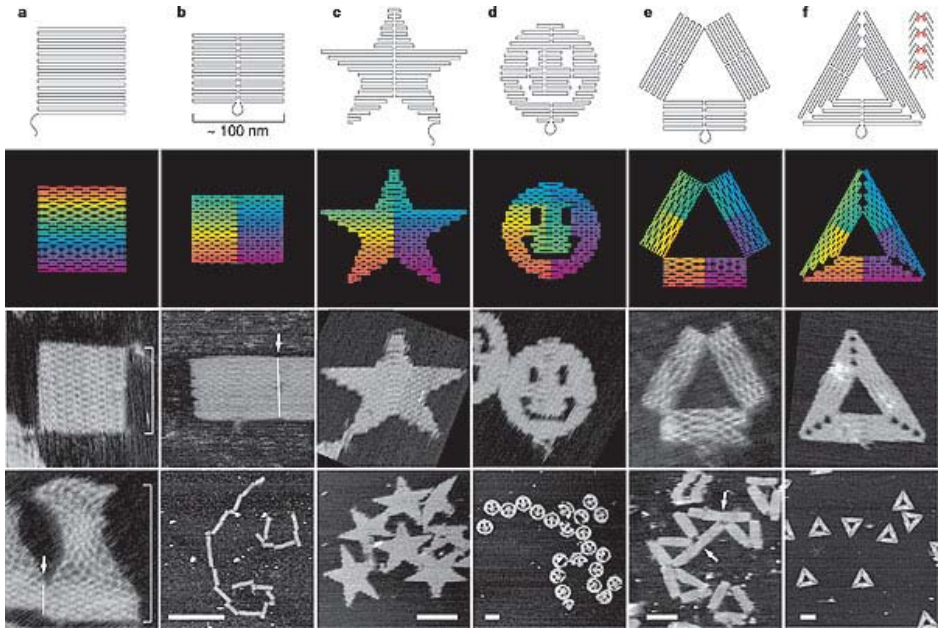

Folding DNA to Create Nanoscale Shapes and Patterns, Paul W. K. Rothemund, Nature 440, 297-302 (16 March 2006)

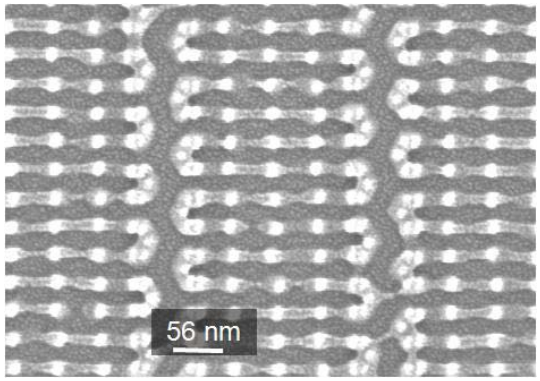

Directed Assembly of Complex Shapes (MIT)

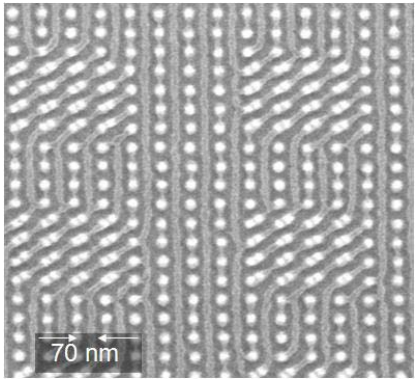

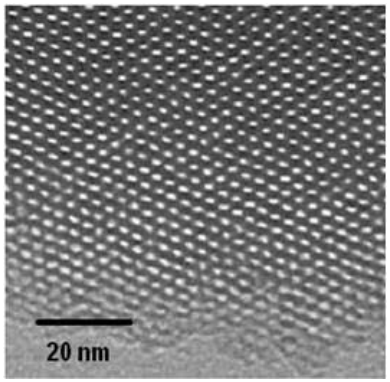

3 nm Mesoporous Silicate pores (UMA-A)

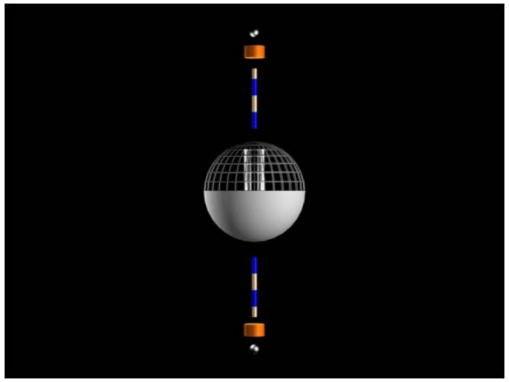

Nanovalves (NWU)